CHARACTERIZATION OF SPRING THAW FOR DIFFERENT FOREST TYPES IN THE SOUTHERN BOREAL FOREST UNDER CURRENT AND FUTURE CLIMATE

A Thesis Submitted to the

College of Graduate and Postdoctoral Studies

in Partial Fulfillment of the Requirements

for the degree of Doctor of Philosophy

in the Department of Civil, Geological and Environmental Engineering

University of Saskatchewan

Saskatoon

By

Hafiz Faizan Ahmed

PERMISSION TO USE

In presenting this thesis/dissertation in partial fulfillment of the requirements for a Postgraduate degree from the University of Saskatchewan, I agree that the Libraries of this University may make it freely available for inspection. I further agree that permission for copying of this thesis/dissertation in any manner, in whole or in part, for scholarly purposes may be granted by the professor or professors who supervised my thesis/dissertation work or, in their absence, by the Head of the Department or the Dean of the College in which my thesis work was done. It is understood that any copying or publication or use of this thesis/dissertation or parts thereof for financial gain shall not be allowed without my written permission. It is also understood that due recognition shall be given to me and to the University of Saskatchewan in any scholarly use which may be made of any material in my thesis/dissertation.

DISCLAIMER

Reference in this thesis/dissertation to any specific commercial products, process, or service by trade name, trademark, manufacturer, or otherwise, does not constitute or imply its endorsement, recommendation, or favoring by the University of Saskatchewan. The views and opinions of the author expressed herein do not state or reflect those of the University of Saskatchewan, and shall not be used for advertising or product endorsement purposes.

Requests for permission to copy or to make other uses of materials in this thesis/dissertation in whole or part should be addressed to:

Head of the Department of Civil, Geological and Environmental Engineering
3B48 Engineering Building, 57 Campus Drive
University of Saskatchewan
Saskatoon, Saskatchewan S7N 5A9 Canada

OR

Dean, College of Graduate and Postdoctoral Studies
University of Saskatchewan
116 Thorvaldson Building, 110 Science Place
Saskatoon, Saskatchewan S7N 5C9 Canada

ABSTRACT

Spring thaw timing is of great significance for ecological, biogeochemical, and hydrological processes in seasonally-frozen boreal forests. Site characteristics such as canopy architecture, ground cover type, thickness of organic soils, and mineral soil texture can influence thaw dynamics causing spring thaw variability for different forest types. The objective of this research was to characterize the existing and future variability of spring thaw between the two coniferous (black spruce and jack pine) and one deciduous (aspen) forests located in the southern boreal forest of Western Canada. Long-term observations (1997-98 to 2015-16) were used to explore existing inter-site variability of spring thaw. During the observation period, seasonal snowfall was similar at all three sites, but snow accumulation on the ground was 15% to 20% higher for the deciduous than the coniferous forests. The timing for the onset of snowmelt and soil thaw were similar between the sites, but varied considerably for soil thaw completion. The soil thawed at the aspen site about 2.5 and 4.5 weeks earlier than the jack pine and black spruce sites, respectively. This was likely driven by the higher sub-canopy net radiation of the leafless deciduous canopy. The differences between the two coniferous forest sites were driven by the thicker forest floor at the black spruce site causing higher ice content and providing better insulation effects. Carbon uptake was strongly correlated with snowmelt and soil thaw at both the coniferous forest sites but the correlations were not statistically significant for the aspen site.

The Simultaneous Heat and Water (SHAW) model was used to predict the future spring thaw variability for the study sites. The model was selected after its performance evaluation against the observations and simulations of the Canadian Land Atmosphere Surface Scheme (CLASS) and Cold Regions Hydrological Model (CRHM) for winter-spring transition at the jack pine site. All three models simulated similar snow ablation date, with a difference of 1 to 5 days, despite large differences in snowmelt rates. The SHAW model performed better for simulating soil thaw timing (the maximum difference between observations and simulations was about 1 week for SHAW, 3 weeks for CLASS, and 6 weeks for CRHM) but spring evapotranspiration was overestimated (by 40 to 95 mm) by all three models. After a rigorous parameter sensitivity analysis and calibration of SHAW, it was determined that the ground cover layer in the model is important for improved simulations of soil temperature/soil thaw and an additional term in Jarvis-Stewart resistance

scheme to consider the influence of low soil temperatures on stomatal conductance is needed for improving simulations of spring evapotranspiration. An approach based on the growing degree days (GDD) was proposed to indirectly consider the soil thermal environment in modelling the functioning of stomatal conductance. The consideration of ground cover layer reduced model bias up to 2.5 weeks and the proposed GDD factor reduced root mean square error for evapotranspiration by 35 to 40 mm.

Future (2085-2097) weather data over Western Canada was generated by the Weather Research and Forecasting (WRF) model using the Pseudo Global Warming approach. The future climate at the study sites is projected to be wetter (18%) and warmer (5.8°C). In response, SHAW predicted significant changes in spring thaw processes. For example, future snow ablation and soil thaw timing are predicted to advance relative to historical conditions (2000-2012) by about 2.5 weeks and 6 to 7 weeks, respectively. The frozen ground depth is predicted to reduce by 45% to 58% with the highest reduction at the black spruce site which has the highest average soil water content. The mean annual soil temperature is projected to rise by 3.3°C to 3.9°C at all three sites. The evapotranspiration is predicted to increase by 26% to 28%. This study advances our understanding about the existing variability of spring thaw for different forest types in the southern boreal forest and predicts future changes in spring thaw dynamics at these sites.

ACKNOWLEDGEMENTS

First and foremost, I am indebted to Almighty Allah for blessing me with the motivation, strength and perseverance to take this long journey to its destination. I am also grateful to holy prophet Muhammad (PBUH) who inspired me to pursue higher education through his teachings. I always remember his saying “Acquire knowledge and impart it to the people”.

I would like to extend my gratitude to Dr. Warren Helgason for his guidance, unwavering support, and encouragement. I am highly grateful to Dr. Alan Barr for his support and positive critique which helped me improving scientific writing skills. I am also very thankful to all member of advisory committee including, Dr. Howard Wheater, Dr. John Pomeroy and Dr. Christopher Hawkes as well as to the external examiner Dr. Timothy Link for providing their thoughtful comments, guidance and support.

I am truly indebted to all my family including parents, siblings, father-in-law and mother-in-law for their prayers, well wishes, encouragement and unconditional support. I am thankful to my best friend Haider Abbas for always being there whenever I needed him. A very special thanks to my colleagues Amber Peterson and Sopan Kurkute for their continued support in this journey.

Last but not the least, I would like to express my warm-hearted appreciation for my beautiful wife, Aleena Suhail, for always believing in me and keeping me motivated. I couldn’t have completed this journey without her incredible company, care, and support.

DEDICATION

It is my genuine gratefulness and warmest regard that I dedicate this work to my beloved parents: “Zahoor Ahmad” and “Shagufta Zahoor (late)”.

TABLE OF CONTENTS

LIST OF TABLES

LIST OF FIGURES

LIST OF ABBREVIATION

AS	Aspen
BERMS	Boreal Ecosystem Research and Monitoring Sites
BOREAS	Boreal Ecosystem Atmosphere Study Program
BS	Black spruce
CO_2	Carbon Dioxide
CLASS	Canadian Land Surface Scheme
CRHM	Cold Regions Hydrological Model
DDS	Dynamically Dimensioned Search Algorithm
ET	Evapotrasnpiration (mm)
G	Ground Heat Flux (W m^{-2})
GCM	General Circulation Model
GDD	Growing Degree Days
GDD_{cum}	Cumulative Growing Degree Days
GDD_{cri}	Critical Growing Degree Days
GEP	Gross Ecosystem Photosynthesis
H	Sensible Heat Flux (W m^{-2})
IPCC	Intergovernmental Panel of Climate Change
JP	Jack pine
LAI	Leaf Area Index (m^2 m^{-2})
LHF	Latent Heat Flux (W m^{-2})
MAE	Mean Absolute Error
MBE	Mean Bias Error
NDVI	Normalized Difference Vegetation Index
NEE	Net Ecosystem Exchange
NEP	Net Ecosystem Production
PAR	Photosynthetically Active Radiation
PGW	Pseudo Global Warming
R	Respiration
RCM	Regional Circulation Model

RCP	Representative Concentration Pathways
RMSE	Root Mean Square Error
SHAW	Simultaneous Heat and Water model
SWE	Snow Water Equivalent (mm)
T	Temperature (°C)
TDR	Time Domain Reflectometry
Tr	Transpiration (mm)
VPD	Vapor Pressure Deficit (Pa)
WRF	Weather Research and Forecasting model

CHAPTER 1 INTRODUCTION

1.1 BACKGROUND

The boreal forest is one of the world's largest ecosystems which covers about 11% of the earth's terrestrial surface (Boonstra et al., 2016). It is considered to be a vital part of the global carbon cycle (Bonan et al., 1995). About 27% of the world's vegetation carbon, and 25-30% of soil carbon is stored in boreal forests (Turetsky et al., 2007). These forests are sensitive to climate change and their quick response to warming has already been observed by northern upslope migration of treeline, decline in growth of white spruce because of moisture stress, and an increase in infestation and wildfire disturbances across the circumpolar vegetation zone (Soja et al., 2007). They are not only sensitive to climate change but can also provide strong and quick feedback to climate by altering global carbon, energy and water budgets because of their size (Hari and Kulmala, 2008). The net annual exchange of CO_2 is highly variable in these environments (Welp et al., 2007) and linked with snow cover properties (Hardy et al., 1995), water availability (Ueyama et al., 2006), as well as air and soil temperatures (Barr et al., 2009). In Canada, the boreal region occupies more than half of the land's area, about 21% to 27% of the global boreal forests (Brandt, 2009). In addition to its global significance on climate, wildlife and carbon storage (Frelich et al., 2021), the sub-humid and seasonally frozen southern boreal forest of Western Canada is of great regional importance for creating jobs, stabilizing forest sector economy, providing timber and non-timber products, generating mineral and energy resources, and promoting tourism or recreational opportunities.

Spring thaw timing in boreal forests is critical for several ecological, biogeochemical and hydrological processes because of its influence on growing season length (Danielewska et al., 2015). Stem growth of trees as well as the uptake of nutrients and carbon dioxide are strongly dependant on soil thaw timing (Jarvis and Linder, 2000). Increased carbon uptake is associated with early spring warming at both field and ecosystem scales (Welp et al., 2007; Xu et al., 2013).

Soil thaw timing has also been strongly correlated with annual evapotranspiration at northern high latitudes (Zhang et al., 2011). Frozen soils influence partitioning of snowmelt into surface runoff and infiltration (Stahli et al., 2001) which results in an increased lateral water movement. Furthermore, soil temperature and moisture content strongly influence decomposition of organic matter in boreal forests (Wickland and Neff, 2008). Thus, an advanced understanding about the potential future changes in soil thaw timing is vital for reliably projecting the response of boreal ecosystems to climate change.

The timing of spring thaw may differ amongst forest types growing in a similar region because of variability in below canopy available energy, differences in the amount of energy required for thaw, and the relative importance of individual energy exchange processes. For example, snow cover provides insulation to the underlying soil; therefore, ablation processes play a critical role in moderating soil thaw rates. The forest canopy directly influences snow accumulation (Pomeroy et al., 2002) and melt rates (Gelfan et al., 2004) by altering snow interception (Hedstrom and Pomeroy, 1998) and energy penetration through the canopy (Mahat and Tarboton, 2012). Similarly, properties of the forest floor and underlying soil can also vary among different forests and have a strong influence on soil thaw. Soil surface temperatures and the ground heat flux density are influenced by ground cover types (Blok et al., 2011; Stoy et al., 2012). Thus, the soil-frost depth, and the degree of soil cooling in winter, are influenced by the insulating effects of the forest floor. The soil water holding capacity, as well as many thermal properties vary substantially between mineral and organic soils (Letts et al., 2000; Rawls et al., 1982). Therefore, the ice content can vary among sites depending on soil texture and thickness of organic layers. Inter-site variability of any of the aforementioned physical characteristics can lead to variations in thaw timing. For example, early soil thaw might be expected at sites with lower snow accumulation or where rapid snow ablation occurs due to increased energy availability. In contrast, soil thaw may be delayed at ice-rich sites. Understanding the extent and dynamics of the variability in thaw timing for different forest types is crucial for reliably projecting their response in a changing future climate. At present, our knowledge about the temporal and spatial variability of spring thaw, particularly in the southern boreal forest, is limited.

North America, northern Europe, and northern Asia, have all experienced air warming and increased precipitation during the past century (Lemmen et al., 2008). This trend is projected to continue into the future because the effects of global warming are expected to be the greatest at high northern latitudes (Li et al., 2019; Solomon, S. et al., 2007; Xarpell et al., 2010). The annual global temperature has been increasing at a rate of 0.2 °C per decade since 1981 and the top 5 warmest years have been recorded in the present decade (NOAA, 2020). The effects of global warming are increasingly becoming more evident with increased observations of sea level rise (Lindsey, 2019), glacier melt (Zemp et al., 2019), increased tropical storm activity (Bhatia et al., 2019), flooding, heatwaves and drought (Dai, 2013), and wildfires (Rossiello and Szema, 2019). The anticipated change in climate will likely have significant impacts on spring thaw processes in the boreal region. However, the exact implications of this are difficult to ascertain because of complex interactions between climate, vegetation, snow cover, forest floor and soil systems. As a prediction tool, land surface models (LSMs) could be combined with climate models to better understand and evaluate future changes in the spatial and temporal variability of thaw dynamics. However, critical evaluation of model performance, including the representation of important hydrological and energy transfer processes, is a key first step for reliable projections.

Applications of LSMs in boreal forests for modelling soil temperatures have presented some limitations. For example, Essery et al. (2009) evaluated the performance of 33 LSMs for predicting winter-time snow processes and soil temperatures. They concluded that snow processes are generally well captured but all the models predicted much colder temperatures compared to the observations. Conversely, the tendency of LSMs to predict warmer soil temperatures in spring has also been observed (Zhang et al., 2008). Canopy architecture, ground cover type, thickness of organic soil layer, and mineral soil properties are important characteristics that influence the soil thermal regime. Canopy controls on critical processes are presently well-understood and modelled: snow interception and unloading (Hedstrom and Pomeroy, 1998), sublimation (Pomeroy et al., 1998b), snow accumulation (Pomeroy et al., 2002), radiation penetration through the canopy (Mahat and Tarboton, 2012; Pomeroy and Dion, 1996; Yang and Friedl, 2003), and snowmelt (Barlett et al., 2006; Gelfan et al., 2004; Mahat and Tarboton, 2014; Pomeroy and Granger, 1997). Similarly, important hydraulic properties of organic (Letts et al., 2000) and mineral soils (Cuenca et al., 1997; Rawls et al., 1982) have been determined and incorporated into LSMs (Chen et al.,

2016) for better representing land-atmosphere interactions in climate models. However, ground covers such as lichen, moss, or litter, are simply treated as an organic soil layer in LSMs – which may not be appropriate because of their unique hydraulic and thermal characteristics. Surface temperature has been documented to vary with different forest floor vegetation (Stoy et al., 2012) because of differences in albedo, water holding capacity (Liljedahl et al., 2011), thermal characteristics, and evaporative cooling among species (Nichols and Brown, 1980). For example, moss can retain and evaporate more water compared to lichen (Moore et al., 2019) which results in varying net energy availability for heat conduction and thermal conductivity. Thus, model simulations for soil temperature and thaw timing could likely be improved by considering site specific characteristics of the soil and understory vegetation or ground cover, but this requires further investigation.

Another known weakness of LSMs for simulating hydro-thermal processes in boreal forests is a tendency to overestimate spring evapotranspiration. Kuchment and Demidov (2006) developed a coupled model of the hydrological and carbon cycles in a forested ecosystem and tested its performance on an hourly time-scale at a jack pine stand in the southern boreal forest. The simulated net carbon uptake was found to be in good agreement with observations but spring evapotranspiration was biased high. Bonan et al. (1997) evaluated the outputs of a land surface model (NCAR LSM1) with the observed fluxes at coniferous and deciduous forests on a daily time scale. This model similarly overestimated spring latent heat fluxes for coniferous forests. Bartlett et al. (2003) evaluated the performance of an offline mode of Canadian Land Atmosphere Surface Scheme (CLASS) at three coniferous forest sites (young jack pine, old jack pine, and old black spruce) located in Manitoba, Canada and found that the latent heat fluxes were overestimated at all sites. Davison et al. (2016) used Modélisation Environnementale communautaire - Surface Hydrology (MESH) which combines CLASS with a routing algorithm and concluded that the model estimates of evapotranspiration remained biased high even after a rigorous calibration of the model parameters. A recent study investigated the controls on evapotranspiration at a jack pine forest using the CLASS and CLASS-CTEM models (Nazarbakhsh et al., 2019). They reported that the overestimation of spring evapotranspiration cannot be explained by parameterizations for soil hydraulic properties or plant characteristics such as roots distribution and leaf area index. However, the authors also concluded that the stomatal resistance is one of the most important

factors for partitioning of net available energy into sensible and latent heat fluxes. Thus, better seasonal controls on stomatal resistance, limiting spring evapotranspiration, may need to be incorporated in LSMs for improving their predictability in these environments.

Before boreal tree species start transpiring in spring, they must awake from dormancy. Several phenology models with varying level of complexity have been developed to mark the beginning of the growing season, most of which are based on surface meteorology. They can be broadly classified into single-phase models, which include those based on a moving mean of air temperature (Tanja et al., 2003), growing degree days (GDD), or thermal time (Cannell and Smith, 1983; Wu et al., 2013) and relatively more complex double-phase models which break dormancy into endogenous and environmental factors (Lang et al., 1987; Sarvas, 1972). Chill accumulation and forcing temperatures are driving factors for two-phase models (Kramer, 1994; Yu et al., 2010). A comparison of spring phenology models for boreal trees including simple thermal-time models, chilling-forcing models, and novel models that reverse the effect of warm temperature by intermittent cold temperatures suggested that the simple thermal-time models are more accurate for predicting onset of photosynthesis in spring for mature stands (Linkosalo et al., 2006). Typically, phenology models are used to mark the beginning of growing season; however, biological awakening is a gradual process (Saxe et al., 2001) and should be modelled as such. Low soil temperatures in spring influence biological functioning of boreal trees by depressing root water uptake and stomatal conductance (Ensminger et al., 2008).

1.2 PROBLEM STATEMENT

In seasonally frozen boreal forests, spring thaw timing is critical for several biogeochemical and hydrological processes. The existing extent of spring thaw variability for different forest types in the southern boreal forest and its driving forces are not well understood. It is also unclear how the timing of spring thaw will respond to climate change for varying forest types. Models can be a useful tool to answer these questions but there are some known modelling limitations particularly for simulating soil thermal regime and spring evapotranspiration in boreal forests.

1.3 STUDY OBJECTIVES

The overall objective of this study is to explore the present and future variability of spring thaw for contrasting forest types. This is achieved through the following specific objectives:

1. Characterize the variability of spring thaw for different forest-cover type (aspen, jack pine, and black spruce) under recent climate conditions and identify critical factors causing inter-site variability.
2. Conduct a diagnostic evaluation of three modelling platforms (CLASS, CRHM, and SHAW) for simulating winter-spring processes (snow accumulation, snowmelt, soil thaw timing, and spring evapotranspiration) and select an appropriate model for further testing, application and improvement.
3. Improve simulations of the selected model for spring thaw and evapotranspiration through better parametrization or improving algorithms of relevant processes.
4. Assess the impact of climate change on spring thaw for contrasting forest-cover types in the southern boreal forest using improved/parametrized model with future climate projections.

1.4 THESIS FRAMEWORK

This dissertation follows a traditional structure: chapter 1 provides background information along with stating research objectives, chapter 2 provides an overview of the relevant literature, chapter 3 describes adopted methodology to address research questions, chapter 4 through 7 present results and discussions corresponding to specific objectives 1 to 4, and chapter 8 summarizes research findings along with providing recommendations for future work. A more detailed outline of each chapter is given below.

A general overview of boreal forest such as its geographical location, climate, vegetation, and soils is provided in chapter 2 along with relevant literature for critical processes related to soil thaw, land surface models and their applications in boreal forests, and usage of climate change forcing data for impact studies. Much of the specific literature review is presented throughout this thesis in different chapters where deemed appropriate. Chapter 3 provides a description of the study sites, field instrumentation, available observations, adopted methodology and analysis techniques to

address each study objective. Chapter 4 (Objective 1) quantifies the differences in thaw timing between the two coniferous (jack pine and black spruce) and one deciduous (aspen) forest sites and identifies controlling factors for inter-site variability in thaw timing by using long-term (1997-98 to 2014-15) hydrometeorological observations. The relationship between spring thaw and carbon uptake was also explored. Chapter 5 (Objective 2) compares the performance of three models: Canadian Land Surface Scheme (CLASS); Cold Regions Hydrological Model (CRHM); and Simultaneous Heat and Water model (SHAW) for simulating various winter-spring processes including snow accumulation, snow ablation, soil thaw, and spring evapotranspiration at a coniferous forest (jack pine) site. Based on the results of this diagnostic model evaluation, particularly for soil thaw, the SHAW model was adopted for modelling spring thaw timing at all three study sites. Chapter 6 (Objective 3) presents the SHAW model application for simulating soil thaw timing and spring evapotranspiration for contrasting forest-cover types. The influence of ground cover on soil temperatures and thaw timing was explored. In addition, a simple formulation to incorporate thermal time approach in Jarvis-Stewart resistance scheme for predicting the recovery and development of stomatal functioning was tested to improve the model simulations for spring evapotranspiration. Chapter 7 (Objective 4) then combines the SHAW model with future climate forcing to assess the impact of climate change on spring thaw in the southern boreal forest. Chapter 8 summarizes the key study findings and provides recommendations for future work.

CHAPTER 2 REVIEW OF LITERATURE

2.1 BOREAL FORESTS

2.1.1 Geographical Distribution

The boreal zone is a broad circumpolar vegetation zone at high northern latitudes which is dominated by forests but also consists of other woodland, naturally treeless areas including alpine areas on mountains, heathlands, wetlands, lakes, rivers, and some grassland in drier areas (Brandt, 2009). This is one of the world's largest biomes covering about 11% of the earth terrestrial surface (Boonstra et al., 2016). The extent of the boreal region is mainly contained within Russia (60%) and Canada (29%) as presented in Figure 2.1 but the presence is extended to several other countries including the United States of America (4%), Finland, Sweden, Norway, Iceland, and Mongolia (Brandt et al., 2013).

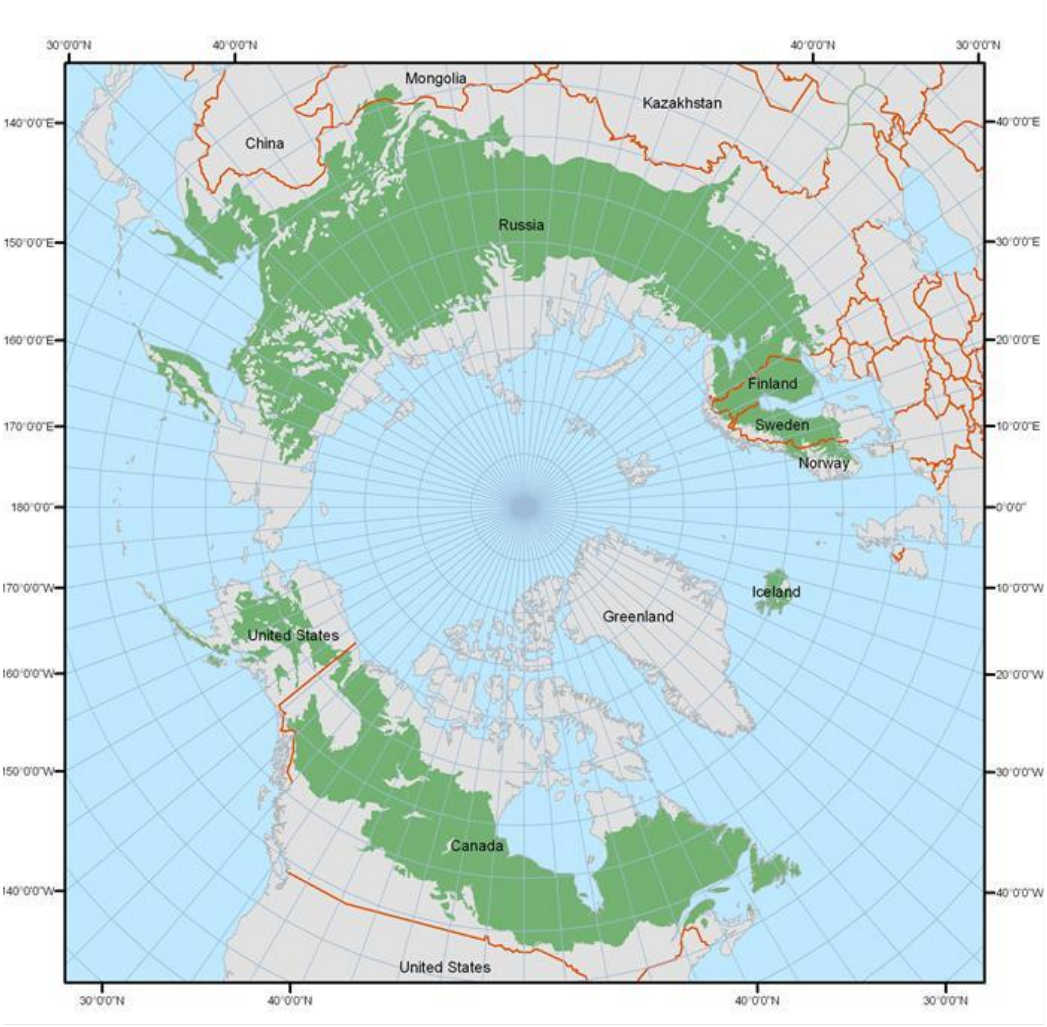

Figure 2.1 Worldwide distribution of the boreal forest (shown in green). Note: This map is the property of the Regional Aquatics Monitoring Program (RAMP) and is reproduced under the license and permission by RAMP (www.ramp-alberta.org).

The boreal zone in Canada stretches across the country from the Yukon territory to Newfoundland and Labrador (Figure 2.2) covering an area of about 552 million ha. The boreal region is 49% forest, 7% other wooded land, 13% open water (lakes, rivers, streams) while the remaining 31% is wetlands and naturally treeless areas (Brandt et al., 2013). The boreal forest is the largest ecosystem of Canada, occupying about 75% of forested land and 35% of total land area of the country (RAMP, 2019). The health of the boreal zone is of paramount importance because of its significant ecosystem services, including the wood industry, recreation services, regional climatic

controls, natural water purification systems, hydro-power generation, cultural and spiritual value, and wildlife habitat.

Figure 2.2 Distribution of boreal zone in Canada (Source: NRCan, 2019)

2.1.2 Classification of Vegetation and Climate

The dominant tree species of the boreal zone are within genera *Picea* (Spruce), *Pinus* (Pine), *Abies* (Fir), *Larix* (Larch), *Betula* (Birch) and *Populus* (Poplar) (Brandt et al., 2013). In Canada, tree species within the genera *Picea* are the most prevalent and comprises about 65% of the forest area (National-Forest-Inventory, 2013). The boreal zone corresponds to subarctic and cold continental climate in the Koeppen's climate classification system (SLW, 1996) which displays large seasonal variability and can be characterized by cool short summers with increased photoperiod (long days) and cold long winters with reduced photoperiod. The precipitation occurs in the form of snow in winter and rain in summer with an annual average of 300 mm to 850 mm (ISC-Audubon, 2013). Snowpack covers the ground for about 5 months in the southern portion of the region and for about 7 to 8 months in northern latitudes (Juday, 2020). Evapotranspiration during the short summer is

generally lower than rainfall resulting in a moist climate (Eugster et al., 2000). The boreal zone experiences cold, below freezing, temperatures for more than 6 months in winter. The mean annual temperature generally ranges from -5°C to 5°C (Marietta, 2013) but can be as low as -10°C in some parts such as in eastern Siberia (Jakutsk, 2020). The winter temperature ranges from -54°C to -1°C whereas air temperature in summer can get as high as 21°C to 30°C (ISC-Audubon, 2013). The length of growing season is generally short in boreal forests because of the long cold winters and short summers. It varies from 2.5 to 4 months for boreal forests in Canada with an overall average of 130 days (UCMP, 2020).

2.1.3 Forest Floor and Soils

Forest stands exert important controls on light transmittance and nutrient cycling, and this influences growth of understory vegetation or forest floor (Légaré et al., 2001). Lichens and mosses are common in coniferous forests whereas herbs and berries grow in deciduous forests or in forest clearings (National Geographic, 2020). The roots of these organisms are very shallow, and they can grow in limited light. Field observations suggest that the surface temperature can vary amongst different forest floor vegetation (Stoy et al., 2012) because of differences in albedo, water holding capacity (Liljedahl et al., 2011), thermal conductivity, specific heat, and evaporative cooling among species (Nichols and Brown, 1980).

Forest soils are typically comprised of layered organic and mineral horizons. The organic soils are broadly classified into three categories based on level of decomposition of organic matter: fibric (early stage), mesic (moderate level of decomposition), and humic (highly decomposed organic matter). Hydraulic conductivity of these layers can vary by several orders of magnitude (Dettmann et al., 2014). Soil bulk density and porosity (Saxton et al., 1986; Wagner et al., 1999), water retention characteristics (Rawls et al., 1982), and hydraulic conductivity (Western et al., 2002) are important soil physical properties for modulating the water content. Thus, soil moisture content, which is a critical variable for heat transport processes (Hayashi et al., 2007) because of its large influence on the heat capacity and thermal conductivity, can vary significantly for different peat types. Letts et al. (2000) summarized some hydraulic properties of organic soils based on an extensive review of literature (Table 2.1). In addition to soil texture, soil water content in boreal

forests is influenced by canopy density because of its control on intercepted precipitation, and vegetation water use through transpiration (Elliott et al., 1998).

Table 2.1 Hydraulic properties of different organic soils in boreal forests

Type of Organic Soil	Saturated hydraulic conductivity (m/s)	Residual Water Content (cm^3/cm^3)	Saturated Water Content (cm^3/cm^3)
Fibric Peat	$3x10^{-7}$ to $1x10^{-3}$	0.04	0.90-0.93
Hemic (Mesic) Peat	$1x10^{-9}$ to $2x10^{-4}$	0.15	0.88-0.95
Sapric (Humic) Peat	$1x10^{-12}$ to $3x10^{-6}$	0.22	0.83-0.85

The Luvisol (B horizon enriched with illuvial clay) and Brunisol (poorly developed or immature soil) are the common mineral soil orders of boreal forests in Western Canada whereas Organic and Podzolic (well-developed A and B horizon and primarily found on sandy deposits in ecozones where mean annual precipitation is above 700-mm) soil orders are present on the east side of the country (Canadian Society of Soil Science, 2020). The organic and mineral soil layers have markedly different hydraulic and thermal properties. Thermal conductivity and specific heat of soil are the most important parameters for defining soil thermal regime (Putkonen, 1998). These thermal parameters of soils vary significantly based on the minerology and fractions of ice, water and air (Table 2.2).

Table 2.2 Typical values of density and thermal properties of soil constituents

Property	Mineral Soil	Organic Soil	Water	Ice	Air
Density (kg/m^3)	1370 to 1450	91 to 156	1000	917	1.2
Particle Density (kg/m^3)	2650	1300	-	-	-
Specific Heat (J/kg C)	733	1926	4182	2030	1005
Thermal Conductivity (W/m K)[(a)]	2.9-8.8	0.25	0.57	2.2	0.024

(a) Thermal conductivity values are based on 10°C temperature for mineral soil, organic matter, and water whereas 0°C for ice (Hillel, 1998).

2.2 SOIL THAW

2.2.1 Description of Soil Freeze/Thaw Processes

In seasonally frozen soils, the liquid water content starts freezing when soil temperature declines to 0°C in the fall. This process starts from the ground surface and advances downwards. Although the freezing point of pure water is 0°C, it is always below 0°C for soils because of their particle surface free energy and presence of chemical substances (Ming et al., 2020). An almost linear increase in freezing point with increasing soil water content has been observed (Kozlowski, 2009) whereas the freezing point decreases with increasing soil salt content (Grechishchev et al., 2001). The freezing process is reversed in spring and soil ice content melts starting from the surface. Both (freeze and thaw) processes co-exist in freezing or thawing soils. The boundary between the frozen and unfrozen soils is referred as the freezing front or thawing front depending upon the soil state. A typical description of the freeze-thaw front is presented in Figure 2.3. Soil water can migrate from the deeper unfrozen soil layers towards the freezing front due to gradients in matric potential and temperature, increasing total water content in frozen soils (Zheng et al., 2020). Seasonal changes in soil freeze/thaw stages strongly influence vegetation growth, organic matter decomposition (Xie et al., 2017), and exchanges of energy, water and greenhouse gases between the land and atmosphere.

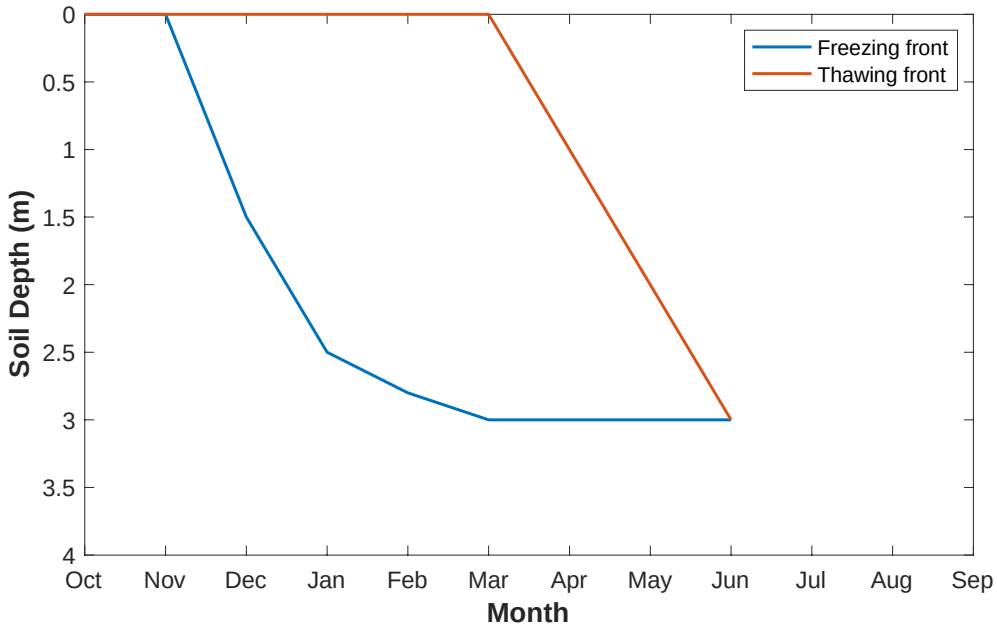

Figure 2.3 Representation of freeze-thaw fronts for seasonally frozen soils. Adapted from (Xie et al., 2017)

2.2.2 Definition of Soil Thaw based on Soil Temperature

Soil thaw lacks a universal definition and has been defined in the literature in different ways based on observed or simulated soil temperatures. For example, Sinha and Cherkauer (2008) defined soil thaw by using a criterion of at least one daily minimum and two daily maximum soil temperature to be greater than 0°C for two consecutive days. Kreyling and Henry (2011) used a positive mean daily soil temperature for two consecutive days as a threshold for reflecting soil thawed state. A simple 0°C threshold has also been used (Peng et al., 2016) for frozen (below 0°C) and thawed soils (above 0°C). Threshold temperatures other than 0°C have also been adopted such as -1°C for frozen soils (Ho and Gough, 2006) and 1-2°C for the thawed soil state (Drake et al., 2015). The timing for completion of soil thaw and number of freeze-thaw cycles may vary based on the selected threshold/criteria. Completion of soil thaw can be more reliably predicted with higher temperature thresholds as soil temperature typically rises sharply after reaching 1°C. The biogeochemical processes rather than soil temperature measurements can also be used to determine soil freeze-thaw state. For example, Bartsch et al. (2007) described an approach of using carbon

fluxes and xylem sap flow data to determine thaw timing and freeze-thaw cycles. However, the scope of this study is limited to using soil temperature data for defining soil thaw timing.

2.2.3 Heat Transport Processes Variably Frozen in Soils

The temperature state equation for a given soil layer can be written as (Flerchinger, 2000):

$$\boldsymbol{C_s \frac{\partial T}{\partial t} - \rho_i \lambda_f \frac{\partial \theta_i}{\partial t} = \frac{\partial}{\partial z}\left[k_s \frac{\partial T}{\partial z}\right] - \rho_l C_l \frac{\partial q_l T}{\partial z} - L_v \left(\frac{\partial q_v}{\partial z} + \frac{\partial \rho_v}{\partial t}\right)} \qquad \textbf{Equation 2.1}$$

where the terms, from left to right, represent change in internal energy, latent heat required to freeze water, net thermal conduction into the layer, net thermal advection into the layer due to water flux, and net latent heat vaporization within the soil layer, respectively. The symbology used in the equation is defined as: C=Volumetric heat capacity (J kg^{-1} °C^{-1}), T=Temperature (°C), t=time, ρ=density (kg m^{-3}), λ_f = latent heat of fusion, θ=volumetric content (m^3 m^{-3}), k=thermal conductivity (W m^{-1} °C^{-1}), z=depth, L=latent heat where subscripts s, i, l, v represent soil, ice, liquid, and water vapor.

Heat transfer in soils is primarily driven by conduction. Soil heat conduction is largely dependent on soil water content (Hayashi et al., 2007) and net energy available at the soil surface (Roulet and Woo, 1986).

2.2.4 Water Transport Processes in Soils

The soil water content is important for soil thaw because of its strong influence on specific heat capacity and thermal conducitivity of soils (Hayashi et al., 2007; Hillel, 1998). In addition to water infiltration from the surface, soil water content is controlled by several sub-surface water transport processes. The soil water flux equation for partially frozen soils is written as (Flerchinger, 2000):

$$\boldsymbol{\frac{\partial \theta_l}{\partial t} + \frac{\rho_i}{\rho_l}\frac{\partial \theta_i}{\partial t} = \frac{\partial}{\partial z}\left[K\left(\frac{\partial \varphi}{\partial z} + 1\right)\right] + \frac{1}{\rho_l}\frac{\partial q_v}{\partial z} + U} \qquad \textbf{Equation 2.2}$$

where the terms, from left to right, represent change in volumetric liquid water content, change in volumetric ice content, net liquid flux into a layer based on unsaturated hydraulic conductivity K

(m/s), net vapor flux into a layer because of water potetnail or temperature gradient, and a source/sink term U.

2.3 MODELLING APPLICATION IN BOREAL FORESTS

2.3.1 Land Surface Schemes

Land-atmosphere exchanges of energy, water, and carbon influence climate, watershed hydrology, and vegetation dynamics. Within climate models, the complex interactions between the land and the atmosphere are represented by land surface models (LSMs). A land surface scheme is a one-dimensional computational model that describes biophysical, geochemical, hydrological, and thermal processes in the soil-plant-atmosphere continuum. Land surface models were initially incorporated into atmospheric models in the mid-1980s for treating water and energy balances on the land surface (Pitman, 2003). However, their capabilities have now been enhanced to predict carbon balances, changes in vegetation (biomass, leaf area index), and soil organic matter. These models typically combine a physical sub-model that considers hydrological processes and heat and energy exchanges, and a plant physiology sub-model that considers biological and biogeochemical processes such as photosynthesis, respiration, phenology, and decomposition of soil organic matter (Sato et al., 2015). The model structure, degree of complexity, process representation, and spatial-temporal resolution varies among land surface schemes based on their development purpose. Thus, the performance of the models for predicting a given process is subject to variability.

2.3.2 Application of Land Surface Models in Boreal Forests

Land surface models have been applied in boreal forests for modelling various processes. For example, Wang et al. (2001) simulated plant, soil and ecosystem CO_2 exchanges using Canadian Land Surface Scheme (CLASS) for a deciduous (aspen) and a coniferous (black spruce) forest located in western Canada. Slevin et al. (2015) applied JULES (the joint UK land environment simulator) model for predicting gross primary productivity in boreal as well as temperate, and tropical ecosystems. Kuchment and Demidov (2006) and Bonan et al. (1997) modelled latent heat fluxes from coniferous forests in Canada using a coupled model of the hydrological & carbon cycles and National Center for Atmospheric Research Land Surface Model (NCAR LSM1),

respectively. The community NOAH land surface model has been used to predict snow depth and snow water equivalent in North America over mid-latitude regions (Yang et al., 2011). The Forest Hydrology Model (ForHyM) has also been applied in boreal forests for simulating snowpack, soil temperature and soil moisture for different forest types (Balland et al., 2006).

2.3.3 Application of CLASS, CRHM and SHAW Models

In this study, modelling of soil temperatures and soil thaw timing in the southern boreal forest was of primary interest. The Simultaneous Heat and Water (SHAW) model was developed for predicting freeze-thaw by considering detailed energy and water transport processes in soils and has been successfully applied in various landscapes but with limited applications in boreal forests (Section 2.3.3.3). It was a rational choice to use the SHAW model for simulating freeze-thaw; however, the model does not consider unloading of intercepted precipitation by the canopy which may lead to erroneous estimates of snow accumulation and ablation processes influencing soil temperature/thaw simulations in boreal forests. To evaluate this deficiency of the SHAW model, two regionaly appropriate models (CRHM and CLASS) were considered. The Cold Regions Hydrological Model (CRHM) was considered because of its various successful applications in modelling snow processes (Section 0). Because the CRHM model had simplified representation of freeze/thaw processes, the Canadian Land Surface Scheme (CLASS) with moderate representation of both snow processes as well as soil heat and water transport processes was also considered. All three models were used to simulate winter-spring processes such as snow accumulation and melt, soil thaw and spring evapotranspiration at the jack pine forest site (Objective 2). A detailed description of the process representation and modelling algorithms used in this study is provided in Section 3.5. The examples of application of these models particularly in the boreal forests or for modelling processes relevant to this study are provided below.

2.3.3.1 Cold Regions Hydrological Model (CRHM)

The Cold Regions Hydrological Model (CRHM) model was developed for modeling hydrological cycle in cold regions for small to medium basins by incorporating several critical winter processes such as snow interception, sublimation, snow redistribution, snowmelt, and infiltration into frozen soils in addition to typical hydrological processes (Pomeroy et al., 2007). The model has been

applied to simulate snow accumulation and snowmelt for needleleaf forests across varying geographical locations (Canada, Switzerland, and United States of America), climate, forest species, and forest cover densities (Ellis et al., 2010). Across sites, model simulations have generally been shown to be in agreement with observations for predicting the quantity and timing of snow accumulation and melt. The CRHM has also been applied in boreal zone to simulate snow hydrology, stream flows, evapotranspiration, and freeze/thaw processes (Krogh et al., 2017; Krogh and Pomeroy, 2019; Pomeroy et al., 2012). The model performance for simulating spring ET in boreal forests is yet to be evaluated.

2.3.3.2 Canadian Land Surface Scheme (CLASS)

The Canadian Land Surface Scheme (CLASS) is a physically based parametrization scheme developed for providing surface feedback to the atmospheric/climate models based on heat and water exchange between the land and atmosphere (Verseghy, 1991). The model was specifically designed to represent the effects of vegetation, snow, and soil properties on these exchanges. The model performance for simulating snow accumulation in the boreal forest has been significantly improved over time through an improved representation of snow processes such as precipitation phase partitioning, snow density variation with temperature, the correlation between maximum snow density and depth, snow interception by the canopy and its unloading (Bartlett et al., 2006). Soil temperature simulations have also been improved by incorporating organic soils in the model (Letts et al., 2000). The root mean square error for daily latent heat flux was 50 W m^{-2} at old jack pine and 48 W m^{-2} at old black spruce site, both located in Manitoba, which was reduced to 15 W m^{-2} and 13 W m^{-2}, respectively by considering the influence of environmental variables such as solar radiation, vapour pressure deficit, and soil moisture stress on stomatal conductance (Bartlett et al., 2003).

2.3.3.3 Simultaneous Heat and Water Model (SHAW)

The Simultaneous Heat and Water (SHAW) model is a point scale, one dimensional (vertical), finite-difference model primarily developed for simulating freeze-thaw processes in agricultural soils (Flerchinger and Saxton, 1989). The SHAW model has been successfully applied for modelling soil hydro-thermal characteristics and free-thaw processes in varying landscapes

including boreal forests (Hejazi and Woodbury, 2011), rangeland (Flerchinger and Hanson, 1989), agricultural soils (Hayhoe, 1994), and sub-arctic peatlands (Mohammed et al., 2017). The model has also performed well in simulating snow accumulation and snowmelt for varying sites (Flerchinger et al., 1996, 1994). Simulations of evapotranspiration from a faber fir forest ecosystem in the eastern Tibetan Plateau of China were in agreement with observations (Yin et al., 2010) but the model has not been specifically evaluated for evapotranspiration from boreal forests.

2.4 FORCING DATA FOR CLIMATE CHANGE IMPACT STUDIES

2.4.1 Emission Scenarios and Climate Change Projections

Greenhouse gases in the atmosphere such as water vapor, carbon dioxide, methane, nitrous oxides, and chlorofluorocarbons absorb and re-radiate thermal energy from the earth surface. Thus, increased concentration of these gases in the atmosphere contributes to global warming. Emission scenarios for greenhouse gases describe the potential pathways for their evolution in the atmosphere as a result of human activities over time. The Intergovernmental Panel on Climate Change (IPCC) adopted two alternate approaches for defining emission scenarios. First is the storyline approach in which potential changes in relevant variables such as world population, socio-economic conditions, technological advancements, land use change, and use of energy resources are articulated by the end of the 21st century (Nebojsa Nakicenovic and Swart, 2000). The impact of these changes on greenhouse gas emissions was then estimated. Second, the most recent approach, is the reverse of the storyline approach in which different endpoint values for radiative forcing (2.6, 4.5, 6.0, and 8.5 W m^{-2}) were defined by the year 2100 and associated factors were then assessed (Stocker et al., 2013). This is known as representative concentration pathways (RCP) emission scenarios. Coupled atmospheric-ocean global climate models (AOGCMs), also referred to as General Circulation Models (GCMs), represent physical processes in the atmosphere, ocean, cryosphere, and land surface, are commonly used to simulate global climate change projections for different emission scenarios. The simulations of GCM for atmospheric variables tend to have spatial-temporal biases which vary in magnitude for different models because of varying assumptions, physical parametrization, numerical solutions, boundary conditions and spatial-temporal resolutions.

2.4.2 Downscaling of Climate Data

The output of AOGCMs cannot be used at regional scales because of the coarse spatial resolution of these models as regional climate is often affected by forcing and circulations that occur at fine scales (Mearns et al., 2003). Therefore, downscaling of AOGCMs is required for regional climate change impact assessment studies which can be carried out by using either dynamical or statistical methods. In the dynamical downscaling approach, regional circulations models (RCMs) that require additional input data or parametrization are used to capture physical processes at desired spatial resolutions; whereas in a statistical downscaling approach, relationships are established between large-scale climate features that are produced by GCMs and local climate characteristics (Trzaska and Schnarr, 2014). Dynamical downscaling methods are based on physically consistent processes, however, they are computationally intensive and generally represent limited emission scenarios. Statistical downscaling methods are computationally efficient and can provide point-scale climate variables from GCMs output but require long and reliable historical data and they don't consider climate feedbacks. Fowler et al. (2007) conducted a thorough review on downscaling methods and concluded that the dynamical downscaling methods provide "added value" in climate change impact studies. However, bias-correction needs to be carried out on the output simulations prior to their use in impact studies (Kleinn et al., 2005).

CHAPTER 3 MATERIAL AND METHODS

3.1 DESCRIPTION OF STUDY SITES

This study considers three long-term CO_2 and energy flux observation sites: two within coniferous forests (jack pine [*Pinus Banksiana*] and black spruce [*Picea Mariana*]) and one in a deciduous (trembling aspen [*Populus tremuloides* Michx.]) forest, all located in central Saskatchewan, Canada (Figure 3.1). All three study sites (old jack pine, old black spruce, and old aspen) were initiated through the Boreal Ecosystem and Atmosphere Study (BOREAS) program during 1994-96 (http://boreas.gsfc.nasa.gov/) and were continued after 1996 under the Boreal Ecosystem Research and Monitoring Sites (BERMS) program. The aspen site is located at the south end of Prince Albert National Park (53.629°N, 106.198°W) about 50 km north west of the city of Prince Albert. The black spruce (53.987°N, 105.117°W) and jack pine (53.916°N, 104.692°W) sites are about 80 km and 105 km north east of the aspen site, respectively. All three sites were naturally established after forest fires: in 1919 for aspen, 1914 for jack pine and approximately 1879 for black spruce (Barr et al., 2012). The aspen site is located in the boreal transition ecoregion, which is characterized by a mix of forest and farmland; dominated by tall trembling aspen and balsam poplar with a thick understory of mixed herbs and tall shrubs. The specific study site was located in a homogeneous region of aspen trees. The coniferous forest sites are located in the mid-boreal upland ecoregion which consists of mixed coniferous and deciduous forests. Medium to tall trembling aspen, balsam poplar, white and black spruce, and balsam fir are the abundant species in this ecoregion; however, jack pine stands dominate areas of dry sandy soils. The soil remains frozen and covered with snow in winter. Spring snowmelt generally begins in late March to early April. Mean annual air temperature varies from 0 to 2°C while precipitation varies from 400 to 600 mm. The topography is generally flat at the site level and gently rolling in the region.

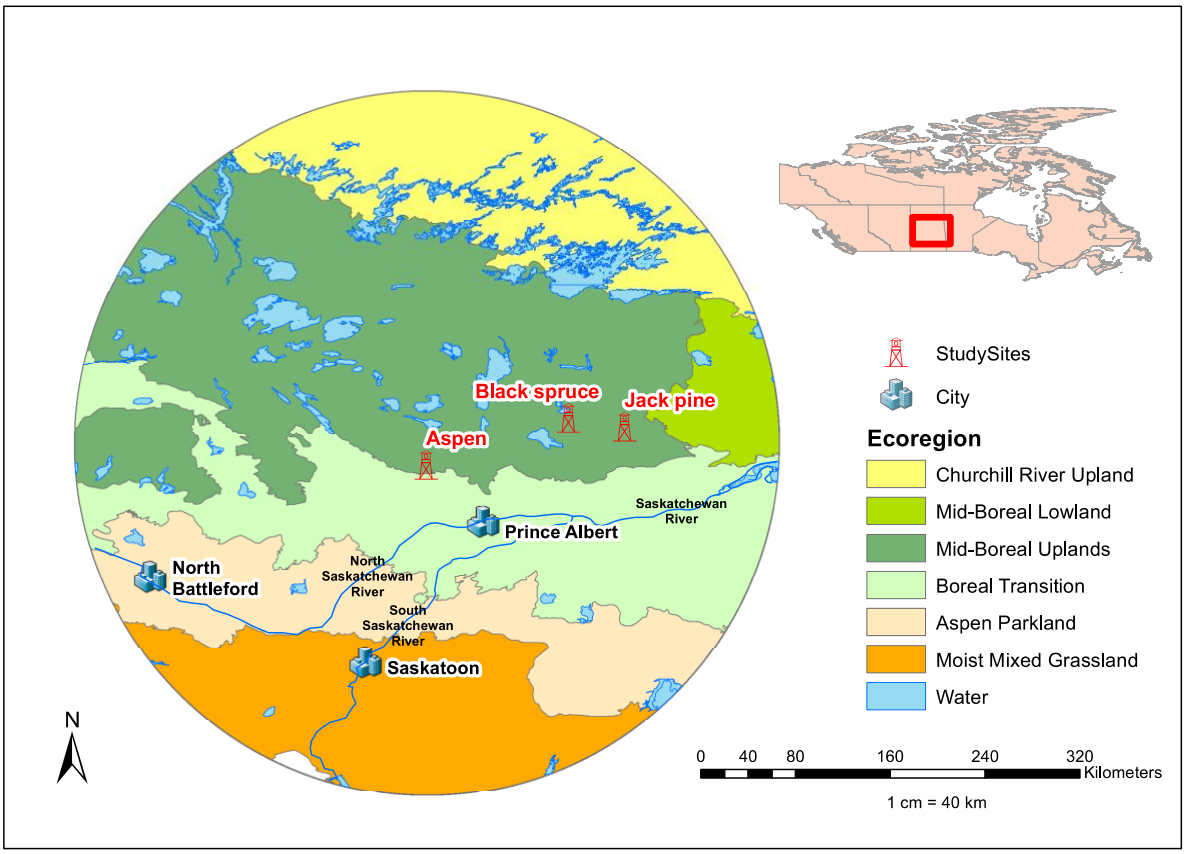

Figure 3.1 Geographical location of the study sites

The canopy architecture, forest floor characteristics and soil properties are distinctive among the study sites. Some major inter-site differences and seasonal variations are shown in Figure 3.2. The tall (21 m average height) aspen forest transitions from a dense canopy in summer (combined leaf area index of 4.4 m^2 m^{-2} for aspen and hazelnut canopies) to a leafless canopy in the fall (Barr et al., 2004). The two coniferous forests are similar in average height (14-15 m) but have considerably different canopy densities; the leaf area index was 2.6 m^2 m^{-2} for jack pine and 3.8 m^2 m^{-2} for black spruce (Chen et al., 2006). The contrasts among sites extend to understory vegetation and soil properties. The understory vegetation at the trembling aspen forest consists of 2 m tall hazelnut (*Corylus cornuta*), compared with a thin layer of lichen (*Cladina mitis*) at the jack pine site and a thick feather moss (*Ptilium Crista-Castrensis*) layer at the black spruce site. The organic soil layer is shallow (2-3 cm thickness) at the jack pine site, extends to 8-10 cm at the aspen site, and is up to 30 cm thick at the black spruce site. The mineral soil below the organic layer at jack pine is very

well drained and sandy in texture, whereas loam to sandy clay loam soil texture dominates at the aspen site with moderate water holding capacity. The soil texture at the black spruce site is sandy loam with a shallow water table depth. More details about the study sites can be found in Balland et al. (2006) and Gower et al. (1997).

Aspen (summer)

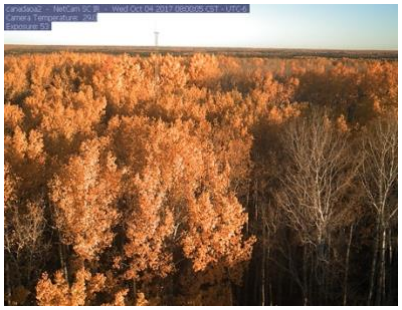

Aspen (fall)

Aspen (winter/Spring)

Jack pine (summer)

Jack pine (winter, below canopy)

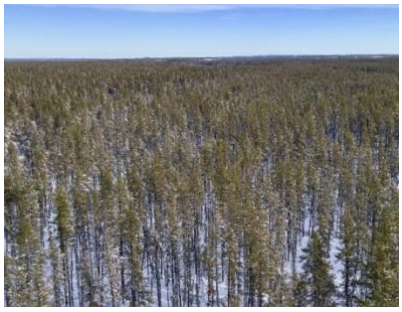

Jack pine (Spring, above canopy)

Black spruce (summer)

Black spruce (winter)

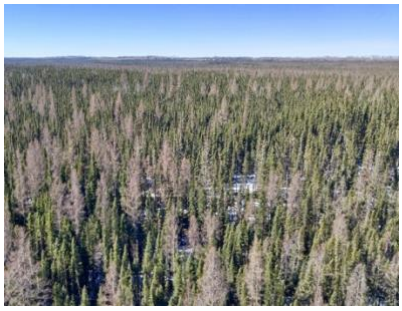

Black spruce (spring)

Figure 3.2 Inter-site seasonal variability among study sites (Photo credit: Bruce Johnson except aspen fall season photo which was downloaded from PhenoCam (https://phenocam.sr.unh.edu/webcam/)

3.2 INSTRUMENTATION AND OBSERVATIONS

All three study sites were equipped with a walk-up scaffold tower (Figure 3.3) fitted with sensors to measure air temperature, relative humidity, wind speed and direction, above canopy shortwave and longwave radiation components, as well as the turbulent fluxes of energy, carbon and water vapour. Other onsite measurements included precipitation, snow depth, snow density, snow temperature, soil temperature, and soil water content profiles. The details about the relevant measurement sensors and observations are provided below.

Jack Pine Aspen

Figure 3.3 Photograph of flux towers installed at jack pine and aspen sites

3.2.1 Precipitation

Precipitation was recorded at a 30-minute interval from 1998 to present by a tipping bucket and weighing gauges. The original precipitation weighing gauge was a Belfort-3000 (Belfort Instruments, Baltimore, MD) at all sites which was replaced by Geonor-T200B (Geonor, Branchville, NJ) in 2010 and 2011 at jack pine and black spruce sites, respectively. The weighing gauges were installed in small forest clearings to minimize canopy and wind effects. At the black spruce site, it was installed on the roof of the hut (about 5 m above the ground), and at the jack pine and aspen sites it was mounted on a stand about 3 m above the ground. The approach used for the precipitation data processing has been described by Pan et al. (2016). Manually-cleaned tipping bucket data, which was only valid for rain events, was used for gap filling and/or adjusting interval precipitation when the weighing gauge data was excessively noisy. Snow catch efficiency was calculated by Smith (2007) but wind effects were minor because of sheltered gauge locations. The distribution of total precipitation into rain and snow was calculated by the Harder and Pomeroy (2013) psychrometric energy balance method.

Figure 3.4 Geonor-T200B weighing gauge for measuring precipitation installed at the jack pine site

Figure 3.5 Tipping bucket rain gauge (TBRG) and Belfort weighing gauge installed at black spruce site for measuring precipitation

3.2.2 Snow Water Equivalent (SWE)

Snow accumulation on the ground was quantified by the measured snow water equivalent (SWE), which is the depth of water that would be produced by instantaneous melt of the snowpack. The SWE (mm) was calculated as $SWE = 10 * (d_s * \rho_s + CV)$ following Pomeroy and Gray (1995), where d_s is snow depth (cm), and ρ_s is snow density (g cm^{-3}) and CV is the covariance between depth and density (which was generally negligible at all sites). Snow surveys were conducted about 8-10 times a year. The snow depth and density were measured at 40 and 5 locations respectively, during each snow survey along a pre-established snow survey transect (Figure 3.6). The snow density was measured by using the recorded snow depth and weighing the snow collected in a snow sampling core of known area. A systematic bias in snow depth measurements at the black spruce site (due the spongy organic layer) was noted and removed (Appendix A).

Deciduous forest (Aspen)

Evergreen Coniferous forest (Jack Pine)

Evergreen Coniferous forest (Black Spruce)

Figure 3.6 Photographs show a portion of snow survey transect at the study sites (fluorescent tape was used to mark the survey transect)

3.2.3 Turbulent Fluxes

The closed-path eddy covariance technique has been widely used in flux tower networks because of its long term stability, low maintenance cost, and good accuracy (Mammarella et al., 2009). Above canopy turbulent fluxes of momentum, heat, CO_2, and H_2O were measured at all three sites using a closed-path eddy covariance (EC) system (Figure 3.7) which included CSAT (Campbell Scientific, Logan, UT) or Gill-R3 sonic anemometers (Gill Instruments Limited, Hampshire, UK) for measuring wind velocity components and a closed-path infrared gas analyzer, LI-7000 (LI-COR, Lincoln). The gas analyzer was replaced by a closed path LI-7200 model in 2012 at the jack pine site. The height above the ground surface for measuring flux densities was 39 m at the aspen site, 28 m at the jack pine site, and 25 m at the black spruce site. Surface fluxes were calculated as the sum of fluxes at the measuring height and change in storage in the underlying air. More details

about the EC system are given by Black et al. (1996). The measured fluxes were processed by using standard FLUXNET-Canada methods (Amiro et al., 2006; Barr et al., 2004).

The measured CO_2 fluxes or net ecosystem exchange (NEE) provided a direct measure of net ecosystem production (NEP) assuming negligible loss of carbon via groundwater flow i.e. NEP = -NEE. The relationship between net ecosystem production, gross ecosystem photosynthesis (GEP), and respiration (R) is defined by equation 3-1. The standard Fluxnet-Canada Research network method was adopted for gap filling of NEP and estimating GEP and R (Barr et al., 2004). The method uses two empirical relationships; one between respiration and soil temperature at shallow depths and the other between gross ecosystem photosynthesis and downwelling photosynthetically active radiation.

$$\boldsymbol{NEP = GEP - R} \qquad \textbf{Equation 3.1}$$

The surface flux data were compiled at a frequency of 30 minutes. The data from 1998 to 2015 were used in this study for analysis and modelling purposes.

Figure 3.7 Above canopy eddy covariance system installed at the jack pine site

3.2.4 Air Temperature, Relative Humidity and Wind Speed

The measurement height for air temperature, relative humidity and winde speed for all three sites is summarized in Table 3.1. A Campbell/Vaisala HMP35CF or HMP45CF Hygrothermometer (Vaisala, Helsinki, Finland) in a 12-plate Gill radiation shield was used to measure relative humidity and air temperature. The wind speed was measured by RM-Young 05103 (Figure 3.8). The data were compiled at 30-minute intervals; however, an hourly average was used in this study for modelling purposes.

Table 3.1 Measurement height (m) above the ground surface for measuring wind speed, relative humidity and air temperature at the study sites

Site	Wind Speed (m/s)	Air Temperature (°C) & Relative Humidity (%)
Aspen	38	37
Jack Pine	29	28
Black Spruce	26	25

Figure 3.8 Sensors for measuring wind speed and direction

3.2.5 Radiation

Instrumentation for measuring radiation varied between sites and years. Downwelling and upwelling shortwave radiation were measured by Kipp and Zonen CM11 pyranometer (Kipp&Zonen, Delft, The Netherlands) at the aspen and black spruce sites. The same sensor was also installed at the jack pine site but was later replaced by a Kipp and Zonen CMP11 in 2010. Downwelling and upwelling longwave radiation were measured by Eppley PIR (precision infrared radiometer) sensors at all three sites; however, these were replaced by Kipp and Zonen CGR4 Pyrgeometers in 2010 at the jack pine site. Net radiation was calculated from the shortwave and longwave components. A second measurement of net radiation was made using a Kipp and Zonen CNR1 net radiometer, consisting of thermopile pyranometer and CG3 pyrgeometer sensors, installed at the aspen site (31 m height) in 2003, at the jack pine site in 2010 and at the black spruce site (20 m height) in 2007. The data from the CNR1 were available to gap-fill primary radiation measurements when needed. Some radiation measuring instruments installed at the study sites are shown in Figure 3.9. The incoming and outgoing fluxes of photosynthetically active radiation (PAR) were measured above and below canopy by paired quantum systems-LI190SA (LI-COR, Lincoln, NE).

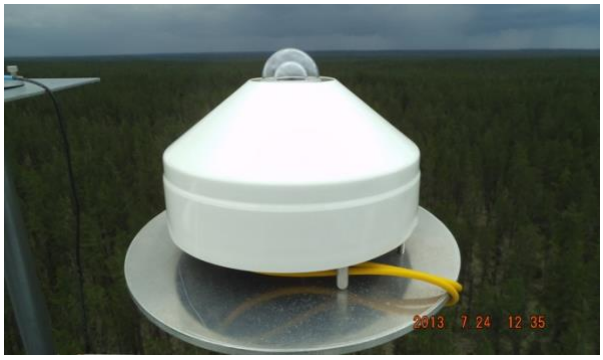

CMP11 pyranometer

CGR4 pyrgeometers

CNR1 boom (top view)

CNR1 (bottom view) along with downward looking pyranometer and pyrgeometer

Figure 3.9 Radiation measurement instruments installed at study sites.

3.2.6 Snow Temperature and Depth

Snow temperature was measured at various heights above the soil surface (1, 2, 5, 10, 20, 30, 40, and 50 cm) using a type-T thermocouple from 2001 onwards. Snow temperature probes (Figure 3.10) tend to bend over time resulting in an inconsistency of measuring depth. In order to address this issue and to increase measurement depth interval, the snow harp was designed and installed at the jack pine site in 2014 (Figure 3.11). A snow harp is rectangular in shape and consists of a frame that supports a graduated series of parallel strings on which thermocouples were mounted at 2, 5, 10, 15, 20, 25, 30, 35, 40, 45, 50, 55, and 60 cm depth. Time-series measurements of snow depth were recorded by an ultrasonic distance sensor (Campbell Scientific SR-50).

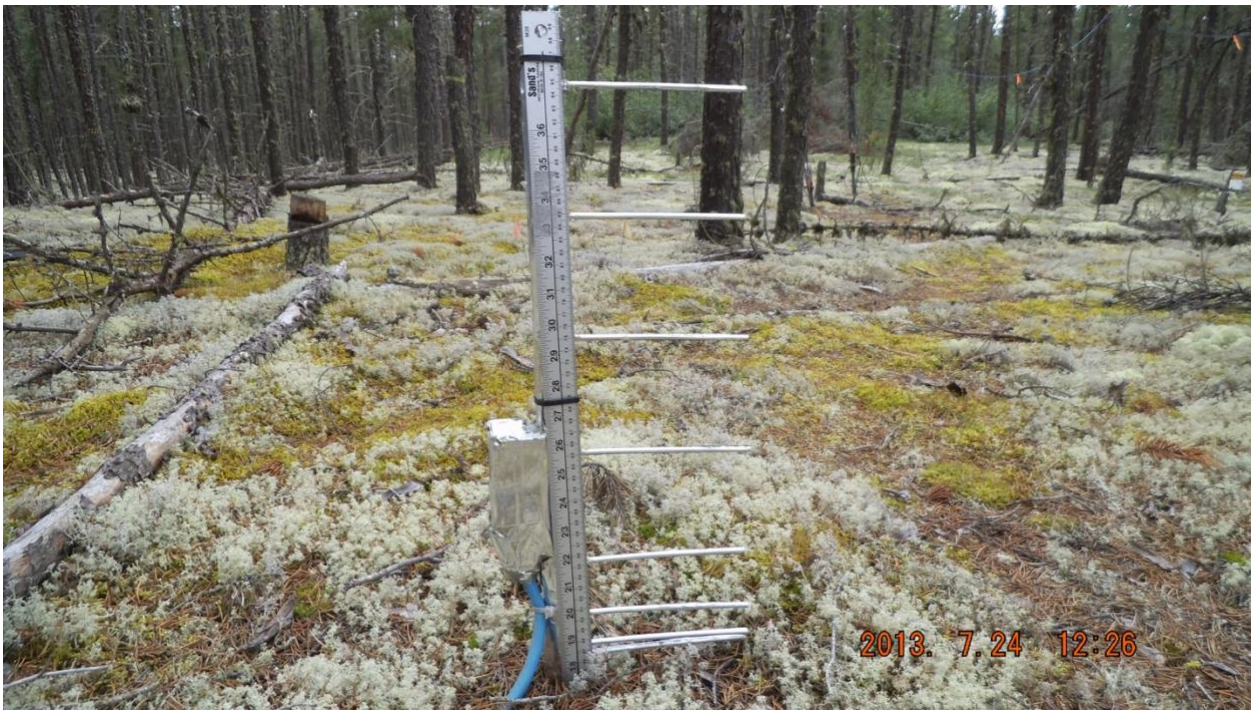

Figure 3.10 Snow temperature probes installed at site

Figure 3.11 Snow harp for measuring snow temperature at every 5 cm depth, and SR-50 for measuring snow depth installed at the jack pine site

3.2.7 Soil Temperature and Moisture

Soil temperature was measured by a type-T thermocouple in two profiles at 2, 5, 10, 20, 50, and 100 cm from the ground surface. The average of the two locations was considered to be the representative temperature for the site. The measurements were available at 30-minute intervals but the daily average was used in this study. Soil volumetric water content was measured by the Campbell Scientific water content reflectometers (CS615/616 or CS-TDR100) at 0-15, 15-30, 30-60, 60-90, 90-120 cm depth. More details about the installation of TDR probes have been provided by Barr et al. (2007).

3.2.8 Photographs

In addition to meteorological observations, photographs were taken during each field visit to capture seasonal changes in site conditions. Moreover, two cameras were installed at the jack pine site in 2014; one above canopy – network camera P1357E-5MP (Axis Communications, Lund) and one below canopy - Wingscapes TimelapseCam (Moultrie, Birmingham, AL) to take time series photos. These photographs were helpful in identifying seasonal changes particularly the development and ablation of the snowpack.

3.3 METHODOLOGY OVERVIEW

A brief description of the adopted approach for each study objective is provided in Figure 3.12. The general approach taken to address objective 1 was to use long-term datasets to explore the inter-site variability of spring thaw. The relative importance of canopy architecture, forest floor and soil properties upon the timing of soil thaw was investigated by comparing among sites the: (1) snow accumulation; (2) snow melt rates and ablation timing; and (3) the theoretical total energy required to thaw each soil profile. In addition, the influence of spring thaw timing on carbon uptake was explored using the observed CO_2 fluxes. For objective 2, the performance of Simultaneous Heat and Water (SHAW) model, Canadian Land Atmosphere Surface Scheme (CLASS), and Cold Regions Hydrological Model (CRHM) was evaluated against the observations for simulating winter-spring transition at the jack pine site. The selection of the jack pine site was based on availability of more reliable observations including above-canopy time-series photographs to better characterize snow ablation timing. For objective 3, an exhaustive parameter uncertainty and sensitivity analysis was first completed to identify key parameters/processes and deficiencies or improvement opportunities of SHAW for simulating evapotranspiration. A Growing Degree Days factor was proposed and tested to improve simulations of spring evapotranspiration by considering the influence of low soil temperatures on stomatal functioning. In addition, the influence of ground cover layer on the simulations of soil temperature/thaw was also explored. Finally, in order to understand climate change impacts on spring thaw for varying forest types (Objective 4), the improved and parametrized SHAW model was run with future climate projections. More specific details about the analysis for each study objective will be provided in the following sections.

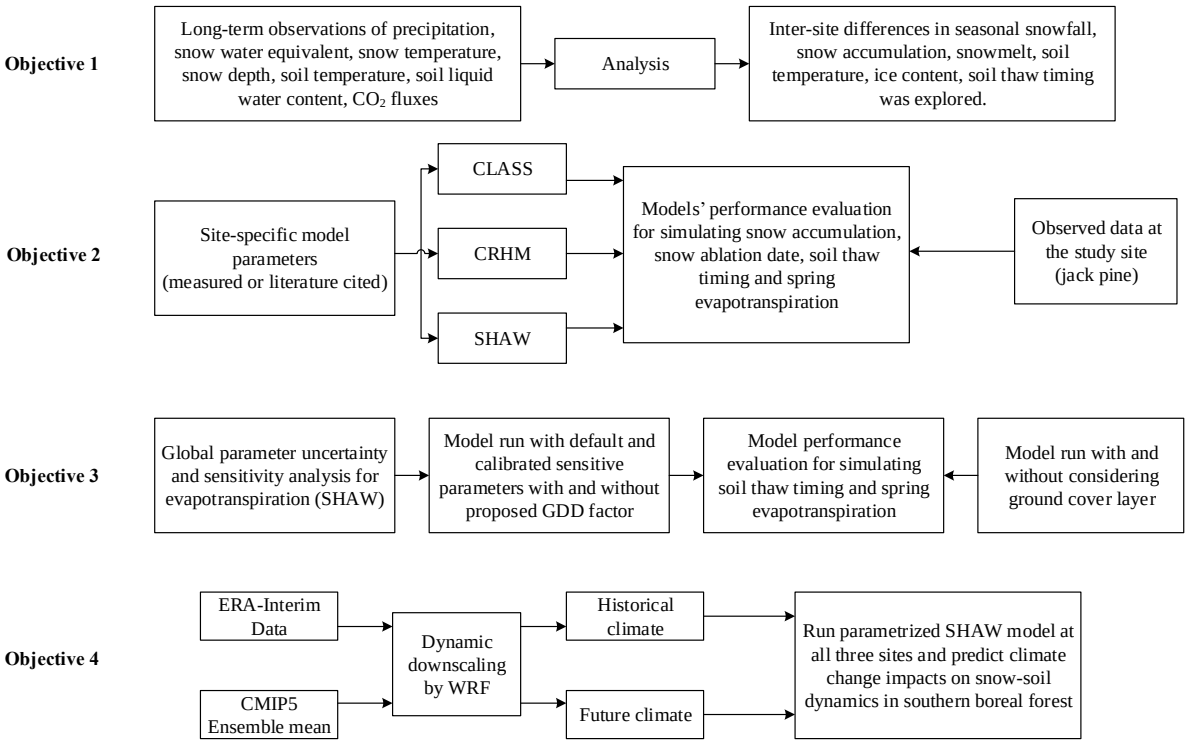

Figure 3.12 A brief overview of methodology for each study objective (All sites were used for objective 1, 3 and 4 and only jack pine site was used for objective 2)

3.4 OBSERVATIONAL ANALYSIS FOR SOIL THAW, ITS CONTROLLING FACTORS AND RELATIONSHIP WITH CARBON UPTAKE

Inter-site variability of spring thaw and its controlling factors were explored by analyzing long-term observations (Objective 1). This section provides definitions of soil thaw, snow accumulation, snow ablation, and onset of net positive carbon uptake based on observations at the study sites. In addition, method for calculating required energy for soil thaw is described.

3.4.1 Timing of Soil Thaw

Daily average soil temperatures were used to define the soil frozen or thawed state. Soil was considered to be frozen when its temperature was below -0.5°C for two consecutive days. The soil thaw start date was associated with the beginning of isothermal (0±0.5°C) conditions near the soil surface (2 cm depth) whereas the thaw end date was defined as the time when soil temperature first rises above 1°C. An example definition of soil thaw at 2 cm depth is presented in Figure 3.13.

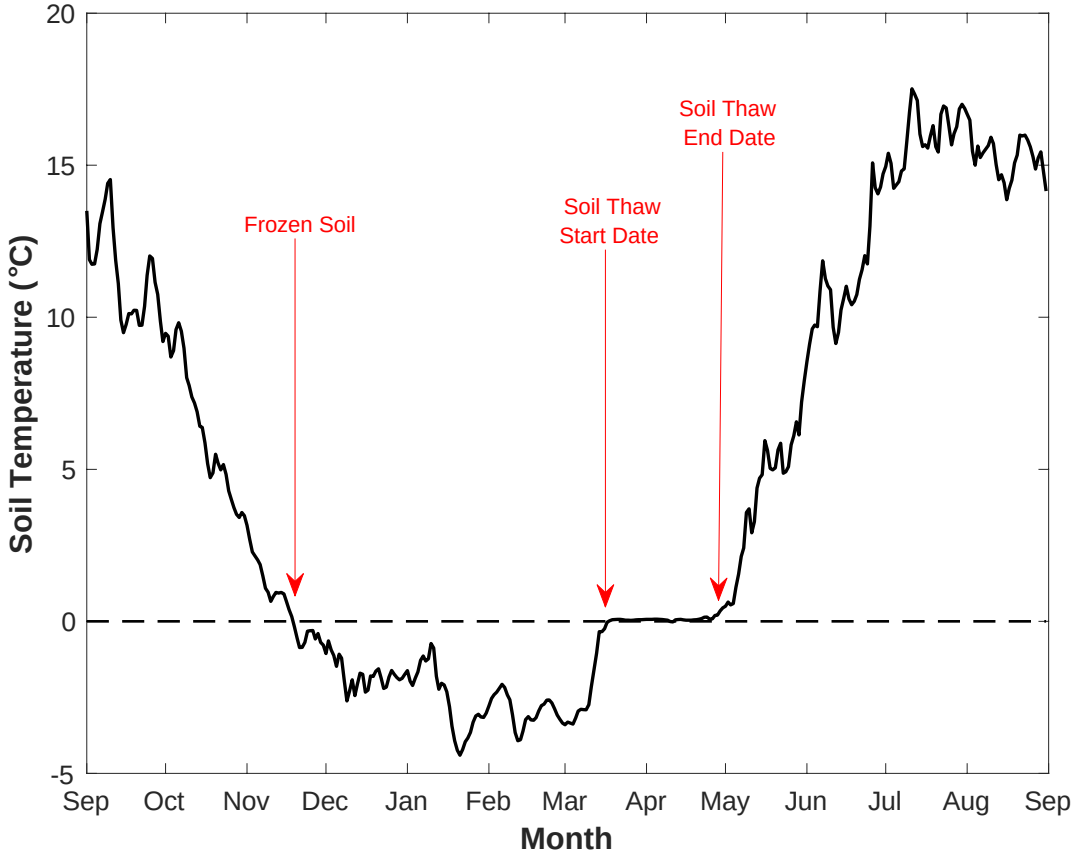

Figure 3.13 Example classification of soil thaw at jack pine site based on 2 cm soil temperature (2011-12)

3.4.2 Snow Accumulation and Ablation

Peak snow water equivalents measured by snow surveys (Section 3.2.2) in early-to-mid March were compared between the sites to quantify differences in seasonal snow accumulation. It was determined from the time-series observations of snow depth that these snow surveys captured the peak reasonably well for the analysis record presented in this study. The snowmelt start date was defined by the continuous snow temperature measurements based on 0°C isothermal snowpack conditions. The snow ablation date was determined from the near surface snow temperature sensor – by its rapid rise above 0°C coincident with the disappearance of snow. The snow ablation date was also determined by the change signal in broadband normalized difference vegetation index (NDVI) following Huemmrich et al. (1999) for the years when snow temperature measurements

were not available. Both estimates agreed well (± 1-2 days) for the years where overlapping data was available.

3.4.3 Estimation of Required Energy for Snowmelt and Soil Thaw

The total energy required for melting the snowpack is the sum of energy required for the warming and melting phases. Assuming heat capacity of the air to be negligible, the required energy for the warming phase of the snowpack was calculated based on the specific heat of ice (C_{pi} = 2100 J kg^{-1} K^{-1}), density of water (ρ_w = 1000 kg m^{-3}), snow water equivalent (SWE in m), and average snowpack temperature minus 0°C (T_s in °C) as:

$$\boldsymbol{Q_{snow\_warming} = -C_{pi}\,\rho_w\,SWE\,T_s} \qquad \textbf{Equation 3.2}$$

The energy required for the snowmelt phase was calculated as:

$$\boldsymbol{Q_{snowmelt} = (SWE - 0.03 d_s)\,\rho_w\,\lambda_f} \qquad \textbf{Equation 3.3}$$

where d_s is the snowpack depth, and λ_f is the latent heat of fusion (0.334 MJ kg^{-1}). The capillary water holding capacity was assumed to be 3% of volume of the snowpack (Würzer et al., 2016); thus, was removed from the total SWE. The amount of energy required to completely thaw the soil profile at each site was estimated from soil properties, temperature and water content. The total energy required for soil thaw was estimated as the sum of the thermal energy required to raise the minimum winter soil temperature to 0 °C ($Q_{soil\_warming}$) and energy required to melt the soil ice content (Q_{Thaw}). The energy required during the warming phase was estimated as:

$$\boldsymbol{Q_{soil\_warming} = \sum_{j=1}^{n}\left(M_{a,j}C_{p(a,j)} + M_{w,j}C_{p(w,j)} + M_{i,j}C_{p(i,j)} + M_{s,j}C_{p(s,j)}\right)\Delta T_j} \qquad \textbf{Equation 3.4}$$

where M is mass, C_p is specific heat, subscripts $a, w, i,$ and s are air, water, ice and soil, respectively, ΔT is change in temperature in degrees Celsius, and n is the number of soil layers. The specific heat values for air, water, ice, fibric peat and mineral soil were 1005, 4182, 2030, 1926 and 733 J kg^{-1} °C^{-1}, respectively. The energy required for melting soil ice was estimated as:

$$Q_{Thaw} = \sum_{j=1}^{n} \theta_{ice,j}\, d_j\, \lambda_f\, \rho_{ice} \qquad \textbf{Equation 3.5}$$

where $\theta_{ice,j}$ is the volumetric ice content of the jth soil layer (m^3 m^{-3}), d is the soil layer (j) depth (m), λ_f is the latent heat of fusion (J kg^{-1}), and ρ_{ice} is the ice density (kg m^{-3}). The ice content was estimated from soil water content measurements by subtracting the minimum winter water content from the antecedent water content at each site. The fall antecedent water content was considered to be the measured soil water content immediately before soil freeze-up.

3.4.4 Carbon Uptake and Soil Thaw

The measured fluxes of CO_2 were used to determine the onset date of net positive carbon uptake. The gap-filled net ecosystem production was integrated for each year starting from January 1 and the spring minimum value, when daily carbon uptake switches from negative to positive values, was used as an indicator for the beginning of net carbon uptake (Figure 3.14).

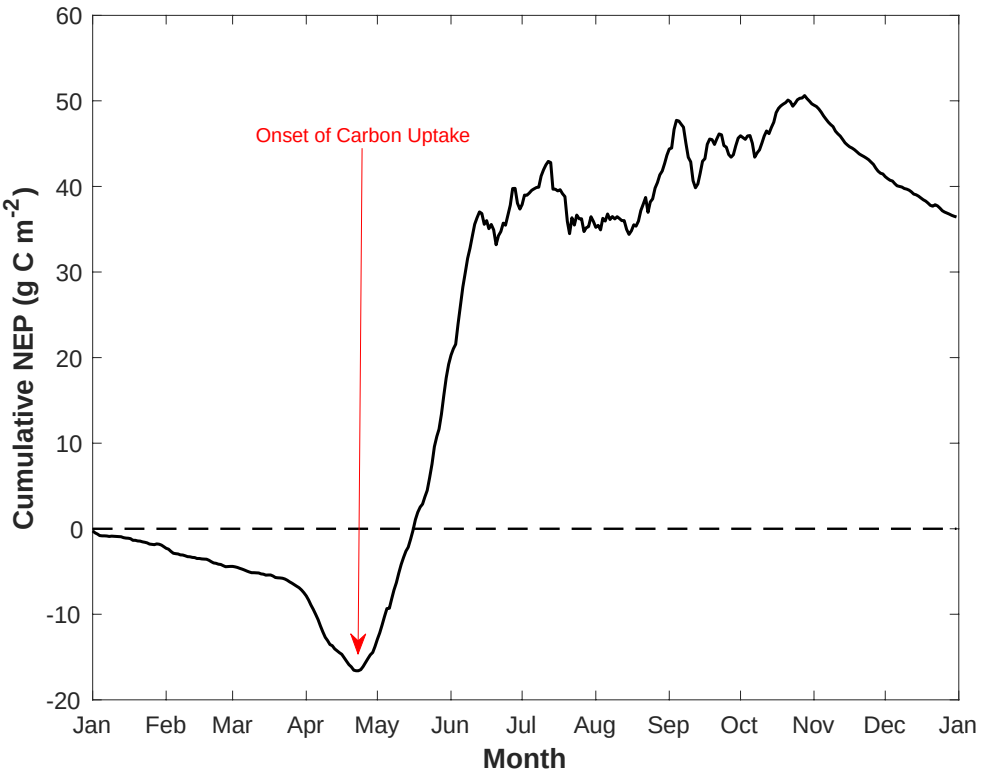

Figure 3.14 Onset of carbon uptake based on accumulated net ecosystem production

3.5 MODEL DESCRIPTION

Three models (CLASS, CRHM, and SHAW) were used in this study as described in Section 3.3. The CLASS and CRHM models were used to address objective 2 only and SHAW was used for objective 2 to 4. Therefore, a brief relevant description is provided for CLASS and CRHM and a more detailed description is provided for SHAW in the following sections.

3.5.1 Canadian Land Surface Scheme

The Canadian Land Surface Scheme (CLASS) originally developed by Verseghy (1991) simulates energy and water balances for a land surface comprised of soil, snow and vegetation. The model is usually coupled to atmospheric models but can also be run in a stand-alone (offline) mode. Snow processes are represented with a moderate level of complexity: an explicit representation of snow interception and unloading processes (Hedstrom and Pomeroy, 1998) and a single layer snowpack system. The maximum snow interception capacity is a function of fresh snow density and modified plant area index for needle leaf trees (Barlett et al., 2006). The model calculates sublimation from canopy-intercepted snow, and calculates sub-canopy fluxes of radiation, sensible and latent heat. Snowpack albedo and density are modelled using empirical decay functions based on the snow state: fresh, dry, and melting. Snowpack surface temperature is estimated by iteratively solving the surface energy budget (Eq. 3-6) with an upper limit of 0°C. The excess energy is then used for melting the snowpack which switches from a continuous to a fractional cover when its depth is reduced to ≤ 10 cm. The terms in equation 3-6 represent change in internal energy (dU/dt), net longwave radiation (Q_{LW}), net shortwave radiation (Q_{SW}), melt energy (Q_M), sensible heat flux (Q_H), latent heat flux (Q_E) and ground heat flux (G), all with units in W m^{-2}.

$$dU/dt = Q_{LW} + Q_{SW} - Q_M - Q_H - Q_E - G \qquad \textbf{Equation 3.6}$$

Soil heat transport processes are primarily driven by conduction which is strongly influenced by soil water content (Hayashi et al., 2007). The classic Clapp and Hornberger (1978) equation is used for the relationship between matric suction and soil moisture content where all the parameters are estimated following Cosby et al (1984) based on soil texture. The model doesn't represent

coexistence of liquid water with ice in the soils through the use of a freezing point depression equation.

Transpiration or canopy latent heat flux (Q_E) is modelled by a mass transfer function (Eq. 3-7) based on the specific humidity gradient between the canopy and the air ($q_c - q_a$), latent heat of vaporization (L_v), air density (ρ), as well as aerodynamic (r_a) and canopy resistances (r_c). The aerodynamic resistance is a function of a surface drag coefficient and wind speed whereas the canopy resistance depends upon the minimum stomatal resistance, extinction coefficient, leaf area index, incoming solar radiation and other environmental drivers following Schulze et al. (1995) coupled with functions based on the Jarvis-Stewart (Jarvis, 1976; Stewart, 1988) approach. The recovery of transpiration in spring is triggered by a threshold air temperature of 5°C. Evaporation from canopy intercepted precipitation is calculated by setting the canopy resistance to zero. For sub-canopy evaporation, the resistance terms are replaced by surface resistance which is determined as a function of the virtual potential temperature difference between the surface and the canopy.

$$\boldsymbol{Q_E = \frac{L_v \rho (q_c - q_a)}{(r_a + r_c)}} \qquad \textbf{Equation 3.7}$$

3.5.2 Cold Regions Hydrological Model

The Cold Regions Hydrological Model (CRHM) incorporates a full range of hydrological processes and provides flexibility of choosing desired algorithm for representing a given hydrological process based on research needs (Pomeroy et al., 2007). Snow interception, and unloading processes are represented by Hedstrom and Pomeroy (1998). The CRHM simulates canopy intercepted snow sublimation by considering a particle-scale mass and energy balance which is scaled-up for intercepted snow load considering the exposure of intercepted snow in the canopy (Pomeroy et al., 1998b). The model also has a detailed representation of sub-canopy shortwave and longwave radiation, which is important for snowmelt. The trasmisivity of above canopy shortwave radiation is a function of effective leaf area index and solar elevation angle whereas sub-canopy longwave radiation is the sum of above canopy longwave tranmistance based on open sky and canopy emissions propotional to canopy cover. Like CLASS, snowmelt is based on an energy balance approach but the snowpack albedo decay is a function of time since the last

snowfall event. However, CRHM uses the Gray and Landine (1988) approach for estimating internal energy state of the snowpack based on the minimum air temperature. Evapotranspiration is modelled by the Penman-Monteith approach (Monteith, 1965) with the same Jarvis-Stewart resistance scheme as in CLASS. The onset of spring transpiration is associated with the timing of snow ablation but transpiration is restricted because of unfrozen soil water content above the thawing front.

Heat transport processes are not represented in detail, but the model uses a modified Stefan equation (Changwei and Gough, 2013) for simulating the depth of freezing and thawing front (ξ) for a multi-layered soil system. The approach takes the following form:

$$\xi = \begin{cases} \sqrt{\frac{2k_1F}{L_f\theta\rho_s}}, & \xi \leq Z_1 \\ Z_1 + \frac{\xi_1 - Z_1}{P_{12}}, & \xi > Z_1 \end{cases} \qquad \textbf{Equation 3.8}$$

where k = thermal conductivity, L_f = latent heat of fusion, θ = water content, ρ_s = bulk density of soil, Z = soil layer thickness, F = surface freeze-thaw index calculated based on soil surface temperature following (Williams et al., 2015), and P_{12} is defined as $(k_1\rho_2\theta_2/k_2\rho_1\theta_1)^{0.5}$ with 1 & 2 represents two subjacent soil layers. The freeze-thaw algorithm interacts with the soil module and restricts downward percolation of water for frozen soils.

3.5.3 Simultaneous Heat and Water Model

The Simultaneous Heat and Water (SHAW) model simulates one-dimensional fluxes of energy, water and solute flow through a system comprised of vegetation, snow, dead plant residue, and soil based on prescribed boundary conditions in a finite-difference numerical solution framework (Flerchinger, 2017; Flerchinger and Hanson, 1989). Soil heat transport processes are represented in detail; however, some snow processes are simplified. In particular, the model does not have an explicit representation of canopy unloading and assumes that all intercepted precipitation is lost to evaporation. The maximum canopy interception capacity is limited to a user-specified depth of water per unit leaf area index, which typically varies between 0 and 1 mm. Like CLASS and CRHM, the SHAW model simulates sub-canopy shortwave and longwave radiation considering

canopy architecture (leaf area index, leaf orientation). The model develops a multi-layer snowpack in winter which changes its density due to compaction, settling, and vapor transfer. An energy balance approach is used for simulating snowmelt, similar to CLASS and CRHM. The change in liquid water content is modelled by considering the change in volumetric ice content for partially frozen soils, net liquid flux into a layer driven by the potential gradient and hydraulic conductivity, net vapour flux into a layer driven by the water potential and temperature gradient, and water extraction by roots (Section 2.2.4). The hydraulic conductivity is determined from the moisture retention curve but is linearly reduced when ice is present assuming negligible conductiviy at an available porosity of 0.13. There are multiple algorithms available for representing soil water retention curve but the Brooks and Corey (1966) model was used in this study because of its superior performance at the study sites. In the presence of ice, the soil matric potential (ψ) was determined by the freezing point depression curve (Fuchs et al., 1978) using equation 3.9, assuming soil water osmotic potential to be negligible, where λ_f is latent heat of fusion (J kg^{-1}), T is soil temperature (°C), and g is acceleration due to gravity (m s^{-2}).

$$\boldsymbol{\psi = \frac{\lambda_f T}{g(T+273.15)}} \qquad \textbf{Equation 3.9}$$

Changes in soil temperature (Eq. 3-9) are based on net thermal conduction (term II), net thermal advection into the soil layer (term III) due to water flux, net latent heat of vaporization (term IV), and latent heat required to freeze water (term V). The symbology used in equation 3-9 is defined as: C = Volumetric heat capacity (J kg^{-1} °C^{-1}), T = Temperature (°C), t = time, ρ = density (kg m^{-3}), θ = volumetric water content (m^3 m^{-3}), k = thermal conductivity (W m^{-1} °C^{-1}), z = depth, L = latent heat where subscripts s, i, l, v represent soil, ice, liquid, and water vapor.

$$\underset{(\boldsymbol{I})}{\boldsymbol{C_s \frac{\partial T}{\partial t}}} = \underset{(\boldsymbol{II})}{\boldsymbol{\frac{\partial}{\partial z}\left[k_s \frac{\partial T}{\partial z}\right]}} - \underset{(\boldsymbol{III})}{\boldsymbol{\rho_l C_l \frac{\partial q_l T}{\partial z}}} - \underset{(\boldsymbol{IV})}{\boldsymbol{L_v \left(\frac{\partial q_v}{\partial z} + \frac{\partial \rho_v}{\partial t}\right)}} + \underset{(\boldsymbol{V})}{\boldsymbol{\rho_i L_f \frac{\partial \theta_i}{\partial t}}} \qquad \textbf{Equation 3.10}$$

The SHAW model was originally developed for agricultural applications in which a residue layer is added to account for heat and water transport processes through the crop residue left on the ground surface after the harvest. Forest floor vegetation or ground cover is represented by this residue layer in the model and is hereafter referred to as the ground cover layer. The change in

stored energy of the ground cover depends upon net thermal conduction/convection, net latent heat of evaporation, and net absorption of radiant heat as:

$$\boldsymbol{C_{GC}\frac{\partial T}{\partial t} = \frac{\partial}{\partial z}\left(K_r \frac{\partial T}{\partial z}\right) - L_v \frac{\partial}{\partial z}\left(\frac{(RH_{GC} \cdot \rho'_{vs} - \rho_v)}{r_h}\right) + \frac{\partial R_n}{\partial z}} \qquad \textbf{Equation 3.11}$$

where C_{GC} = specific heat capacity of ground cover, K_r = sum of conduction and convection coefficients, RH_{GC} = relative humidity in the ground cover layer, ρ'_{vs} = saturated vapour density in the ground cover elements, ρ_v = vapour density in the air, r_h = boundary layer resistance, and R_n = net absorbed radiation which is a function of fractional coverage and density of the ground cover. The heat transfer coefficient K_r is a function of thermal conductivities of water, air, and ground cover, wind speed within the ground cover layer, its density, temperature, gravimetric water content and an empirical parameter. The relative humidity is an important term for calculating evaporation from the ground cover which is a function of gravimetric water content (θ_{GC}) and two empirical coefficients (a_r & b_r) as:

$$\boldsymbol{RH_{GC} = \exp\left(a_r \theta_{GC}^{b_r} \frac{M_w \cdot g}{R \cdot T}\right)} \qquad \textbf{Equation 3.12}$$

where M_w is the molecular weight of water, and R is the gas constant. The maximum water content for the ground cover is back calculated from equation 3-11 for a relative humidity of 99.9%.

Canopy transpiration rate, T (kg m^{-2} s^{-1}) in the model is determined by vapor density within the stomatal cavities (ρ_{st}) which is assumed to be saturated, vapor density of the air (ρ_{air}), stomatal resistance (r_s), resistance to water vapor from the canopy leaves (r_v), and leaf area index (LAI) as:

$$\boldsymbol{T = \frac{\rho_{st} - \rho_{air}}{r_s + r_v} LAI} \qquad \textbf{Equation 3.13}$$

Resistance from the canopy is a function of the characteristic dimension of its leaves, the canopy temperature, and wind speed. Stomatal resistance in equation 3-12 is determined from equation 3-13 where r_{s_min} = minimum stomatal resistance, ψ_l = leaf water potential, ψ_c = critical leaf water potential at which stomatal resistance becomes twice of its minimum value, n_s = empirical exponent, and f_{ST}, f_T, f_{VPD} = are the factors to account for solar radiation, air temperature, and

vapor pressure deficit influences on stomatal resistance respectively. The influence of soil moisture on stomatal resistance was implicitly represented in equation 3-13 as it considers leaf water potential which is simulated by the model.

$$\boldsymbol{r_s = r_{s\_min}\left(\left[1 + \frac{\psi_l}{\psi_c}\right]^{n_s} \Big/ f_{ST} f_T f_{VPD} \right)} \qquad \textbf{Equation 3.14}$$

f_{ST} is determined as $S(1000 + K_{st})/(1000(S + K_{st}))$ where S is incoming solar radiation and K_{st} is an empirical coefficient. The influence of vapor pressure deficit depends on two parameters as $f_{VPD} = K_{VPD} + [1 - K_{VPD}]r\_vpd^{VPD}$. The temperature influence (f_T) is incorporated based on lower transpiring temperature T_l, higher transpiring temperature T_H, and optimum temperature for transpiration T_{opt} as $f_T = (T - T_l)\ (T_H - T)^{n_T}/(T_{opt} - T_l)\ (T_H - T_{opt})^{n_T}$ where T is ambient air temperature and n_T is calculated as $(T_H - T_{opt})/(T_{opt} - T_l)$.

3.6 DIAGNOSTIC MODEL COMPARISON

This section describes the methodology adopted to address objective 2 of this study which deals with evaluating the performance of different models for simulating winter-spring transition at the jack pine site. Previous multi-site snow model intercomparison projects such as PILPS and SnowMIP (Essery et al., 2009; Nijssen et al., 2003; Slater et al., 2001) have reported largest differences in SWE simulations at warmer sites during spring snowmelt (Krinner et al., 2018). An intercomparison of 33 snow models (SnowMIP2) at the same old jack pine site as used for the present study also revealed large differences in simulated SWE where divergence between models was larger for spring snowmelt than for winter snow accumulation (Rutter et al., 2009). In the present study, the performance of three models (CLASS, CRHM, and SHAW) was evaluated at the jack pine site for simulating snow accumulation, snowmelt, soil thaw timing, and spring evapotranspiration. The general aspects of the models are summarized in Table 3.2 with more details provided in Section 3.5.

Table 3.2 General characteristics and structural formulations of the models

Description	Model		
	CLASS	**CRHM**	**SHAW**
Model version	CLASS v3.6.2	CRHM 06/14/17	SHAW 3.0
Runtime resolution	1 hr	1 hr	1 hr
Canopy layer	Single	Single	Multiple (11 max.)
Canopy-snow interception	Yes	Yes	Yes
Unloading of intercepted precipitation	Yes	Yes	No
Snow layer	Single	Single/Multiple	Multiple
Snowpack temperature simulation	Yes	No	Yes
Physically based snowmelt model	Yes	Yes	Yes
Forest floor/understory vegetation	No	No	Dead plant residue layer
Infiltration into frozen soil	Yes	Yes	Yes
Soil layer	Multiple	Multiple	Multiple
Provision of organic soil representation	Yes	No	Yes
Lower boundary condition required	No	No	Yes

3.6.1 Model Setup and Parametrization

For the last two decades, extensive research has been conducted at the study locations (as described in Section 1.1 and Section 2.3); therefore, it was desirable to use site-specific model parameters which were either directly measured or well representative of the study site. These parameters are listed in Table 3.3.

Table 3.3 Common model parameters for BERMS old jack pine site

Parameters	Unit	Value	Source
Silt- mineral soil	%	15	Soil survey 1993
Clay- mineral soil	%	5	
Average tree height	m	14	(Gower et al., 1997)
Leaf area index	$m^2\ m^{-2}$	2.6	(Chen et al., 2006)
Clumping factor	fraction	0.85	
Residual water content	$cm^3\ cm^{-3}$	0.001	SHAW water retention characteristics (WRC) parameters (derived from CLASS WRC by curve fitting which was developed based on site soil texture)
Saturated water content	$cm^3\ cm^{-3}$	0.24	
Air entry	m	-0.476	
Pore size distribution	-	0.168	
Saturated hydraulic conductivity	$cm\ hr^{-1}$	5.54	(Cosby et al., 1984)
Critical leaf water potential	m	-255	(Bonan et al., 2014)
Canopy albedo	-	0.09	(Betts and Ball, 1997)

For canopy snow interception and unloading processes, within CRHM the maximum intercepted snow load was set to 6.3 kg m^{-2} and the threshold ice-bulb temperature for snow unloading was set to -2°C based on the vegetation type (Hedstrom and Pomeroy, 1998; Pomeroy et al., 2007). The maximum snow interception and unloading rate coefficient were hard coded in CLASS; thus, could not to be specified. The SHAW model does not account for unloading of intercepted

precipitation. Accordingly, snow interception was reduced by calibrating the maximum intercepted precipitation which was set to 0.05 mm per unit leaf area index.

For simulating the latent heat flux, the minimum stomatal resistance was the sensitive parameter for all three models and was set to 250 s m^{-1} for CLASS, 100 s m^{-1} for CRHM, and 500 s m^{-1} for SHAW. These values were all determined from manual calibration by visual assessment of simulated daily latent heat fluxes against the observations. The Jarvis-Stewart functions to consider the influence of environmental variables (such as solar radiation, air temperature and vapor pressure deficit) on stomatal conductance were switched off for SHAW in this analysis.

All three models were run on a multi-layer soil system. Within CLASS, there are three standard soil layers (with thicknesses of 0.1, 0.25, and 3.75 m), but the third layer can be sub-divided into several layers with desired thickness. The third layer was sub-divided into 13 layers to simulate soil temperature at desired depths. Thus, fifteen soil layers were specified in total for CLASS: the top five soil layers were 0.1 m, 0.25 m, 0.3 m, 0.25 m, and 0.2 m thickness followed by 0.3 m increment to a depth of 4.1 m. Eleven soil layers were specified for the CRHM model: the top three layers with 0.1 m thickness followed by 0.2 m increment to a depth of 0.9 m, and then 0.4 m increment to a depth of 2.9 m. The SHAW model required a constant temperature lower boundary condition which can either be specified or simulated. The option of simulated lower boundary condition was selected and the soil profile was extended to 11 m, well past the expected frozen depth (1-2 m) to avoid any influence of lower boundary conditions on the simulations. Twenty eight soil layers were specified: the first two with 0.05 m thickness followed by 0.10 m increment to a depth of 1 m, 0.25 m increment from 1 m to 3 m and then 1 m increment from 3 to 11 m. The SHAW model also has a dead plant residue layer which was used to evaluate the insulation effects of lichen on soil thaw timing by running the model with and without this layer. The thickness of this layer was set to 2 cm with 100% fractional coverage and 0.25 albedo.

All three models were run on an hourly time-step from October 2012 to June 2016 with observed meteorological forcing data at the jack pine site. The first year was considered as model spin-up time and was excluded from the analysis. For boreal forest applications, a 1-year model spin-up time has been used, both at stand and catchment scales (Launiainen et al., 2019). It is also believed that 1-year model spin-up time would be sufficient in this study because the initial soil moisture

conditions are known (Kim et al., 2018) and the model run is started in the fall (Rahman et al., 2016). All three models simulated lateral water flow in the form of surface runoff considering the influence of frozen soils on infiltration. However, lateral sub-surface water flow was omitted. This assumption was reasonable because of the flat topography of the study sites and dominance of coarse-textured parent material causing minimal lateral saturated flow while promoting significant vertical drainage and groundwater recharge (Ireson et al., 2015). Lateral groundwater flow is generally significant in souther boreal environments, which typically drains to fen complexes depending upon their water table depth and hydraulic properties of the peat. This study focussed on upland forest sites where soil moisture in the shallow root-zone was of primary interest; thus, lateral sub-surface water flow was not considered.

3.6.2 Model Performance Evaluation

Simulated daily snow water equivalent (SWE) was compared against the periodically observed SWE to explore differences in simulated snow accumulation, snowmelt rates and snow ablation timing. Simulated soil thaw timing (Julian day) at 10-, 20-, 50-, and 100-cm depths was also compared against the observations. Measured or simulated (CLASS and SHAW) soil temperature data were used to define soil thaw timing i.e. the time when soil temperatures rapidly rises above zero degree Celsius (Tanja et al., 2003). The CRHM does not simulate soil temperatures; thus, soil thaw timing at different depths was determined by the simulated thawing front as it reached the corresponding depth. Daily evapotranspiration was calculated from the measured and simulated latent heat flux densities and then integrated over the spring season (April 1 to June 15). The observed seasonal values were compared with model estimates for three years (2014 to 2016). Two statistical measures, Mean Absolute Error (Eq. 3-14) and Mean Bias Error (Eq. 3-15), were used to determine the accuracy of the models. The total number of observations, model predicted value and observation value are represented by n, P_i, and O_i in the following equations.

$$\boldsymbol{MAE = \frac{1}{n}\sum_{i=1}^{n}|P_i - O_i|} \qquad \textbf{Equation 3.15}$$

$$\boldsymbol{MBE = \frac{1}{n}\sum_{i=1}^{n}(P_i - O_i)} \qquad \textbf{Equation 3.16}$$

3.7 MODELING SOIL THAW AND SPRING EVAPOTRANSPIRATION USING THE SIMULTANEOUS HEAT AND WATER (SHAW) MODEL

This section describes the methodology adopted to address objective 3 of this study. The SHAW model was used to simulate soil thaw timing and spring evapotranspiration at all three sites. The model was run on an hourly time step by considering a single canopy layer, a multi-layer snowpack, a single ground cover (residue) layer, and a multi-layer soil system. Snowpack layer thicknesses were automatically defined by the model based on snow depth, but soil layers were specified (Section 3.6.1). The depth of the organic soil layer was set to 0.03 m for jack pine, 0.10 m for aspen, and 0.30 m for black spruce based on historical site observations. The required inputs were precipitation, incoming shortwave and longwave radiation, air temperature, wind speed, and relative humidity. Observed soil temperature and above canopy latent heat fluxes were used for model validation. The details about the instrumentation used for measuring these variables, and procedures adopted for data integrity and quality checks have been previously described (Section 3.2).

3.7.1 Model Parameterization for Soil Thaw

The soil heat transport processes strongly depend upon water content (Hayashi et al., 2007), which is controlled by water retention characteristics of soils. The site-specific mineral soil water retention curve parameters for the van Genuchten (1980) model had been previously determined by Cuenca et al. (1997) and were determined for the Brooks and Corey (1966) model using a curve fitting approach implemented via an online SWRC-fit tool (Seki, 2007). Water retention characteristics for the organic soils at jack pine, aspen, and the top shallow layer (10-cm) at black spruce were obtained from Letts et al. (2000) and were calibrated to soil moisture and temperature observations for a more decomposed (11-30 cm) layer at black spruce using Dynamically Dimensioned Search (DDS) algorithm (Tolson and Shoemaker, 2007). For calibration, the refined index of agreement (Willmott et al., 2012) was used to evaluate model performance which is defined as:

$$d_r = 1 - \sum_{i=1}^{n}|P_i - O_i| \Big/ 2\sum_{i=1}^{n}|O_i - O_{mean}| \text{ , when}$$

$$\sum_{i=1}^{n}|P_i - O_i| \leq 2\sum_{i=1}^{n}|O_i - O_{mean}|$$

And **Equation 3.17**

$$d_r = \begin{cases} 2\sum_{i=1}^{n}|O_i - O_{mean}| \Big/ \sum_{i=1}^{n}|P_i - O_i| - 1 & \text{when } \sum_{i=1}^{n}|P_i - O_i| \leq 2\sum_{i=1}^{n}|O_i - O_{mean}| \\ \end{cases}$$

$$\sum_{i=1}^{n}|P_i - O_i| > 2\sum_{i=1}^{n}|O_i - O_{mean}|$$

where n represents number of observations, P is model simulation, O is observations and O_{mean} is the mean observation value for the time duration. The value of d_r varies between -1 and 1 where negative values indicate poor model performance and a value of 1 represents the best or perfect model. The model parameters used in this study are listed in Table 3.4 for all three sites. In this study, the refined index of agreement was consistently used as an objective function for any calibration, parameter sensitivity or uncertainty analysis. The function compared predicted and observed variability about the observed mean and allowed estimation of true mean (varied over space and time rather than averaged over the entire domain). Therefore, it was anticipated that the function may be better suited for analyzing time-series climate variables. For reporting overall simulation errors/biases (in the same units as measurement) MAE, MBE and/or Root Mean Square Error (RMSE) were used.

Table 3.4 Model parameters for the study sites

Parameters	Unit	Typical/Default Value			Source
		JP	BS	AS	
Residual water content-mineral	$cm^3\ cm^{-3}$	0.03	0.01	0.05	(Cuenca et al., 1997) (Seki, 2007)
Saturated water content-mineral	$cm^3\ cm^{-3}$	0.40	0.51	0.49	
Air entry-mineral	m	-0.077	-0.168	-0.303	
Pore size distribution-mineral	-	0.461	0.244	0.189	
Saturated hydraulic conductivity-mineral	$cm\ hr^{-1}$	6.08	3.29	1.04	
Residual water content-fibric	$cm^3\ cm^{-3}$	0.04	0.04	0.04	(Letts et al., 2000) (Seki, 2007)
Saturated water content-fibric	$cm^3\ cm^{-3}$	0.93	0.93	0.93	
Air entry-fibric	m	-0.074	-0.074	-0.074	
Pore size distribution-fibric	-	0.682	0.682	0.682	
Saturated hydraulic conductivity-fibric	$cm\ hr^{-1}$	100.8	100.8	100.8	
Residual water content-humic	$cm^3\ cm^{-3}$	-	0.19	-	Calibrated
Saturated water content-humic	$cm^3\ cm^{-3}$	-	0.86	-	
Air entry-humic	m	-	-0.219	-	
Pore size distribution-humic	-	-	0.5	-	
Saturated hydraulic conductivity-humic	$cm\ hr^{-1}$	-	68.5	-	
Minimum stomatal resistance	$s\ m^{-1}$	200	200	125	(Verseghy, 2011)
Leaf area index	$m^2\ m^{-2}$	2.6	3.8	4.4	(Barr et al., 2004)
Critical leaf water potential	m	-255	-255	-225	(Bonan et al., 2014)
Canopy albedo	-	0.09	0.08	0.156	(Betts and Ball, 1997)
Clumping factor	%	0.85	0.9	-	(Chen et al., 2006)
Dry weight of surface cover	$kg\ ha^{-1}$	2200	2220	1440	(Gower et al., 1997)

It was established through observations (Section 4.5.2) and modelling (Section 5.4) that the ground cover influences soil temperatures and thaw. The ground cover at all three sites was represented by a dead plant residue layer in the SHAW model. There were seven parameters related to ground cover including its dry weight, albedo, thickness, fractional coverage, boundary layer resistance for evaporation and two empirical coefficients for relating water content with humidity. The information for site specific dry weight was derived from literature (Table 3.4). A manual, one-at-a-time sensitivity analysis suggested that soil temperature simulations were insensitive to evaporation-related parameters (i.e., the empirical coefficients in equation 3-11 and boundary layer resistance in equation 3-10); thus, were kept as model defaults. The most sensitive parameters (thickness, fractional coverage, and albedo of ground cover) were calibrated for soil temperature simulations using Dynamically Dimensioned Search (DDS) algorithm (Tolson and Shoemaker, 2007) by three independent trials. The calibration period was 2009-2011 for the aspen site, and 2013-2015 for the jack pine and black spruce sites. The parameter ranges used for calibration are provided in Table 3.5. The insulation effects of the ground cover on underlying soils were evaluated by running the SHAW model with and without representation of ground cover layer at all three sites. The water retention curve parameters for 10-30 cm organic soil layer at black spruce site were calibrated independently of residue layer parameters to explore the difference residue layer would make on soil temperature simulations against the model run without the residue layer but with the best known all other parameters.

Table 3.5 Feasible range of model parameters used for calibration

Parameter (unit)	Lower Bound	Upper Bound
Thickness of surface cover (cm)	0.5	10
Fractional surface coverage	0.5	1
Albedo	0.1	0.25

3.7.2 Modelling Evapotranspiration

The problem of models' overestimation of spring evapotranspiration within boreal coniferous forests has been reported in the literature (Section 1.1) and was also observed in this study (Section

5.4). The following approach was adopted for improved SHAW simulations of evapotranspiration for coniferous forests:

Uncertainty Analysis – A model parameter uncertainty analysis was conducted to better understand model behavior. The parameter uncertainty analysis was conducted using the Generalized Likelihood Uncertainty Estimation (GLUE) framework (Beven and Binley, 1992). A large number of parameters were considered in the analysis and are listed along with their feasible ranges in Table 3.6. The analysis was completed with and without considering environmental control variables (air temperature, solar radiation and vapor pressure deficit) for stomatal conductance. All parameters were sampled from a uniform distribution. The model was run 50,000 times for both scenarios and the top 5% model runs were retained as behavioural simulations. The model performance evaluation metric was refined index of agreement, d_r (Eq. 3-16).

Sensitivity Analysis – The critical model parameters for evapotranspiration were identified by global sensitivity analysis using Variogram Analysis of Response Surfaces (VARS) method (Razavi and Gupta, 2016). Forest transpiration is controlled by stomatal conductance (Collins and Avissar, 1994; Nazarbakhsh et al., 2019). Thus, all the parameters related to stomatal resistance (equation 3-13) which is a reciprocal of stomatal conductance, were considered for the analysis. The analysis was completed with and without considering minimum stomatal resistance using 200 stars which corresponds to 16,400 and 14,600 model runs, respectively. The refined index of agreement (Eq. 3-16) was evaluating objective function and parameter ranges used in the analysis are provided in Table 3.7.

Model Development – In order to improve the ability of the model to capture spring evapotranspiration, an additional environmental control factor based on growing degree days was proposed for the Jarvis-Stewart resistance scheme using observed data. The detailed description of model development has been provided in Section 6.3.3.

Model Evaluation – The model performance was evaluated for both the coniferous forest sites with and without considering proposed growing degree days factor. The model calibration/evaluation matric was root mean square error (RMSE), which is the standard deviation of the residuals or prediction errors and calculated from equation 3-17 where all the variables have

previously been defined. In addition, other statistical measures such as mean absolute error and mean bias error were also used to quantify errors in simulations of evapotranspiration.

$$RMSE = \sqrt{\frac{\sum_{i=1}^{n}(P_i - O_i)^2}{n}} \qquad \textbf{Equation 3.18}$$

Table 3.6 Parameter ranges for uncertainty analysis at jack pine

Parameters	Unit	Lower Bound	Upper Bound	Default
Slope	%	2	5	2
Surface roughness for momentum transfer	cm	0.5	4	4
Max. ponding depth	cm	0	10	5
Max. intercepted precipitation	mm	0.1	1	0.1
Albedo of canopy	-	0.1	0.3	0.12
Min. transpiring temperature	◦C	0	10	5
Stomatal resistance min	s/m	100	500	400
Leaf water potential	m	-100	-300	-200
Clumping factor	%	0.5	1	0.7
Dry biomass of plant species	kg/m^2	2	5	3
Leaf area index	m^2/m^2	1.5	3	2.5
Rooting depth	m	1	5	2
Max. temp. at precipitation is now	◦C	0	3.6	2
Thickness of residue layer	cm	3	10	6
Dry weight of residue on surface	kg/ha	1500	4000	3000
Fraction of surface covered by residue	-	0.7	1	0.9
Albedo of residue	-	0.2	0.4	0.3
Resistance to vapour transfer from residue	s/m	1000	50000	15000
Albedo of dry soil	-	0.1	0.3	0.2
Exponent for calculating albedo of moist soil	-	0	3.5	3.5
Hydraulic conductivity of mineral soil	cm/hr	5	30	25
Air entry	cm	-0.2	-0.3	-0.1598
Pore size distribution	-	0.3	0.4	0.698
Saturated content	-	0.4	0.44	0.41
Residual content	-	0.03	0.057	0.05

Parameter for Radiation function	-	100	400	200
Empirical parameter for VPD function	-	0	1	0.5
Minimum temperature for transpiration	◦C	0	5	5
Maximum temperature for transpiration	◦C	30	45	35
Optimum temperature for transpiration	◦C	10	30	25

Table 3.7 Model parameters used for sensitivity analysis at jack pine

Parameters	**Unit**	**Jack pine**	
		LB	**UB**
Minimum stomatal resistance, RSmin	s m^{-1}	100	400
Rooting depth, Rd	m	0.5	4
Critical leaf water potential, LWPc	m	-300	-100
Radiation influence parameter, Kst	W m^{-2}	100	400
Temperature influence parameter- Tl	℃	-5	5
Temperature influence parameter- Th	℃	30	45
Temperature influence parameter- Topt	℃	10	30
VPD function parameter r-VPD	-	0.1	0.9
Maximum reduction in conductance- k-VPD	-	0.05	0.4
Root resistance, Rr	m^3 s kg^{-1}	5e4	7e4
Exponent, n	-	1	5

3.8 MODELLING CLIMATE CHANGE IMPACT ON SPRING THAW

This section describes the approach taken to evaluate climate change impacts on spring thaw processes for different forest-cover types in the southern boreal forest (objective 4). The overall modelling approach is described in Figure 3.15. The Weather Research and Forecasting (WRF) model was used to generate weather data for historical and future scenarios, which were bias-corrected using observed the meteorological data at the study sites. The WRF simulations for both scenarios were used as off-line forcing for a optimized SHAW model and simulated changes in soil frost, soil thaw completion, evapotranspiration, and soil water content were evaluated, in addition to exploring projected changes in climate i.e. air temperature and precipitation. More details about generating weather input data for both scenarios and its bias correction are provided in the following sections.

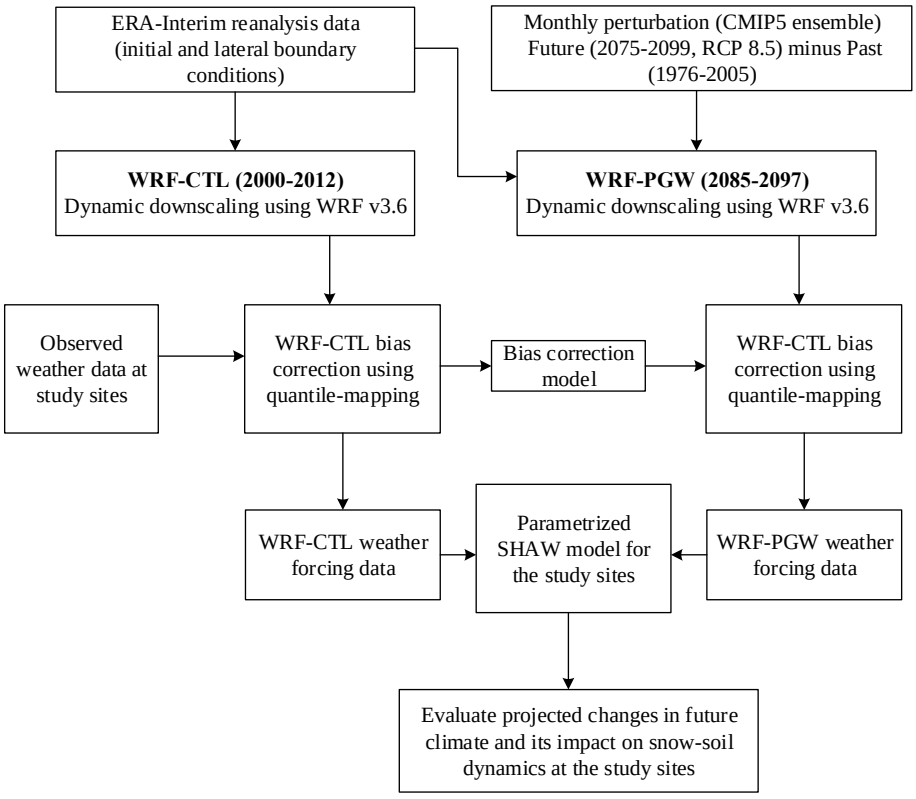

Figure 3.15. Modelling flowchart for evaluating climate change impacts on spring thaw processes

3.8.1 Historical Simulations (WRF-CTL)

The historical weather data (2000 to 2012) were simulated by the convection-permitting, Weather Research and Forecasting (WRF) model version 3.6.1 coupled with the Noah Land Surface Scheme (Chen and Dudhia, 2001). The WRF model is a numerical weather prediction and atmospheric simulation system developed through multi-agency collaborations and for the prediction of mesoscale weather for research and operational applications (Skamarock et al., 2008). The model was run over Western Canada, covering the Mackenzie and South Saskatchewan river basin with a horizontal resolution of 4 km and at 37 vertical levels topped at 50 hPa in the lower stratosphere (Li et al., 2019). The initial and lateral boundary conditions for the WRF model were derived from 6-hourly ERA-Interim reanalysis data at a spatial resolution of 0.7° (Dee et al., 2011). The WRF simulated hourly time-series of precipitation, air temperature, wind speed, specific humidity, and solar radiation at the ground surface were used in this study excluding the first year (2000) which was considered as the model spin-up time. The SHAW model was run from January 1, 2001 to June 30, 2012 for historical simulations and the first year (2001) was considered as warm-up period for SHAW. The SHAW model output were analysed for 10 years from 2002 to 2011.

3.8.2 Future Simulations (WRF-PGW)

The Pseudo Global Warming (PGW) approach (Kimura and Kitoh, 2007) was adopted for future weather prediction. In this method, mean monthly perturbations were added to initial and lateral boundary conditions for the WRF-CTL scenario. These perturbations were calculated as the mean monthly difference between 1976-2005 and 2071-2100 projections which were derived from simulations of a 19-member ensemble mean of Coupled Model Inter-comparison Project Phase 5, CMIP5 under the high emission scenario of RCP8.5 (Taylor et al., 2012). The high emission scenario (RCP 8.5), which is now debated to be the business-as-usual scenario, is consistent with current pace of global emissions. The cumulative CO_2 emissions, which is an important metric to assess usefulness of the emission scenarios, agrees within 1% from 2005 to 2020 with RCP 8.5 scenario (Schwalm et al., 2020). The WRF-PGW is considered to be 2085-2097 equivalent. For the same model spin-up/warm-up times as for historical simulations, SHAW analysis based on this forcing data is representative of 2087-2096.

The PGW approach allows reproducibility of the current climate, thus, reflects actual global warming effects relative to the current climate which is a major advantage of this approach over traditional practices (Sato et al., 2007). Additionally, an ensemble mean of the GCM's can be used for the detection of change signal which can reduce the noise and uncertainty. The adaption of this approach is still challenged by computational resources and efficiency but the method has been implemented in several climate change impact studies (Kusaka et al., 2012; Taniguchi and Sho, 2015).

3.8.3 Bias Correction of WRF Data

The outputs of GCMs or RCMs are subject to biases despite fine resolution because of imperfect knowledge of climate processes, simplified physics, and uncertainties in the input data and model parametrization. Hydrological simulations improve against the observations when biased corrected climate variables of RCMs are used as compared to uncorrected variables (Teutschbein and Seibert, 2012). Several bias correction methods are available including direct methods based on mean and/or variance statistics (Hawkins et al., 2013), delta change (Karyn and Williams, 2010), and a more sophisticated quantile mapping approach in which a transfer function minimizes the difference between cumulative density functions of climate model outputs and observations (Grillakis et al., 2017). The quantile mapping method has been proven to outperform other simplified approaches for bias correction (Chen et al., 2013). In this study, the WRF weather data (WRF-CTL and WRF-PGW) were corrected by univariate bias correction based on quantile delta mapping (Cannon et al., 2015) using an available online R package "MBC" (https://cran.r-project.org/web/packages/MBC/index.html). The bias correction was applied to hourly precipitation, air temperature, wind speed, relative humidity, and solar radiation data by combining WRF output with observed time series at study sites. The precipitation and air temperature data were separately bias corrected for summer and winter months.

CHAPTER 4 INTER-SITE VARIABILITY OF SOIL THAW AND ITS RELATIONSHIP WITH CARBON UPTAKE

4.1 CHAPTER OVERVIEW

This chapter addresses objective 1, which was to characterize the variability of spring thaw for different forest-cover type (aspen, jack pine, and black spruce) under recent climate conditions and identify critical factors causing inter-site variability. The relationships between spring thaw and carbon uptake are also explored. The site characteristics are described in Section 3.1. The analytical approach has been described in Section 3.4. Within this chapter, the observed inter-site differences in soil thaw timing, seasonal snowfall, snow accumulation on ground, snowmelt and ablation timing, soil hydro-thermal characteristics, ice content in the soil profile, and energy required for spring thaw are presented (Section 4.2 and 4.3). The relationships between carbon uptake and spring thaw timing are then explored (Section 4.4) followed by a discussion about uncertainty in observations, controlling factors for soil thaw variability, relationship between carbon uptake and spring thaw, and implications of study results for modelling work.

4.2 DIFFERENCES IN SNOWFALL, SNOW ACCUMULATION, ABLATION, AND ICE CONTENT

Seasonal snowfall (from 1 October to 30 March) was similar at all three sites (Figure 4.1) as expected because of regional proximity, with the exception of only a few years. For example, the aspen site received about 40 to 60 mm more snow in 1998-99 compared to the coniferous forest sites. Similarly, both the jack pine and the black spruce sites received about 50 mm more snow in 2003-04 compared to the aspen site. The differences in these years were likely caused by local snowstorm events; it is believed that the measurement errors were small.

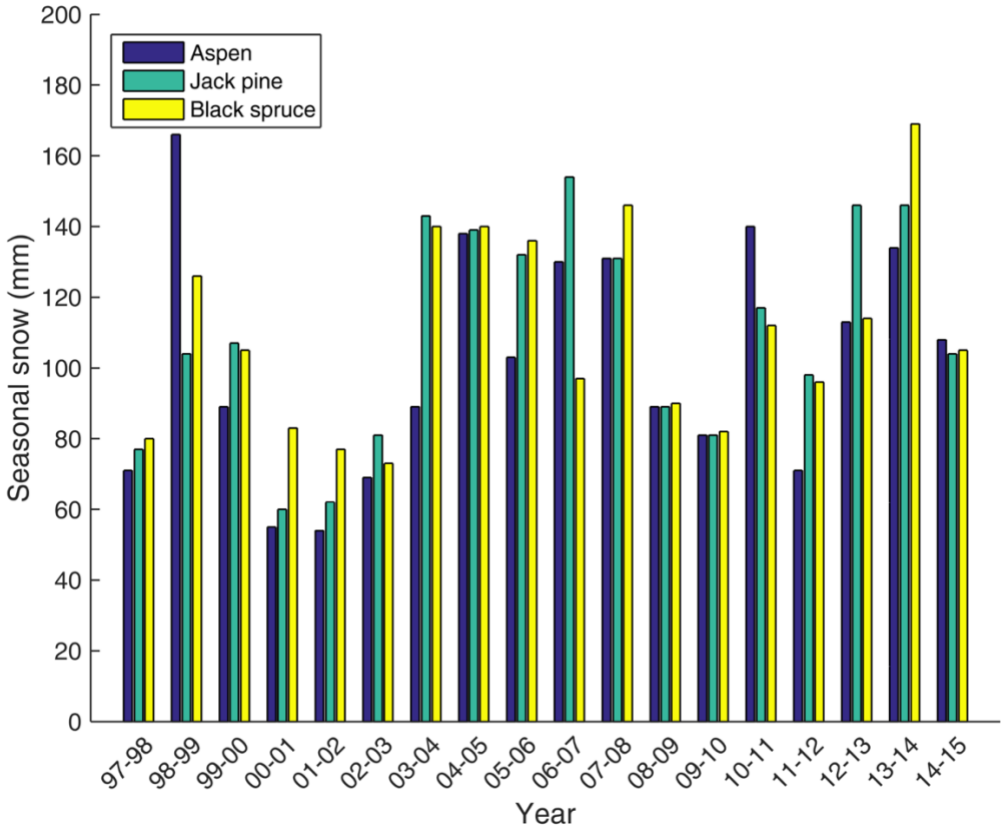

Figure 4.1 Seasonal snowfall estimates at the study sites from the precipitation data from 1 Oct to 30 March Note: *p*-value for one way ANOVA was found to be 0.676 which was greater than significance level at α=0.05, therefore, null hypothesis was accepted that all sites receives similar precipitation

Despite similar snowfall at all sites, the accumulation of snow on the ground can vary because of differences in snow interception and sublimation from the canopy, resulting in lower snow accumulation for coniferous than deciduous forests (Rahmat, 2019). In this study, snow accumulation on the ground was higher for the deciduous forest site compared to the two coniferous forest sites (Table 4.1). The average annual peak snow water equivalent (SWE) for the aspen site was 14 mm and 19 mm higher than jack pine and black spruce sites, respectively. Peak snow accumulation relative to total snowfall was estimated to be 96% for aspen, 81% for jack pine and 76% for black spruce. These estimates indicate sublimation losses of 5%, 20% and 23% respectively, which are lower than the previously reported 13% to 40% sublimation losses for

varying deciduous and coniferous forests west of the study sites in boreal forests (Pomeroy et al., 1998b). This may be because snow accumulation estimates in this study were based on the time of peak SWE rather than snow ablation.

Table 4.1 Annual measured snowfall and peak snow water equivalent (mm) at the study sites

Date	Aspen		Jack pine		Black spruce	
	Snowfall (mm)	**Peak SWE (mm)**	**Snowfall (mm)**	**Peak SWE (mm)**	**Snowfall (mm)**	**Peak SWE (mm)**
March 17-18, 2004	90	67	118	59	117	55
March 14-15, 2006	102	109	130	90	135	84
March 11-20, 2007	122	101	118	100	81	94
March 18-19, 2008	128	104	128	103	143	92
March 21-23, 2011	139	141	116	98	109	93
March 23-25, 2014	130	149	145	134	169	133
March 11-12, 2015	109	112	95	100	99	103
Mean	**117**	**112**	**122**	**98**	**122**	**93**

Note: Only those years when peak SWE was captured by snow surveys were included.

Canopy leaf area index influences radiation penetration through the canopy which directly relates to the energy availability for snowmelt. Snowmelt characteristics, including snowmelt start date, snow ablation date, and snowmelt duration, were compared between the sites to explore the relative significance of canopy architecture. Snowmelt typically commenced in March with large inter-annual variability in the start date but very small differences between the sites (Figure 4.2). This suggests that the snowmelt start date was generally governed by the regional climate. In contrast, the snow ablation date ranged from late-March to mid-May and was quite similar for the aspen and jack pine sites, but often delayed by a few days for the black spruce site. Snowmelt duration ranged from about 2 to 8 weeks at all three sites. On average, snowmelt duration was 4 weeks for the aspen and jack pine sites and about 4 days longer for black spruce.

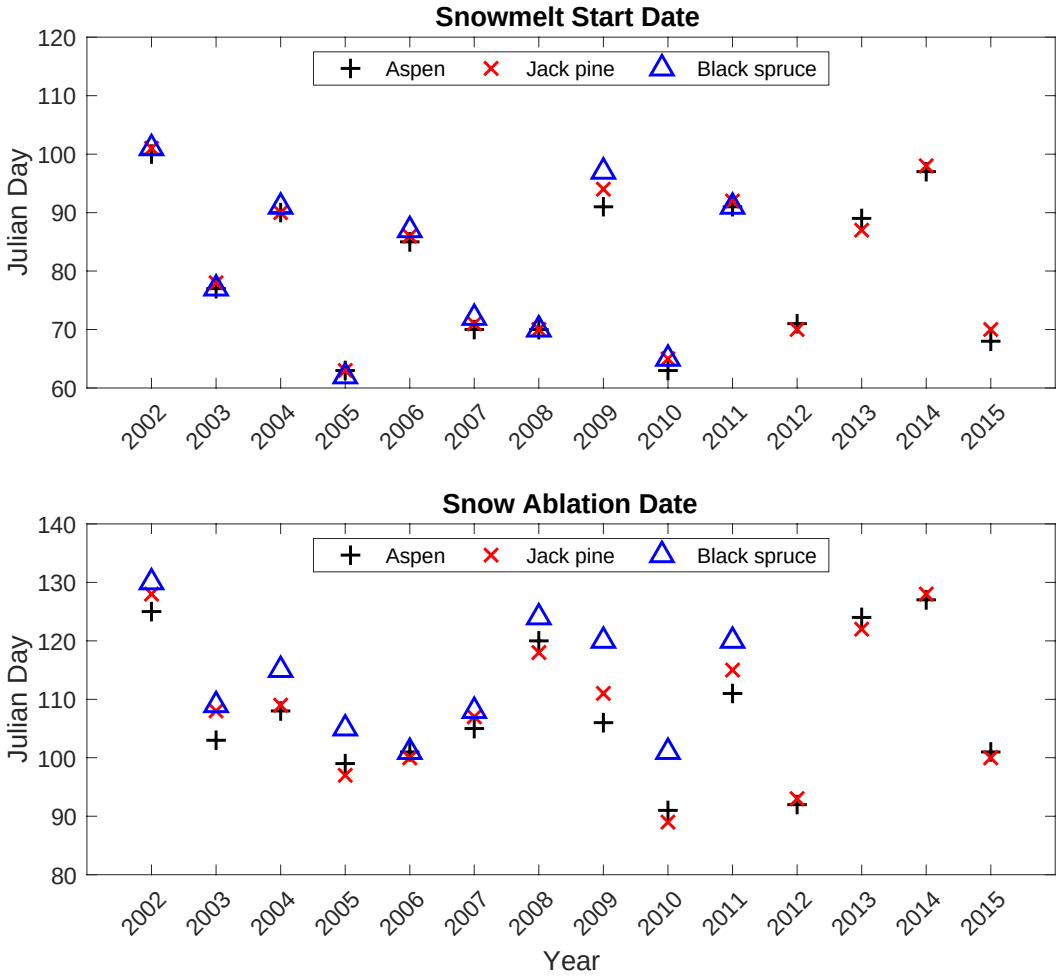

Figure 4.2 A comparison of snowmelt start date and ablation among sites

The energy required for soil thaw may vary between the study sites, depending upon the soil thermal and water retention properties. Soil temperature and soil water content measurements showed significant contrasts between the sites (Figure 4.3). The average frost depth was greatest at jack pine (>1 m) followed by aspen and black spruce (Figure 4.3a). The soil was also consistently colder at the jack pine site compared to the aspen and black spruce sites. Autumn antecedent soil water content was the highest at the black spruce site for 15-30 cm or deeper soil depths and the lowest for the jack pine site (Figure 4.3b). The inter-annual variability of the minimum soil temperature was similar for all three sites but the total ice content was less variables at the jack pine and black spruce sites (Figure 4.3c and Figure 4.3d). The median ice content was the lowest for the jack pine site and the highest for the black spruce site. The average annual ice

contents for 1 m deep soil profile were 67, 65, and 38 mm of water equivalent for the aspen, black spruce, and jack pine sites, respectively. The estimated average ice content for different depths at all three sites are provided in Appendix B.

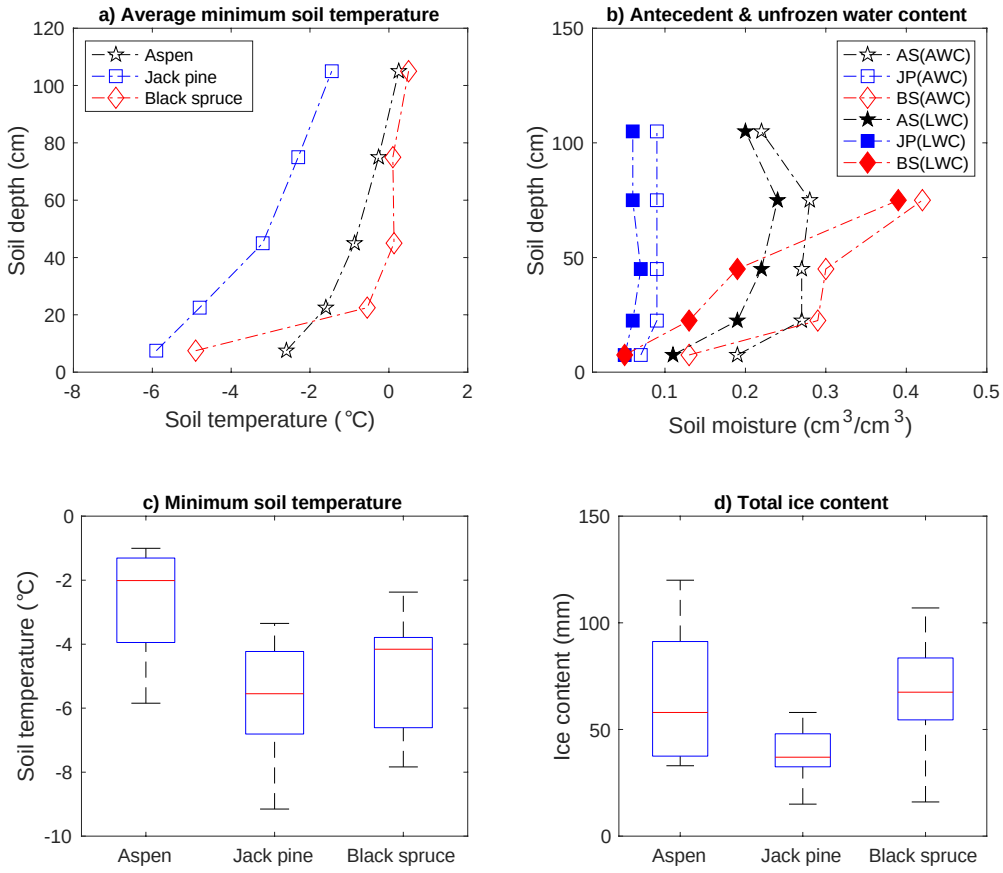

Figure 4.3 A comparison of a) mean annual minimum soil temperature as a function of depth, b) soil water content (AWC is the antecedent and LWC is the minimum liquid water content) as a function depth, c) inter-annual variability in average minimum soil temperature, and d) variability in total ice content among the study sites. Note: The length of the box in the plots represents the inter-quartile range (25th and 75th inter-quartiles), with the median denoted by a horizontal line within the box. The whiskers represent the minimum and the maximum values of the dataset and outliers were represented by "+".

The amount of energy required for melting the average snowpack and soil ice content (based on the observations from 2001 to 2015) was estimated and compared between sites (Figure 4.4). The total energy required for snowmelt and soil thaw was higher for the aspen site, by about 9-11 MJ m^{-2}, but was similar for jack pine and black spruce with a difference of about 2 MJ m^{-2}. The required energy for the warming phase (removing cold content) was smaller than the snowmelt phase and ranged from 7% to 19% of the total required energy for all sites. The energy required for the soil warming phase was the highest at the jack pine site because of higher mineral soil content, colder soil temperatures and deeper frozen depth. In general, the energy required for snowmelt was higher than energy required for soil thaw.

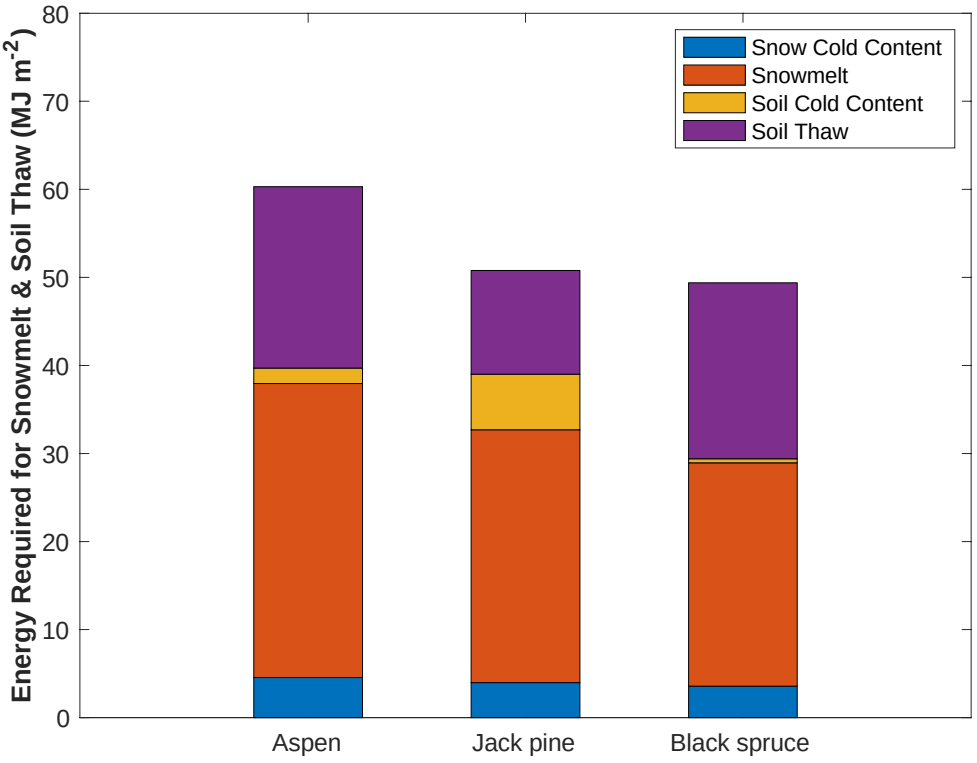

Figure 4.4 Energy requirement for snowmelt and soil thaw. Note: The average minimum snowpack temperature was assumed to be -20 °C at all sites for estimating energy required for warming phase.

4.3 INTER-SITE VARIABILITY OF SOIL THAW

The onset of soil thaw was similar at all three sites, but large differences were observed for soil thaw completion (Figure 4.5). For most years, soil thaw started from late March to early April, with smaller inter-annual variability compared to snowmelt start date (Figure 4.4). On average, the soil thaw start date lagged the onset of snowmelt by 12 days, with no difference among sites. Soil thaw end date was the earliest for aspen followed by jack pine and black spruce sites, respectively. The mean difference in thaw end date was 18 days between aspen and jack pine and 30 days between aspen and black spruce sites. Soil thaw completion typically occurred towards the end of April or early May for aspen, compared with the beginning of June for black spruce. The soil thaw duration varied from 2.5 to 5 weeks for aspen, 4 to 8 weeks for jack pine, and 6 to 10 weeks for black spruce site from 2001 to 2015. The average thaw duration was 4 weeks for aspen, 6 weeks for jack pine, and 8 weeks for black spruce.

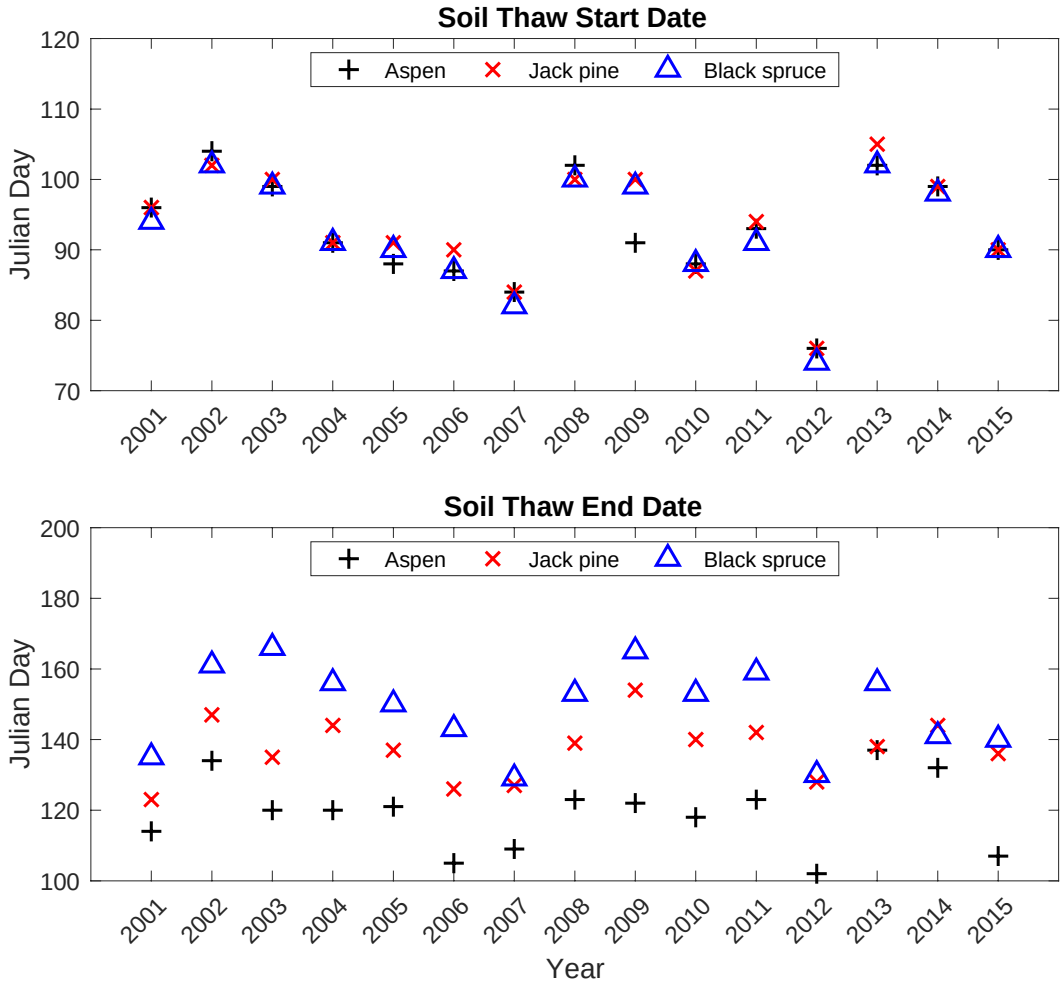

Figure 4.5 Onset and completion of soil thaw at aspen, jack pine and black spruce sites

4.4 INFLUENCE OF SOIL THAW ON CARBON UPTAKE

At both coniferous forest sites and for all years, net positive carbon uptake started after the onset of soil thaw but before its completion (Figure 4.6). However, uptake was delayed until well after completion of soil thaw for the deciduous forest. The average lag time was about 4 weeks, which is expected because the start of photosynthesis at aspen is delayed until leaf emergence. The onset date of carbon uptake was quite similar at both coniferous forest sites with a mean difference of only about 3 days.

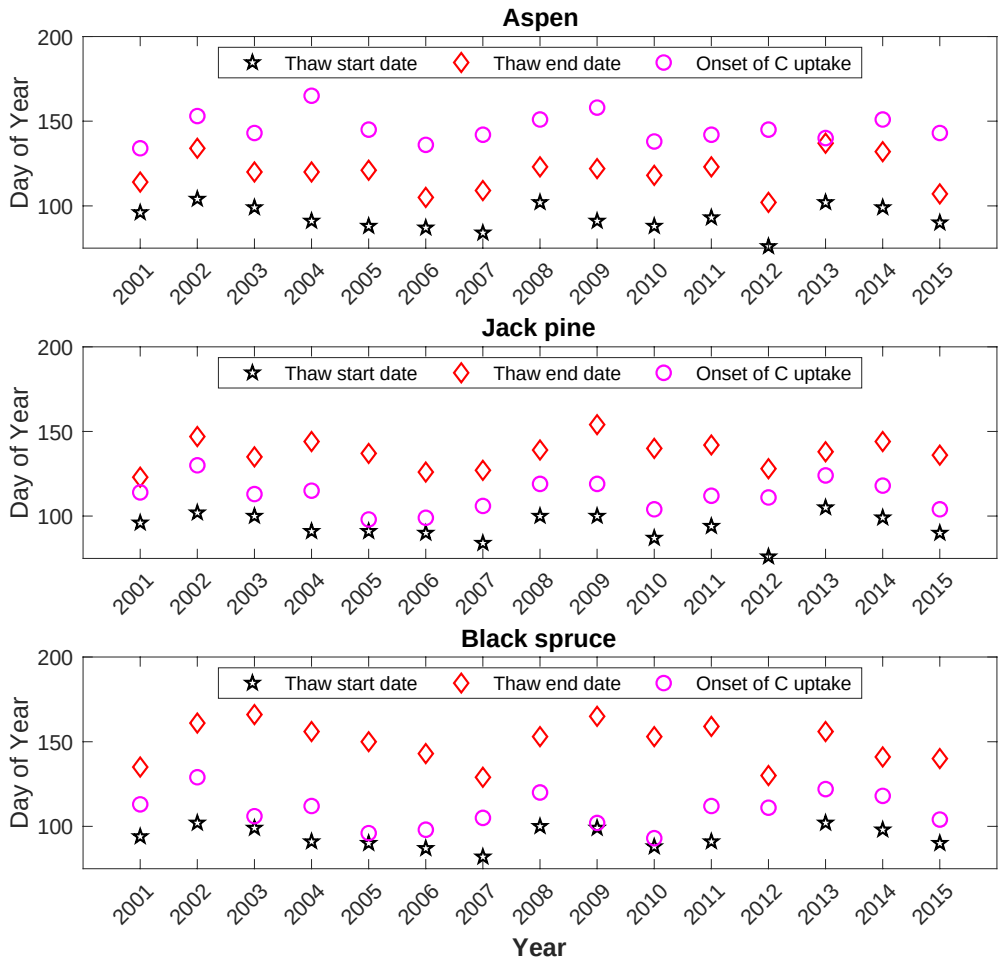

Figure 4.6 Onset of net positive carbon uptake, onset of soil thaw (2 cm depth), and completion of soil thaw for fifteen years (2001-2015)

Both the onset date of carbon uptake and the net annual carbon uptake were poorly correlated with the timing of snowmelt and soil thaw for the aspen site but a strong correlation was found for the coniferous forests (Table 4.2). This is not surprising as the onset of carbon uptake is associated with leaf emergence for deciduous forests which depends on other climatic controls (Barr et al., 2004). The onset of net positive carbon uptake was better correlated with snow ablation date than soil thaw start or end dates at any depth for the coniferous forests. The mean difference between onset of carbon uptake and snow ablation date was only 3 days at both coniferous forest sites. Net annual carbon uptake was also strongly (negatively) correlated with the completion of soil thaw

for coniferous forests; however, the correlation was stronger for deeper soil depths at jack pine and shallower depths at black spruce.

Table 4.2 A relationship of carbon uptake with snowmelt and soil thaw (mean absolute difference and correlation coefficient) based on 15 years of data (2001-2015). Statistically significant correlation between the variables at significance level $\alpha = 0.05$ is denoted by (*) sign.

Variable	Aspen		Jack pine		Black spruce	
	Correlation (r)	Mean Difference (Days)	Correlation (r)	Mean Difference (Days)	Correlation (r)	Mean Difference (Days)
Onset of net positive carbon uptake						
Snowmelt start date	0.44	67	0.66*	31	0.51	29
Snow ablation date	0.34	37	0.82*	3	0.89*	3
Soil thaw start date	0.23	53	0.66*	18	0.50*	17
Thaw end date (5 cm)	0.32	31	0.61*	11	0.36	17
Thaw end date (10 cm)	0.37	30	0.63*	12	0.19	26
Thaw end date (20 cm)	0.40	29	0.67*	14	0.06	38
Thaw end date (50 cm)	0.32	23	0.59*	19	-	-
Thaw end date (100 cm)	-	-	0.51*	25	-	-
Net Annual Carbon Uptake						
Snowmelt start date	0.34	-	-0.81*	-	-0.47	-
Snow ablation date	0.24	-	-0.63*	-	-0.83*	-
Soil thaw start date	0.35	-	-0.68*	-	-0.23	-
Thaw end date (5 cm)	0.24	-	-0.41	-	-0.76*	-
Thaw end date (10 cm)	0.23	-	-0.44	-	-0.55*	-
Thaw end date (20 cm)	0.24	-	-0.54*	-	-0.47	-
Thaw end date (50 cm)	0.25	-	-0.48*	-	-	-
Thaw end date (100 cm)	-	-	-0.58*	-	-	-
Soil thaw duration	-0.03		0.04		-0.27	

4.5 DISCUSSION

4.5.1 Measurement Uncertainty

The estimates of snow water equivalent and soil ice content both had important sources of uncertainty. For example, a systematic bias of +5.5 cm in snow depth measurements was identified and removed after field validation at the black spruce site, caused by soft forest floor (fluffy feather moss layer with organic soils) not providing a firm base for the snow depth measurement rod. This bias was not present at jack pine because of the firmer soil-snow interface. It was not investigated at aspen, but it is believed that the firm forest floor would have contributed negligible bias. The SWE estimates are sensitive to snow depth, where a bias of 5.5 cm could translate to an overestimation of SWE by 5 to 25 mm, depending upon snow density. However, after bias correction, it is believed that the SWE estimates reported in this study are accurate. In regards to reported soil ice contents, it can be considered that these are best estimates but contain uncertainty from several sources. First, the sensors for measuring soil water content were not calibrated for frozen conditions. Second, the estimates of antecedent water content were based on near zero soil temperature in fall but potential snowmelt and infiltration in the fall was ignored and assumed to be small, as was drainage below the freezing front. Third, the soil moisture sensors were not calibrated for site-specific soil types but this would likely have a small influence on the results because coarse-textured soils are present, where the default calibration works reasonably well. However, the soil ice content at the black spruce site is likely underestimated because of the thick organic soil layer at this site.

4.5.2 Influence of Site Characteristics on Soil Thaw

Completion of soil thaw at the aspen site was 18 and 30 days earlier than the jack pine and black spruce sites, respectively (Figure 4.5). The difference in soil thaw end date also varied by 2 weeks between the coniferous forests. These differences can be attributed to inter-site differences in net available energy beneath the canopy as well as to ice content and forest-floor characteristics influencing heat transport processes in the soil.

The early observed thaw at the aspen site, despite the higher energy requirements (Figure 4.4), was likely driven by higher available energy at the snowpack/ground surface. Below-canopy net radiation is controlled by several factors such as sky cover (cloudiness), solar elevation, topography (slope and aspect), vegetation architecture and density, surface albedo, and physical properties of the snow and ground surface (Chen et al., 1997; Gelfan et al., 2004; Kumar et al., 1997; Pomeroy et al., 2009; Seyednasrollah et al., 2013). Direct measurements of below canopy net radiation were not available for this study; however, canopy influences on radiation penetration are well established. The transmissivity of thermal as well as direct and diffuse shortwave radiation through the canopy has been observed to be much higher for deciduous compared to coniferous forests (Link and Marks, 1999; Timothy E. Link et al., 2004). The higher transmittance of radiation for deciduous forest is partially offset by the increased absorption and re-emittance of longwave radiation from the coniferous canopy (Essery et al., 2008; Pomeroy et al., 2009). In general, net radiation on the ground surface during the cold season tends to be the highest for forest clearings, followed by deciduous then coniferous forests (Mahat and Tarboton, 2012; Pomeroy and Granger, 1997; Rasmus et al., 2016). This would almost certainly have contributed to the relatively early completion of thaw for the aspen site in this study, despite its higher energy requirement.

The duration of soil thaw was similar to, or larger than, that of snow ablation (Figure 4.2 and Figure 4.5). This was at first surprising because the measured maximum SWE exceeded the estimated soil ice content requiring higher energy for melting snowpack (Figure 4.4), and because soil thaw occurred during a period of higher net radiation. Moreover, the inter-site differences were larger for soil thaw duration than snowmelt duration. This suggests that forest floor and soil properties strongly influence soil heat transport processes and are critical for soil thaw. The presence of moss and lichens at the coniferous sites could have contributed to insulating the underlying soil. Beringer et al. (2001) reported that the presence of a moss layer can reduce ground heat flux density by more than 50%. Furthermore, the thickness of the organic soil layer varied by an order of magnitude between the sites, from 2-3 cm at jack pine to 25-30 cm at black spruce. Compared to mineral layers, organic layers have higher water retention, lower thermal conductivity and about three times higher specific heat (Hillel, 1998). Thus, differences in the soil organic layer could explain the variability in heat transport processes between study sites. Since snow accumulation and ablation timing were quite similar for the two coniferous forest sites, the

delayed thaw at the black spruce site was likely caused by the differences in forest floor characteristics and soil properties which influenced ice content and heat transport processes.

4.5.3 Relationship between Soil Thaw and Carbon Uptake

The correlation between spring thaw (snowmelt and soil thaw) and carbon uptake was explored at all three sites. Carbon uptake started during spring thaw at both the coniferous forest sites and was better correlated ($r = 0.82$ to 0.89) with the date of snow ablation (Table 4.2) than soil thaw timing. These results are consistent with other studies relating the onset date of spring photosynthesis recovery with air temperature (Tanja et al., 2003) and snowmelt (Pulliainen et al., 2017) for boreal evergreen forests. In this study, net annual carbon uptake for the coniferous forest sites was also negatively correlated with the soil thaw end dates. This relationship was stronger for deeper depths at the jack pine site and shallower depths at the black spruce site. This was likely caused by the shallower rooting systems and higher soil water content at the black spruce site. In boreal forests, which have short growing seasons, soil thaw timing critically affects the length of the period when resources can be captured, which in turn affects the annual carbon uptake through the combined effects of soil warming on photosynthesis in spring and nitrogen mineralization in summer (Jarvis and Linder, 2000). Few previous boreal forest studies have related carbon uptake with soil thaw, and enhanced ecosystem productivity is commonly linked with other indirect metrices such as early spring warming (Grant et al., 2009; Welp et al., 2007) and increased growing season length (Piao et al., 2007). The timing of soil thaw may be a more robust indicator than the growing season length for annual NEP, because interannual variability of NEP is the highest in spring, controlled by the differential impact of the soil thermal environment on photosynthesis and respiration (Barr et al., 2009). No statistically significant correlation was found between carbon uptake and spring thaw date at the deciduous forest site. As opposed to the coniferous forests, photosynthesis is delayed until leaf emergence for the aspen site, which is dependent on other environmental variables such as soil temperatures or cumulative degree days (Barr et al., 2004). In this study, the onset of carbon uptake started at the aspen site when the 5-day moving mean of soil temperature at 10 cm and 20 cm depths reached at 7.4 ± 1.0°C and 6.7 ± 1.0°C based on 15 years (2001-2015) of observations.

4.5.4 Modelling Implications

Early soil thaw at the deciduous forest was almost certainly associated with increased below-canopy net radiation as compared to the coniferous forests. In contrast, differences in soil thaw timing between the two coniferous forests were governed by the varying characteristics of forest floor and mineral soil properties, as only small differences were noticed in snow accumulation and ablation at these sites. This suggests that appropriate representation of canopy-radiation interactions as well as heat and water transport processes of forest floor and underlying soil systems are critical for a reliable simulation of seasonal changes in the soil thermal environment by land surface models. Soil thaw modelling is particularly important for coniferous forests because of the strong inverse relationship between soil thaw end date and annual net ecosystem production (Table 4.2). In this study, large variability of soil thaw timing (2 to 4 weeks) was observed among proximate but contrasting forest stands, which suggests that consideration of site characteristics on soil thaw dynamics is critical when modelling and evaluating an ecosystem composed of different forest types. It was also observed that the correlation between soil thaw end date and annual carbon uptake was stronger at deeper depths for the dry jack pine forest and at shallow depths for the moist black spruce stand. We conclude that the relationship between soil thaw and biological awakening needs to be well understood and represented in climate models for reliable simulations of carbon, heat, and water fluxes.

4.6 SUMMARY

Site characteristics exert great control on soil thaw timing in seasonally frozen boreal forests. The inter-site variability of soil thaw was contrasted between two coniferous (jack pine and black spruce) forests and one deciduous (aspen) forest, using 15 years of data. All three sites received similar seasonal snowfall but net snow accumulation at the deciduous site was 15% to 20% higher than the coniferous forests. Similar snowmelt and soil thaw start dates were observed at all sites. Small differences were observed among sites in snow ablation dates, whereas large differences were observed for soil thaw end date. The soil thaw completion at the aspen site was about 2.5 weeks earlier than the jack pine site and about 1 month earlier than the black spruce site despite higher energy requirements for spring thaw, which was likely caused by increased energy availability because of leafless canopy in spring. The difference in thaw timing between the two

coniferous forest sites was driven by coarser soil texture and thicker forest floor at the black spruce site causing higher ice content and providing better insulation. Thus, appropriate representation of canopy-radiation interactions and heat and water transport processes in forest floor and underlying soil systems in land surface models is critical for realistic simulations of soil thaw in boreal forests. Net annual carbon uptake was negatively correalted with soil thaw timing for coniferous forest sites but no statistically significant correlation was found for the deciduous forest site. It was also observed that the correlation between carbon uptake and soil thaw end date was stronger for shallower depths at the black spruce site and deeper depths at the jack pine site. These results highlight the ecological importance of soil thaw timing in the southern boreal forest: its high interannual variability, its variability among forest-cover types, and its strong influence on ecosystem productivity for coniferous forests.

CHAPTER 5 SIMULATING WINTER-SPRING HYDRO-THERMAL PROCESSES IN THE SOUTHERN BOREAL FORESTS: DIAGNOSTIC MODEL COMPARISON

Acknowledgement: A very special thanks to Amber Peterson and Mahtab Nazarbakhsh for providing technical support in running and compiling results for CRHM and CLASS models for this study.

5.1 CHAPTER OVERVIEW

In support of the goal to model the winter-spring transition in the southern boreal forest, a diagnostic evaluation of three models (CLASS, CRHM and SHAW) was completed at the jack pine site to help select the most appropriate model. This evaluation was also useful to identify key areas for model improvement. The ability of these models to simulate the relevant processes was expected to vary because of differences in process representation, and also because of their development purposes. For example, SHAW was developed for simulating soil freeze/thaw processes; thus, has a very detailed representation of heat and water transport processes in soils but a simplified representation of canopy-snow interactions. In contrast, CLASS and CRHM have more detailed representation of canopy-snow processes but the soil thermal regime is modelled with fewer details. In this chapter, differences between the models for simulating snow accumulation, snowmelt, soil thaw timing, and spring evapotranspiration are reported and potential causes for any divergences are discussed. The model setup and parametrization details have been provided in Section 3.6.1 and the performance evaluation criteria described in Section 3.6.2.

5.2 SNOW ACCUMULATION AND MELT

Snow interception by the canopy and its subsequent unloading will influence sublimation losses and snow accumulation on the ground. The total observed seasonal sublimation values (17 mm for 2013-14, 16 mm for 2014-15, and 18 mm for 2015-16) were constrained by small vapour pressure gradients and accounted for about 15% to 20% of the seasonal snowfall. This was consistent with the previously reported observations and CLASS simulations for this site (Barlett et al., 2006). Differences between observed and simulated seasonal (mid-November to mid-April) sublimation losses (surface sublimation + intercepted snow sublimation) were small for all the years (Figure 5.1). The sublimation losses were overestimated by CLASS (2 to 6 mm) and underestimated by CRHM (4 to 6 mm). The SHAW bias was slightly lower (up to 4 mm) with its calibrated maximum intercepted precipitation parameter.

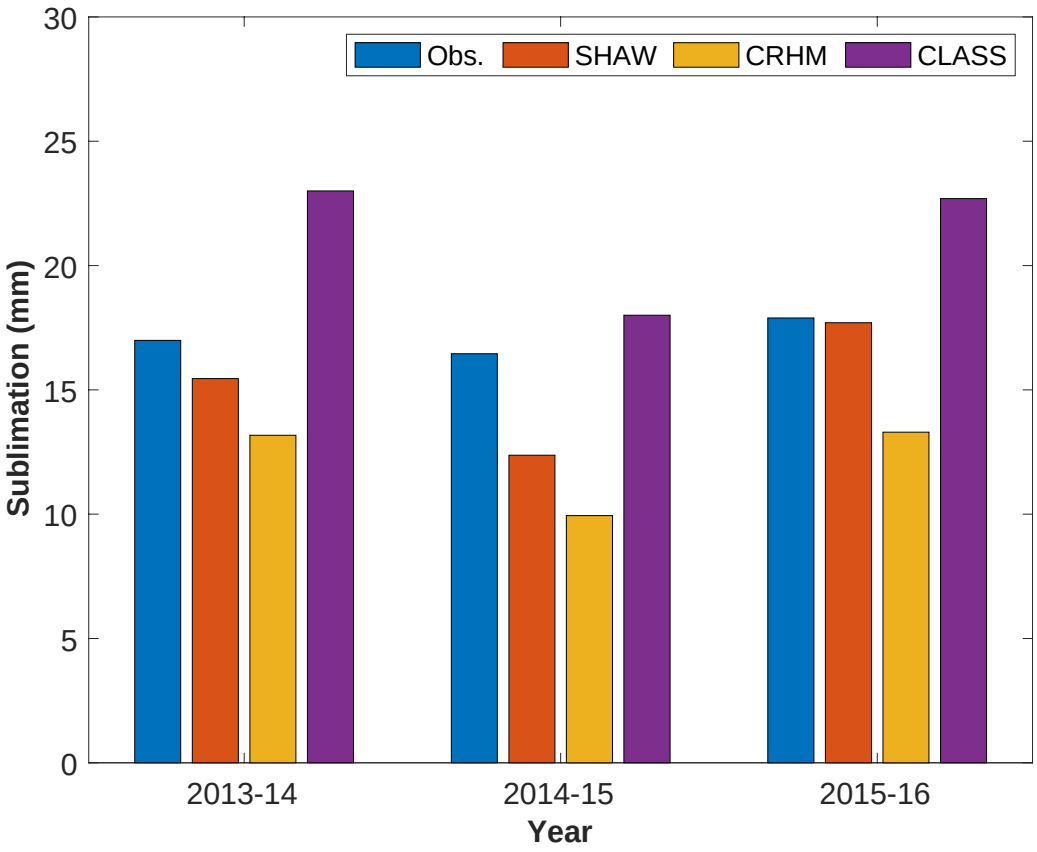

Figure 5.1 Seasonal sublimation loss estimates from November 15 to April 15 at BERMS old jack pine site

The observed snow accumulation and melt, compared to the model simulations are shown in Figure **5.2**. All three models simulated similar snow accumulation in winter (November to February) except for 2014-15 when CLASS underestimated snow accumulation by about 20 mm compared to the CRHM and SHAW. This was caused when CLASS simulated a large snowmelt (about 15 mm) in early fall of 2014 because of a warming event. For spring snowmelt, the three models produced distinct patterns. In CLASS, melt began earlier and initially proceeded faster, followed by a more gradual snowpack ablation at the end. In contrast, SHAW simulated very small melt events in early spring and rapid snowpack ablation later in the season. For CRHM, the snowmelt pattern was similar to CLASS in early spring and to SHAW near ablation but with smaller magnitudes. Based on these 3 years of observation, SHAW underestimated intermittent melt events in spring, CRHM performed better for capturing snowmelt in 2014-15 and 2015-16

whereas CLASS performance was superior in 2013-14. Surprisingly, all the models predicted similar snow ablation timing despite the differences in melt rates (Table 5-1). The difference between simulated and mean observed snow ablation date, when snowpack completely disappeared from the ground, ranged from 1 to 9 days. Simulated snow ablation was consistently late by 1 to 4 days for CLASS and SHAW. The CRHM simulated snow ablation timing varied by 1 day for the last two years (2014-15 and 2015-16) and by 9 days for the first year (2013-14). An example snow ablation week for 2015 is shown in Figure 5.3 with the aid of above and below canopy time-series photographs.

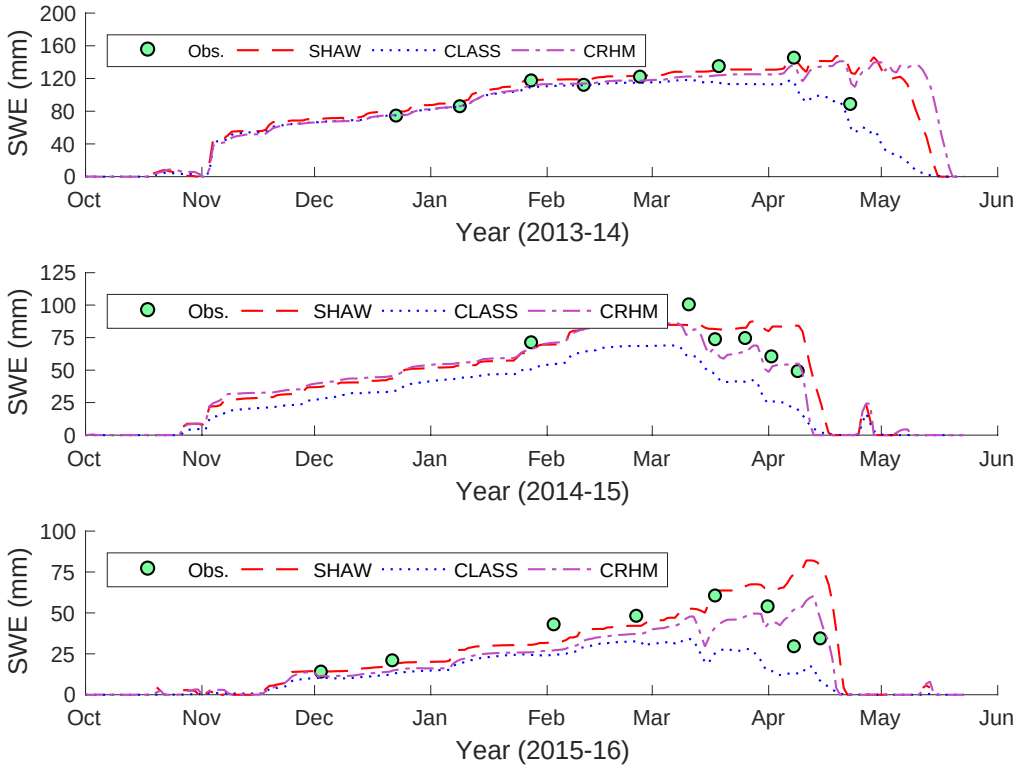

Figure 5.2 **Simulated and observed snow water equivalent (SWE) at the jack pine forest site**

Table 5.1 Modelled and observed snow ablation time

Methods	Snow ablation time		
	2013-14	**2014-15**	**2015-16**
Observation			
NDVI	10-May	12-Apr	18-Apr
Snow Temperature	-	12-Apr	17-Apr
Snow depth SR-50 (snow harp)	-	13-Apr	19-Apr
Snow depth SR-50 (Geonor)	12-May	15-Apr	19-Apr
Snow depth SR-50 (soil pit)	2-May	11-Apr	16-Apr
Photographs			
Cryocam	-	17-Apr	19-Apr
Snowharp camera	-	15-Apr	18-Apr
Mean Observed	**11-May**	**14-Apr**	**18-Apr**
Models			
SHAW	15-May	18-Apr	20-Apr
CLASS	15-May	16-Apr	19-Apr
CRHM	20-May	13-Apr	19-Apr

Note: The three automated snow depth measurements by SR-50 show differences in ablation date of up to 10 days, reflecting the onset of a patchy snowcover. The latest of the three was used to estimate the ablation date.

Figure 5.3 Photographs taken during a week of snow ablation in 2015. (Photographs in the bottom row were taken on April 09, 12, and 17, 2015)

5.3 SOIL THAW

With respect to soil thaw timing, SHAW outperformed both CLASS and CRHM (Figure 5.4). The SHAW model had a small early bias of 1 to 7 days but had a remarkable ability to simulate thaw progression from 10 cm to 100 cm depth. CLASS had an early, but more variable, bias in soil thaw end date that ranged from 1 to 22 days. The CRHM model had the most inconsistent performance, predicting thaw 7 to 42 days late in 2014 and an early thaw by 2 to 20 days in 2015 and 2016. Hejazi and Woodbury (2011) also reported that the soil temperature simulations by the SHAW model were in good agreement with the observations (higher correlation and smaller absolute error) based on 10 years of data 1997-2006 at this site.

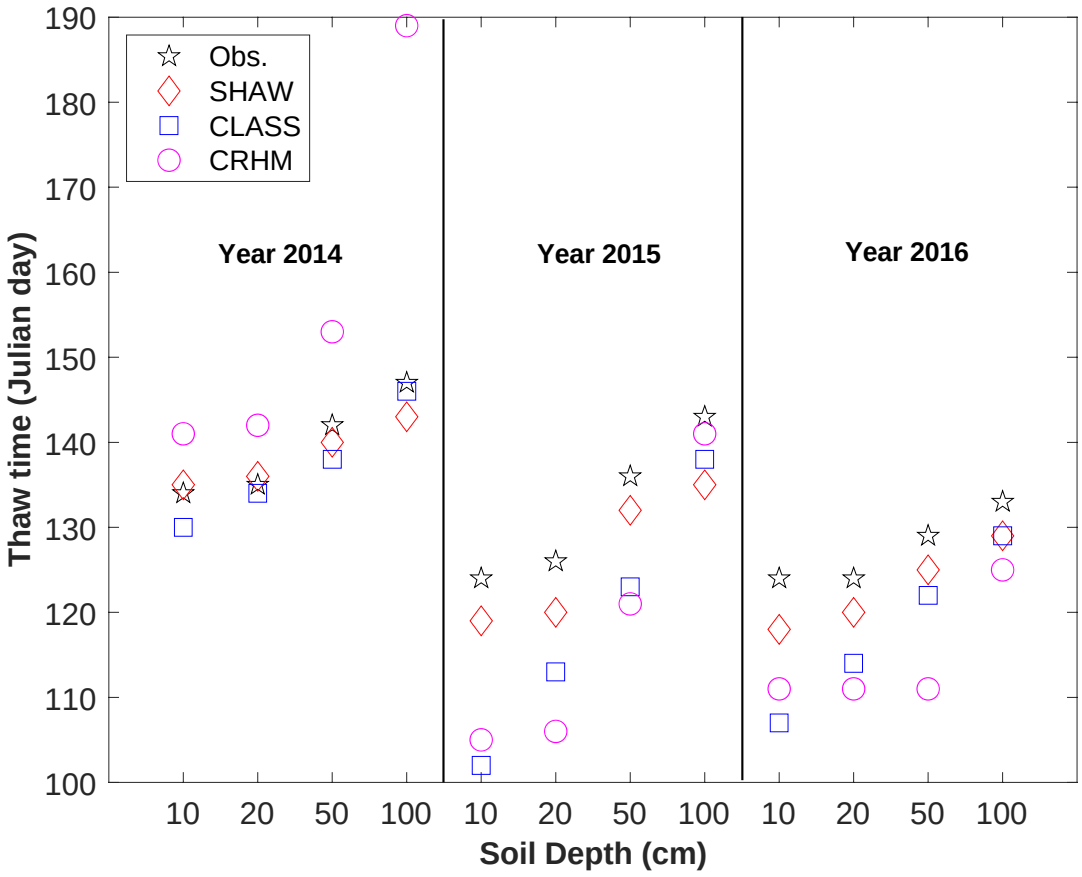

Figure 5.4 Simulated and observed last day of thaw at different soil depths

5.4 SPRING EVAPOTRANSPIRATION

All three models reproduced fall, winter and summer fluxes of daily latent heat reasonably well but the spring (April 1 to June 15) was not adequately captured (Figure 5.5). Although CLASS and SHAW performed well in simulating the timing of the spring transition (the time when latent heat flux starts to increase in early spring), but both models overestimated daily latent heat fluxes during the spring season. For CRHM, the timing of the 2014 spring transition was simulated to occur considerably late and displayed an on-off behavior in 2015. This behaviour is caused by CRHM using the timing of snow ablation as a trigger for evapotranspiration, whereas CLASS and SHAW use an air temperature threshold for the onset for spring evapotranspiration. After snow ablation, CRHM also overestimated the daily latent heat fluxes in the spring. The mean absolute error between the observed and simulated latent heat flux was highest in May and ranged from 21 W m^{-2} to 34 W m^{-2} for CRHM, 24 W m^{-2} to 40 W m^{-2} for CLASS, and 25 W m^{-2} to 34 W m^{-2} for SHAW. The mean bias error was similar to the mean absolute error for CLASS and SHAW (23 W m^{-2} to 40 W m^{-2}) but much smaller for CRHM (-5 W m^{-2} to 22 W m^{-2}). The smaller bias for CRHM occurred because evapotranspiration was not triggered until snow ablation, resulting in underestimation of latent heat flux in early spring.

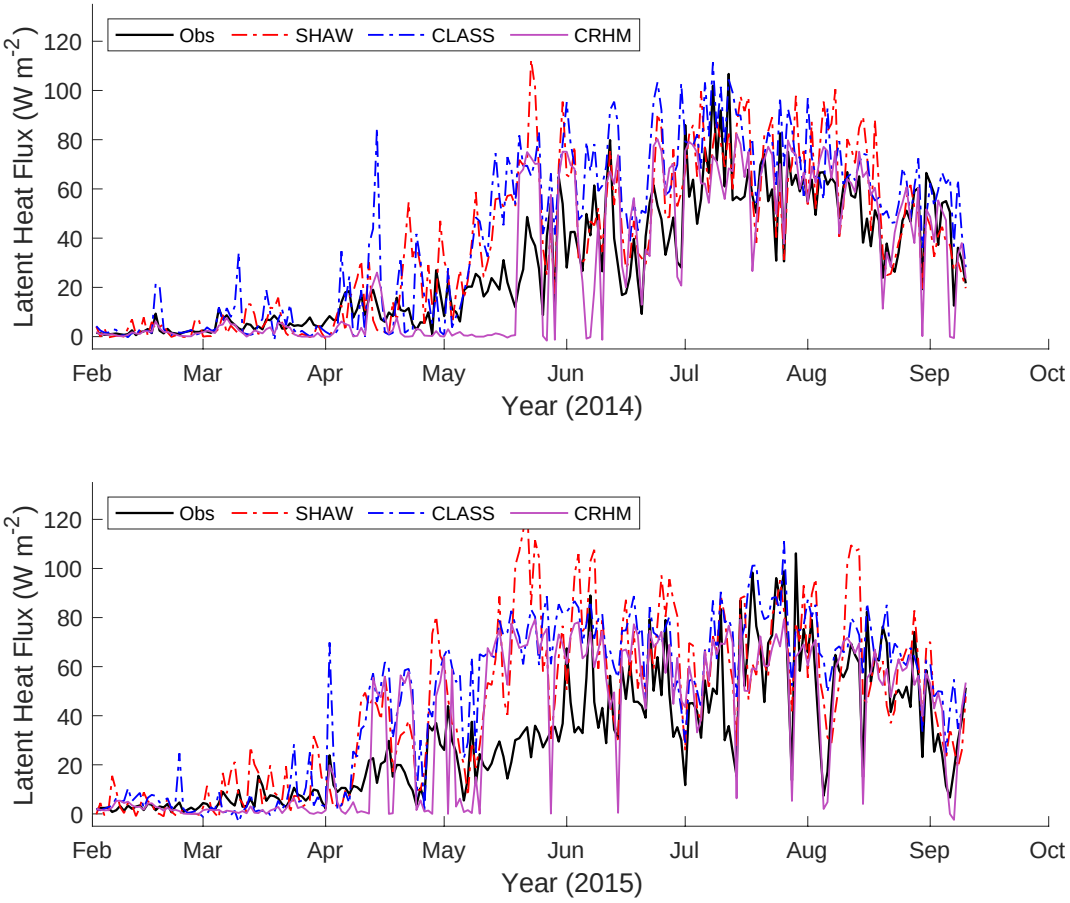

Figure 5.5 Simulated and observed daily latent heat fluxes at old jack pine site

The cumulative spring evapotranspiration was overestimated with large inter-annual variability (Figure 5.6). The difference between observed and simulated spring evapotranspiration was smaller (ranging from 6 to 60 mm) for the year 2013-14 when the snow ablation date was late, as compared to 40 to 95 mm for early ablation years 2014-15 and 2015-16. The CLASS model simulated the largest difference of 60 to 95 mm followed by SHAW (40 to 75 mm) and CRHM (6 to 40 mm). The mean absolute error in cumulative ET was 80 mm for CLASS, 64 mm for SHAW, and 29 mm for CRHM.

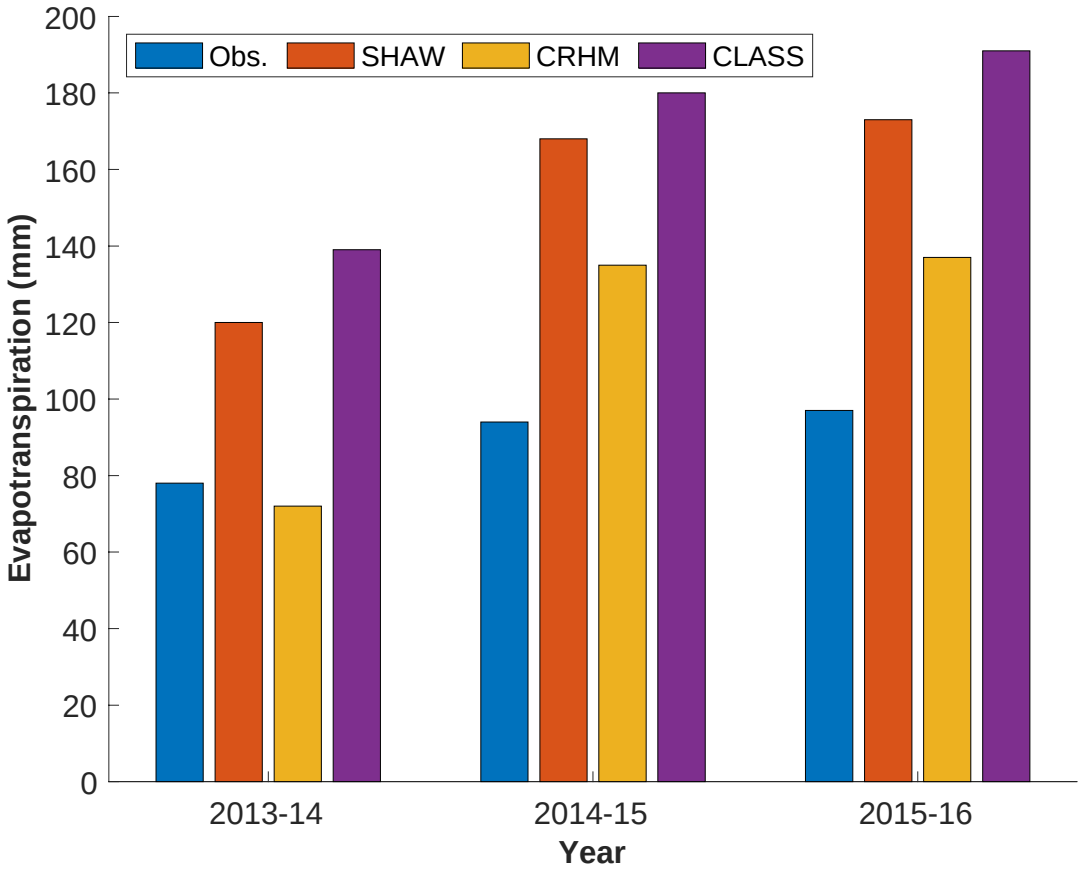

Figure 5.6 Simulated and observed spring evapotranspiration (April 01 to June 15)

5.5 DISCUSSION

Snow interception and unloading processes influence sublimation losses and snow accumulation on the ground (Essery et al., 2003; Mahat et al., 2013; Molotch et al., 2007). Total seasonal (November 15 to April 15) snow interception by the canopy was 80, 56, and 87 mm for CLASS, 68, 50, and 62 mm for CRHM, and only 11, 8, and 10 mm for SHAW for 2013-14, 2014-15, and 2015-16, respectively. Although CLASS and CRHM simulated much higher snow interception than SHAW, the simulated seasonal sublimation losses were similar between the models. This is because only CLASS and CRHM consider snow unloading from the canopy and both models simulated unloading of large fractions of intercepted snow. Total seasonal unloading of intercepted snow was 64% to 75% for CLASS and 92% to 94% for CRHM. The intercepted snow unloaded from the canopy in 2 to 5 days for CLASS and 1 to 4 days for CRHM. The differences between CLASS and CRHM for canopy snow interception and subsequent unloading were caused by their differences in parametrization routines for maximum interception capacities and unloading. For example, the maximum interception capacity is an input parameter within CRHM but is determined from the fresh snow density in CLASS. Snow unloading is also a function of the ice bulb temperature in CRHM in addition to an exponential function of time as in CLASS. Bartlett et al. (2008) also reported that the intercepted snow at this old jack pine site quickly unloads (within 1 to 2 days) from the canopy based on the observations of above canopy albedo and photographs, which may be caused by high wind speed (inter-quartile range of half-hourly observations from November 15 to April 15 is 2.1 m s^{-1} to 3.6 m s^{-1} with a maximum of 11 m s^{-1}). In the present study, SHAW captured sublimation losses and snow accumulation reasonably well without an unloading mechanism but with far less snow interception than would have actually occurred. For typical snowfall events of 0.1-5 mm at the study site, snow interception could be up to 2 mm, or potentially much higher for larger snow events (Pomeroy et al., 1998a). However, the maximum instantaneous canopy interception simulated by SHAW was only 0.3 mm. Overall, the snow accumulation was better simulated by calibrating the maximum intercepted precipitation parameter thereby significantly reducing snow interception. A caveat of this approach is that calibration of the parameters for snow interception should also be applicable to rain interception for modelling evapotranspiration throughout the year as SHAW does not differentiate between rain and snow for interception. Although, canopy water storage and evaporation loss from the

intercepted rainfall are not well established for the study site yet it can be anticipated that the rain interception would be underestimated (Hadiwijaya et al., 2021; Pypker et al., 2005) by the use of calibrated maximum interception capacity parameter (0.05 mm per unit leaf area index). This deficiency didn't result in underestimation of the latent heat fluxes in summer (Figure 5.5), likely because of two reasons: (1) the SHAW model doesn't have unloading mechanism so all intercepted rain evaporated (2) transpiration from the canopy dominates evapotranspiration losses in the southern boreal forest (Rebeca Quiñonez-Piñón and Valeo, 2020). The simplified representation of canopy snow interception/unloading processes like SHAW may not be suitable for modelling snow accumulation in areas with high sublimation losses and/or where snow is retained on the canopy for longer durations.

All three models simulated large differences in spring snowmelt rates (Figure **5.2**). The SHAW model missed or simulated much smaller snowmelt events in early spring likely because of two main reasons. First, large temperature gradients are simulated in its multi-layer snowpack system and snow surface melt is likely refrozen in colder snowpack layers. Second, the simulated cumulative below-canopy fluxes of sensible and latent heat accounted for 15% to 30% of the below-canopy net radiation during the time of melt (March 1 to snow ablation), reducing the available energy for snowmelt (Appendix C). Like SHAW, CRHM simulated higher below canopy turbulent fluxes (30% to 35% of below canopy net radiation fluxes) but the model does not track snow temperatures and snowmelt signal is activated by an albedo subroutine (Gray and Landine, 1988). Also, the change in internal energy of the snowpack is associated with minimum air temperature. The snowmelt/snowpack energy balance approach in CRHM worked well for two out of three years (Figure **5.2**). The CLASS model tended to overestimate snowmelt in early spring and underestimate it towards the end of the season. The higher snowmelt in early spring may be caused by smaller below-canopy turbulent fluxes (up to 5% of below canopy net radiation). The gradual snowpack ablation simulated by CLASS later in the season was inconsistent with the other models (Figure **5.2**), as well as with previously reported historical observations and simulations (Barlett et al., 2006; Gelfan et al., 2004; Mahat and Tarboton, 2014). For example, the CRHM and SHAW models simulated 4-5 times larger magnitude of snowmelt than CLASS after the point when the snowpack was reduced to about 20 mm. This was caused by the fractional snow coverage routine of the CLASS model which distributes available energy between the snowpack and the

ground surface when snow depth is reduced to 10 cm. A patchy snowpack was developed in CLASS about 2 weeks earlier than actually observed for 2014-15 and 2015-16 and about the same time for 2013-14. The observation for patchy snowpack was based on automated snow depth measurements for the first year and above canopy time series photographs for the later years. The fractional snow covered area in CLASS is determined by dividing the simulated snow depth as it reaches to the threshold of 0.1 m by this limiting depth (MacDonald et al., 2016). Other studies have also reported the problem of gradual melt of the snowpack which resulted in simulating delayed snow ablation (Pomeroy et al., 1998a; Slater et al., 2001). Local horizontal advection is an important process for patchy snowpack which significantly increases snowmelt (Mott et al., 2018) but could not be considered in a vertical one-dimensional CLASS model; thus, may be a limiting factor for representing patchy snowpack in the model.

Soil thaw completion was better simulated by SHAW than by CLASS and CRHM (Figure 5.4). The SHAW provision for considering the insulation effects of ground cover by a residue layer in the model played an important role in this performance. For instance, an earlier and more variable soil thaw completion was predicted by SHAW at different soil depths (10-, 20-, 50-, and 100-cm) that ranged from 3 to 17 days when the model was run without ground cover layer (Table 5.2). Porada et al. (2016) also reported that lichens significantly impact soil temperatures at high latitudes and a process-based representation of their thermal properties is crucial for simulating a realistic soil thermal environment. Both CLASS and CRHM lacked this ability to represent ground cover in the model. The CLASS model consistently predicted earlier soil thaw end dates than observed and with larger differences at shallower depths than deeper depths which may also be caused by earlier development of fractional snow coverage than observed as discussed above. The CRHM model predicted delayed soil thaw completion for the first year (2014) and earlier than observed for the following years. This pattern may be caused by reduced soil water content for the later years as the freeze-thaw algorithm interacts with the soil module to restrict infiltration to thawing soils in spring.

Table 5.2 Difference (Observed - simulated) in SHAW simulated soil thaw timing (days) at different depths with and without considering residue layer in the model

Soil depth (cm)	2013-14		2014-15		2015-16	
	Residue	No residue	Residue	No residue	Residue	No residue
10	-1	-1	5	16	6	10
20	-1	-1	6	15	4	8
50	2	3	4	16	4	10
100	4	6	8	17	4	9
Average	**1**	**2**	**6**	**16**	**5**	**9**

All three models simulated similar fluxes of latent heat in summer (Figure 5.5) despite using different input values for the minimum stomatal resistance. This is because the CRHM uses Penman-Monteith equation and bulk surface resistance (100 s m^{-1}) was input in the model which would be 260 s m^{-1} for leaf resistance based on leaf area index of 2.6 m^2 m^{-2}, similar to what was used for CLASS (250 s m^{-1}). For SHAW, a higher value (500 s m^{-1}) was used as environmental controls (such as air temperature, radiation, vapor pressure deficit) on stomatal conductance were switched off as opposed to CLASS and CRHM. A value of 200 s m^{-1} for stomatal conductance, similar to other models, was obtained for SHAW when the model was calibrated by considering these environmental controls.

The common problem of all three models overestimating spring evapotranspiration was noted (Figure 5.6). Many modelling studies have reported similar overestimation of spring evapotranspiration in boreal coniferous forests at high latitudes. For example, Kuchment and Demidov (2006) developed a coupled model of the hydrological and carbon cycles in a forested ecosystem. The testing of the model on an hourly time scale at the same jack pine site as in this study resulted in high-biased simulations for spring evapotranspiration. Bonan et al. (1997) also reported similar results for a coniferous forest on a daily time scale. Nazarbakhsh et al. (2019) recently documented the overestimation of spring evapotranspiration by the CLASS and CLASS-CTEM models and investigated its controls. They concluded that the problem cannot be resolved

by the parametrization of soil hydraulic properties, root distribution, leaf area index or stomatal conductance. Mellander et al. (2004) reported that low soil temperatures reduced transpiration for scot pine in northern Sweden. Mellander et al. (2006) showed that simulated spring evapotranspiration can be greatly improved by considering the effects of low soil temperatures on stomatal conductance in the models. In this study, all three models lacked this ability which may have likely led to large errors in simulating latent heat fluxes in spring.

5.6 SUMMARY

The performance of three models (CLASS, CRHM, and SHAW) was evaluated for simulating winter-spring transition within a jack pine forest for 3 winters (2013-14 to 2015-2016). The SHAW model simulated seasonal sublimation losses and snow accumulation that were similar to CLASS and CRHM after reducing its interception capacity to smaller than expected actual magnitudes. This interception capacity was reduced because SHAW does not consider unloading and it was demonstrated that most of the intercepted snow (64% to 94%) quickly unloaded from the canopy in both CRHM and CLASS. All three models simulated distinct snowmelt patterns but surprisingly similar snow ablation dates (with a difference of only 1 to 5 days). The SHAW model predicted soil thaw completion dates at different depths (10-, 20-, 50-, and 100-cm) which were more accurate than CLASS and CRHM. The SHAW ability to represent ground cover (lichen) by a dead plant residue layer for considering its insulation effects on underlying soils played an important role for its better performance. All three models performed well for simulating winter, fall, and summer fluxes of latent heat flux but spring evapotranspiration was overestimated by 40 to 95 mm during 3-year of analysis. The mean absolute error ranged from 29 to 80 mm. The problem of overestimation of spring evapotranspiration by the models for coniferous boreal forests should be further investigated.

CHAPTER 6 MODELLING SOIL THAW TIMING AND SPRING EVAPOTRANSPIRATION USING SHAW

6.1 CHAPTER OVERVIEW

The SHAW model was selected for extended modelling of the winter-spring transition at all three study sites based on its performance evaluation for three years at the jack pine site (Chapter 5). However, it is clear that additional work will be needed to optimize or enhance the model to correctly simulate spring evapotranspiration. Conveniently, the model uses a Jarvis-Stewart type resistance scheme, so additional controls on stomatal conductance can be easily integrated. The model parametrization details for simulating soil thaw at all sites have been described in Section 3.7.1 and relevant results are presented in this chapter (Section 1.1). Regarding spring evapotranspiration, the results of model parameters uncertainty and sensitivity analysis are first presented (Section 6.3.1). An additional control on stomatal conductance to consider the influence of low soil temperatures in spring using cumulative growing degree days is then proposed based on long-term site observations (Section 6.3.3). The results for model performance evaluation at the jack pine site are presented in Section 6.3.4 with and without considering the proposed growing degree days factor. The model validation for all three sites and for extended record is presented in Section 6.3.5.

6.2 MODELLING SOIL TEMPERATURE/THAW COMPLETION

6.2.1 Parametrization of Ground Cover Layer

Ground cover parameters (thickness, fractional coverage, and albedo) were calibrated for soil temperature (described in Section 3.7.1). All three independent trials of parameter optimization produced similar parameter values (Table 6.1.) Without a ground cover layer , soil temperature simulations were cold biased throughout the year at the aspen site and warm biased in summer at the jack pine and black spruce sites (Figure 6.1). The maximum difference between observed and simulated soil temperature decreased from 5.5°C to 2.9°C for the aspen site, 6.0°C to 2.7°C for the jack pine site, and 4.9°C to 3.9°C for the black spruce site by considering a ground cover layer in the model. The mean absolute error was reduced from 1.5°C to 0.4°C for the aspen site, 1.2°C to 0.6°C for the jack pine site, and 1.2°C to 0.7°C for the black spruce site.

Table 6.1 Calibrated model parameters for ground cover properties

Properties	Unit	Aspen	Jack Pine	Black Spruce
Ground cover thickness	cm	4	2	5
Fractional coverage	%	80	100	100
Albedo	-	0.10	0.25	0.25

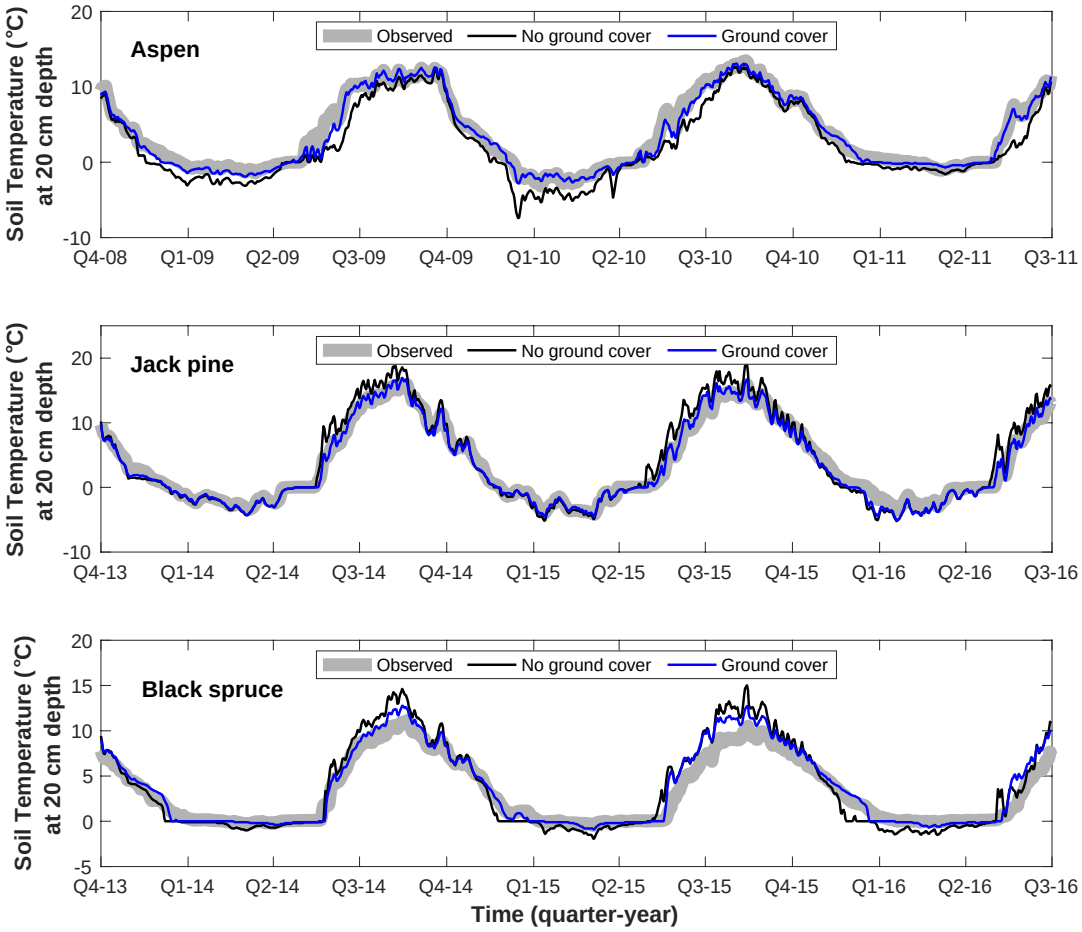

Figure 6.1 Observed and model simulated soil temperatures with and without considering surface cover layer

6.2.2 Modelling Soil Thaw Completion

The simulated soil thaw end dates were improved at all three sites by considering a ground cover layer in the model (Figure 6.2). The maximum difference between the observed and simulated soil thaw timing was reduced from 2 to 2.5 weeks to about 4 days. The model also captured the inter-annual variability of soil thaw, which varied from 4 to 6 weeks, at all three sites.

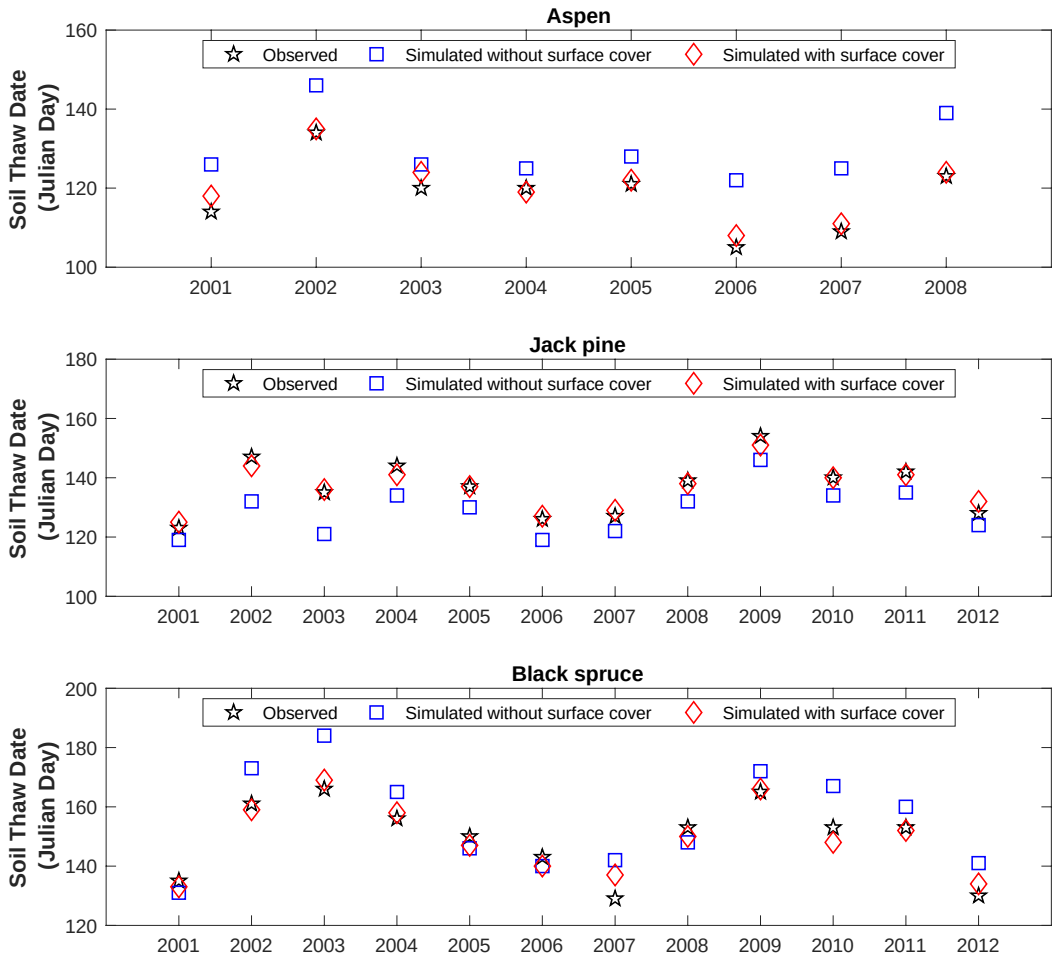

Figure 6.2 Observed and model simulated soil thaw timing (1-m depth) with and without surface cover layer

6.3 MODELLING EVAPOTRANSPIRATION

6.3.1 Uncertainty and Sensitivity Analysis

The global sensitivity and uncertainty analyses were completed for both the coniferous forest sites. However, very similar results were obtained for both the sites. Therefore, only results for the Jack Pine study site are presented and discussed here.

For uncertainty analysis, the top 5% simulations (2500 model runs) for latent heat flux were compared against the observations. The model consistently overestimated latent heat flux in spring when controls of environmental variables (solar radiation, air temperature, vapor pressure deficit) on stomatal conductance were not considered (Figure 6.3). Spring simulations were improved by considering environmental variable controls (Figure 6.4); however, the model consistently underestimated latent heat flux in summer. Overall, no combination of model parameters adequately captured observed fluxes of latent heat thorughout the year. This suggests that the problem of overestimation of spring evapotranspiration (ET) by SHAW cannot be resolved with existing model structure and some additional controls on ET in boreal coniferous forests need to be understood and incorporated in the model.

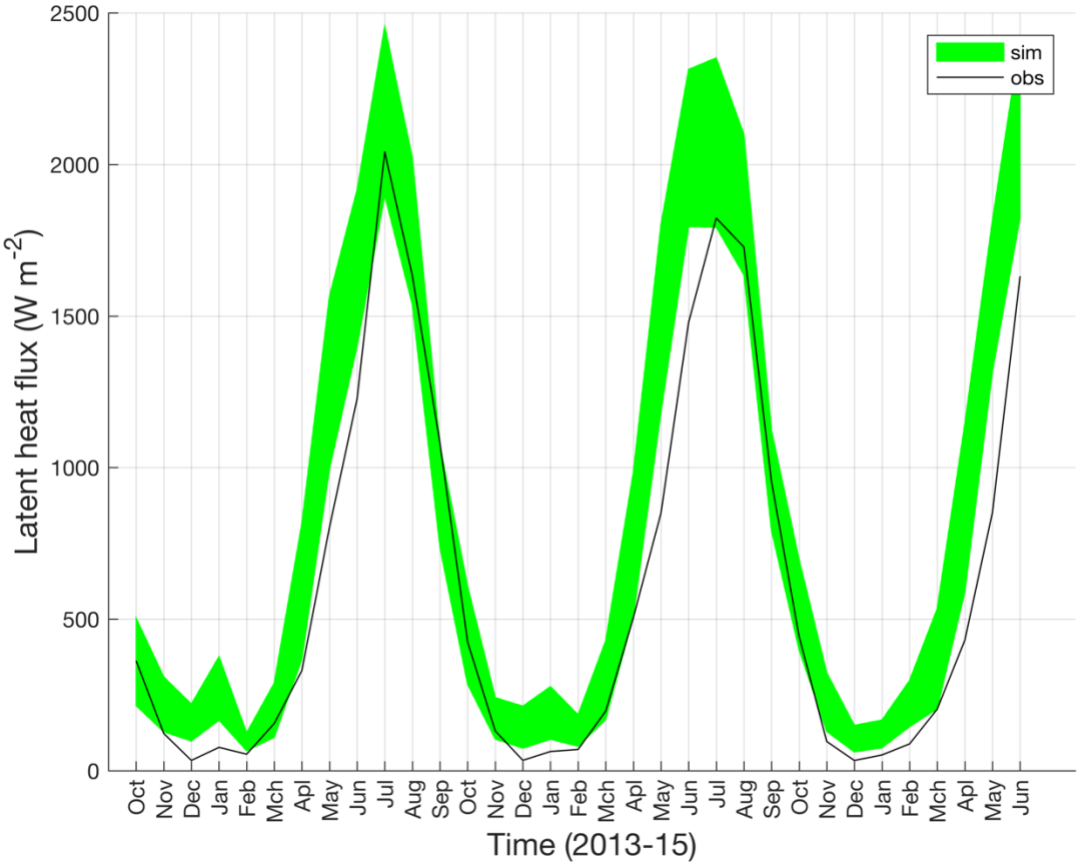

Figure 6.3 Observed and simulated (without considering controls of environmental variables on stomatal conductance) latent heat flux at jack pine

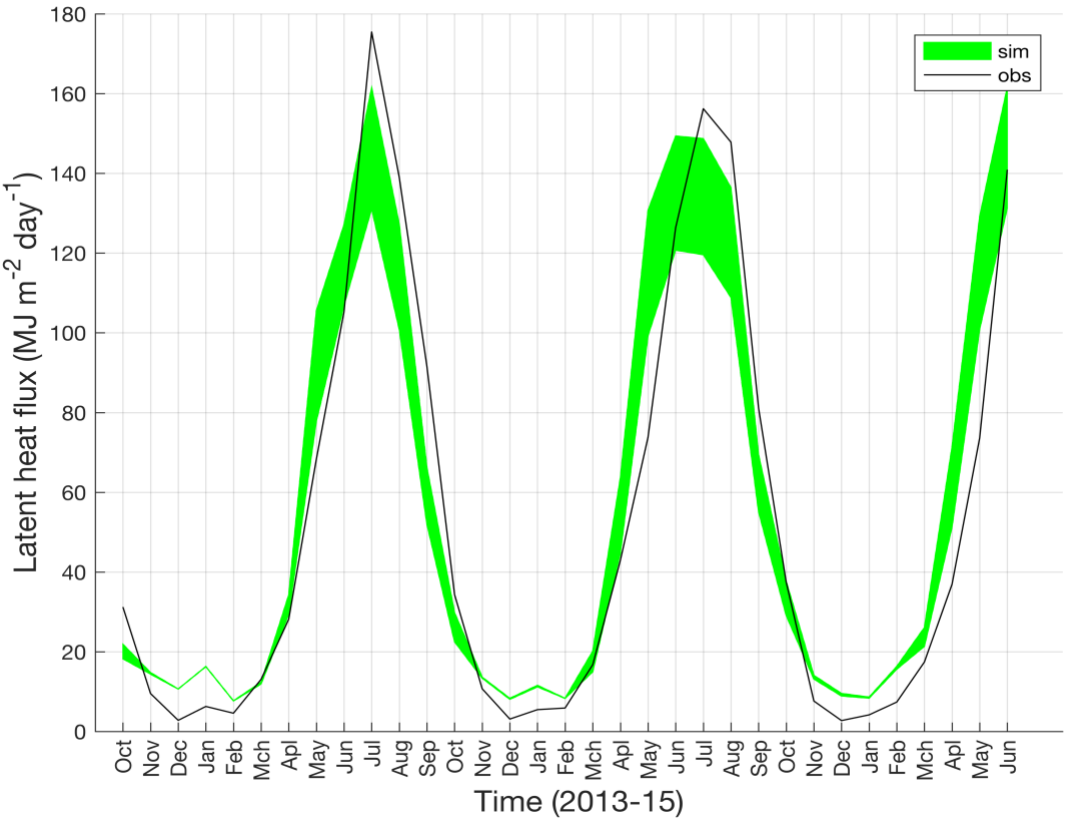

Figure 6.4 Observed and simulated (considering controls of environmental variables on stomatal conductance) latent heat flux at jack pine

The global sensitivity analysis showed that the SHAW was most sensitive to minimum stomatal resistance and vapor pressure deficit function parameters (Figure 6.5 and Figure 6.6) for simulating latent heat flux. The results suggested that for the known value of minimum stomatal resistance, the r-VPD parameter of vapor pressure deficit function dominates uncertainty in simulations i.e. parameter sensitivity was 92%.

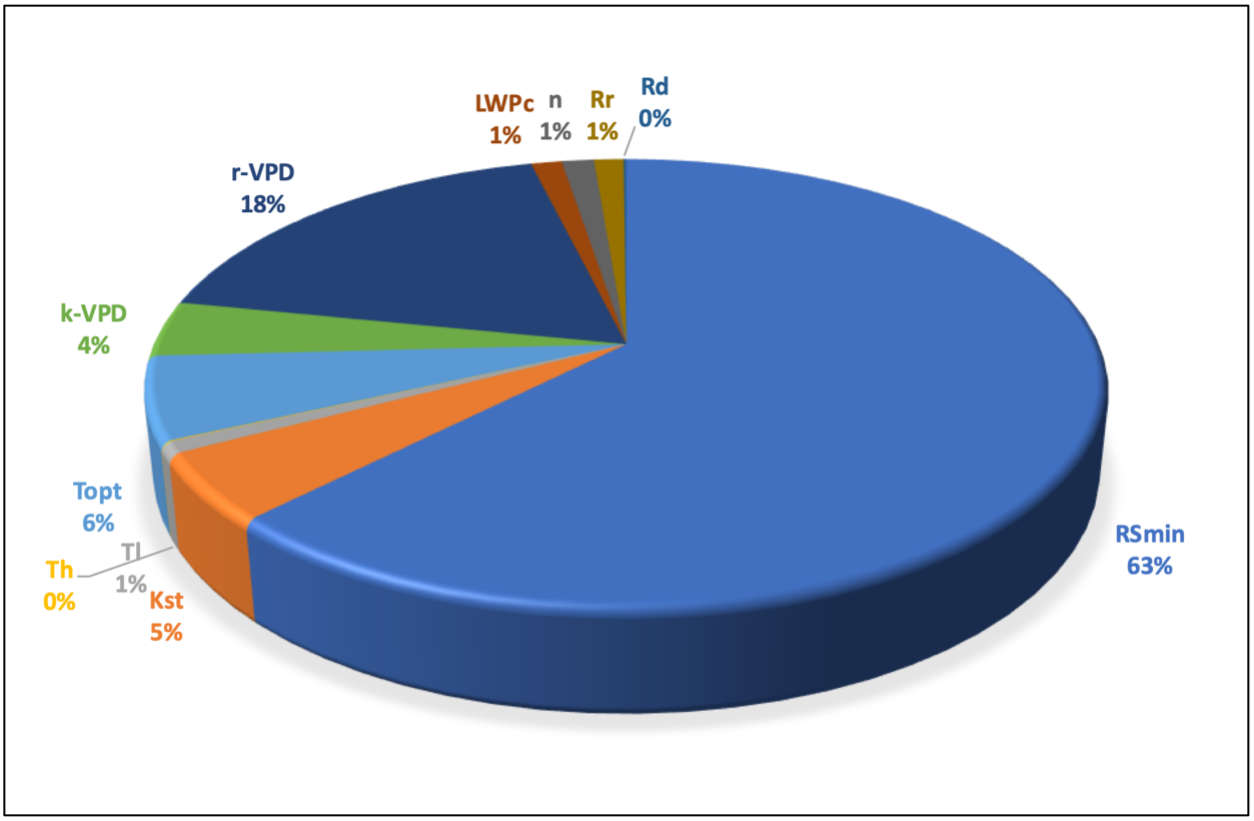

Figure 6.5 Model parameters sensitivity to latent heat flux at jack pine

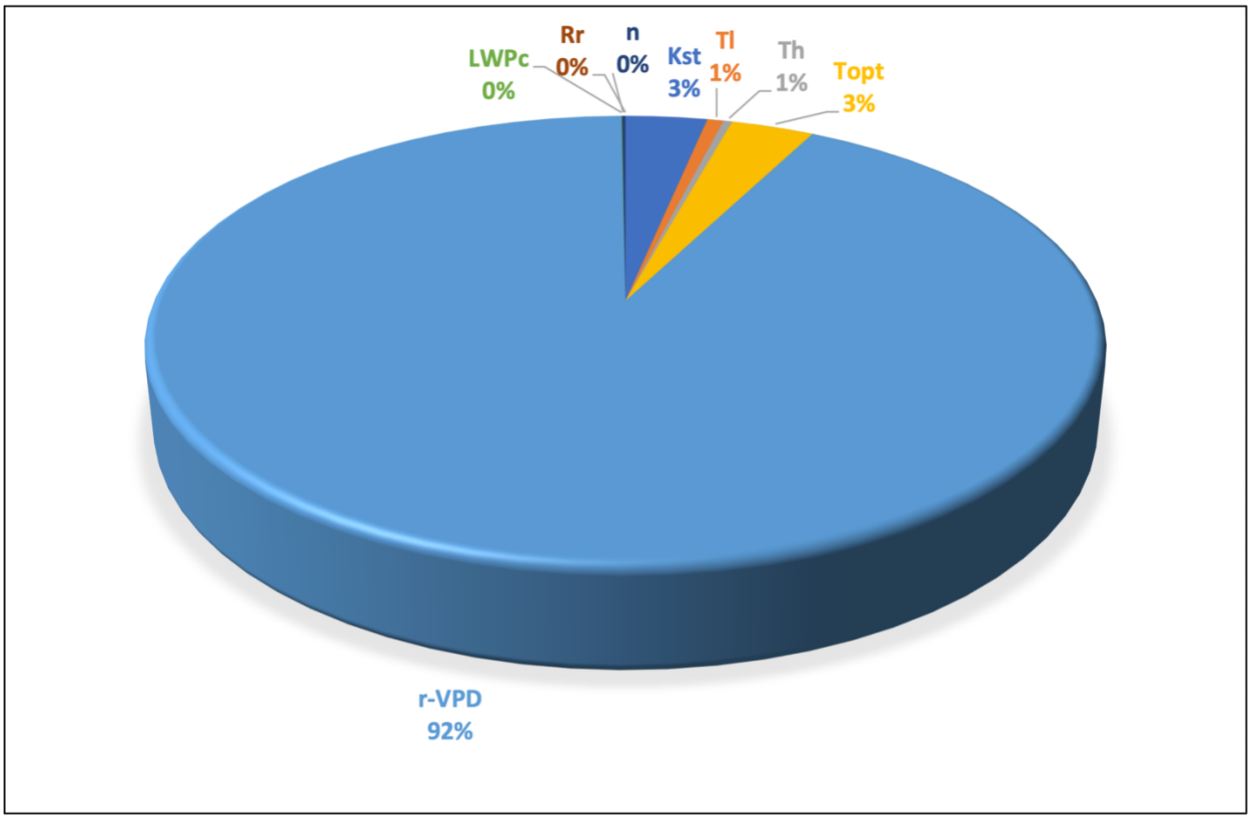

Figure 6.6 Model parameters sensitivity to latent heat flux at jack pine

6.3.2 Model Parametrization for Simulating Evapotranspiration

The minimum stomatal resistance and r-VPD parameter of vapor pressure deficit function were identified as the most dominant parameters for evapotranspiration. This suggests that any parameter optimization algorithm would likely face a parameter unidentifiability challenge for other parameters, or it would result in an inappropriate parameter estimation if their ranges are not well constrained. Accordingly, all parameters were specified based on the best available information. For instance, leaf area index, the minimum stomatal resistance, and critical leaf water potential (eq. 3-12 and 3-13) were assigned site-specific values from literature (Table 3.4) and the exponent (n) for relating actual stomatal resistance to leaf water 'potential was set to its typical value of 5 (Flerchinger et al., 1998). The influence of air temperature on stomatal conductance was not directly considered as it is positively correlated with both vapor pressure deficit and solar radiation (Bartlett et al., 2003). For the solar radiation function, a site specific parameter, $K_{ST,}$ was

determined based on observed data (Appendix D). For considering vapor pressure deficit influence on stomatal conductance in the model, the following vapor pressure deficit function f_{VPD} is used:

$$\boldsymbol{f_{VPD} = K_{VPD} + [1 - K_{VPD}] r\_vpd^{VPD}} \qquad \textbf{Equation 6.1}$$

Where K_{VPD} is the maximum stomatal conductance reduction factor at high vapor pressure deficit which was set to 0.15 (Link et al., 2004) and r_vpd is the empirical fitting parameter. Since the vapor pressure deficit was identified as the most sensitive environmental variable for evapotranspiration, which has also been reported by Zha et al. (2013), the impact of using default/typical and calibrated parameter values was explored (Section 6.3.4). The default r-VPD parameter (0.8 for coniferous and 0.38 for deciduous forests) was determined based on vegetation type (Appendix E).

6.3.3 Model Development

The existing model structure of SHAW was demonstrated to inadequately reproduce spring evapotranspiration in coniferous forests (Section 5.4 and Section 6.3.1). Transpiration is controlled by stomatal conductance in SHAW which is influenced by environmental variables including soil moisture status, air temperature, solar radiation, and vapor pressure deficit. However, the influence of soil warming on stomatal conductance in spring is ignored.

Soil warming is important for spring recovery of photosynthesis in boreal forests as cold or frozen soils restrict root activity, water and nutrients uptake (Bergh and Linder, 1999; Jarvis and Linder, 2000; Repo et al., 2005). In these environments, mycorrhizal fungi play a fundamental role in the uptake and transport of nutrients and water (Egerton-Warburton et al., 2007; Read et al., 2004; Xu and Zwiazek, 2020). Low positive soil temperatures reduces mycorrhizae formation (Husted, 1991) whereas the number of root tips and mycorrhizae increases with increase in soil temperatures (Domisch et al., 2002) improving nutrients and water uptake. Other studies have also reported that low soil temperatures can reduce soil and plant hydraulic conductance (van Bavel, 1996) by increasing water viscosity, decreasing membrane permeability (Kaufmann, 1975) and hampering the production of new roots (Vapaavuori et al., 1992) which affects stomatal conductance (Fuchs and Livingston, 1996; Strand et al., 2002). Ensminger et al. (2008) discovered in a controlled

experiment on boreal scot pine seedlings that spring recovery rate of photosynthesis were inhibited by cold soil temperatures by reducing root water uptake, water potential of needles, and stomatal conductance. Mellander et al. (2004) reported that liquid water availability in spring was not sufficient for scot pine trees to transpire and soil temperatures below +8 °C restricted transpiration by lowering stomatal conductance. These studies suggest that the influence of soil temperatures on stomatal conductance of boreal conifers should be considered in the models for better simulating spring evapotranspiration.

Axelsson and Agren (1976) proposed a transpiration reduction factor for Swedish conifers based on soil temperature which was later modified by Mellander et al. (2006) by incorporating a threshold soil temperature as:

$$f_{T(z)} = \begin{cases} 1 - \exp\{-t_1[T_{(z)} - t_3]^{t_2} & T_{(z)} > t_3 ℃ \\ 0 & T_{(z)} \leq t_3 ℃ \end{cases} \qquad \textbf{Equation 6.2}$$

where t_1 and t_2 are empirical parameters, t_3 is a threshold soil temperature below which no water uptake takes place, and $T_{(z)}$ is the soil temperature at depth z. The application of this formulation in hydrological models is challenging. First, determining the actual critical soil depth and relevant parameters at which the soil temperature is related with stomatal conductance may require demanding observations. Second, several hydrological/land surface models don't simulate soil temperatures, and model simulations are often biased, particularly in winter and spring, for those models that do include soil temperature algorithms (Essery et al., 2009; Zhang et al., 2008). Thus, a simplified representation in models for considering the influence of soil thermal environment on stomatal conductance would be of great practical use. Accumulated growing degree days (thermal time) can be associated with the soil thermal environment during snow free periods (Dwyer et al., 1990) and can provide a simple alternative. Moreover, A comparison of spring phenology models for boreal trees has suggested that the simple thermal-time models are accurate for predicting the onset of photosynthesis in spring for mature stands (Linkosalo et al., 2006). Thus, the same approach can be used not only to mark the beginning of growing season but also to consider the influence of soil thermal environment on stomatal conductance.

The cumulative growing degree days were calculated by taking the integral of warmth (temperature) above a base temperature of 5 °C. For all three sites, cumulative growing degree days (GDD_{cum}) are strongly correlated (correlation coefficient r = 0.81 to 0.94) with post-thaw soil temperatures at different depths (Figure 6.7). The correlation was stronger at the relatively drier jack pine site than at the black spruce and aspen sites. The coefficient of determination decreased from 0.73 to 0.65 from 10 cm to 20 cm at the black spruce site which has the highest soil water content between the sites.

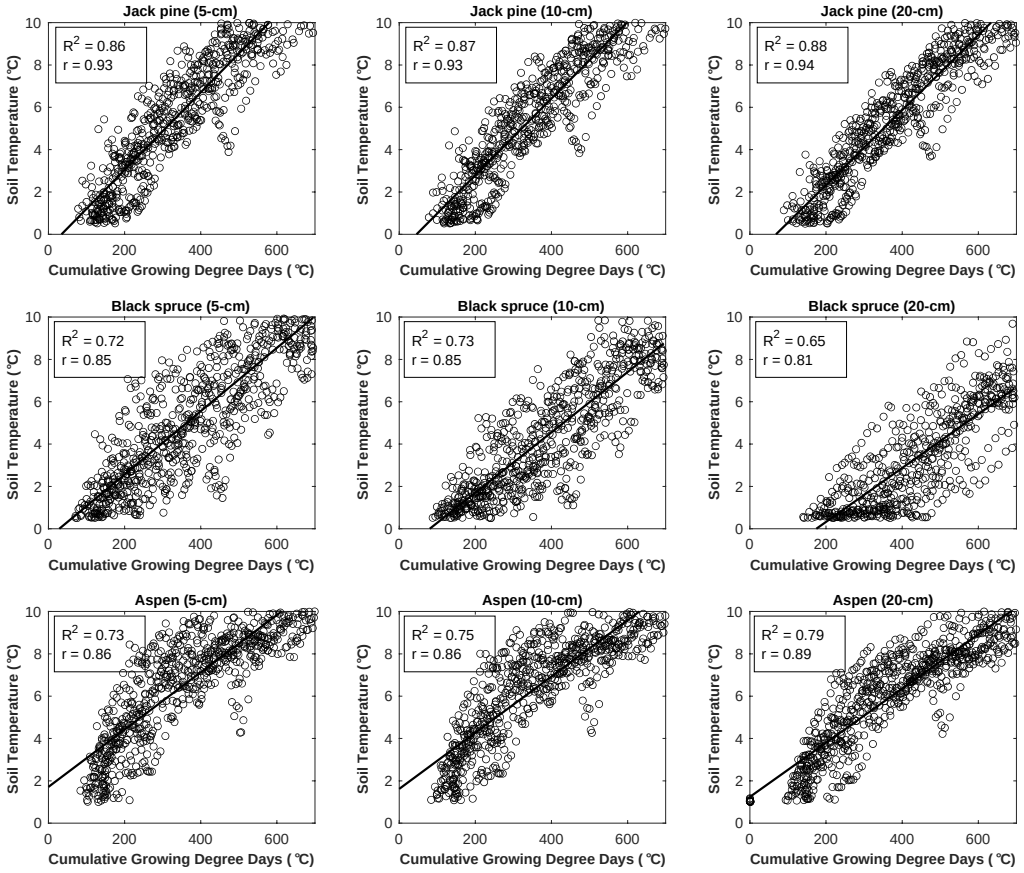

Figure 6.7 Relationship between cumulative growing degree days (T-base = 0 °C) and soil temperatures at different depths

A relationship between cumulative growing degree days (starting from January 1 each year) and gross ecosystem photosynthesis (GEP) was explored using the long-term (1998-2015)

observations. The GEP was used as a proxy for canopy conductance. For GDD, a base temperature of +5°C was used for mean daily temperatures, similar to other studies in the boreal forests of Finland (Kauppi et al., 2014) and Siberia (Brazhnik and Shugart, 2015). The data showed that the development of stomatal functioning advances with an increase in accumulated growing degree days until it reaches its full capacity. Two points in the GEP data were identified where the mean and the slope of the signal changed most abruptly using a built-in change-point detection function ("findchangepts") in MATLAB which divided the data into three groups. A linear regression model was fitted for each group and the intersecting points were related to onset and full recovery of stomatal functioning as shown in Figure 6.8. The recovery process started with the start of growing degree days accumulation (GDD_{cum} = 15 to 20) for the coniferous forests and after accumulating about 90 GDD at the aspen site. The number of cumulative growing degree days required for full recovery were approximately 300, 400, and 440 for the aspen, jack pine and black spruce sites, respectively. The testing of 0°C base temperature produced similar results with a GDD_{cum} threshold of about 675 (Appendix F).

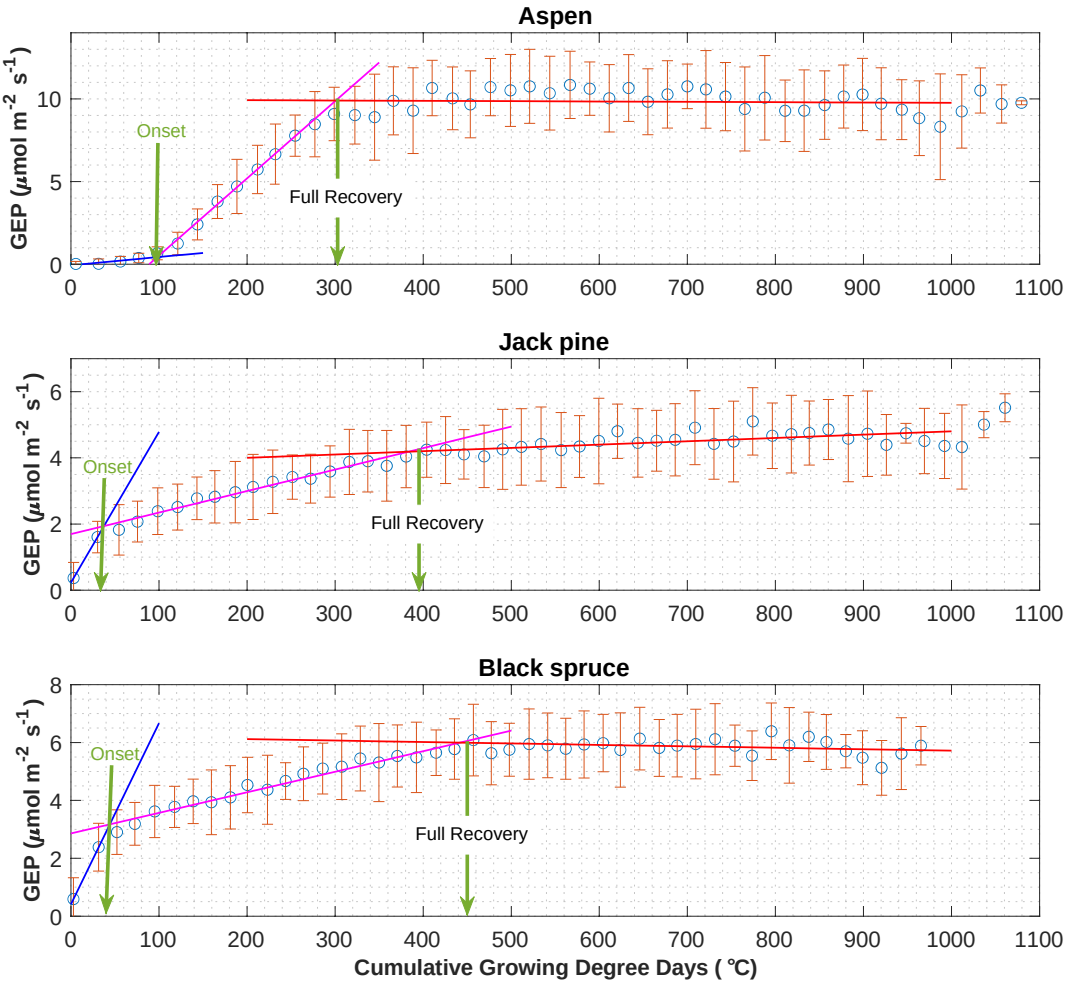

Figure 6.8 A relationship between bin averaged gross ecosystem photosynthesis (GEP) and accumulated growing degree days (5 degree base, mean daily air temperatures) based on 18 years of data (1998-2015). Bin size was determined by taking the square root of total number of observations

Based on the above analysis, a simple formulation is proposed to consider the influence of soil thermal environment on stomatal conductance through the cumulative growing degree days approach, which is hereafter termed as the growing degree days factor (f_{GDD}). A conceptualization of the proposed factor is presented in Figure 6.9. The value of f_{GDD} will vary between 0 and 1 like other meteorological influences on stomatal conductance within Jarvis-Stewart type approaches.

Two required species-dependent parameters are: (1) GDD_{onset} at which biological awakening or recovery of stomatal functioning starts, and GDD_{Cri} at which it reaches to its full capacity. The proposed GDD factor will take the following mathematical form:

$$f_{GDD} = \begin{cases} 0, & GDD_{cum} \leq GDD_{onset} \\ \frac{(GDD_{cum} - GDD_{onset})}{(GDD_{cri} - GDD_{onset})}, & GDD_{onset} < GDD_{cum} < GDD_{cri} \\ 1, & GDD_{cum} \geq GDD_{cri} \end{cases} \qquad \textbf{Equation 6.3}$$

where GDD_{cum} is the cumulative growing degree days on a daily time scale. The proposed GDD factor was included in SHAW (eq. 3-13) as modifier of stomatal resistance along with other environmental variable influences as follows, where all terms have previously been defined.

$$r_s = r_{s\_min}\left(\left[1 + \frac{\psi_l}{\psi_c}\right]^{n_s} \Big/ f_{ST} f_T f_{VPD} f_{GDD} \right) \qquad \textbf{Equation 6.4}$$

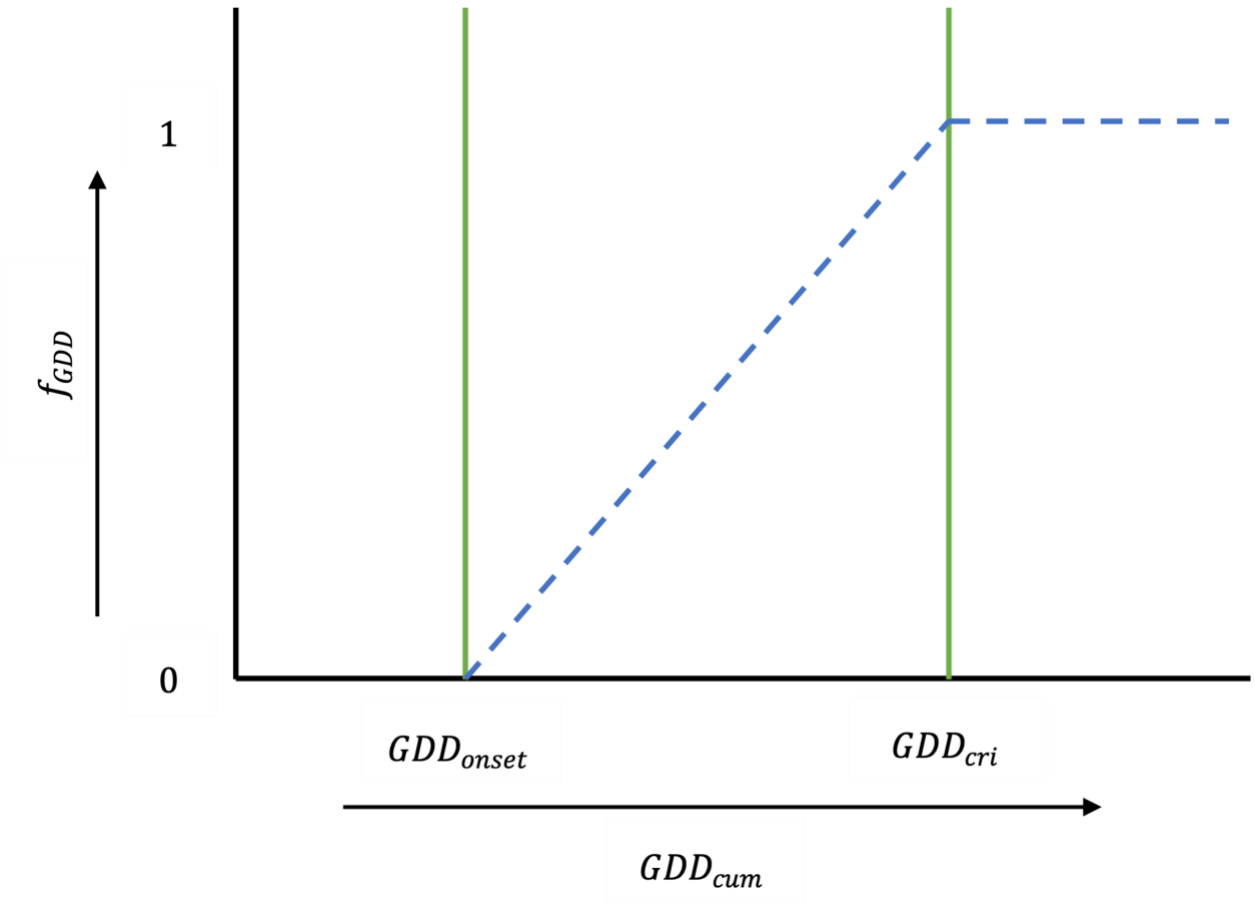

Figure 6.9 A graphical representation of proposed GDD factor

6.3.4 The Model Performance Evaluation

The performance of SHAW was evaluated for simulating latent heat flux with and without considering the proposed GDD factor. Four combinations of model formulations were compared with the observations: (1) model run with default/typical values for r-VPD parameter without considering GDD factor, (2) optimized r-VPD parameter without GDD factor, (3) default r-VPD with GDD factor, and (4) optimized r-VPD parameter with GDD factor. The calibrated empirical fitting parameter (r-VPD) values for VPD function are listed in Table 6.2.

Table 6.2 Calibrated r-VPD parameter values

Site	Calibrated r-VPD	
	Without GDD factor	**With GDD factor**
Black Spruce	0.44	0.55
Jack Pine	0.24	0.55
Aspen	0.43	-

Note: The GDD function was not considered for aspen as transpiration is delayed until leaf emergence which occurs well after soil thaw/warming.

The model performance for different parametrization schemes to consider the influence of vapor pressure deficit (VPD) and cumulative growing degree days (GDD_{cum}) on stomatal conductance is shown in Figure 6.10. Simulated fluxes of latent heat were biased high when the default r-VPD parameter was used without considering the proposed GDD factor (Figure 6.10a). The calibration of r-VPD, without adding the GDD factor, improved the simulation in spring but under-predicted latent heat flux in summer (Figure 6.10b). Spring latent heat flux simulation was also improved when the proposed GDD factor was included in the model while keeping the default VPD parametrization (Figure 6.10c). Year-round latent heat flux simulations were significantly improved by incorporating the GDD factor and calibrating r-VPD parameter (Figure 6.10d). The mean absolute error was 25 MJ m^{-2} $month^{-1}$ for scenario (a), 15 MJ m^{-2} $month^{-1}$ for (b) and (c), and 6 MJ m^{-2} $month^{-1}$ for (d).

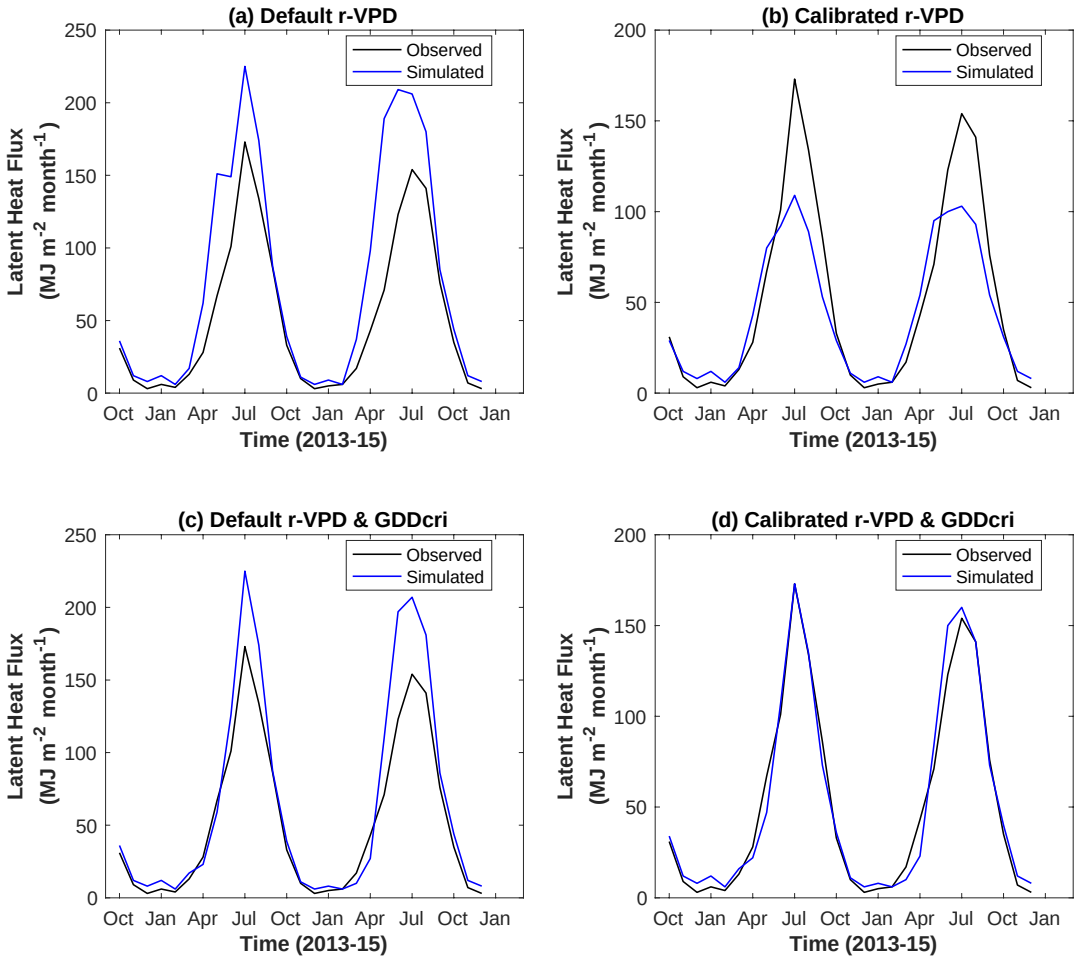

Figure 6.10 Monthly observed and simulated latent heat flux at Jack pine site for the four model formulations; (a) Default VPD function, (b) Calibrated VPD function, (c) Default VPD function with GDD factor, (d) Calibrated VPD function with GDD factor

6.3.5 Model Validation for Extended Record and at All Three Study Sites

The model was validated for longer periods (11 years for coniferous sites and 7 years for aspen) compared to their calibration period of 3 years. Latent heat fluxes were overestimated for both coniferous forests but matched well with the observations for aspen when the default parametrization for VPD function was used (Figure 6.11). The mean absolute error was similar

(32.5 MJ m^{-2} $month^{-1}$) for both coniferous forest sites, which was reduced to 11.97 MJ m^{-2} $month^{-1}$ for jack pine and 12.83 MJ m^{-2} $month^{-1}$ for black spruce by calibrating the r-VPD parameter. Consideration of the GDD factor further reduced this error to about 10 MJ m^{-2} $month^{-1}$.

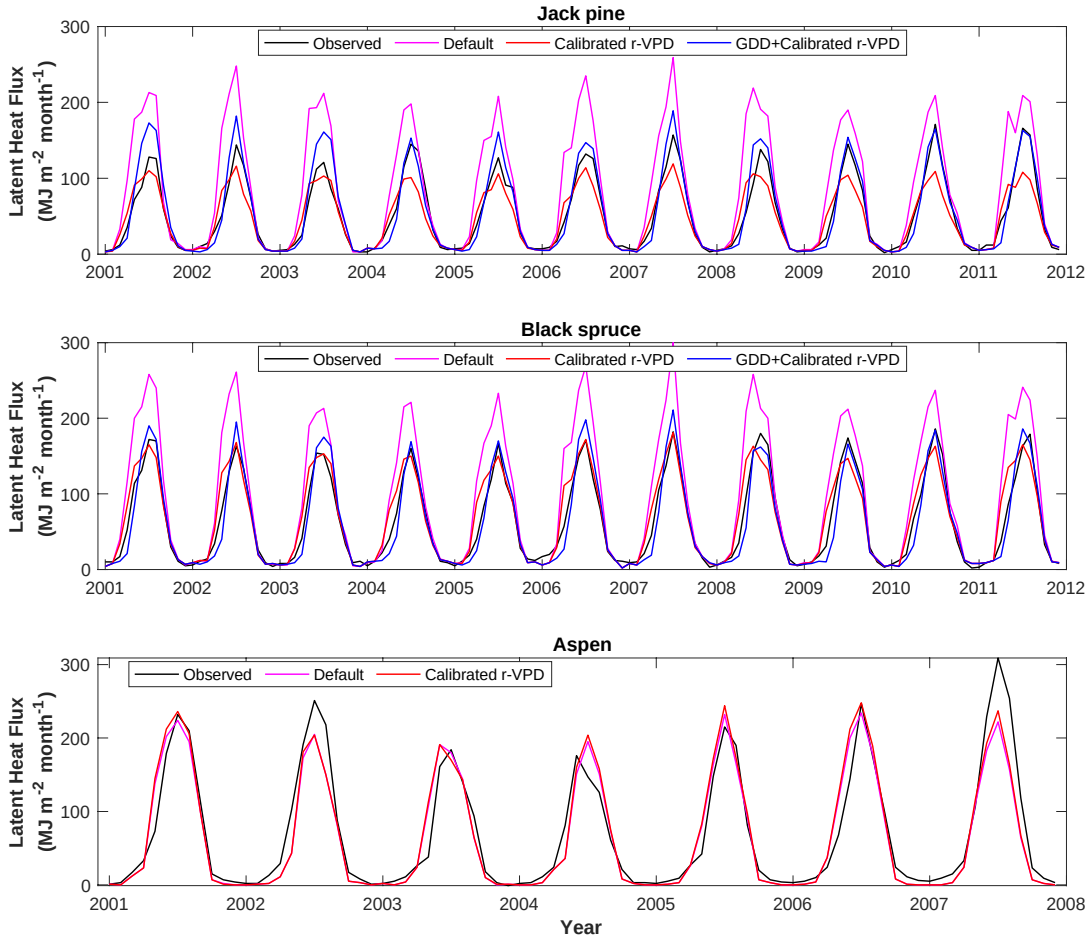

Figure 6.11 Observed and model simulated latent heat flux at the study sites during validation period based on different model formulations

Seasonal variability between observed and simulated latent heat fluxes at both coniferous sites (jack pine and black spruce) for different model parametrizations is shown in Figure 6.12. The default r-VPD resulted in overestimation of latent heat flux throughout the growing season at both sites (Figure 6.12 a & b). The calibration of this parameter significantly improved the model

performance. However, two contrasting trends were noted at both sites: (1) at jack pine, latent heat fluxes were better predicted in spring but were underestimated in summer, and (2) the model overestimated spring latent heat fluxes at the black spruce site but simulations matched well with observations during summer months (Figure 6.12d). Both of these problems were addressed and model simulations were improved when the vapor pressure deficit function was calibrated with the proposed growing degree days function included in the model (Figure 6.12 e and f). Root mean square error was reduced by 2.67 to 3.02 MJ m^{-2} $month^{-1}$ which translates into 35 to 40 mm of water loss to evapotranspiration (about 50% of the spring evapotranspiration).

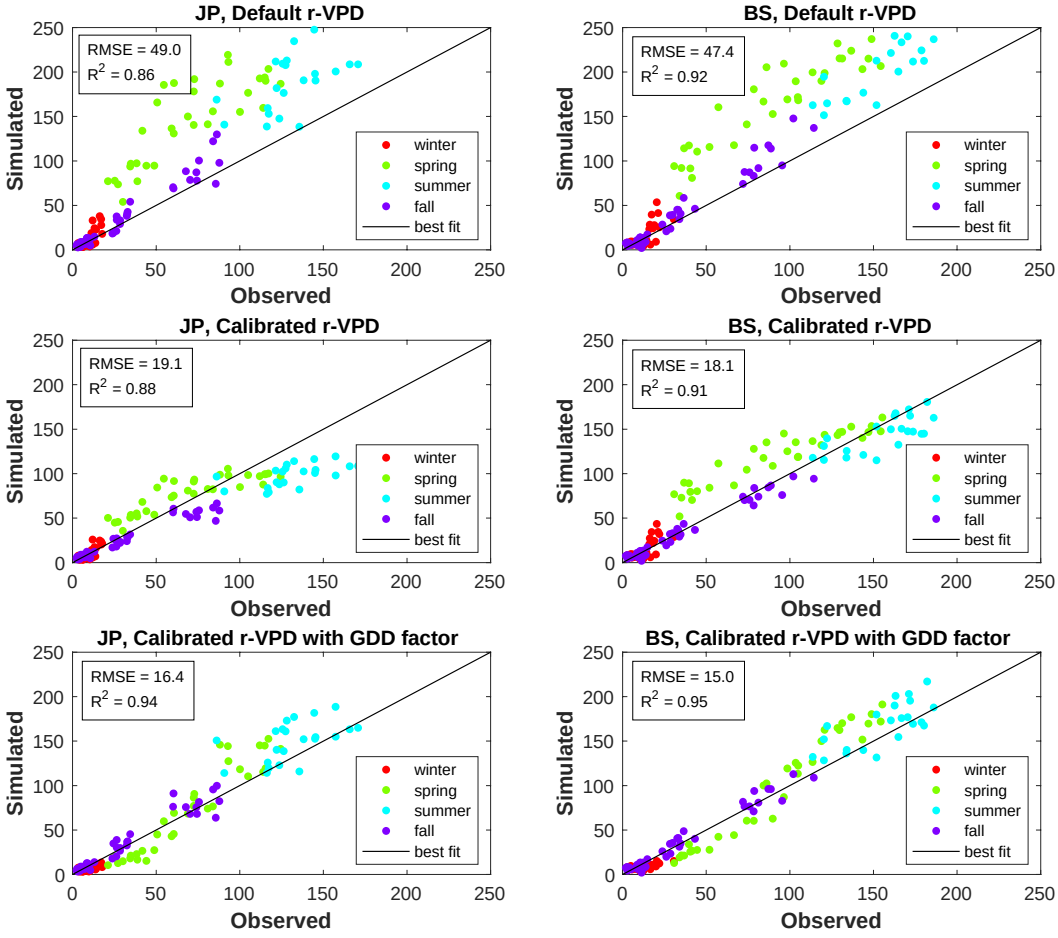

Figure 6.12 Observed and modelled latent heat flux (MJ m^{-2} $month^{-1}$) for different model parametrizations at jack pine (JP) and black spruce (BS) sites. Seasons were

defined as: winter (January to March), spring (April-June), summer (July-August), and fall (September-December).

6.4 DISCUSSION

6.4.1 Modelling Soil Temperature and Soil Thaw

Soil temperature simulations improved at all three sites when a ground cover layer was included in the model (Figure 6.1). The mean absolute error was reduced by 0.6°C to 1.1°C at 20 cm depth. The influence of ground cover on soil temperatures at high northern latitudes have also been documented by other studies. For example, the average insulations effects of mosses/lichen on soil temperatures to a depth of 1 m varied from 0.3°C to 0.7°C at 169 °E, 63 °N (Druel et al., 2017). Similarly, parametrization of moss reduced the root mean square error by 0.7°C at 32 cm depth during August-September months in the Lena River Delta, Siberia (Chadburn et al., 2015). In the present study, improved soil temperature simulations also resulted in better prediction of soil thaw timing at all three sites (Figure 6.2). The mean difference between observed and simulated soil thaw end date was reduced by 1.5 to 2 weeks. These results suggest that the consideration of ground cover in modelling significantly improve simulations for soil thermal environment in boreal forests.

The insulation effects of ground cover on soil temperatures and soil thaw timing varied between sites not only in magnitude but also in temporal patterns. For example, without a ground cover layer, simulated soil temperatures were cold biased at aspen throughout the year, warm biased in summer at jack pine, and cold biased in winter but warm biased in summer at black spruce (Figure 6.1). For soil thaw end date, the model simulated earlier soil thaw at jack pine and delayed thaw at aspen and black spruce without considering a ground cover layer (Figure 6.2). These differences were likely driven by varying forest floor and soil characteristics between the sites. A relatively deeper organic soil layer at the aspen and black spruce sites than the jack pine site likely played a key role. The thermal conductivity of organic soils is much lower than mineral soils (Table 2.2) which may have resulted in higher cold bias in winter soil temperatures and warm bias in summer at the black spruce site. At the aspen site, winter cold bias in soil temperatures was larger than the black spruce site which may have contributed to year around cold bias. This may be caused by

relatively lower soil water content at the aspen site than the black spruce site as water has significantly higher thermal conductivity than air. This cold bias in winter soil temperatures at the aspen and black spruce sites would have resulted in deeper frosts and delayed thaw when ground cover layer was not considered. At the jack pine site, a winter bias in soil temperatures was not present but warm bias in spring/summer was noted resulting in an earlier soil thaw end date simulation without considering ground cover layer. It should be noted that the aspen understory is considered in the model by using a combined leaf area index of aspen trees and hazelnut, but a ground cover layer was also added to consider the effects of fallen leaves/liter in fall when the model simulation was started.

The insulation effects of ground cover were represented by a dead plant residue layer in this study. Ground cover has varying forms of representation in modeling applications for improving soil temperature simulations including an increased thickness of organic soil layer (Chadburn et al., 2015; Ekici et al., 2014) and a dynamic vegetation layer (Launiainen et al., 2015; Park et al., 2018). This allows for a portion of the below-canopy available energy to be consumed by evaporation from the ground cover and to change its temperature state. Similar to the organic soil layer, conduction through the ground cover layer is strongly influenced by water content. The major difference between these 2 layers is that the ground cover layer does not allow drainage and all the intercepted water, which is limited by a maximum water content parameter, is lost to evaporation. In contrast, the top organic soil layer (fibric peat) has very low water holding capacity (Letts et al., 2000). Since lichens/mosses have high water holding capacities (Liljedahl et al., 2011), a ground cover layer may be a more appropriate representation in the model. In addition, varying reflectance characteristics between sites and convective heat transfer by air are also considered by the ground cover layer. Thus, overall the physical processes are better represented by a ground cover layer in the model than increased thickness of organic soil layer. It is noted that dynamic vegetation could not be considered using SHAW; however, it is believed that a uniform coverage and slow growth rate of lichens and mosses can be safely assumed at the study sites.

6.4.2 Modelling Latent Heat Flux

Evergreen boreal trees awake from dormancy early in spring when air temperatures are favourable (Tanja et al., 2003) but soil warming (Jarvis and Linder, 2000) and water availability

(D'Orangeville et al., 2018) may be the limiting factors for stomatal functioning and transpiration. Abundant water is available in spring due to snowmelt infiltration (Nazarbakhsh et al., 2019; Stahli et al., 2001; Zhao et al., 2002); however, soil temperatures remain low for extended periods restricting root activity and water uptake (Repo et al., 2005). Field observations for scot pine forest in southern Finland have also revealed that transpiration is restricted by low soil temperatures (Sevanto et al., 2006). Thus, spring soil warming strongly influences annual evapotranspiration (Zhang et al., 2011) in the northern cryosphere ($\geq 40°N$).

The SHAW model does not have any algorithm to consider the influence of soil temperatures on stomatal conductance. A simple indirect method to relate soil thermal environment with cumulative growing degree days was proposed in this study based on long-term observations. It was demonstrated that spring evapotranspiration can be largely overestimated without considering effects of low soil temperatures on stomatal conductance. The root mean square error was 35 mm for the jack pine site and 40 mm for the black spruce site. The high bias in spring evapotranspiration without considering the proposed GDD factor can also influence soil moisture and temperatures in the rootzone.

The proposed GDD factor has two parameters: (1) GDD_{onset} and (2) GDD_{cri}. Pulliainen et al. (2017) found a strong correlation between the onset of spring biological recovery and snow ablation for northern boreal evergreen forests. Thus, onset of stomatal functioning in spring (GDD_{onset}) can be set to begin with the start of growing degree days accumulation because cold soil temperatures and unfrozen liquid water content would restrict transpiration in early stage of awakening. The GDD_{cri} parameter essentially identifies the soil temperature threshold at a critical depth at which stomatal conductance becomes independent of soil temperature. This threshold depends upon species and soil hydro-thermal characteristics and can vary by more than 10°C (Mellander et al., 2006). In this study, GDD_{cri} was about 700 for jack pine and 675 for black spruce. This corresponds to soil temperature of greater than +10°C at the jack pine site and +6 to +10°C at the black spruce site for the top 20 cm soil profile (Figure 6.7). Mellander et al. (2004) reported similar threshold soil temperature of +8°C at 10 cm depth for scot pine in boreal zone of northern Sweden.

Although the proposed GDD factor worked well for considering the influence of low soil temperatures on stomatal conductance, it has some limitations. First, the relationship between

cumulative growing degree days (GDD_{cum}) and soil temperatures may be weak for sites with high soil water content particularly at deeper depths. This may have little limitation in boreal coniferous forests where more than 80% fine roots are located within the top 20 cm soil profile from the surface (Ruess et al., 2003), and most of the living fine roots are present in the top 10 cm (Read et al., 2004; Stober et al., 2000). Second, the intermittent frost events or reversal of warm soil temperatures into cold temperatures in spring could not be considered. It is, however, believed that this may also likely have limited influence because soil thaw/warming is a gradual process and abrupt changes in air temperature would likely give smaller change signals to soil temperatures. Moreover, stomatal conductance would increase because of limited liquid water availability in case of refreezing. Third, the model assumes a steady response of root system and/or stomatal conductance to soil warming from year to year and any long-term effects of low soil temperatures are not considered.

6.5 SUMMARY

Soil temperature simulations are often biased in boreal forests and simulated spring evapotranspiration is largely overestimated for coniferous forests. The influence of considering the insulating effects of ground cover (lichen/moss/litter) on soil temperatures/thaw was explored. In addition, a simple cumulative degree days approach was proposed to account for the influence of low soil temperatures on stomatal conductance for improving the simulated latent het flux in spring. The performance of the Simultaneous Heat and Water (SHAW) model was evaluated with and without considering these changes using observed data. The soil temperature response to the presence of a ground cover layer varied between sites in magnitude and temporal patterns but simulated soil temperatures and thaw timing improved at all three sites. The maximum difference in observed and simulated soil temperatures was reduced by 2.6°C for aspen, 3.3°C for jack pine, and 1.0°C for black spruce when a ground cover layer was considered in the model. Simulated soil thaw end dates were also significantly improved with a difference of up to 2 weeks. Regarding spring evapotranspiration, the proposed growing degree days factor improved simulations for spring evapotranspiration at coniferous forests and the errors were reduced by 35 mm to 40 mm. The proposed GDD factor was a simple alternative to consider direct soil temperature influence on stomatal conductance and was proposed for easy integration in hydrological models. This study

concludes that consideration of insulation effects of ground cover on underlying soils and low soil temperatures on stomatal conductance may significantly improve simulations for soil temperature and latent heat flux, respectively.

CHAPTER 7 CLIMATE CHANGE IMPACT ON SOIL TEMPERATURE AND THAW TIMING IN THE SOUTHERN BOREAL FORESTS

7.1 CHAPTER OVERVIEW

This chapter addresses objective 4 and explores how spring thaw processes will respond to climate change for contrasting forest cover types in the southern boreal forest. The Simultaneous Heat and Water (SHAW) model was forced with climate variables from runs of Weather Research and Forecasting (WRF) model. The runs were made for historical (WRF-CTL, 2001-2012) and future periods (WRF-PGW, 2086-2097) over Western Canada, and bias corrections were applied for study sites (Sections 3.8.1-3). This chapter summarizes the projected change in climate in the southern boreal forest and explores its impact on spring thaw processes. At first, precipitation simulations of WRF are presented for all three study sites (Section 1.1) followed by bias-correction results (section 7.3). The projected change in climate is then quantified (Section 7.4) and its implications for soil hydro-thermal environment and evapotranspiration are explored (Section 7.5 and 7.6). A discussion is then provided in Section 7.7 about uncertainty in modelling and climate change impacts on hydrological/hydro-thermal processes as well as its implications for boreal forests.

7.2 OBSERVED AND SIMULATED PRECIPITATION

Daily observed and WRF-simulated ([historical WRF-CTL 2001-2012] and [future WRF-PGW, 2086-2097]) precipitation for all three sites is presented in Figure 7.1. Mean annual precipitation was 501 mm based on the observed data (2001-2012), 567 mm for WRF-CTL and 620 mm for WRF-PGW. The differences in mean annual precipitation among sites for the historical record (2001-2012) ranged from 30 to 40 mm based on observed data and from 15 to 20 mm for WRF-CTL. The difference in precipitation among sites was the highest for WRF-PGW which ranged from 50 to 90 mm (9% to 16%). A one-way analysis of variance multi-comparison test suggested that the mean precipitation is not statistically different among sites for the historical precipitation record (both based on observations and WRF-CTL) but varies significantly for WRF-PGW (Appendix G). Mean annual precipitation for WRF-PGW prior to bias-correction was 572 mm for aspen, 623 mm for jack pine, and 663 mm for black spruce. In order to reduce uncertainty in evaluating climate change impacts between sites because of variability in forcing data, the climate variables for the black spruce site were selected to be used at all three sites. The black spruce site was selected because of better agreement of WRF-CTL simulated precipitation with observations compared to the other sites.

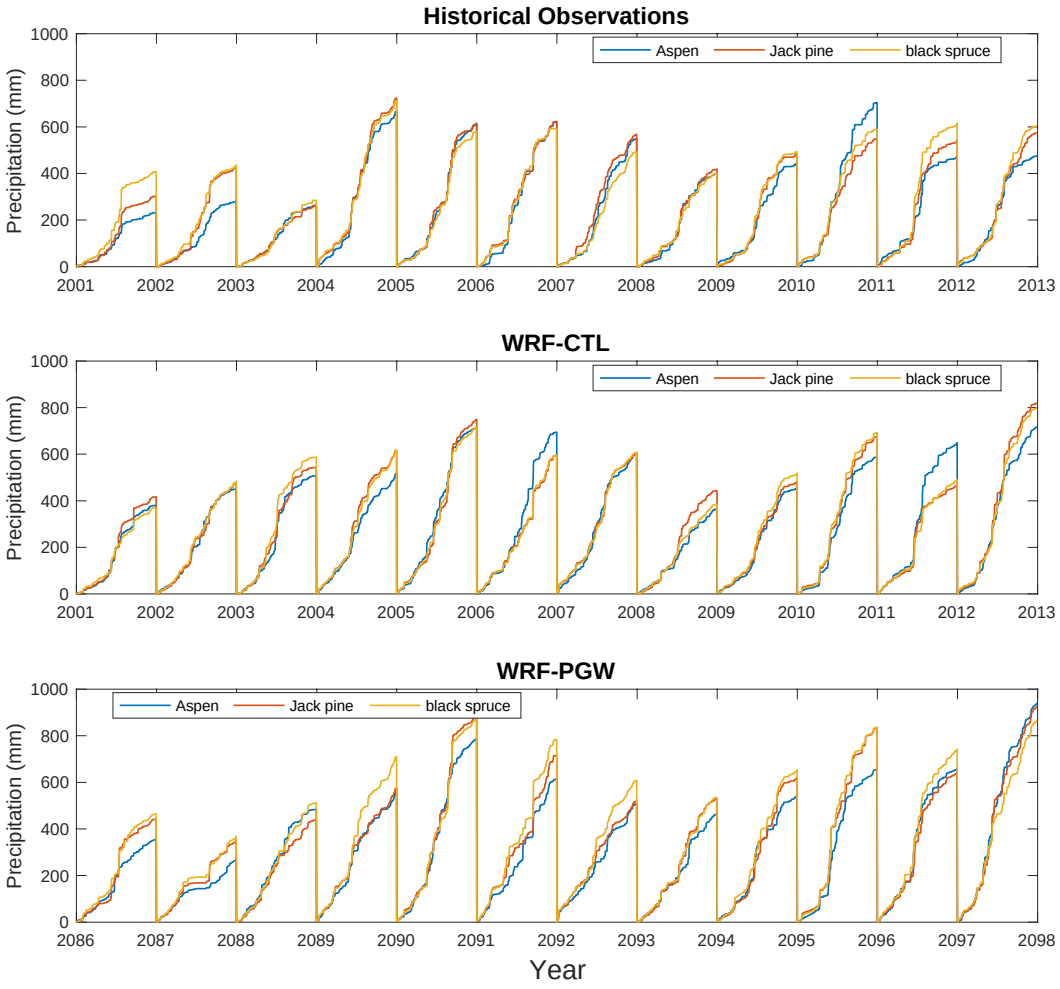

Figure 7.1 Observed and WRF simulated daily precipitation (mm) at all three study sites

7.3 BIAS CORRECTION OF WRF DATA

The WRF-CTL mean annual precipitation was biased high by about 10% (Figure 7.2). This was removed using the quantile-mapping method (Section 3.8.3). Similarly, WRF-CTL simulations for air temperature displayed a cold bias; the difference in mean monthly air temperature between the WRF-CTL and observations was -3.9°C. After bias correction, the WRF-CTL simulations matched well with the observations throughout the year. The quantile-quantile plots between WRF simulations and observations for precipitation and air temperature before and after bias correction are shown in Figure 7.3. Similar to precipitation and air temperature, a high biases of mean annual

daily wind speed (0.3 m s^{-1}), incoming shortwave radiation (10.4 W m^{-2}) and relative humidity (15%) were also removed (Appendix H).

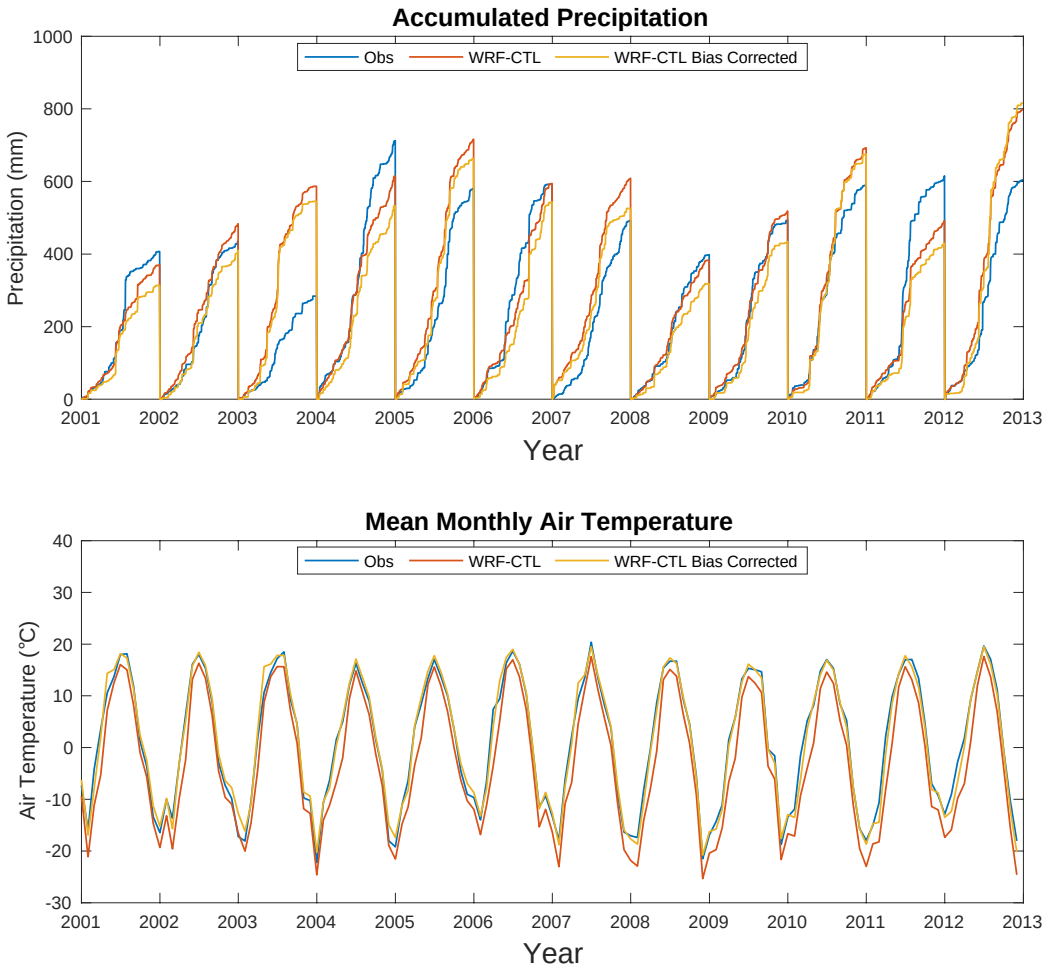

Figure 7.2 A comparison of observed annual daily accumulated precipitation and mean monthly air temperature with WRF data (with and without biased correction)

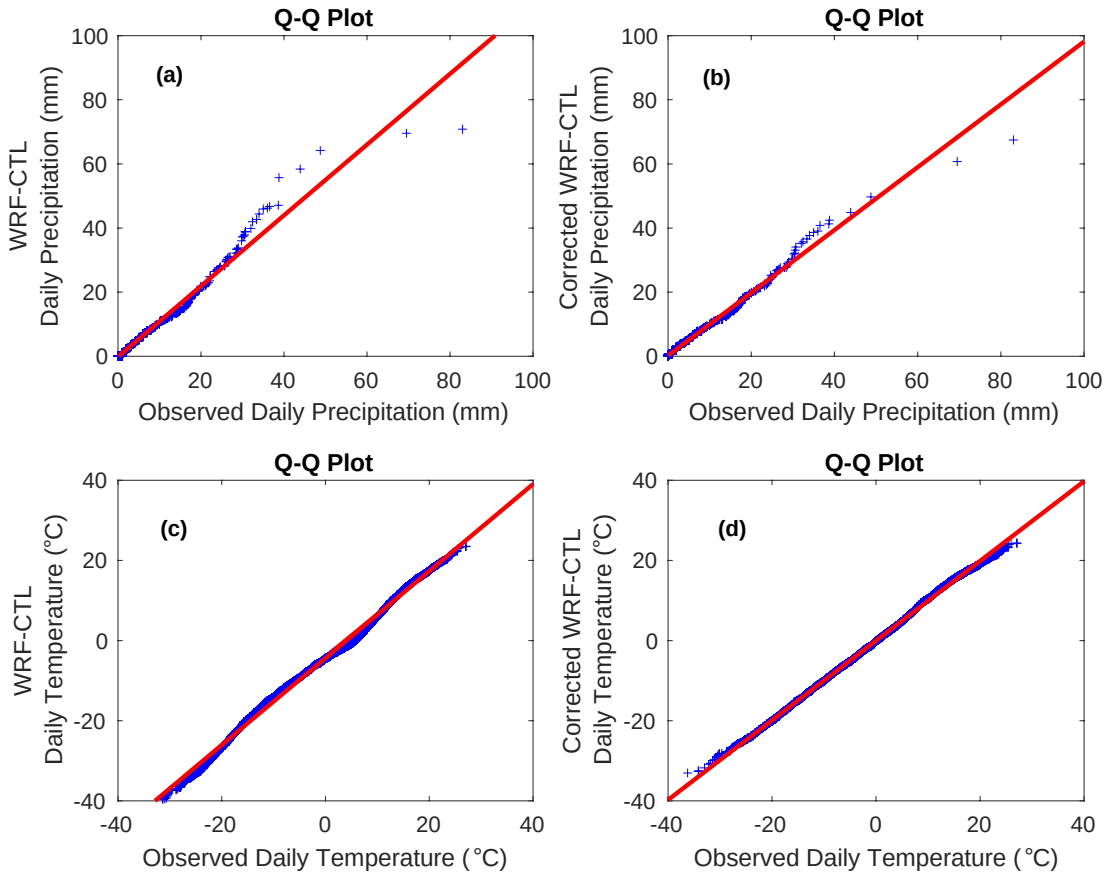

Figure 7.3. Quantile-quantile plot between (a) observed daily precipitation and raw WRF-CTL daily precipitation, (b) observed daily precipitation and bias corrected WRF-CTL daily precipitation, (c) observed daily air temperature and WRF-CTL daily air temperature, (d) observed daily air temperature and bias corrected WRF-CTL daily air temperature

7.4 PROJECTED CHANGE IN CLIMATE

The future climate (WRF-PGW, 2086-2097) compared to historical climate (WRF-CTL, 2001-2012) is projected to be wetter and warmer (Figure 7.4). The total change in annual precipitation based on mean daily values for future and historical climate is predicted to be 160 mm along with an increase in mean daily air temperature of 5.9°C. As a result, the spring warming season (when air temperature rises above zero) was shifted 2 to 2.5 weeks earlier and the winter frost was delayed

for about 3 weeks. This trend was also reported by Yang and Wang (2019). Bias corrected annual precipitation for WRF-CTL and WRF-PGW scenarios is presented in Table 7.1 which shows that mean annual precipitation is predicted to increase from 517 to 609 mm.

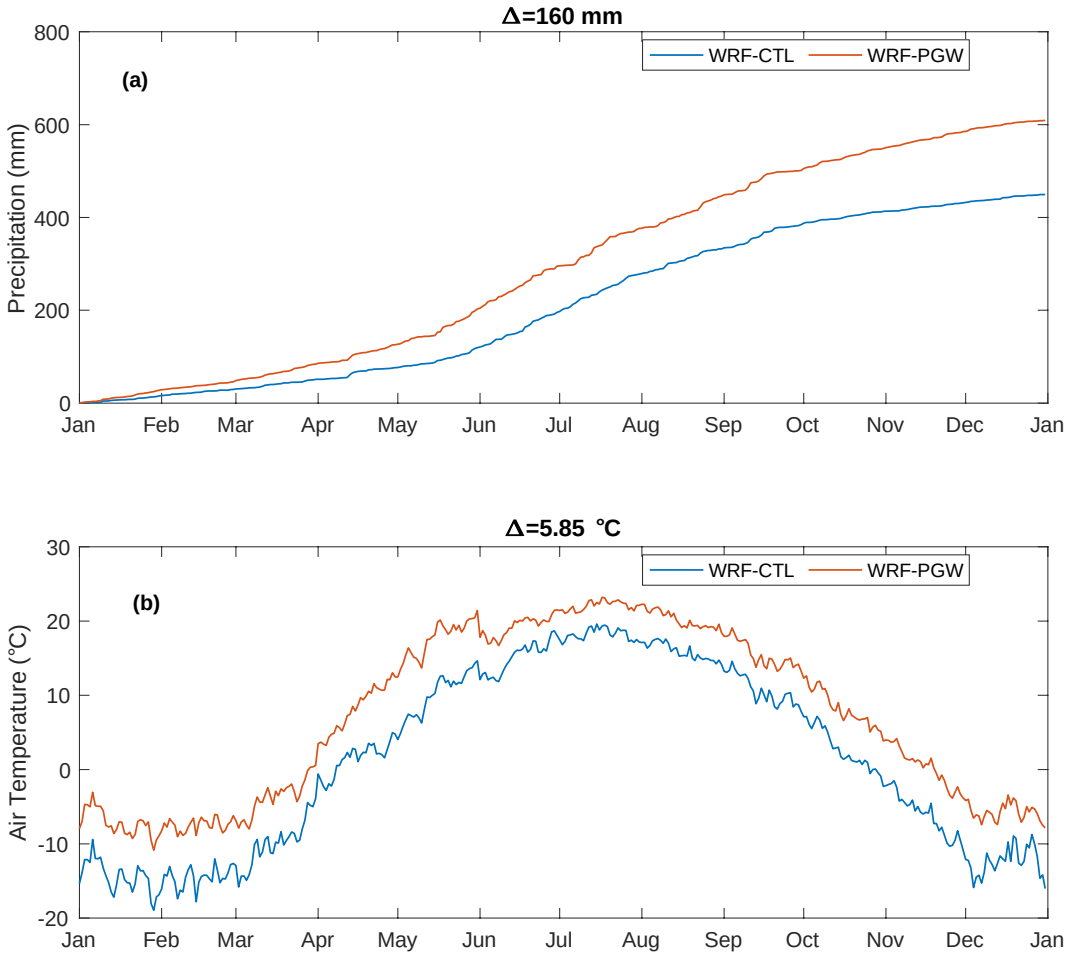

Figure 7.4 WRF simulated (a) mean daily precipitation (accumulated) and (b) mean daily air temperature

Table 7.1. Biased-corrected annual precipitation for WRF-CTL (2001-2012) and WRF-PGW (2086-2097) scenarios

Year	WRF-CTL	WRF-PGW
Year 1	314	426
Year 2	410	291
Year 3	545	452
Year 4	533	660
Year 5	663	811
Year 6	543	756
Year 7	525	543
Year 8	318	475
Year 9	434	597
Year 10	675	797
Year 11	430	692
Year 12	816	803
Minimum	314	291
25th Percentile	410	452
Average	517	609
75th Percentile	575	766
Maximum	816	811

Mean monthly changes in precipitation phase partitioning from WRF-CTL (2001-2012) to WRF-PGW (2086-2097) are presented in Figure 7.5. This demonstrates that the increased precipitation in the future is mainly associated with an increase in rain. The total rain is predicted to increase from 426 mm (WRF-CTL) to 529 mm (WRF-PGW) whereas the total snow is projected to decrease from 91 to 80 mm. About 18% precipitation falls as snow for WRF-CTL which changes to 13% for WRF-PGW. The mean monthly rain is expected to increase in early spring and early

fall which will impact the evolution and ablation of the snowpack. Rain is projected to increase by about 60 mm in spring and 40 mm in fall. Net change in summer precipitation is projected to be small i.e. about 10 mm.

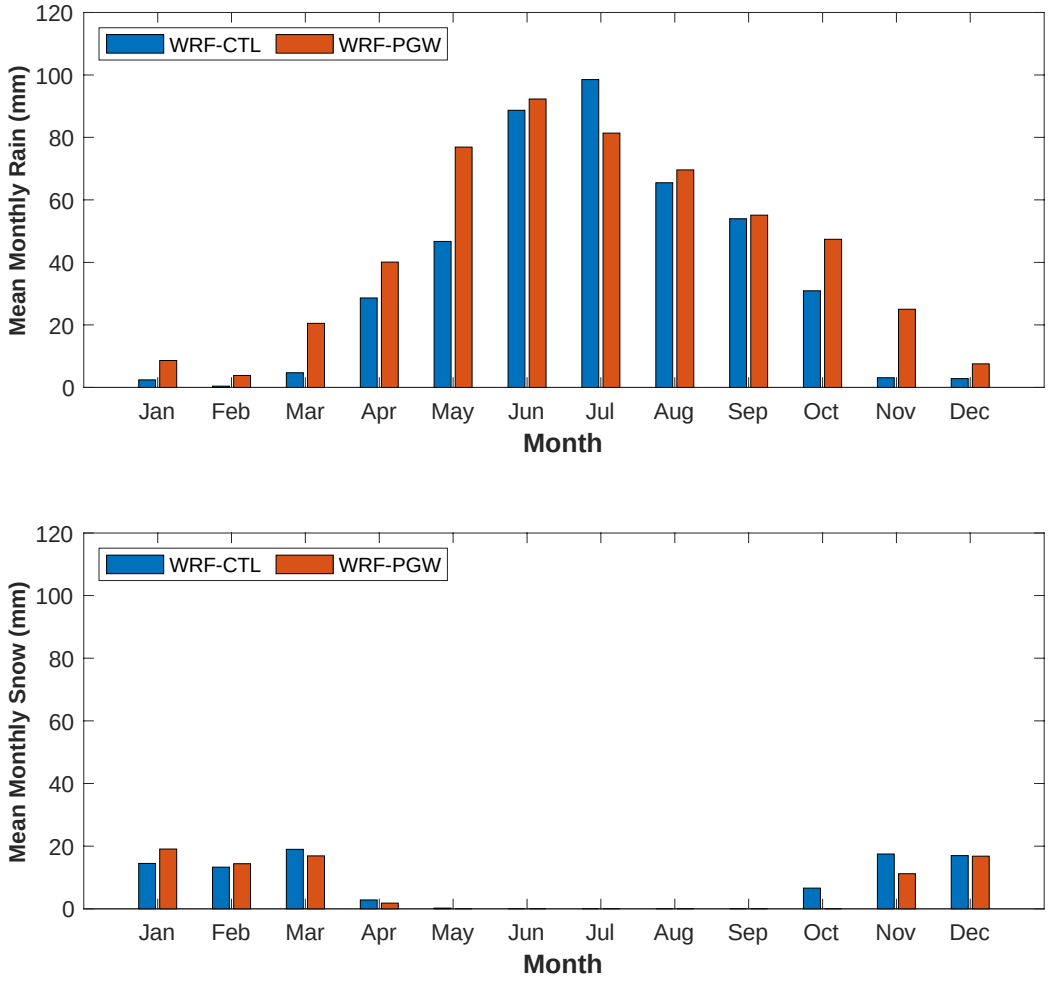

Figure 7.5 Projected mean monthly change in rain and snow

7.5 SHAW SIMULATED PROJECTED CHANGE IN SOIL TEMPERATURE AND SOIL THAW

Mean annual air temperature is projected to increase from 1.3°C (WRF-CTL, 2001-2012) to 7.2°C (WRF-PGW, 2086-2097). Correspondingly, soil temperatures at the 10 cm depth are projected to

increase throughout the year at all three sites (Figure 7.6). The mean annual soil temperature is projected to rise from 3.1°C to 6.7°C for aspen, 3.0°C to 6.9°C for jack pine and 3.5°C to 7.1°C for black spruce. Soil temperatures are projected to rise above 0°C earlier in spring, following the trend of air temperature. The model projections preserve the observed relative differences among sites; the jack pine site continues to have the coldest soil temperatures in winter and the warmest soil temperatures in summer.

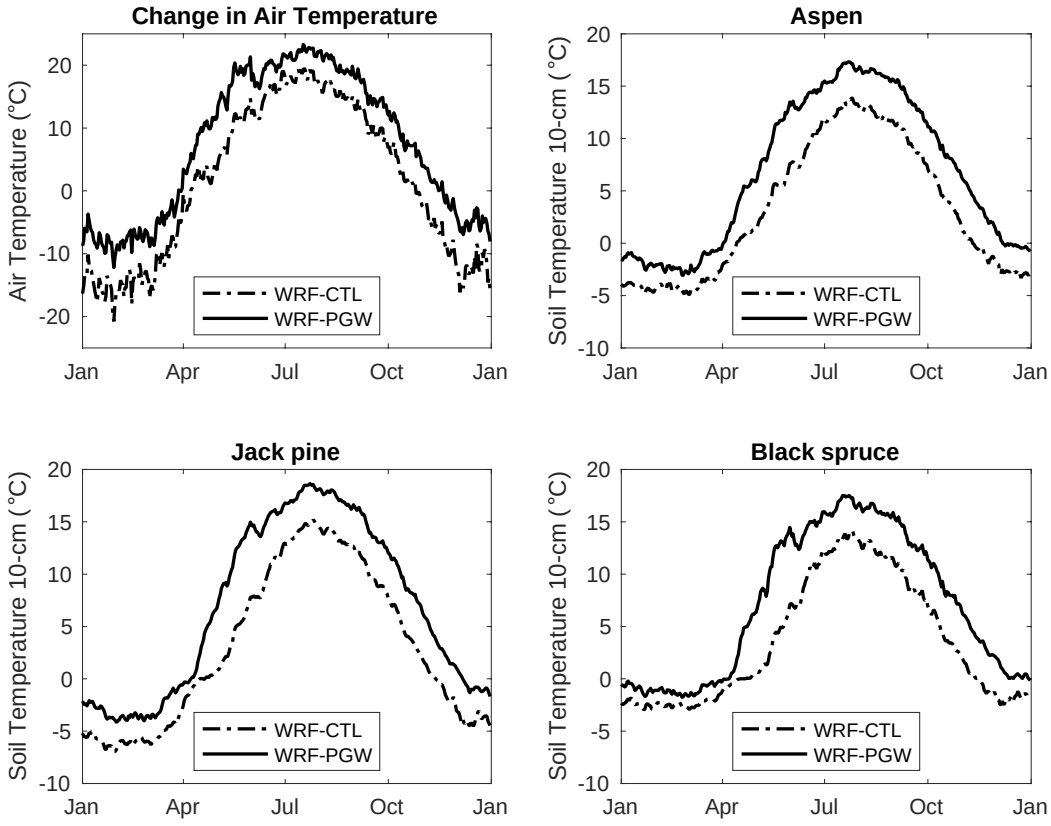

Figure 7.6 Changes in mean daily air temperature and soil temperature at 10-cm depth at all three sites between WRF-CTL and WRF-PGW scenarios

The difference between simulated soil temperatures for WRF-PGW (2087-2096) and WRF-CTL (2002-2011) scenarios shows that soil temperatures are expected to markedly increase at all depths and at all three sites with large seasonal variability (Figure 7.7). The projected change in mean daily soil temperature at 10 cm depth ranged from 0.9°C to 8.2°C for jack pine, 1.4°C to 6.5°C for

aspen, and 0.7°C to 8.3°C for black spruce. The maximum change was projected in spring and was the highest for black spruce (8.3°C) at the 10 cm depth. The projected change in mean annual soil temperature ranged from 3.3°C to 3.9°C for all depths at all three sites. The average annual change in soil temperature was 3.5°C for aspen, 3.7°C for jack pine, and 3.5°C for black spruce. The projected change in soil temperature at shallow depths was the smallest at aspen; however, a similar change was projected for the aspen and black spruce sites for deeper layers (50 cm and 100 cm depth). This was likely caused by the differences in soil moisture content at these sites which are examined in Section 7.6. However, It has been observed (Chapter 4) that the below-canopy snow accumulation was highest at aspen which could lead to greater water content at shallow depths when snow is melted in spring. At deeper layers, black spruce tends to have similar or slightly higher moisture content than aspen. Jack pine is the driest site among all and the largest change in soil temperature for deep layers was projected for this site.

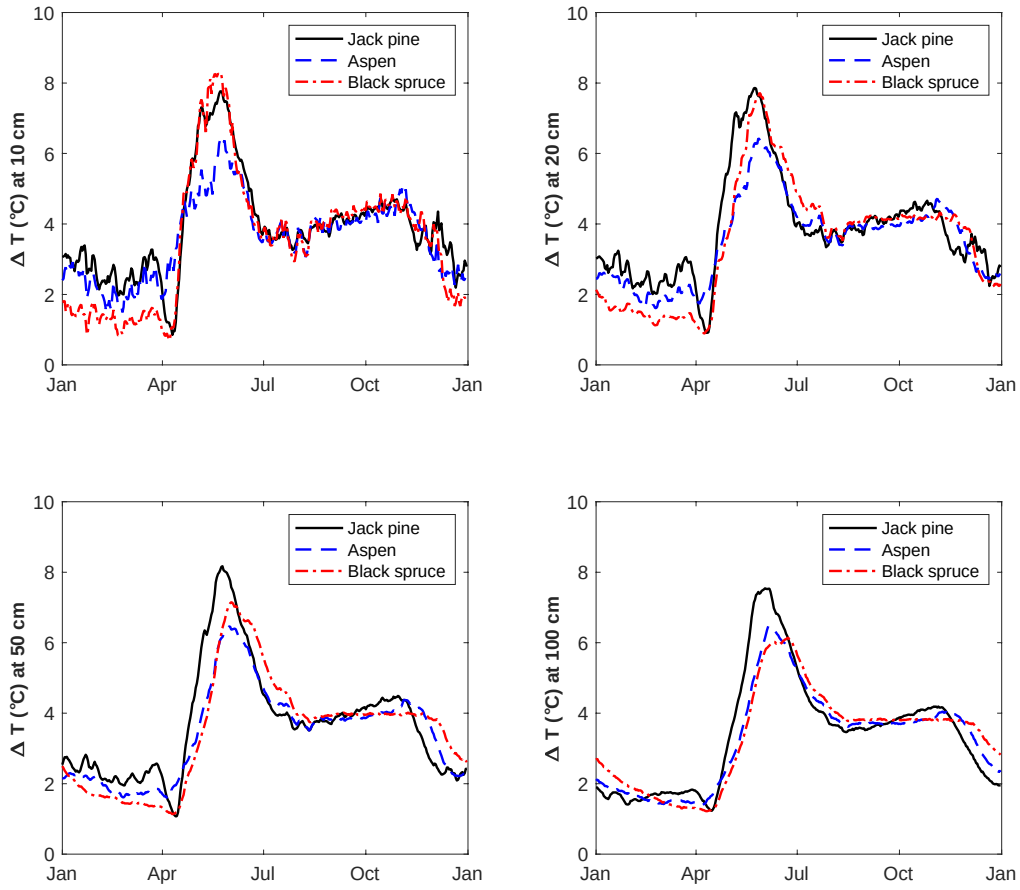

Figure 7.7 Projected change in soil temperature, ΔT(WRF-PGW – WRF-CTL) at different depths for the study sites

The depth of soil frost is projected to decrease at all three sites in future (Figure 7.8). Jack pine freezes to the deepest average depth of 145 cm followed by aspen at 130 cm and black spruce at 70 cm under historical conditions (WRF-CTL, 2002-2011). The projected frozen depths in future (WRF-PGW, 2087-2096) are 73 cm, 71 cm, and 29 cm for aspen, jack pine and black spruce sites, respectively.

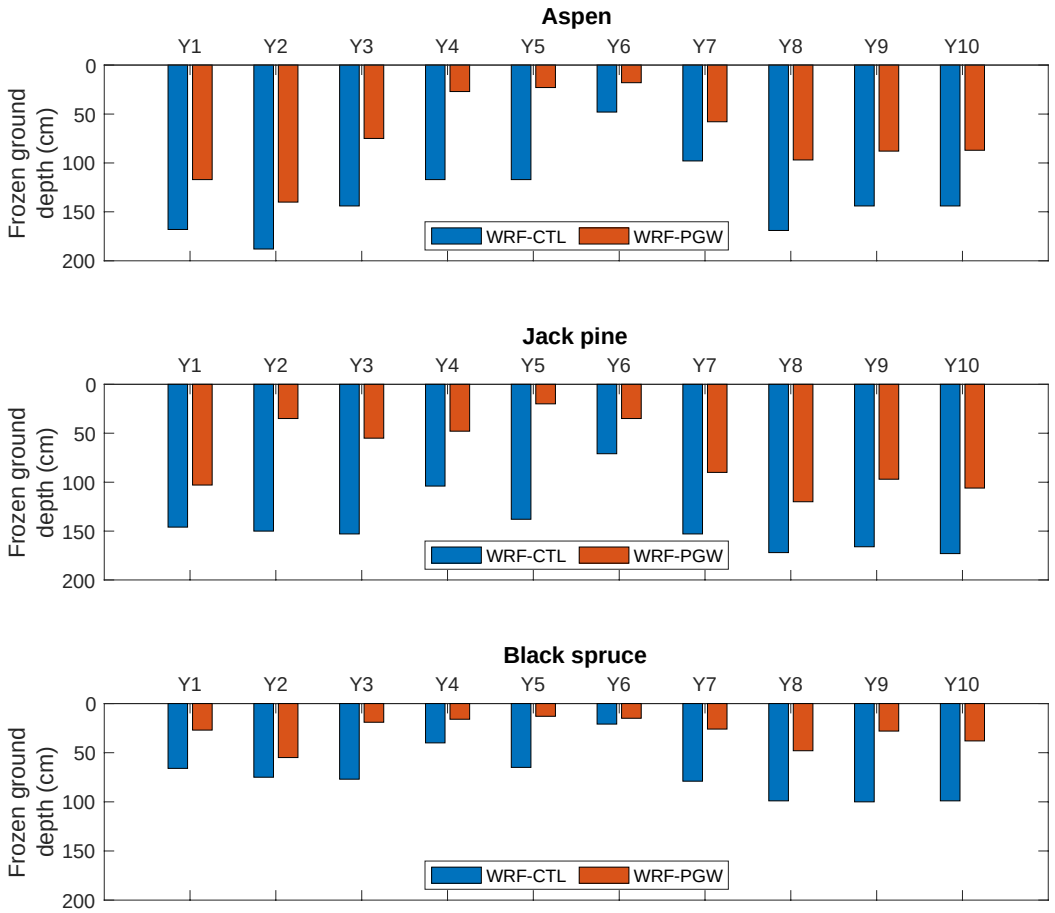

Figure 7.8 Model simulated frozen ground depth for current and future scenarios

An earlier soil thaw is projected in the future at all three sites in response to climate change (Figure 7.9). Based on historical simulations, aspen thaws first followed by jack pine and black spruce with a mean difference of about 1.5 and 3 weeks, respectively. On average, the soil thaw timing is projected to advance by 6 weeks for aspen and jack pine, and by 7 weeks for black spruce. Thus, both coniferous forest sites are projected to thaw at a similar time.

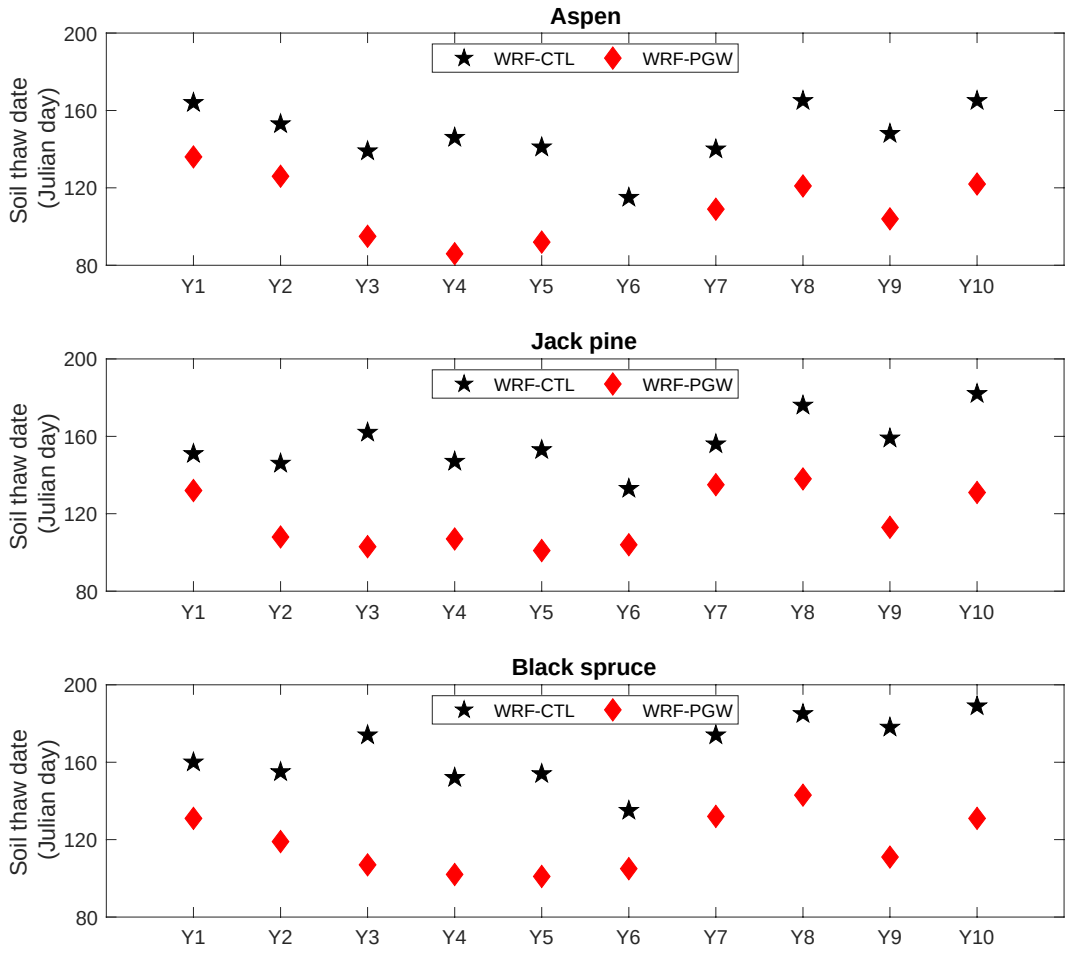

Figure 7.9 Model simulated soil thaw timing for historical and future climate

7.6 SHAW SIMULATED PROJECTED CHANGE IN EVAPOTRANSPIRATION AND SOIL MOISTURE CONTENT

The projected increase in annual evapotranspiration from WRF-CTL to WRF-PGW scenarios ranged from 3 to 62 mm for the aspen site, 32 to 123 mm for the jack pine site, and 57 to 105 mm for the black spruce site (Figure 7.10). A limitation of future climate runs is that they did not consider any advance in the timing of leaf out at the aspen site. In reality, the projected spring warming would cause earlier aspen leaf out, which in turn would add to the projected increase in evapotranspiration and reduce the differences among sites.

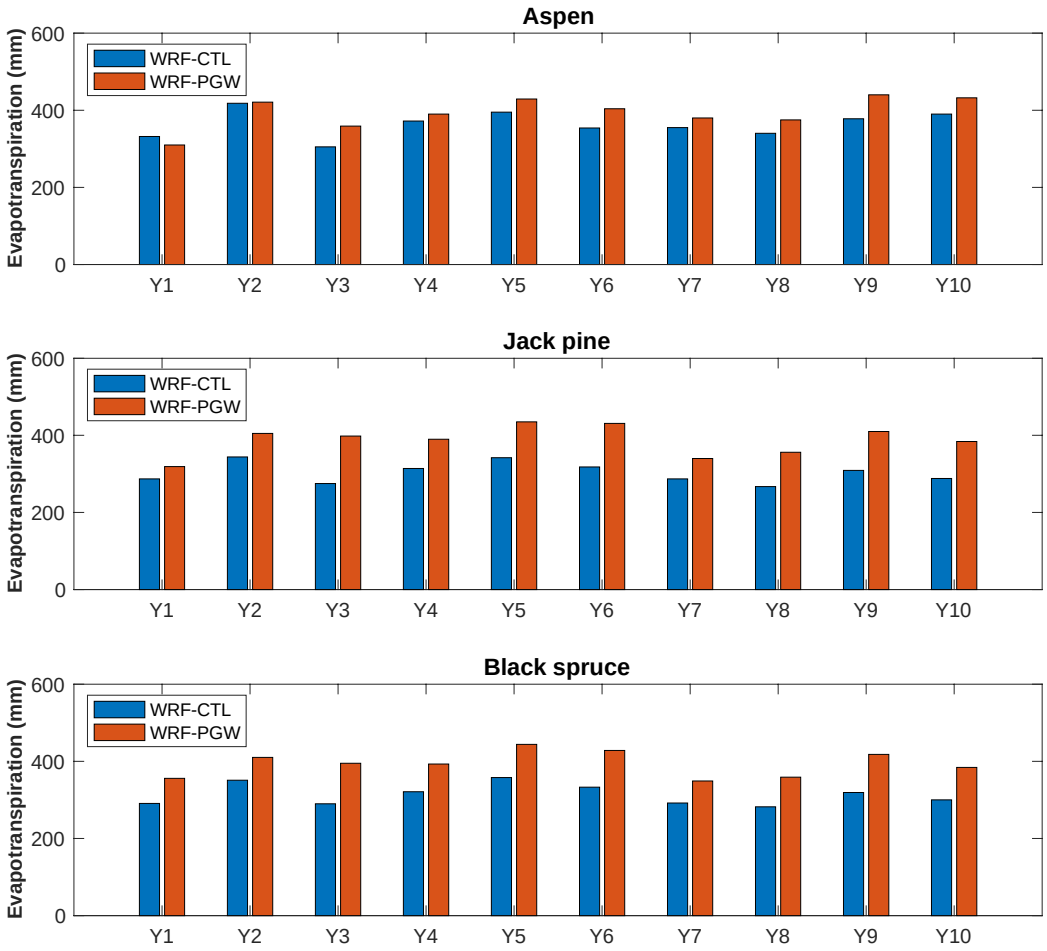

Figure 7.10 Annual evapotranspiration for historical (WRF-CTL, 2002-2011) and future (WRF-PGW, 2087-2096) conditions

In the future period, the mean daily soil liquid water content is projected to be higher in fall and winter months but slightly lower in summer at all three sites (Figure 7.11). The average increase in winter (January to April) was 0.06 m^3/m^3 for aspen, 0.03 m^3/m^3 for jack pine, and 0.10 m^3/m^3 for black spruce. The average drop in liquid water content in summer (May to September) was 0.01 m^3/m^3 for aspen, 0.02 m^3/m^3 for jack pine, and 0.04 m^3/m^3 for black spruce. An earlier rise in soil water content in spring was simulated because of earlier snowmelt with a mean difference of 2 to 2.5 weeks.

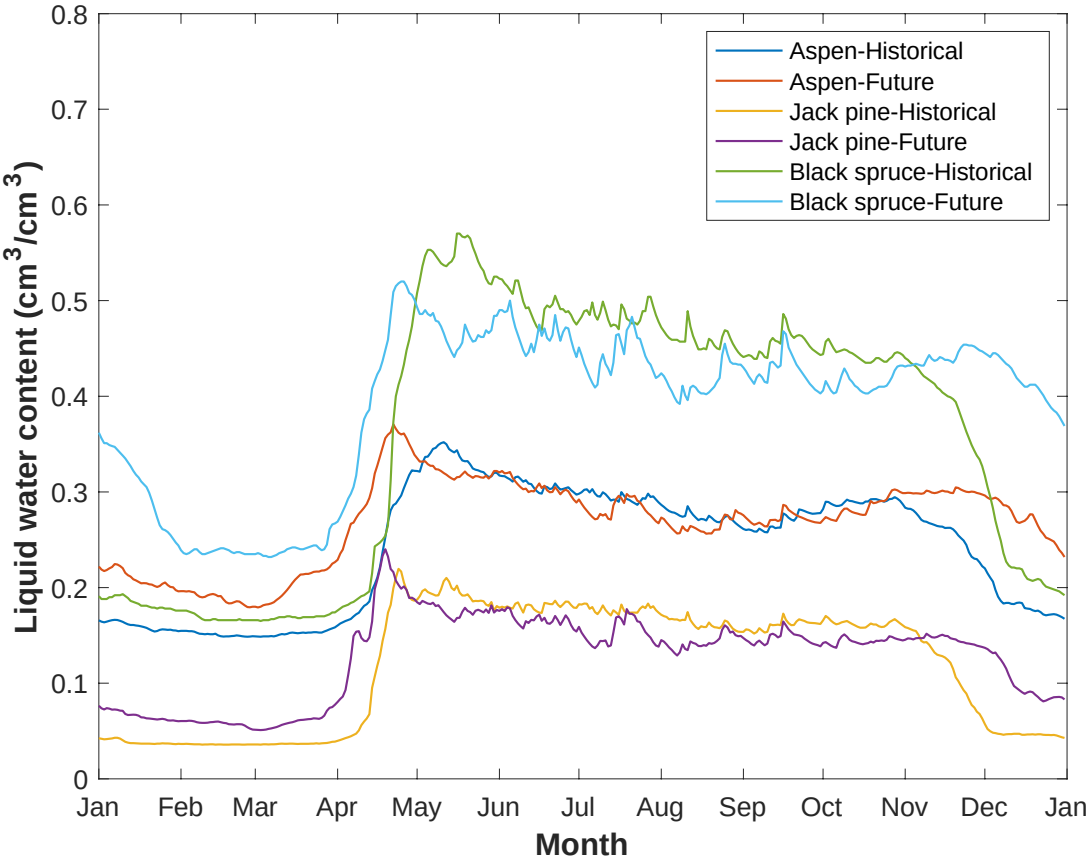

Figure 7.11 Simulated mean daily soil volumetric liquid water content at 20-cm depth from the ground surface for WRF-CTL and WRF-PGW climate scenarios

7.7 DISCUSSION

7.7.1 Uncertainty in modelling

Climate forcing data are one of the major sources of uncertainty in climate change impact studies. The future climate was derived using the PGW method, which does not consider future teleconnections, droughts, wet periods, and their impacts on future weather; thus, misses non-linear interaction between warming and atmospheric changes (Sato et al., 2007) but reduces large errors in reproducing current climate because of biases in RCMs' boundary conditions from GCMs

(Kimura and Kitoh, 2007). The dynamic downscaling of future climate by a high resolution (4 km) convective-permitting WRF model may also provide added-value in the Canadian Prairies where summer precipitation events are mostly governed by convection (Li et al., 2019). Thus, the PGW method has increasingly been adopted in western north Canada for climate change impact studies. These include evaluation of future hydrological changes in Marmot Creek Research Basin in Canadian Rockies (Fang and W. Pomeroy, 2020), an assessment of projected changes in future water budgets over western Canada (Kurkute et al., 2020), investigation of the hydrological cycle of shallow groundwater in the Prairie Pothole Region and its response to climate change (Zhang et al., 2020), and evaluation of climate change impacts on the hydrology of an Arctic headwater basin (Krogh and Pomeroy, 2019). In the present study, biased corrected WRF simulations for the current climate were comparable to the observations (Figure 7.2) and a significantly wetter (18%) and warmer (5.9°C) future climate was projected. These results are consistent with, but slightly lower than, the mean estimates of 29 global climate models over Canada (Zhang et al., 2019).

7.7.2 Projected Hydrological Changes in Southern Boreal forest

In this study, the projected increase in precipitation (18%) and air temperature (up to 5.8°C) for the southern boreal forest is in-line with other studies projecting a wetter and warmer climate in snow-dominated boreal ecosystems (Brown and Robinson, 2011; Mellander et al., 2007). This will have significant implications for several hydrological processes in the region. More precipitation is projected to occur in fall and spring and in the form of rain (Figure 7.5); thus, reduced snow depth and a longer snow-free period can be expected (Krogh and Pomeroy, 2019; Oni et al., 2017). On average, snow ablation is projected to advance by 2 to 2.5 weeks (Table 7.2) because of spring warming. Thus, the spring freshet, which dominates hydrograph in the region, will likely change its magnitude and timing (earlier) in response to climate change. The peak flow can be anticipated to be lower compared to current climate because of reduced snow accumulation but can also be higher because of projected increased rainfall in spring and expected more frequent extreme storm events (Price et al., 2013). Evapotranspiration can also be expected to increase in future in response to warming and because of larger snow-free ground period. The projected increase in mean annual evapotranspiration for coniferous forests ranged from 26% to 28% (Figure 7.10). The mean annual difference between precipitation and evapotranspiration (P-ET) was 144 mm for aspen, 205 mm

for jack pine and 194 mm for black spruce for WRF-CTL (2002-2011) which was increased for WRF-PGW (2087-2096) to 213 mm for aspen, 221 mm for jack pine and 214 mm for black spruce. However, the evapotranspiration for aspen was likely underestimated for aspen because of using same leaf phenology for future as historically observed. All these changes may influence other hydrological variables/processes such as soil water storage and ground water recharge. Soil volumetric water content is expected to be higher in the future during fall and spring seasons but slightly lower in summer months (Figure 7.11).

Table 7.2 Model simulated snow ablation date for historical and future scenarios

Year	Aspen		Jack pine		Black spruce	
	Historical	**Future**	**Historical**	**Future**	**Historical**	**Future**
Y1	106	98	112	103	114	102
Y2	100	95	105	95	107	95
Y3	100	86	111	95	116	100
Y4	97	81	107	93	108	92
Y5	98	89	101	97	103	99
Y6	108	89	117	103	123	105
Y7	105	80	107	99	109	102
Y8	101	82	105	90	111	88
Y9	90	65	94	65	95	60
Y10	106	92	111	97	117	95
Average	**101**	**86**	**107**	**94**	**110**	**94**

7.7.3 Projected Changes in Soil Temperature and Thaw for Different Forest-Cover Types

Soil temperatures and thaw timing are important for several hydrological and biogeochemical processes in boreal forests. The mean annual soil temperature (1-m profile depth) is projected to increase by 3.3°C to 3.9°C at the study sites to the end of this century. The results are consistent with previous research findings. For example, an increase of 0.6°C in soil temperature for 1°C rise

in air temperature was projected for Canadian soils during the 20th century (Zhang et al., 2005). Similarly, Houle et al. (2012) projected an increase of 3.3°C in mean annual soil temperature at three forest sites in Quebec. Soil thaw timing is projected to advance in the future by 2 to 7 weeks for different years because of early spring warming (Figure 7.6), reduced frozen ground depth (Figure 7.8), and early snow ablation (Table 7.2). An early soil thaw in response to climate change has also been predicted for scot pine stands in Swedish boreal forests (Mellander et al., 2007).

In seasonally frozen boreal forests, the response of the soil thermal environment to future air warming is subject to variability between seasons and forest types. This is because the snowpack decouples the air and soil in winter, and site characteristics further influence energy exchange processes. In this study, the largest increase in soil temperature (6.5°C to 8.3°C) was projected during spring at shallow depths (Figure 7.7), which has also been reported in other modelling studies (Jungqvist et al., 2014; Oni et al., 2017). Generally, all three sites followed the same trend of projected increases in soil temperature but with relatively different magnitudes. This variability was higher in winter and spring compared to summer and autumn months, similar to that predicted by Zhang et al. (2005). Regarding soil thaw, it also dynamically varied among study sites. For example, the depth of frozen ground was projected to decline by 58% for black spruce, 50% for jack pine, and 45% for aspen (Figure 7.8). However, the absolute depth of frozen ground is anticipated to follow the same relative order as recent observations i.e. jack pine was frozen to the deepest depth and black spruce to the shallowest depth. Sthli et al. (2001) also reported deeper winter soil frost for relatively drier sandy mineral soils compared to organic-rich soils with higher water retention capacities in Swedish boreal forests. The timing of soil thaw was projected to advance by 6 weeks for jack pine and aspen and by 7 weeks for black spruce. These results suggest that a large spatial variability of soil temperature change and thaw timing can be expected at local-scales, especially for sites with low snow cover (Mellander et al., 2007). The variability is controlled by canopy density, ground cover properties, thickness of organic soils and mineral soil texture (chapter 4).

7.7.4 Implications for Boreal Ecosystems

The projected future changes in soil temperatures and soil thaw timing will have strong influence on several ecological and biogeochemical processes. For example, late soil frost in fall and early

thaw in spring will increase growing season length. Soil freezing is expected to be delayed by 3 weeks (Figure 7.6) and soil thaw to advance by 2 to 7 weeks (Figure 7.9); thus, the length of growing season could increase up to 5-10 weeks. An extension of the growing season by about 2.5 weeks has already been observed from 1981 to 2008 in Swedish boreal forests (Oni et al., 2013). The predicted changes to the growing season may have a significant positive impact on the productivity of boreal forests, particularly at the stand scale. It has been shown in Chapter 4 (Section 4.5.3) through observed data that increased net annual carbon uptake has a statistically strong inverse relationship with early snow ablation or soil thaw. Soil moisture stress in the summer because of higher evapotranspiration could reduce this potential (Belyazid and Giuliana, 2019), but is not predicted to be a limiting factor in this study (Figure 7.11). Thus, an increase in carbon uptake can be expected in the future (Barnard et al., 2018; Danielewska et al., 2015). Pulliainen et al. (2017) report that an advancement of soil thaw by only 8 days over the period of 1979 to 2014 has resulted in increasing carbon uptake by 4% per decade for evergreen boreal forests. An enhanced CO_2 sink in response to a warming climate has also been projected at larger scales in the boreal forests (Grant et al., 2009; Zhang et al., 2017). However, respiration of boreal forests is also expected to increase in response to air and soil warming (Carey et al., 2016; Öquist and Laudon, 2008) which may partially offset the increased projected CO_2 uptake. The increased respiration could also be offset by greater nutrient cycling and availability which enhances productivity (Bonan and Van Cleve, 1992; Jarvis and Linder, 2000). The projected changes in net ecosystem productivity is subject to uncertainty because of unknown complex factors including changes to forest aging because of altered disturbance patterns (Girardin et al., 2011) and forest insect pests outbreaks (Price et al., 2013). The decomposition of organic matter could also expected to increase by many folds with early soil thaw and warmed soil temperatures (Goulden et al., 1998) as predicted for the study sites (Figure 7.7 and Figure 7.9). The decomposition rate exponentially grows with soil warming; for example a 1°C increase in soil temperature may increase organic matter decomposition rate up to 10% (Kirschbaum, 1995; Zheng et al., 1993). This may also have implications for water quality as increased solute mobility can be anticipated via streams as well as through groundwater (Oni et al., 2017), particularly at shallow water table locations such as the black spruce site.

7.7.5 Study Limitations

One of the limitations of this study is that the analysis was based on the highest future precipitation prediction among all three sites (1.1). The use of a relatively less wet future climate would likely not significantly affect the change in thaw dates but would suppress future summer and annual ET and could result in a higher degree of water stress that could more than offset the benefits of an earlier growing season. However, the SHAW model does not simulate net ecosystem production (NEP); a limiting factor in exploring the relative importance of increased growing season length (due to air warming) or soil moisture stress (because of changes in precipitation and evapotranspiration patterns) on potential changes in NEP. For the same reason, the variable NEP response for future wetter and drier years could not be explored.

Another limitation of this study is the use of static vegetation i.e., the leaf area index (LAI) and leaf on-off timings for the deciduous forest site were kept the same for the historical and future climates. These changes in vegetation characteristics can influence several hydro-thermal processes such as precipitation interception and unloading, snow accumulation on the ground, evapotranspiration, radiation penetration through the canopy, and soil thaw timing. It can be expected that potential changes in vegetation characteristics and its implications may be of lesser magnitude for the evergreen coniferous forest sites than the deciduous forest site as large seasonal changes in LAI are anticipated for the aspen site because of earlier air warming/snow ablation and thus leaf emergence.

Forest composition or land cover may change in the future because of changes in atmospheric CO_2 concentration, air warming, soil moisture variability, wildfires frequency, insect outbreaks, flooding and droughts. The assessment of land cover changes in the study region was beyond the scope of this study; thus, was not considered. Accordingly, the impacts of future land cover changes on the variables of interest of this study were not explored.

As described in Section 3.6.1, the lateral sub-surface water flow was omitted in the modelling exercise because of moderately flat to gently rolling topography of the study region and coarse texture of parent material, which encourages vertical drainage and limits lateral sub-surface flow.

The results of this study may not be extrapolated to the areas where lateral sub-surface water fow is a source of advected energy for thawing soils or influences soil liquid/ice content.

7.8 SUMMARY

The potential impact of climate change on spring thaw was explored for two coniferous (jack pine and black spruce) and one deciduous forest (aspen) sites in the southern boreal forest. The SHAW model was forced with historical and future climate projections which were derived by Pseduo Global Warming (PGW) approach using Weather Research and Forecasting (WRF) model. A significantly wetter and warmer climate was projected to the end of the century with a mean increase of 18% in total annual precipitation and about 5.8°C rise in mean annual air temperature. Large hydrological changes were simulated in response to climate change including increased rainfall (23%), reduced snowfall (5%), increased evapotranspiration (26% to 28%), and earlier snow ablation (up to 2.5 weeks). A non-linear soil warming response to projected changes in air temperature was simulated by the model. The largest increase in soil temperature (6.5°C to 8.3°C) was simulated for spring with a mean annual increase of 3.3°C. The simulated projected changes in soil temperature showed local-scale spatial variability particularly during winter and spring seasons, suggesting that modelling climate change impacts on soil thermal environment in boreal ecosystems is a complex problem. Similar to soil temperature simulations, the projected changes in soil thaw also showed variability among sites. Frozen soil depth was projected to reduce (45% to 58%) at all three sites and soil thaw to advance by 6 to 7 weeks by the end of 21st century. The length of growing season was projected to increase by 5 to 10 weeks. As a result of these changes, net ecosystem productivity, water and energy fluxes, and biogeochemical processes can be expected to be significantly altered in future in the southern boreal forests.

CHAPTER 8 CONCLUSIONS AND RECOMMENDATIONS

8.1 SUMMARY AND CONCLUSIONS

This study explores the present and potential future variability of spring thaw between the two boreal coniferous (black spruce and jack pine) forests and one deciduous (aspen) forest in Western Canada with the aid of long-term observations and application of a process-based model. All three study sites were distinct in canopy coverage/leaf area index, ground cover, thickness of organic soils, and mineral soil properties.

Long-term (1997-98 to 2015-16) hydro-meteorological observations were used to describe the influence of these site characteristics on several hydro-thermal processes particularly during winter-spring transition. Precipitation and air temperature were similar at all three sites. For soil water content, the jack pine was the driest and the black spruce was the wettest site; the depth of soil freezing displayed an inverse relationship with site wetness. The mean winter soil temperatures for the frozen soil layers were -3.2°C, -1.7°C and -1.0°C for the jack pine, black spruce, and aspen sites, respectively. Snow accumulation was 15% to 20% higher for the deciduous forest site than the coniferous forest sites despite similar seasonal snowfall. Snowmelt started at a very similar time at all three sites, but snow ablation was slightly delayed (3-4 days) at the black spruce site. Inter-site variability for soil thaw end dates was large despite similar soil thaw onset dates. Soil thaw completed at the aspen site about 2.5 weeks and 4.5 weeks in advance of the jack pine and black spruce sites, respectively. The earlier soil thaw completion at the aspen site was associated with higher sub-canopy net radiation because of its leafless canopy in spring. The differences between the coniferous forests were driven by the thicker forest floor at the black spruce site which caused higher ice content and provided better insulation to the underlying soils. It was also observed that carbon uptake started during soil thaw at the coniferous forest sites (after soil thaw start date but before soil thaw completion date) and well after soil thaw for the deciduous forest site. The net annual carbon uptake was negatively correlated to spring thaw.

The application of a process-based model at the study sites was needed to explore future changes in thaw dynamics due to climate change. The simultaneous heat and water (SHAW) model was a rational choice because of its detailed representation of freeze-thaw processes and its ability to include a residue layer to represent the insulation effects of ground vegetation on the underlying soils. However, SHAW has a simplified representation of canopy-snow interactions (no unloading mechanism) which could potentially lead to erroneous snow accumulation and ablation estimates influencing spring thaw processes. A diagnostic evaluation of SHAW, the Canadian Land Surface Scheme (CLASS), and the Cold Regions Hydrological Model (CRHM) at the jack pine site suggested that the limitation of no unloading in SHAW can be offset by reducing snow interception through the calibration of maximum intercepted precipitation parameter at the study site. The SHAW model simulated snow accumulation and sublimation losses that were comparable to CLASS and CRHM. Snowmelt rates were better simulated by CRHM for 2 out of 3 years and by CLASS for 1 year; however, all three models simulated similar snow ablation dates. SHAW outperformed both CLASS and CRHM for simulating thaw timing. The difference in thaw timing for different depths (10-, 20-, 50-, and 100-cm) ranged from 1 to 7 days for SHAW, 1 to 22 days for CLASS, and 7 to 42 days for CRHM. The better performance of SHAW model was associated with a 2 cm thick residue layer which provided insulation to the underlying soil. Spring evapotranspiration was overestimated by all three models in the range of 29 mm to 80 mm likely because of no consideration of the influence of cold soil temperatures on stomatal conductance.

Following the diagnostic evaluation of model performance, the application of SHAW was extended to all three sites but with an improved algorithm for modelling stomatal functioning to indirectly consider the influence of soil thermal environment on stomatal conductance through cumulative growing degree days. The proposed factor was derived based on the observed relationship between gross ecosystem photosynthesis (used as a proxy for stomatal functioning) and air temperature/growing degree days. Spring evapotranspiration simulations for the coniferous forest sites were greatly improved with the consideration of proposed GDD factor and errors were reduced by 35 to 40 mm. In addition, it was also demonstrated that soil temperature/soil thaw simulations were improved when insulation effects of ground cover were considered by the dead plant residue layer in SHAW. The mean absolute error for soil temperature simulations at 20 cm depth were reduced from 1.5°C to 0.4°C for the aspen site, 1.2°C to 0.6°C for the jack pine site,

and 1.2°C to 0.7°C for the black spruce site. The difference in observed and simulated soil thaw timing was 2 to 2.5 weeks without considering the ground cover layer and reduced to only 2 to 3 days when insulation effects of ground cover were considered.

In order to understand the impacts of climate change on spring thaw at the study sites, the parameterized SHAW model was run with future climate projections. The Pseudo Global Warming (PGW) approach was adopted to derive future climate data and Weather Research and Forecasting (WRF) model was used for dynamic downscaling. In future, precipitation is projected to increase by 18% and mean annual air temperature by 5.8°C to the end of the 21st century. In response, the mean annual soil temperature (10 cm depth) is projected to increase by 3.6°C for the aspen site, 3.9°C for the jack pine site and 3.5°C for the black spruce site. The highest increase in soil temperature was projected in early spring and ranged from 6.5°C to 8.3°C. Frozen ground depth is projected to reduce in future at all three sites with a mean difference of 72 cm for the jack pine, 59 cm for the aspen, and 41 cm for the black spruce site. Snow ablation and soil thaw completion are projected to advance by 2 weeks, and 6 to 7 weeks, respectively. Thus, a significant increase in growing season length is anticipated. Evapotranspiration is projected to increase by 30 to 80 mm without causing moisture stress in the soil profile because of increased precipitation. Accordingly, the productivity of southern boreal forests will likely increase in the future unless constrained by biological factors because of warmer air and soil temperatures.

8.2 SIGNIFICANT CONTRIBUTIONS

There is a growing interest in better understanding the implications of climate change for boreal forests. Typically, less attention has been given to understand its impacts on spring thaw/soil warming which is important for several biogeochemical and hydrological processes. In this study, variability of spring thaw/soil temperatures was explored under present and future climate in the southern boreal forest. The specific significant contributions of this research work are listed below.

- This study advances our understanding about existing spring thaw variability between two coniferous sites (jack pine and black spruce) and one deciduous (aspen) forest sites in the southern boreal region, identifies its controlling factors, and examines the relationship between spring thaw and carbon uptake with the aid of long-term observations. Inter-site variability of spring thaw was quantified and associated with differences in canopy architecture as well as forest floor characteristics and soil texture. The key findings have been summarized in Section 8.1.

- From a modelling perspective, accurate simulations for soil temperatures/thaw timing and spring evapotranspiration have been challenging in boreal forests. This study demonstrates that soil temperature/soil thaw simulations can be greatly improved by considering insulation effects of ground cover. For spring evapotranspiration, it was demonstrated that soil temperature influence on stomatal functioning needs to be considered for boreal coniferous forests. A new term for the Jarvis-Steward resistance scheme based on cumulative growing degree days was proposed and tested which significantly improved simulations for spring evapotranspiration.

- This study also advances our understanding about the potential future changes in snow-soil dynamics at the study sites due to climate change. Large spatial variability of soil temperatures and thaw timing is predicted between the sites. In general, lower snow accumulation, earlier snowmelt, warmer soil temperatures, earlier soil thaw timing, higher evapotranspiration, and increased growing season length was projected at all three sites. The predicted magnitude of change in these processes has been summarized in Section 8.1.

8.3 RECOMMENDATIONS

Based on the work completed in this study, the following recommendations are made:

- The simulations of SHAW for soil temperature and spring evapotranspiration improved by considering ground cover layer (Section 6.2.2) and proposed growing degree days factor (Section 6.3.4), respectively. These algorithms should be considered and further evaluated by other models such as CLASS and CRHM for simulating soil temperatures and spring evapotranspiration in boreal forests.

- Site characteristics control spring thaw variability (Section 4.5.2) which is not only important for hydrological processes but also has a strong association with carbon uptake. Thus, local-scale variability of spring thaw must be captured and its linkages with runoff, infiltration, evapotranspiration and carbon uptake should be well represented in models when simulating water and carbon fluxes at ecosystem scales.

- The forest floor characteristics are important for soil thaw because of its insulation effects on underlying soils. Future work should advance our understanding about the climate change impacts on spatial-temporal changes in forest floor of boreal ecosystems to better characterize the impacts of climate change in these environments.

- The assessment of future land cover changes in the southern boreal forest and the use of a carbon coupled model such as CLASS-CTEM that combines Canadian Land Surface Scheme and Canadian Terrestrial Ecosystem Model may be of great use for evaluating relative significance of air warming and increased precipitation on net ecosystem production under changing future climate.

REFERENCES

Amiro, B.D., Barr, A.G., Black, T.A., Iwashita, H., Kljun, N., McCaughey, J.H., Morgenstern, K., Murayama, S., Nesic, Z., Orchansky, A.L., Saigusa, N., 2006. Carbon, energy and water fluxes at mature and disturbed forest sites, Saskatchewan, Canada. Agric. For. Meteorol. 136, 237–251. https://doi.org/10.1016/j.agrformet.2004.11.012

Axelsson, B., Agren, G., 1976. Tree growth model (PT 1)—a development paper. Swedish Coniferous Forest Project Internal Report 41.

Balland, V., Bhatti, J., Errington, R., Castonguay, M., Arp, P.A., 2006. Modeling snowpack and soil temperature and moisture conditions in a jack pine, black spruce and aspen forest stand in central Saskatchewan (BOREAS SSA). Can. J. Soil Sci. 86, 203–217. https://doi.org/10.4141/S05-088

Barlett, P.A., MacKay, M.D., Verseghy, D.L., 2006. Modified snow algorithms in the Canadian Land Surface Scheme: Model runs and sensitivity analysis at three boreal forest stands. Atmos. - Ocean. https://doi.org/10.3137/ao.440301

Barnard, D.M., Knowles, J.F., Barnard, H.R., Goulden, M.L., Hu, J., Litvak, M.E., Molotch, N.P., 2018. Reevaluating growing season length controls on net ecosystem production in evergreen conifer forests. Sci. Rep. https://doi.org/10.1038/s41598-018-36065-0

Barr, A., Black, T.A., Mccaughey, H., 2009. Climatic and phenological controls of the carbon and energy balances of three contrasting boreal forest ecosystems in Western Canada, in: Phenology of Ecosystem Processes. Springer, New York, NY, pp. 3–34. https://doi.org/10.1007/978-1-4419-0026-5_1

Barr, A.G., Black, T.A., Hogg, E.H., Griffis, T.J., Morgenstern, K., Kljun, N., Theede, A., Nesic, Z., 2007. Climatic controls on the carbon and water balances of a boreal aspen forest, 1994-2003. Glob. Chang. Biol. https://doi.org/10.1111/j.1365-2486.2006.01220.x

Barr, A.G., Black, T.A., Hogg, E.H., Kljun, N., Morgenstern, K., Nesic, Z., 2004. Inter-annual

variability in the leaf area index of a boreal aspen-hazelnut forest in relation to net ecosystem production. Agric. For. Meteorol. 126, 237–255. https://doi.org/10.1016/j.agrformet.2004.06.011

Barr, A.G., van der Kamp, G., Black, T.A., McCaughey, J.H., Nesic, Z., 2012. Energy balance closure at the BERMS flux towers in relation to the water balance of the White Gull Creek watershed 1999-2009. Agric. For. Meteorol. https://doi.org/10.1016/j.agrformet.2011.05.017

Bartlett, P.A., Mackay, M., Neumann, M., Verseghy, D., Barr, A.., 2008. Modelling snow interception and unloading in the Canadian Land Surface Scheme, in: Atmospheric Modeling and Data Assimilation of Land-Surface Climate Interactions. 28th Conference of Agriculture and Forest Meteorology. American Meteorological Society.

Bartlett, P.A., McCaughey, J.H., Lafleur, P.M., Verseghy, D.L., 2003. Modelling evapotranspiration at three boreal forest stands using the class: Tests of parameterizations for canopy conductance and soil evaporation. Int. J. Climatol. https://doi.org/10.1002/joc.884

Bartsch, A., Kidd, R.A., Wagner, W., Bartalis, Z., 2007. Temporal and spatial variability of the beginning and end of daily spring freeze/thaw cycles derived from scatterometer data. Remote Sens. Environ. https://doi.org/10.1016/j.rse.2006.09.004

Belyazid, S., Giuliana, Z., 2019. Water limitation can negate the effect of higher temperatures on forest carbon sequestration. Eur. J. For. Res. https://doi.org/10.1007/s10342-019-01168-4

Bergh, J., Linder, S., 1999. Effects of soil warming during spring on photosynthetic recovery in boreal Norway spruce stands. Glob. Chang. Biol. https://doi.org/10.1046/j.1365-2486.1999.00205.x

Beringer, J., Lynch, A.H., Chapin, F.S.I., Mack, M., Bonan, G.B., 2001. The representation of arctic soils in the land surface model: The importance of mosses. J. Clim. 14, 3324–3335. https://doi.org/10.1175/1520-0442(2001)014<3324:TROASI>2.0.CO;2

Betts, A.K., Ball, J.H., 1997. Albedo over the boreal forest. J. Geophys. Res. Atmos.

https://doi.org/10.1029/96JD03876

Beven, K., Binley, A., 1992. The future of distributed models: Model calibration and uncertainty prediction. Hydrol. Process. 6, 279–298. https://doi.org/10.1002/hyp.3360060305

Bhatia, K.T., Vecchi, G.A., Knutson, T.R., Murakami, H., Kossin, J., Dixon, K.W., Whitlock, C.E., 2019. Recent increases in tropical cyclone intensification rates. Nat. Commun. https://doi.org/10.1038/s41467-019-08471-z

Black, T.A., Den Hartog, G., Neumann, H.H., Blanken, P.D., Yang, P.C., Russell, C., Nesic, Z., Lee, X., Chen, S.G., Staebler, R., Novak, M.D., 1996. Annual cycles of water vapour and carbon dioxide fluxes in and above a boreal aspen forest. Glob. Chang. Biol. 2, 219–229. https://doi.org/10.1111/j.1365-2486.1996.tb00074.x

Blok, D., Heijmans, M.M.P.D., Schaepman-Strub, G., van Ruijven, J., Parmentier, F.J.W., Maximov, T.C., Berendse, F., 2011. The cooling capacity of mosses: Controls on water and energy fluxes in a Siberian Tundra site. Ecosystems 14, 1055–1065. https://doi.org/10.1007/s10021-011-9463-5

Bonan, G.B., Chapin, F.S., Thompson, S.L., 1995. Boreal forest and tundra ecosystems as components of the climate system. Clim. Change. https://doi.org/10.1007/BF01094014

Bonan, G.B., Davis, K.J., Baldocchi, D., Fitzjarrald, D., Neumann, H., 1997. Comparison of the NCAR LSM1 land surface model with BOREAS aspen and jack pine tower fluxes. J. Geophys. Res. 102, 29065. https://doi.org/10.1029/96JD03095

Bonan, G.B., Van Cleve, K., 1992. Soil temperature, nitrogen mineralization, and carbon source-sink relationships in boreal forests. Can. J. For. Res. 22, 629–639. https://doi.org/10.1139/x92-084

Bonan, G.B., Williams, M., Fisher, R.A., Oleson, K.W., 2014. Modeling stomatal conductance in the earth system: Linking leaf water-use efficiency and water transport along the soil-plant-atmosphere continuum. Geosci. Model Dev. 7, 2193–2222. https://doi.org/10.5194/gmd-7-

2193-2014

Boonstra, R., Andreassen, H.P., Boutin, S., Hušek, J., Ims, R.A., Krebs, C.J., Skarpe, C., Wabakken, P., 2016. Why do the boreal forest ecosystems of Northwestern Europe differ from those of Western North America? Bioscience. https://doi.org/10.1093/biosci/biw080

Brandt, J.P., 2009. The extent of the North American boreal zone. Environ. Rev. https://doi.org/10.1139/A09-004

Brandt, J.P., Flannigan, M.D., Maynard, D.G., Thompson, I.D., Volney, W.J.A., 2013. An introduction to Canada's boreal zone: ecosystem processes, health, sustainability, and environmental issues. Environ. Rev. 21, 207–226. https://doi.org/10.1139/er-2013-0040

Brazhnik, K., Shugart, H.H., 2015. 3D simulation of boreal forests: Structure and dynamics in complex terrain and in a changing climate. Environ. Res. Lett. https://doi.org/10.1088/1748-9326/10/10/105006

Brooks, R.H., Corey, A.T., 1966. Properties of Porous Media Affecting Fluid Flow. J. Irrig. Drain. Div. https://doi.org/10.3758/s13423-011-0165-y

Brown, R.D., Robinson, D.A., 2011. Northern Hemisphere spring snow cover variability and change over 1922-2010 including an assessment of uncertainty. Cryosphere 5, 219–229. https://doi.org/10.5194/tc-5-219-2011

Canadian Society of Soil Science, 2020. Soils of Canada [WWW Document]. Univ. Saskatchewan.

Cannell, M.G.R., Smith, R.I., 1983. Thermal Time, Chill Days and Prediction of Budburst in Picea sitchensis. J. Appl. Ecol. 20, 951–963. https://doi.org/10.2307/2403139

Cannon, A.J., Sobie, S.R., Murdock, T.Q., 2015. Bias correction of GCM precipitation by quantile mapping: How well do methods preserve changes in quantiles and extremes? J. Clim. https://doi.org/10.1175/JCLI-D-14-00754.1

Carey, J.C., Tang, J., Templer, P.H., Kroeger, K.D., Crowther, T.W., Burton, A.J., Dukes, J.S.,

Emmett, B., Frey, S.D., Heskel, M.A., Jiang, L., Machmuller, M.B., Mohan, J., Panetta, A.M., Reich, P.B., Reinschj, S., Wang, X., Allison, S.D., Bamminger, C., Bridgham, S., Collins, S.L., De Dato, G., Eddy, W.C., Enquist, B.J., Estiarte, M., Harte, J., Henderson, A., Johnson, B.R., Larsen, K.S., Luo, Y., Marhan, S., Melillo, J.M., Peñuelas, J., Pfeifer-Meister, L., Poll, C., Rastetter, E., Reinmann, A.B., Reynolds, L.L., Schmidt, I.K., Shaver, G.R., Strong, A.L., Suseela, V., Tietema, A., 2016. Temperature response of soil respiration largely unaltered with experimental warming. Proc. Natl. Acad. Sci. U. S. A. https://doi.org/10.1073/pnas.1605365113

Chadburn, S., Burke, E., Essery, R., Boike, J., Langer, M., Heikenfeld, M., Cox, P., Friedlingstein, P., 2015. An improved representation of physical permafrost dynamics in the JULES land-surface model. Geosci. Model Dev. 8, 1493–1508. https://doi.org/10.5194/gmd-8-1493-2015

Changwei, X., Gough, W.A., 2013. A simple thaw-freeze algorithm for a multi-layered soil using the stefan equation. Permafr. Periglac. Process. https://doi.org/10.1002/ppp.1770

Chen, F., Dudhia, J., 2001. Coupling an Advanced Land Surface–Hydrology Model with the Penn State–NCAR MM5 Modeling System. Part I: Model Implementation and Sensitivity. Mon. Weather Rev. 129, 569–585. https://doi.org/10.1175/1520-0493(2001)129<0569:CAALSH>2.0.CO;2

Chen, J., Brissette, F.P., Chaumont, D., Braun, M., 2013. Finding appropriate bias correction methods in downscaling precipitation for hydrologic impact studies over North America. Water Resour. Res. 49, 4187–4205. https://doi.org/10.1002/wrcr.20331

Chen, J.M., Blanken, P.D., Black, T.A., Guilbeault, M., Chen, S., 1997. Radiation regime and canopy architecture in a boreal aspen forest. Agric. For. Meteorol. 86, 107–125. https://doi.org/10.1016/S0168-1923(96)02402-1

Chen, J.M., Govind, A., Sonnentag, O., Zhang, Y., Barr, A., Amiro, B., 2006. Leaf area index measurements at Fluxnet-Canada forest sites. Agric. For. Meteorol. 140, 257–268. https://doi.org/10.1016/j.agrformet.2006.08.005

Chen, L., Li, Y., Chen, F., Barr, A., Barlage, M., Wan, B., 2016. The incorporation of an organic soil layer in the Noah-MP land surface model and its evaluation over a boreal aspen forest. Atmos. Chem. Phys. https://doi.org/10.5194/acp-16-8375-2016

Clapp, R.B., Hornberger, G.M., 1978. Empirical equations for some soil hydraulic properties. Water Resour. Res. https://doi.org/10.1029/WR014i004p00601

Collins, D.C., Avissar, R., 1994. An evaluation with the Fourier amplitude sensitivity test (FAST) of which land-surface parameters are of greatest importance in atmospheric modeling. J. Clim. https://doi.org/10.1175/1520-0442(1994)007<0681:AEWTFA>2.0.CO;2

Cosby, B.J., Hornberger, G.M., Clapp, R.B., Ginn, T.R., 1984. A statistical exploration of the relationships of soil moisture characteristics to the physical properties of soils. Water Resour. Res. 20, 682–690. https://doi.org/10.1029/WR020i006p00682

Cuenca, R., Stangel, E.D., Kelly, F.S., 1997. Soil water balance in a boreal forest. J. Geophys. Res. 102, 355–365.

D'Orangeville, L., Houle, D., Duchesne, L., Phillips, R.P., Bergeron, Y., Kneeshaw, D., 2018. Beneficial effects of climate warming on boreal tree growth may be transitory. Nat. Commun. https://doi.org/10.1038/s41467-018-05705-4

Dai, A., 2013. Increasing drought under global warming in observations and models. Nat. Clim. Chang. 3, 52–58. https://doi.org/10.1038/nclimate1633

Danielewska, A., Urbaniak, M., Olejnik, J., 2015. Growing season length as a key factor of cumulative net ecosystem exchange over the pine forest ecosystems in Europe. Int. Agrophysics 29, 129–135. https://doi.org/10.1515/intag-2015-0026

Davison, B., Pietroniro, A., Fortin, V., Leconte, R., Mamo, M., Yau, M.K., 2016. What is missing from the prescription of hydrology for land surface schemes? J. Hydrometeorol. 17, 2013–2039. https://doi.org/10.1175/JHM-D-15-0172.1

Dee, D.P., Uppala, S.M., Simmons, A.J., Berrisford, P., Poli, P., Kobayashi, S., Andrae, U.,

Balmaseda, M.A., Balsamo, G., Bauer, P., Bechtold, P., Beljaars, A.C.M., van de Berg, L., Bidlot, J., Bormann, N., Delsol, C., Dragani, R., Fuentes, M., Geer, A.J., Haimberger, L., Healy, S.B., Hersbach, H., Hólm, E. V., Isaksen, L., Kållberg, P., Köhler, M., Matricardi, M., Mcnally, A.P., Monge-Sanz, B.M., Morcrette, J.J., Park, B.K., Peubey, C., de Rosnay, P., Tavolato, C., Thépaut, J.N., Vitart, F., 2011. The ERA-Interim reanalysis: Configuration and performance of the data assimilation system. Q. J. R. Meteorol. Soc. https://doi.org/10.1002/qj.828

Dettmann, U., Bechtold, M., Frahm, E., Tiemeyer, B., 2014. On the applicability of unimodal and bimodal van Genuchten-Mualem based models to peat and other organic soils under evaporation conditions. J. Hydrol. https://doi.org/10.1016/j.jhydrol.2014.04.047

Domisch, T., Finér, L., Lehto, T., Smolander, A., 2002. Effect of soil temperature on nutrient allocation and mycorrhizas in Scots pine seedlings. Plant Soil 239, 173–185. https://doi.org/10.1023/A:1015037127126

Drake, T.W., Wickland, K.P., Spencer, R.G.M., McKnight, D.M., Striegl, R.G., 2015. Ancient low-molecular-weight organic acids in permafrost fuel rapid carbon dioxide production upon thaw. Proc. Natl. Acad. Sci. U. S. A. https://doi.org/10.1073/pnas.1511705112

Druel, A., Peylin, P., Krinner, G., Ciais, P., Viovy, N., Peregon, A., Bastrikov, V., Kosykh, N., Mironycheva-Tokareva, N., 2017. Towards a more detailed representation of high-latitude vegetation in the global land surface model ORCHIDEE (ORC-HL-VEGv1.0). Geosci. Model Dev. 10, 4693–4722. https://doi.org/10.5194/gmd-10-4693-2017

Dwyer, L.M., N, H.H., B, C.J.L., 1990. Prediction of soil temperature from air temperature for estimating corn emergence. Can. J. Plant Sci. 70, 619–628.

Egerton-Warburton, L.M., Querejeta, J.I., Allen, M.F., 2007. Common mycorrhizal networks provide a potential pathway for the transfer of hydraulically lifted water between plants. J. Exp. Bot. 58, 1473–1483. https://doi.org/10.1093/jxb/erm009

Ekici, A., Beer, C., Hagemann, S., Boike, J., Langer, M., Hauck, C., 2014. Simulating high-latitude

permafrost regions by the JSBACH terrestrial ecosystem model. Geosci. Model Dev. https://doi.org/10.5194/gmd-7-631-2014

Elliott, J.A., Toth, B.M., Granger, R.J., Pomeroy, J.W., 1998. Soil moisture storage in mature and replanted sub-humid boreal forest stands. Can. J. Soil Sci. 78, 17–27. https://doi.org/10.4141/S97-021

Ellis, C.R., Pomeroy, J.W., Brown, T., MacDonald, J., 2010. Simulation of snow accumulation and melt in needleleaf forest environments. Hydrol. Earth Syst. Sci. https://doi.org/10.5194/hess-14-925-2010

Ensminger, I., Schmidt, L., Lloyd, J., 2008. Soil temperature and intermittent frost modulate the rate of recovery of photosynthesis in Scots pine under simulated spring conditions. New Phytol. 177, 428–442. https://doi.org/10.1111/j.1469-8137.2007.02273.x

Essery, R., Pomeroy, J., Ellis, C., Link, T., 2008. Modelling longwave radiation to snow beneath forest canopies using hemispherical photography or linear regression. Hydrol. Process. 22, 2788–2800. https://doi.org/10.1002/hyp.6930

Essery, R., Pomeroy, J., Parviainen, J., Storck, P., 2003. Sublimation of snow from coniferous forests in a climate model. J. Clim. https://doi.org/10.1175/1520-0442(2003)016<1855:SOSFCF>2.0.CO;2

Essery, R., Rutter, N., Pomeroy, J., Baxter, R., Stähli, M., Gustafsson, D., Barr, A., Bartlett, P., Elder, K., 2009. SNOWMIP2: An Evaluation of Forest Snow Process Simulations. Bull. Am. Meteorol. Soc. 90, 1120–1136. https://doi.org/10.1175/2009BAMS2629.1

Eugster, W., Rouse, W.R., Pielke, R.A., Mcfadden, J.P., Baldocchi, D.D., Kittel, T.G.F., Chapin, F.S., Liston, G.E., Vidale, P.L., Vaganov, E., Chambers, S., 2000. Land-atmosphere energy exchange in Arctic tundra and boreal forest: Available data and feedbacks to climate. Glob. Chang. Biol. https://doi.org/10.1046/j.1365-2486.2000.06015.x

Fang, X., W. Pomeroy, J., 2020. Diagnosis of future changes in hydrology for a Canadian Rockies

headwater basin. Hydrol. Earth Syst. Sci. 24, 2731–2754. https://doi.org/10.5194/hess-24-2731-2020

Flerchinger, G.N., 2017. The simultaneous heat and water (SHAW) model: Technical documentation. Biose, Idaho.

Flerchinger, G.N., 2000. The Simultaneous Heat and Water (SHAW) Model: Technical documentation.

Flerchinger, G.N., Baker, J.M., Spaans, E.J.A., 1996. A test of the radiative energy balance of the shaw model for snowcover. Hydrol. Process. https://doi.org/10.1002/(sici)1099-1085(199610)10:10<1359::aid-hyp466>3.3.co;2-e

Flerchinger, G.N., Cooley, K.R., Deng, Y., 1994. Impacts of spatially and temporally varying snowmelt on subsurface flow in a mountainous watershed: 1. Snowmelt simulation. Hydrol. Sci. J. https://doi.org/10.1080/02626669409492771

Flerchinger, G.N., Hanson, C.L., 1989. Modeling soil freezing and thawing on a rangeland watershed. Trans. Am. Soc. Agric. Eng. https://doi.org/10.13031/2013.31188

Flerchinger, G.N., Kustas, W.P., Weltz, M. a., 1998. Simulating Surface Energy Fluxes and Radiometric Surface Temperatures for Two Arid Vegetation Communities Using the SHAW Model. J. Appl. Meteorol. 37, 449–460. https://doi.org/10.1175/1520-0450(1998)037<0449:SSEFAR>2.0.CO;2

Flerchinger, G.N., Saxton, K.E., 1989. Simultaneous Heat and Water Model of a freezing snow-residue-soil system i. theory and development. Trans. ASAE. https://doi.org/10.13031/2013.31040

Fowler, H.J., Blenkinsop, S., Tebaldi, C., 2007. Linking climate change modelling to impacts studies: Recent advances in downscaling techniques for hydrological modelling. Int. J. Climatol. https://doi.org/10.1002/joc.1556

Frelich, L.E., Montgomery, R.A., Reich, P.B., 2021. Seven ways a warming climate can kill the

southern boreal forest. Forests 12. https://doi.org/10.3390/f12050560

Fuchs, E.E., Livingston, N.J., 1996. Hydraulic control of stomatal conductance in Douglas fir [Pseudotsuga menziesii (Mirb.) Franco] and alder [Alnus rubra (Bong)] seedlings. Plant, Cell Environ. 19, 1091–1098. https://doi.org/10.1111/j.1365-3040.1996.tb00216.x

Fuchs, M., Campbell, G.S., Papendick, R.I., 1978. An Analysis of Sensible and Latent Heat Flow in a Partially Frozen Unsaturated Soil. Soil Sci. Soc. Am. J. 42, 379–385. https://doi.org/10.2136/sssaj1978.03615995004200030001x

Gelfan, A.N., Pomeroy, J.W., Kuchment, L.S., 2004. Modeling forest cover influences on snow accumulation, sublimation, and melt. J. Hydrometeorol. 5, 785–803. https://doi.org/10.1175/1525-7541(2004)005<0785:MFCIOS>2.0.CO;2

Girardin, M.P., Bernier, P.Y., Gauthier, S., 2011. Increasing potential NEP of eastern boreal North American forests constrained by decreasing wildfire activity. Ecosphere. https://doi.org/10.1890/ES10-00159.1

Goulden, M.L., Wofsy, S.C., Harden, J.W., Trumbore, S.E., Crill, P.M., Gower, S.T., Fries, T., Daube, B.C., Fan, S.M., Sutton, D.J., Bazzaz, A., Munger, J.W., 1998. Sensitivity of boreal forest carbon balance to soil thaw. Science (80-.). https://doi.org/10.1126/science.279.5348.214

Gower, S.T., Vogel, J.G., Norman, M., Kucharik, C.J., Steele, S.J., 1997. Carbon distribution and aboveground net primary production in aspen , jack pine , and black spruce stands in Saskatchewan and Manitoba , Canada. J. Geophys. Res. 102, 29029–29041. https://doi.org/10.1029/97JD02317

Grant, R.F., Margolis, H.A., Barr, A.G., Black, T.A., Dunn, A.L., Bernier, P.Y., Bergeron, O., 2009. Changes in net ecosystem productivity of boreal black spruce stands in response to changes in temperature at diurnal and seasonal time scales. Tree Physiol. 29, 1–17. https://doi.org/10.1093/treephys/tpn004

Gray, D.M., Landine, P.G., 1988. An energy-budget snowmelt model for the Canadian Prairies. Can. J. Earth Sci. https://doi.org/10.1139/e88-124

Grechishchev, S.E., Instanes, A., Sheshin, J.B., Pavlov, A. V., Grechishcheva, O. V., 2001. Laboratory investigation of the freezing point of oil-polluted soils. Cold Reg. Sci. Technol. https://doi.org/10.1016/S0165-232X(01)00030-1

Grillakis, M.G., Koutroulis, A.G., Daliakopoulos, I.N., Tsanis, I.K., 2017. A method to preserve trends in quantile mapping bias correction of climate modeled temperature. Earth Syst. Dyn. 8, 889–900. https://doi.org/10.5194/esd-8-889-2017

Hadiwijaya, B., Isabelle, P.E., Nadeau, D.F., Pepin, S., 2021. Observations of canopy storage capacity and wet canopy evaporation in a humid boreal forest. Hydrol. Process. 35. https://doi.org/10.1002/hyp.14021

Harder, P., Pomeroy, J., 2013. Estimating precipitation phase using a psychrometric energy balance method. Hydrol. Process. 27, 1901–1914. https://doi.org/10.1002/hyp.9799

Hardy, J.P., Davis, R.E., Winston, G.C., 1995. Evolution of factors affecting gas transmissivity of snow in the boreal forest. Biogeochem. Seas. snow-covered catchments. Proc. Symp. Boulder, 1995.

Hari, P., Kulmala, L., 2008. Boreal forest and climate change, in: Advances in Global Change Research. https://doi.org/10.1007/978-1-4020-8718-9

Hawkins, E., Osborne, T.M., Ho, C.K., Challinor, A.J., 2013. Calibration and bias correction of climate projections for crop modelling: An idealised case study over Europe. Agric. For. Meteorol. 170, 19–31. https://doi.org/10.1016/j.agrformet.2012.04.007

Hayashi, M., Goeller, N., Quinton, W.L., Wright, N., 2007. A simple heat-conduction method for simulating the frost-table depth in hydrological models, in: Hydrological Processes. https://doi.org/10.1002/hyp.6792

Hayhoe, H.N., 1994. Field testing of simulated soil freezing and thawing by the SHAW model.

Can. Agric. Eng. 36, 279–285.

Hedstrom, N.R., Pomeroy, J.W., 1998. Measurements and modelling of snow interception in the boreal forest. Hydrol. Process. 12, 1611–1625. https://doi.org/10.1002/(SICI)1099-1085(199808/09)12:10/11<1611::AID-HYP684>3.0.CO;2-4

Hejazi, A., Woodbury, A.D., 2011. Evaluation of land surface scheme SABAE-HW in simulating snow depth, soil temperature and Soil moisture within the BOREAS Site, Saskatchewan. Atmos. - Ocean. https://doi.org/10.1080/07055900.2011.587238

Hillel, D., 1998. Environmental soil physics: Fundamentals, applications, and environmental considerations, Environmental Soil Physics. Elsevier Science Publishing Co Inc, San Diego, United States.

Ho, E., Gough, W.A., 2006. Freeze thaw cycles in Toronto, Canada in a changing climate. Theor. Appl. Climatol. https://doi.org/10.1007/s00704-005-0167-7

Houle, D., Bouffard, A., Duchesne, L., Logan, T., Harvey, R., 2012. Projections of future soil temperature and water content for three Southern Quebec forested sites. J. Clim. https://doi.org/10.1175/JCLI-D-11-00440.1

Huemmrich, K.F., Black, T.A., Jarvis, P.G., McCaughey, J.H., Hall, F.G., 1999. High temporal resolution NDVI phenology from micrometeorological radiation sensors. J. Geophys. Res. Atmos. 104, 27935–27944. https://doi.org/10.1029/1999JD900164

Husted, L., 1991. Low soil temperature and efficacy of ectomycorrhizal fungi. University of British Columbia.

Ireson, A.M., Barr, A.G., Johnstone, J.F., Mamet, S.D., van der Kamp, G., Whitfield, C.J., Michel, N.L., North, R.L., Westbrook, C.J., DeBeer, C., Chun, K.P., Nazemi, A., Sagin, J., 2015. The changing water cycle: the Boreal Plains ecozone of Western Canada. WIREs Water 2, 505–521. https://doi.org/10.1002/wat2.1098

ISC-Audubon, 2013. Taiga Biome - Boreal Forest Climate (Dfc) [WWW Document]. Köppen

Clim. Classif.

Jakutsk, 2020. Weather Station Jakutsk [WWW Document]. World Clim. URL http://www.worldclimate.com/cgi-bin/data.pl?ref=N62E129+1102+24959W (accessed 1.19.20).

Jarvis, P., Linder, S., 2000. Constraints to growth of boreal forests. Nature 405, 904–905. https://doi.org/10.1038/35016154

Jarvis, P.G., 1976. The interpretation of the variations in leaf water potential and stomatal conductance found in canopies in the field. Philos. Trans. R. Soc. B Biol. Sci. https://doi.org/10.1098/rstb.1976.0035

Juday, G.P., 2020. Environmental Conditions [WWW Document]. Britannica.

Jungqvist, G., Oni, S.K., Teutschbein, C., Futter, M.N., 2014. Effect of climate change on soil temperature in Swedish boreal forests. PLoS One. https://doi.org/10.1371/journal.pone.0093957

Karyn, T., Williams, J.W., 2010. Globally downscaled climate projections for assessing the conservation impacts of climate change. Ecol. Appl. https://doi.org/10.1890/09-0173.1

Kaufmann, M., 1975. Leaf Water Stress in Engelmann Spruce: Influence of the Root and Shoot Environments. Plant Physiol. 58, 841–844. https://doi.org/10.1104/pp.56.6.841

Kauppi, P.E., Posch, M., Pirinen, P., 2014. Large impacts of climatic warming on growth of boreal forests since 1960. PLoS One. https://doi.org/10.1371/journal.pone.0111340

Kim, K.B., Kwon, H.H., Han, D., 2018. Exploration of warm-up period in conceptual hydrological modelling. J. Hydrol. 556. https://doi.org/10.1016/j.jhydrol.2017.11.015

Kimura, F., Kitoh, A., 2007. Downscaling by Pseudo Global Warning Method, The Final Report of ICCAP.

Kirschbaum, M.U.F., 1995. The temperature dependence of soil organic matter decomposition, and the effect of global warming on soil organic C storage. Soil Biol. Biochem. 27, 753–760. https://doi.org/10.1016/0038-0717(94)00242-S

Kleinn, J., Frei, C., Gurtz, J., Lüthi, D., Vidale, P.L., Schär, C., 2005. Hydrologic simulations in the Rhine basin driven by a regional climate model. J. Geophys. Res. D Atmos. https://doi.org/10.1029/2004JD005143

Kozlowski, T., 2009. Some factors affecting supercooling and the equilibrium freezing point in soil–water systems. Cold Reg. Sci. Technol. 59, 25–33. https://doi.org/10.1016/j.coldregions.2009.05.009

Kramer, K., 1994. Selecting a Model to Predict the Onset of Growth of Fagus sylvatica. J. Appl. Ecol. 31, 172–181. https://doi.org/10.2307/2404609

Kreyling, J., Henry, H.A.L., 2011. Vanishing winters in Germany: Soil frost dynamics and snow cover trends, and ecological implications. Clim. Res. https://doi.org/10.3354/cr00996

Krinner, G., Derksen, C., Essery, R., Flanner, M., Hagemann, S., Clark, M., Hall, A., Rott, H., Brutel-Vuilmet, C., Kim, H., Ménard, C.B., Mudryk, L., Thackeray, C., Wang, L., Arduini, G., Balsamo, G., Bartlett, P., Boike, J., Boone, A., Chéruy, F., Colin, J., Cuntz, M., Dai, Y., Decharme, B., Derry, J., Ducharne, A., Dutra, E., Fang, X., Fierz, C., Ghattas, J., Gusev, Y., Haverd, V., Kontu, A., Lafaysse, M., Law, R., Lawrence, D., Li, W., Marke, T., Marks, D., Ménégoz, M., Nasonova, O., Nitta, T., Niwano, M., Pomeroy, J., Raleigh, M.S., Schaedler, G., Semenov, V., Smirnova, T.G., Stacke, T., Strasser, U., Svenson, S., Turkov, D., Wang, T., Wever, N., Yuan, H., Zhou, W., Zhu, D., 2018. ESM-SnowMIP: assessing snow models and quantifying snow-related climate feedbacks. Geosci. Model Dev. 11, 5027–5049. https://doi.org/10.5194/gmd-11-5027-2018

Krogh, S.A., Pomeroy, J.W., 2019. Impact of future climate and vegetation on the hydrology of an Arctic headwater basin at the tundra-taiga transition. J. Hydrometeorol. 20, 197–215. https://doi.org/10.1175/JHM-D-18-0187.1

Krogh, S.A., Pomeroy, J.W., Marsh, P., 2017. Diagnosis of the hydrology of a small Arctic basin at the tundra-taiga transition using a physically based hydrological model. J. Hydrol. 550, 685–703. https://doi.org/10.1016/j.jhydrol.2017.05.042

Kuchment, L.S., Demidov, V.N., 2006. Modeling of influence of hydrological processes on the carbon cycle of a forest ecosystem. Environ. Model. Softw. 21, 111–114. https://doi.org/10.1016/j.envsoft.2005.01.002

Kumar, L., Skidmore, A.K., Knowles, E., 1997. Modelling topographic variation in solar radiation in a GIS environment. Int. J. Geogr. Inf. Sci. 11, 475–497. https://doi.org/10.1080/136588197242266

Kurkute, S., Li, Z., Li, Y., Huo, F., 2020. Assessment and projection of the water budget over western Canada using convection-permitting weather research and forecasting simulations. Hydrol. Earth Syst. Sci. 24, 3677–3697. https://doi.org/10.5194/hess-24-3677-2020

Kusaka, H., Hara, M., Takane, Y., 2012. Urban climate projection by the WRF model at 3-km horizontal grid increment: Dynamical downscaling and predicting heat stress in the 2070's August for Tokyo, Osaka, and Nagoya metropolises. J. Meteorol. Soc. Japan. https://doi.org/10.2151/jmsj.2012-B04

Lang, G., Early, J., Martin, G., Darnell, R., 1987. Endo-, para-, and ecodormancy: physiological terminology and classification for dormancy research. HortScience.

Launiainen, S., Guan, M., Salmivaara, A., Kieloaho, A.J., 2019. Modeling boreal forest evapotranspiration and water balance at stand and catchment scales: a spatial approach. Hydrol. Earth Syst. Sci. 23, 3457–3480. https://doi.org/10.5194/hess-23-3457-2019

Launiainen, S., Katul, G.G., Lauren, A., Kolari, P., 2015. Coupling boreal forest CO2, H2O and energy flows by a vertically structured forest canopy - Soil model with separate bryophyte layer. Ecol. Modell. https://doi.org/10.1016/j.ecolmodel.2015.06.007

Légaré, S., Bergeron, Y., Leduc, A., Paré, D., 2001. Comparison of the understory vegetation in

boreal forest types of southwest Quebec. Can. J. Bot. https://doi.org/10.1139/cjb-79-9-1019

Lemmen, D.S.D.S., Warren, F.J.F.J., Lacroix, J., Bush, E., 2008. From Impacts to Adaptation: Canada in a Changing Climate 2007., Environment.

Letts, M.G., Comer, N.T., Roulet, N.T., Skarupa, M.R., Verseghy, D.L., 2000. Parametrization of peatland hydraulic properties for the Canadian land surface scheme. Atmos. - Ocean. https://doi.org/10.1080/07055900.2000.9649643

Li, Y., Li, Z., Zhang, Z., Chen, L., Kurkute, S., Scaff, L., Pan, X., 2019. High-resolution regional climate modeling and projection over Western Canada using a Weather Research Forecasting model with a pseudo-global warming approach. Hydrol. Earth Syst. Sci. Discuss. 1–38. https://doi.org/10.5194/hess-2019-201

Liljedahl, A.K., Hinzman, L.D., Harazono, Y., Zona, D., Tweedie, C.E., Hollister, R.D., Engstrom, R., Oechel, W.C., 2011. Nonlinear controls on evapotranspiration in Arctic coastal wetlands. Biogeosciences. https://doi.org/10.5194/bg-8-3375-2011

Lindsey, R., 2019. Climate Change: Global Sea Level [WWW Document]. Clim. Magzine.

Link, T., Marks, D., 1999. Distributed simulation of snowcover mass- and energy-balance in the boreal forest. Hydrol. Process. 13, 2439–2452. https://doi.org/10.1002/(SICI)1099-1085(199910)13:14/15<2439::AID-HYP866>3.0.CO;2-1

Link, T E, Flerchinger, G.N., Unsworth, M., Marks, D., 2004. Simulation of water and energy fluxes in an old-growth seasonal temperate rain forest using the Simultaneous Heat and Water (SHAW) model. J. Hydrometeorol. 5, 443–457. https://doi.org/10.1175/1525-7541(2004)005<0443:sowaef>2.0.co;2

Link, Timothy E., Marks, D., Hardy, J.P., 2004. A deterministic method to characterize canopy radiative transfer properties. Hydrol. Process. 18, 3583–3594. https://doi.org/10.1002/hyp.5793

Linkosalo, T., Häkkinen, R., Hänninen, H., 2006. Models of the spring phenology of boreal and

temperate trees: Is there something missing? Tree Physiol. https://doi.org/10.1093/treephys/26.9.1165

MacDonald, M.K., Davison, B.J., Mekonnen, M.A., Pietroniro, A., 2016. Comparison of land surface scheme simulations with field observations versus atmospheric model output as forcing. Hydrol. Sci. J. https://doi.org/10.1080/02626667.2016.1177185

Mahat, V., Tarboton, D.G., 2014. Representation of canopy snow interception, unloading and melt in a parsimonious snowmelt model. Hydrol. Process. https://doi.org/10.1002/hyp.10116

Mahat, V., Tarboton, D.G., 2012. Canopy radiation transmission for an energy balance snowmelt model. Water Resour. Res. 48, 1–16. https://doi.org/10.1029/2011WR010438

Mahat, V., Tarboton, D.G., Molotch, N.P., 2013. Testing above- and below-canopy representations of turbulent fluxes in an energy balance snowmelt model. Water Resour. Res. https://doi.org/10.1002/wrcr.20073

Mammarella, I., Launiainen, S., Gronholm, T., Keronen, P., Pumpanen, J., Rannik, Ü., Vesala, T., 2009. Relative humidity effect on the high-frequency attenuation of water vapor flux measured by a closed-path eddy covariance system. J. Atmos. Ocean. Technol. https://doi.org/10.1175/2009JTECHA1179.1

Marietta, 2013. Climate [WWW Document]. Taiga or Boreal For. URL http://w3.marietta.edu/~biol/biomes/boreal.htm (accessed 1.19.20).

Mearns, L.O., Giorgi, F., Whetton, P., Pabon, D., Hulme, M., Lal, M., 2003. Guidelines for use of climate ccenarios developed from Regional Climate Model Experiments. Development 38.

Mellander, P.E., Bishop, K., Lundmark, T., 2004. The influence of soil temperature on transpiration: A plot scale manipulation in a young Scots pine stand. For. Ecol. Manage. https://doi.org/10.1016/j.foreco.2004.02.051

Mellander, P.E., Löfvenius, M.O., Laudon, H., 2007. Climate change impact on snow and soil temperature in boreal Scots pine stands. Clim. Change. https://doi.org/10.1007/s10584-007-

9254-3

Mellander, P.E., Stähli, M., Gustafsson, D., Bishop, K., 2006. Modelling the effect of low soil temperatures on transpiration by Scots pine. Hydrol. Process. https://doi.org/10.1002/hyp.6045

Ming, F., Chen, L., Li, D., Du, C., 2020. Investigation into Freezing Point Depression in Soil Caused by NaCl Solution. Water 12, 2232. https://doi.org/10.3390/w12082232

Mohammed, A.A., Schincariol, R.A., Quinton, W.L., Nagare, R.M., Flerchinger, G.N., 2017. On the use of mulching to mitigate permafrost thaw due to linear disturbances in sub-arctic peatlands. Ecol. Eng. https://doi.org/10.1016/j.ecoleng.2017.02.020

Molotch, N.P., Blanken, P.D., Williams, M.W., Turnipseed, A.A., Monson, R.K., Margulis, S.A., 2007. Estimating sublimation of intercepted and sub-canopy snow using eddy covariance systems, in: Hydrological Processes. https://doi.org/10.1002/hyp.6719

Monteith, J.L., 1965. Evaporation and environment. Symp. Soc. Exp. Biol. https://doi.org/10.1613/jair.301

Moore, P.A., Smolarz, A.G., Markle, C.E., Waddington, J.M., 2019. Hydrological and thermal properties of moss and lichen species on rock barrens: Implications for turtle nesting habitat. Ecohydrology. https://doi.org/10.1002/eco.2057

Mott, R., Vionnet, V., Grünewald, T., 2018. The seasonal snow cover dynamics: Review on wind-driven coupling processes. Front. Earth Sci. https://doi.org/10.3389/feart.2018.00197

National-Forest-Inventory, 2013. Canada's National Forest Inventory, revised 2006 baseline [WWW Document]. Nat. Resour. Canada, Victoria, B.C. URL https://nfi.nfis.org/en

National Geographic, 2020. Taiga [WWW Document]. Resour. Libr. URL https://www.nationalgeographic.org/encyclopedia/taiga/ (accessed 1.19.20).

Nazarbakhsh, M., Ireson, A.M., Barr, A.G., 2019. Controls on evapotranspiration from jack pine

forests in the Boreal Plains Ecozone. Hydrol. Process. 1–14. https://doi.org/10.1002/hyp.13674

Nebojsa Nakicenovic, Swart, R., 2000. Emission Scenarios. (Intergovernmental Panel Clim. Chang. Cambridge Univ. Press. https://doi.org/10.1017/CBO9781107415324.004

Nichols, D.S., Brown, J.M., 1980. Evaporation from a sphagnum moss surface. J. Hydrol. https://doi.org/10.1016/0022-1694(80)90121-3

Nijssen, B., Bowling, L.C., Lettenmaier, D.P., Clark, D.B., El Maayar, M., Essery, R., Goers, S., Gusev, Y.M., Habets, F., van den Hurk, B., Jin, J., Kahan, D., Lohmann, D., Ma, X., Mahanama, S., Mocko, D., Nasonova, O., Niu, G.-Y., Samuelsson, P., Shmakin, A.B., Takata, K., Verseghy, D., Viterbo, P., Xia, Y., Xue, Y., Yang, Z.-L., 2003. Simulation of high latitude hydrological processes in the Torne–Kalix basin: PILPS Phase 2(e). Glob. Planet. Change 38, 31–53. https://doi.org/10.1016/S0921-8181(03)00004-3

NOAA, 2020. State of the Climate: Global Climate Report for Annual 2019.

NRCan, 2019. 8 facts about Canada's boreal forest [WWW Document]. Nat. Resour. Canada.

Oni, S.K., Futter, M.N., Bishop, K., Köhler, S.J., Ottosson-Löfvenius, M., Laudon, H., 2013. Long-term patterns in dissolved organic carbon, major elements and trace metals in boreal headwater catchments: Trends, mechanisms and heterogeneity. Biogeosciences 10, 2315–2330. https://doi.org/10.5194/bg-10-2315-2013

Oni, S.K., Mieres, F., Futter, M.N., Laudon, H., 2017. Soil temperature responses to climate change along a gradient of upland–riparian transect in boreal forest. Clim. Change 143, 27–41. https://doi.org/10.1007/s10584-017-1977-1

Öquist, M.G., Laudon, H., 2008. Winter soil frost conditions in boreal forests control growing season soil CO2 concentration and its atmospheric exchange. Glob. Chang. Biol. https://doi.org/10.1111/j.1365-2486.2008.01669.x

Pan, X., Yang, D., Li, Y., Barr, A., Helgason, W., Hayashi, M., Marsh, P., Pomeroy, J., Janowicz,

R.J., 2016. Bias corrections of precipitation measurements across experimental sites in different ecoclimatic regions of western Canada. Cryosphere 10, 2347–2360. https://doi.org/10.5194/tc-10-2347-2016

Park, H., Launiainen, S., Konstantinov, P.Y., Iijima, Y., Fedorov, A.N., 2018. Modeling the effect of moss cover on soil temperature and carbon fluxes at a tundra site in Northeastern Siberia. J. Geophys. Res. Biogeosciences. https://doi.org/10.1029/2018JG004491

Peng, X., Zhang, T., Cao, B., Wang, Q., Wang, K., Shao, W., Guo, H., 2016. Changes in Freezing-Thawing Index and Soil Freeze Depth over the Heihe River Basin, Western China. Arctic, Antarct. Alp. Res. https://doi.org/10.1657/AAAR00C-13-127

Piao, S., Friedlingstein, P., Ciais, P., Viovy, N., Demarty, J., 2007. Growing season extension and its impact on terrestrial carbon cycle in the Northern Hemisphere over the past 2 decades. Global Biogeochem. Cycles 21, 1–11. https://doi.org/10.1029/2006GB002888

Pitman, A.J., 2003. The evolution of, and revolution in, land surface schemes designed for climate models. Int. J. Climatol. https://doi.org/10.1002/joc.893

Pomeroy, J., Fang, X., Ellis, C., 2012. Sensitivity of snowmelt hydrology in Marmot Creek, Alberta, to forest cover disturbance. Hydrol. Process. 26, 1891–1904. https://doi.org/10.1002/hyp.9248

Pomeroy, J.W., Dion, K., 1996. Winter radiation extinction and reflection in a boreal pine canopy: measurements and modelling. Hydrol. Process. https://doi.org/10.1002/(sici)1099-1085(199612)10:12<1591::aid-hyp503>3.0.co;2-8

Pomeroy, J.W., Granger, R.J., 1997. Sustainability of the western Canadian boreal forest under changing hydrological conditions. I. Snow accumulation and ablation. IAHS-AISH Publ. 240, 237–242.

Pomeroy, J.W., Gray, D.M., 1995. Snowcover accumulation, relocation and management. Saskatoon.

Pomeroy, J.W., Gray, D.M., Brown, T., Hedstrom, N.R., Quinton, W.L., Granger, R.J., Carey, S.K., 2007. The cold regions hydrological model: A platform for basing process representation and model structure on physical evidence, in: Hydrological Processes. https://doi.org/10.1002/hyp.6787

Pomeroy, J.W., Gray, D.M., Hedstrom, N.R., Janowicz, J.R., 2002. Prediction of seasonal snow accumulation in cold climate forests. Hydrol. Process. https://doi.org/10.1002/hyp.1228

Pomeroy, J.W., Gray, D.M., Shook, K.R., Toth, B., Essery, R.L.H., Pietroniro, A., Hedstrom, N., 1998a. An evaluation of snow accumulation and ablation processes for land surface modelling. Hydrol. Process. https://doi.org/10.1002/(SICI)1099-1085(199812)12:15<2339::AID-HYP800>3.0.CO;2-L

Pomeroy, J.W., Marks, D., Link, T., Ellis, C., Hardy, J., Rowlands, A., Granger, R., 2009. The impact of coniferous forest temperature on incoming longwave radiation to melting snow. Hydrol. Process. 23, 2513–2525. https://doi.org/10.1002/hyp.7325

Pomeroy, J.W., Parviainen, J., Hedstrom, N., Gray, D.M., 1998b. Coupled modelling of forest snow interception and sublimation. Hydrol. Process. 12, 2317–2337. https://doi.org/10.1002/(SICI)1099-1085(199812)12:15<2317::AID-HYP799>3.0.CO;2-X

Porada, P., Ekici, A., Beer, C., 2016. Effects of bryophyte and lichen cover on permafrost soil temperature at large scale. Cryosphere 10, 2291–2315. https://doi.org/10.5194/tc-10-2291-2016

Price, D.T., Alfaro, R.I., Brown, K.J., Flannigan, M.D., Fleming, R.A., Hogg, E.H., Girardin, M.P., Lakusta, T., Johnston, M., McKenney, D.W., Pedlar, J.H., Stratton, T., Sturrock, R.N., Thompson, I.D., Trofymow, J.A., Venier, L.A., 2013. Anticipating the consequences of climate change for Canada's boreal forest ecosystems1. Environ. Rev. 21, 322–365. https://doi.org/10.1139/er-2013-0042

Pulliainen, J., Aurela, M., Laurila, T., Aalto, T., Takala, M., Salminen, M., Kulmala, M., Barr, A., Heimann, M., Lindroth, A., Laaksonen, A., Derksen, C., Mäkelä, A., Markkanen, T.,

Lemmetyinen, J., Susiluoto, J., Dengel, S., Mammarella, I., Tuovinen, J.P., Vesala, T., 2017. Early snowmelt significantly enhances boreal springtime carbon uptake. Proc. Natl. Acad. Sci. U. S. A. 114, 11081–11086. https://doi.org/10.1073/pnas.1707889114

Putkonen, J., 1998. Soil thermal properties and heat transfer processes near Ny-Ålesund, northwestern Spitsbergen, Svalbard. Polar Res. https://doi.org/10.1111/j.1751-8369.1998.tb00270.x

Pypker, T.G., Bond, B.J., Link, T.E., Marks, D., Unsworth, M.H., 2005. The importance of canopy structure in controlling the interception loss of rainfall: Examples from a young and an old-growth Douglas-fir forest. Agric. For. Meteorol. 130, 113–129. https://doi.org/10.1016/j.agrformet.2005.03.003

Rahman, M., Lu, M., Kyi, K., 2016. Seasonality of hydrological model spin-up time: a case study using the Xinanjiang model. Hydrol. Earth Syst. Sci. Discuss. https://doi.org/10.5194/hess-2016-316

Rahmat, A., 2019. Hydrological characteristics under deciduous broadleaf and evergreen coniferous forests in central JAPAN. Int. J. GEOMATE 16, 217–224. https://doi.org/10.21660/2019.54.90969

RAMP, 2019. The Distribution of Boreal Forests [WWW Document]. Reg. Aquat. Monit. Progr. URL http://www.ramp-alberta.org/river/boreal/distribution.aspx (accessed 11.12.19).

Rasmus, S., Gustafsson, D., Lundell, R., Saarinen, T., 2016. Observations and snow model simulations of winter energy balance terms within and between different coniferous forests in southern boreal Finland. Hydrol. Res. 47, 201–216. https://doi.org/10.2166/nh.2015.177

Rawls, W.J., Brakensiek, D.L., Saxton, K.E., 1982. Estimation of Soil Water Properties. Trans. ASAE. https://doi.org/10.13031/2013.33720

Razavi, S., Gupta, H. V., 2016. A new framework for comprehensive, robust, and efficient global sensitivity analysis: 2. Application. Water Resour. Res. 52, 440–455.

https://doi.org/10.1002/2015WR017559

Read, D.J., Leake, J.R., Perez-Moreno, J., 2004. Mycorrhizal fungi as drivers of ecosystem processes in heathland and boreal forest biomes. Can. J. Bot. 82, 1243–1263. https://doi.org/10.1139/B04-123

Rebeca Quiñonez-Piñón, M., Valeo, C., 2020. Modelling canopy actual transpiration in the boreal forest with reduced error propagation. Atmosphere (Basel). 11, 1158. https://doi.org/10.3390/atmos11111158

Repo, T., Kalliokoski, T., Domisch, T., Lehto, T., Mannerkoski, H., Sutinen, S., Finér, L., 2005. Effects of timing of soil frost thawing on Scots pine. Tree Physiol. https://doi.org/10.1093/treephys/25.8.1053

Rossiello, M.R., Szema, A., 2019. Health Effects of Climate Change-induced Wildfires and Heatwaves. Cureus. https://doi.org/10.7759/cureus.4771

Roulet, N.T., Woo, M.K., 1986. Hydrology of a wetland in the continuous permafrost region. J. Hydrol. https://doi.org/10.1016/0022-1694(86)90144-7

Ruess, R.W., Hendrick, R.L., Burton, A.J., Pregitzer, K.S., Sveinbjornssön, B., Allen, M.F., Maurer, G.E., 2003. Coupling fine root dynamics with ecosystem carbon cycling in black spruce forests of interior Alaska. Ecol. Monogr. 73, 643–662. https://doi.org/10.1890/02-4032

Rutter, N., Essery, R., Pomeroy, J., Altimir, N., Andreadis, K., Baker, I., Barr, A., Bartlett, P., Boone, A., Deng, H., Douville, H., Dutra, E., Elder, K., Ellis, C., Feng, X., Gelfan, A., Goodbody, A., Gusev, Y., Gustafsson, D., Hellström, R., Hirabayashi, Y., Hirota, T., Jonas, T., Koren, V., Kuragina, A., Lettenmaier, D., Li, W.-P., Luce, C., Martin, E., Nasonova, O., Pumpanen, J., Pyles, R.D., Samuelsson, P., Sandells, M., Schädler, G., Shmakin, A., Smirnova, T.G., Stähli, M., Stöckli, R., Strasser, U., Su, H., Suzuki, K., Takata, K., Tanaka, K., Thompson, E., Vesala, T., Viterbo, P., Wiltshire, A., Xia, K., Xue, Y., Yamazaki, T., 2009. Evaluation of forest snow processes models (SnowMIP2). J. Geophys. Res. 114,

D06111. https://doi.org/10.1029/2008JD011063

Sarvas, R., 1972. Investigations on the annual cycle of development of forest trees. Active period. Metsantutkimuslaitoksen Julk.

Sato, H., Ito, Akihiko, Ito, Akinori, Ise, T., Kato, E., 2015. Current status and future of land surface models. Soil Sci. Plant Nutr. https://doi.org/10.1080/00380768.2014.917593

Sato, T., Kimura, F., Kitoh, A., 2007. Projection of global warming onto regional precipitation over Mongolia using a regional climate model. J. Hydrol. https://doi.org/10.1016/j.jhydrol.2006.07.023

Saxe, H., Cannell, M.G.R., Johnsen, Ø., Ryan, M.G., Vourlitis, G., 2001. Tree and forest functioning in response to global warming. New Phytol. 149, 369–399. https://doi.org/10.1046/j.1469-8137.2001.00057.x

Saxton, K.E., Rawls, W.J., Romberger, J.S., Papendick, R.I., 1986. Estimating generalized soil-water characteristics from texture. Soil Sci. Soc. Am. J. https://doi.org/10.2136/sssaj1986.03615995005000040039x

Schulze, E.D., Leuning, R., Kelliher, F.M., 1995. Environmental regulation of surface conductance for evaporation from vegetation. Vegetatio. https://doi.org/10.1007/BF00044674

Schwalm, C.R., Glendon, S., Duffy, P.B., 2020. RCP8.5 tracks cumulative CO2 emissions, Proceedings of the National Academy of Sciences of the United States of America. https://doi.org/10.1073/PNAS.2007117117

Seki, K., 2007. SWRC fit – a nonlinear fitting program with a water retention curve for soils having unimodal and bimodal pore structure. Hydrol. Earth Syst. Sci. Discuss. https://doi.org/10.5194/hessd-4-407-2007

Sevanto, S., Suni, T., Pumpanen, J., Grönholm, T., Kolari, P., Nikinmaa, E., Hari, P., Vesala, T., 2006. Wintertime photosynthesis and water uptake in a boreal forest. Tree Physiol. https://doi.org/10.1093/treephys/26.6.749

Seyednasrollah, B., Kumar, M., Link, T.E., 2013. On the role of vegetation density on net snow cover radiation at the forest floor. J. Geophys. Res. Atmos. 118, 8359–8374. https://doi.org/10.1002/jgrd.50575

Sinha, T., Cherkauer, K.A., 2008. Time series analysis of soil freeze and thaw processes in Indiana. J. Hydrometeorol. https://doi.org/10.1175/2008JHM934.1

Skamarock, W.C., Klemp, J.B., Dudhia, J.B., Gill, D.O., Barker, D.M., Duda, M.G., Huang, X.-Y., Wang, W., Powers, J.G., 2008. A description of the advanced research WRF Version 3, NCAR Technical Note TN-475+STR. Tech. Rep. 113. https://doi.org/10.5065/D68S4MVH

Slater, A.G., Schlosser, C.A., Desborough, C.E., Pitman, A.J., Henderson-Sellers, A., Robock, A., Vinnikov, K.Y., Mitchell, K., Boone, A., Braden, H., Chen, F., Cox, P.M., De Rosnay, P., Dickinson, R.E., Dai, Y.J., Duan, Q., Entin, J., Etchevers, P., Gedney, N., Gusev, Y.M., Habets, F., Kim, J., Koren, V., Kowalczyk, E.A., Nasonova, O.N., Noilhan, J., Schaake, S., Shmakin, A.B., Smirnova, T.G., Verseghy, D., Wetzel, P., Xue, Y., Yang, Z.L., Zeng, Q., 2001. The representation of snow in land surface schemes: Results from PILPS 2(d). J. Hydrometeorol. https://doi.org/10.1175/1525-7541(2001)002<0007:TROSIL>2.0.CO;2

Slevin, D., Tett, S.F.B., Williams, M., 2015. Multi-site evaluation of the JULES land surface model using global and local data. Geosci. Model Dev. https://doi.org/10.5194/gmd-8-295-2015

SLW, 1996. Taiga or Boreal Forest [WWW Document]. URL http://www.radford.edu/~swoodwar/CLASSES/GEOG235/biomes/taiga/taiga.html (accessed 1.18.20).

Smith, C.D., 2007. Correcting the wind bias in snowfall measurements made with a Geonor T-200B precipitation gauge and alter wind shield, in: 14th SMOI. San Antonio.

Soja, A.J., Tchebakova, N.M., French, N.H.F., Flannigan, M.D., Shugart, H.H., Stocks, B.J., Sukhinin, A.I., Parfenova, E.I., Chapin, F.S., Stackhouse, P.W., 2007. Climate-induced boreal forest change: Predictions versus current observations. Glob. Planet. Change.

https://doi.org/10.1016/j.gloplacha.2006.07.028

Solomon, S., D., Qin, M., Manning, Z., Chen, M., Marquis, K.B., Averyt, M.T., Miller HL, Solomon, S., Qin, D., Manning, M., Chen, Z., Marquis, M., Averyt, K.B., Tignor, M., Miller, H.L., 2007. Summary for Policymakers. In: Climate Change 2007: The Physical Science Basis. Contribution of Working Group I to the Fourth Assessment Report of the Intergovernmental Panel on Climate Change. D Qin M Manning Z Chen M Marquis K Averyt M Tignor HL Mill. New York Cambridge Univ. Press pp. https://doi.org/10.1038/446727a

Stahli, M., Nyberg, L., Mellander, P.E., Jansson, P.E., 2001. Soil frost effects on soil water and runoff dynamics along a boreal transect: 2. Simulations. Hydrol. Process. https://doi.org/10.1002/hyp.232

Stewart, J.B., 1988. Modelling surface conductance of pine forest. Agric. For. Meteorol. https://doi.org/10.1016/0168-1923(88)90003-2

Stober, C., George, E., Persson, H., 2000. Root Growth and Response to Nitrogen. In: Schulze ED. (eds) Carbon and Nitrogen Cycling in European Forest Ecosystems. Ecol. Stud. (Analysis Synth. 142, 99–121.

Stocker, T.F., Qin, D., Plattner, G.K., Tignor, M.M.B., Allen, S.K., Boschung, J., Nauels, A., Xia, Y., Bex, V., Midgley, P.M., 2013. Climate change 2013 the physical science basis: Working Group I contribution to the fifth assessment report of the intergovernmental panel on climate change, Climate Change 2013 the Physical Science Basis: Working Group I Contribution to the Fifth Assessment Report of the Intergovernmental Panel on Climate Change. https://doi.org/10.1017/CBO9781107415324

Stoy, P., Street, L., Johnson, A., Prieto-Blanco, A., Ewing, S., 2012. Temperature, heat flux, and reflectance of common subarctic mosses and lichens under field conditions: Might changes to community composition impact climate-relevant surface fluxes? Arctic, Antarct. Alp. Res. https://doi.org/10.1657/1938-4246-44.4.500

Strand, M., Lundmark, T., Söderbergh, I., Mellander, P.E., 2002. Impacts of seasonal air and soil

temperatures on photosynthesis in Scots pine trees. Tree Physiol. https://doi.org/10.1093/treephys/22.12.839

Taniguchi, K., Sho, K., 2015. Application of the pseudo global warming dynamic downscaling method to the Tokai heavy rain in 2000. J. Meteorol. Soc. Japan. https://doi.org/10.2151/jmsj.2015-043

Tanja, S., Berninger, F., Vesala, T., Markkanen, T., Hari, P., Mäkelä, A., Ilvesniemi, H., Hänninen, H., Nikinmaa, E., Huttula, T., Laurila, T., Aurela, M., Grelle, A., Lindroth, A., Arneth, A., Shibistova, O., Lloyd, J., 2003. Air temperature triggers the recovery of evergreen boreal forest photosynthesis in spring. Glob. Chang. Biol. 9, 1410–1426. https://doi.org/10.1046/j.1365-2486.2003.00597.x

Taylor, K.E., Stouffer, R.J., Meehl, G.A., 2012. An overview of CMIP5 and the experiment design. Bull. Am. Meteorol. Soc. https://doi.org/10.1175/BAMS-D-11-00094.1

Teutschbein, C., Seibert, J., 2012. Bias correction of regional climate model simulations for hydrological climate-change impact studies: Review and evaluation of different methods. J. Hydrol. 456–457, 12–29. https://doi.org/10.1016/j.jhydrol.2012.05.052

Tolson, B.A., Shoemaker, C.A., 2007. Dynamically dimensioned search algorithm for computationally efficient watershed model calibration. Water Resour. Res. https://doi.org/10.1029/2005WR004723

Trzaska, S., Schnarr, E., 2014. A Review of Downscaling Methods for Climate Change Projections. African and Latin American Resilience to Climate Change (ARCC). United States Agency Int. Dev. by Tetra Tech ARD 1–42. https://doi.org/10.4236/ojog.2016.613098

Turetsky, M.R., Mack, M.C., Harden, J.W., Manies, K.L., 2007. Spatial Patterning of Soil Carbon Storage Across Boreal Landscapes, in: Ecosystem Function in Heterogeneous Landscapes. https://doi.org/10.1007/0-387-24091-8_12

UCMP, 2020. The forest biome [WWW Document]. Univ. Calif. Museum Paleontol.

Ueyama, M., Harazono, Y., Ohtaki, E., Miyata, A., 2006. Controlling factors on the interannual CO2 budget at a subarctic black spruce forest in interior Alaska, in: Tellus, Series B: Chemical and Physical Meteorology. https://doi.org/10.1111/j.1600-0889.2006.00205.x

van Bavel, C.H.M., 1996. Water Relations of Plants and Soils. Soil Sci. https://doi.org/10.1097/00010694-199604000-00007

van Genuchten, M.T., 1980. A closed-form equation for predicting the hydraulic conductivity of unsaturated soils1. Soil Sci. Soc. Am. J. https://doi.org/10.2136/sssaj1980.03615995004400050002x

Vapaavuori, E.M., Rikala, R., Ryyppo, A., 1992. Effects of root temperature on growth and photosynthesis in conifer seedlings during shoot elongation. Tree Physiol. 10, 217–230. https://doi.org/10.1093/treephys/10.3.217

Verseghy, D., 2011. Class – the canadian land surface scheme (version 3.5), Tecchnical Document.

Verseghy, D.L., 1991. Class—A Canadian land surface scheme for GCMS. I. Soil model. Int. J. Climatol. https://doi.org/10.1002/joc.3370110202

Wagner, W., Lemoine, G., Rott, H., 1999. A method for estimating soil moisture from ERS Scatterometer and soil data. Remote Sens. Environ. https://doi.org/10.1016/S0034-4257(99)00036-X

Wang, S., Grant, R.., Verseghy, D.., Black, T.., 2001. Modelling plant carbon and nitrogen dynamics of a boreal aspen forest in CLASS — the Canadian Land Surface Scheme. Ecol. Modell. 142, 135–154. https://doi.org/10.1016/S0304-3800(01)00284-8

Welp, L.R., Randerson, J.T., Liu, H.P., 2007. The sensitivity of carbon fluxes to spring warming and summer drought depends on plant functional type in boreal forest ecosystems. Agric. For. Meteorol. 147, 172–185. https://doi.org/10.1016/j.agrformet.2007.07.010

Western, A.W., Grayson, R.B., Blöschl, G., 2002. Scaling of Soil Moisture: A Hydrologic Perspective. Annu. Rev. Earth Planet. Sci.

https://doi.org/10.1146/annurev.earth.30.091201.140434

Wickland, K.P., Neff, J.C., 2008. Decomposition of soil organic matter from boreal black spruce forest: Environmental and chemical controls. Biogeochemistry. https://doi.org/10.1007/s10533-007-9166-3

Williams, T.J., Pomeroy, J.W., Janowicz, J.R., Carey, S.K., Rasouli, K., Quinton, W.L., 2015. A radiative-conductive-convective approach to calculate thaw season ground surface temperatures for modelling frost table dynamics. Hydrol. Process. https://doi.org/10.1002/hyp.10573

Willmott, C.J., Robeson, S.M., Matsuura, K., 2012. A refined index of model performance. Int. J. Climatol. https://doi.org/10.1002/joc.2419

Wu, J., Guan, D., Yuan, F., Wang, A., Jin, C., 2013. Soil temperature triggers the onset of photosynthesis in Korean pine. PLoS One. https://doi.org/10.1371/journal.pone.0065401

Würzer, S., Jonas, T., Wever, N., Lehning, M., 2016. Influence of initial snowpack properties on runoffformation during rain-on-snow events. J. Hydrometeorol. 17, 1801–1815. https://doi.org/10.1175/JHM-D-15-0181.1

Xarpell, L., Koivusalo, H., Laurén, A., Repo, T., 2010. Simulation of soil temperature and moisture under different snow and frost conditions with COUP model, metla.fi.

Xie, Z., Gao, J., Wang, A., 2017. Simulations of soil frost and thaw front (FTF) dynamics using a land surface model. Institute of Atmospheric Physics Chinese Academy of Sciences, pp. 19–22.

Xu, H., Zwiazek, J.J., 2020. Fungal Aquaporins in Ectomycorrhizal Root Water Transport. Front. Plant Sci. https://doi.org/10.3389/fpls.2020.00302

Xu, L., Myneni, R.B., Chapin, F.S., Callaghan, T. V., Pinzon, J.E., Tucker, C.J., Zhu, Z., Bi, J., Ciais, P., Tømmervik, H., Euskirchen, E.S., Forbes, B.C., Piao, S.L., Anderson, B.T., Ganguly, S., Nemani, R.R., Goetz, S.J., Beck, P.S.A., Bunn, A.G., Cao, C., Stroeve, J.C.,

2013. Temperature and vegetation seasonality diminishment over northern lands. Nat. Clim. Chang. 3, 581–586. https://doi.org/10.1038/nclimate1836

Yang, K., Wang, C., 2019. Water storage effect of soil freeze-thaw process and its impacts on soil hydro-thermal regime variations. Agric. For. Meteorol. https://doi.org/10.1016/j.agrformet.2018.11.011

Yang, R., Friedl, M.A., 2003. Modeling the effects of three-dimensional vegetation structure on surface radiation and energy balance in boreal forests. J. Geophys. Res. D Atmos. https://doi.org/10.1029/2002jd003109

Yang, Z.L., Niu, G.Y., Mitchell, K.E., Chen, F., Ek, M.B., Barlage, M., Longuevergne, L., Manning, K., Niyogi, D., Tewari, M., Xia, Y., 2011. The community Noah land surface model with multiparameterization options (Noah-MP): 2. Evaluation over global river basins. J. Geophys. Res. Atmos. https://doi.org/10.1029/2010JD015140

Yin, Z., Ouyang, H., Xu, X., Zhou, C., Zhang, F., Shao, B., 2010. Estimation of evapotranspiration from faber fir forest Ecosystem in the Eastern Tibetan Plateau of China using SHAW model. J. Water Resour. Prot. 2, 143–153. https://doi.org/10.4236/jwarp.2010.22017

Yu, H., Luedeling, E., Xu, J., 2010. Winter and spring warming result in delayed spring phenology on the Tibetan Plateau. Proc. Natl. Acad. Sci. 107, 22151–22156. https://doi.org/10.1073/pnas.1012490107

Zemp, M., Huss, M., Thibert, E., Eckert, N., McNabb, R., Huber, J., Barandun, M., Machguth, H., Nussbaumer, S.U., Gärtner-Roer, I., Thomson, L., Paul, F., Maussion, F., Kutuzov, S., Cogley, J.G., 2019. Global glacier mass changes and their contributions to sea-level rise from 1961 to 2016. Nature. https://doi.org/10.1038/s41586-019-1071-0

Zha, T., Li, C., Kellomäki, S., Peltola, H., Wang, K.Y., Zhang, Y., 2013. Controls of Evapotranspiration and CO2 Fluxes from Scots Pine by Surface Conductance and Abiotic Factors. PLoS One. https://doi.org/10.1371/journal.pone.0069027

Zhang, K., Kimball, J.S., Kim, Y., Mcdonald, K.C., 2011. Changing freeze-thaw seasons in northern high latitudes and associated influences on evapotranspiration. Hydrol. Process. 25, 4142–4151. https://doi.org/10.1002/hyp.8350

Zhang, X., Flato, G., Kirchmeier-Young, M., Vincent, L.A., Wan, H., Wang, X., Rong, R., Fyfe, J.C., L, G., Kharin, V. V., 2019. Changes in temperature and precipitation across Canada. Canada's Chang. Clim. Rep. 112–193.

Zhang, Y., Chen, W., Smith, S.L., Riseborough, D.W., Cihlar, J., 2005. Soil temperature in Canada during the twentieth century: Complex responses to atmospheric climate change. J. Geophys. Res. D Atmos. 110, 1–15. https://doi.org/10.1029/2004JD004910

Zhang, Y., Wang, S., Barr, A.G., Black, T.A., 2008. Impact of snow cover on soil temperature and its simulation in a boreal aspen forest. Cold Reg. Sci. Technol. https://doi.org/10.1016/j.coldregions.2007.07.001

Zhang, Z., Li, Y., Barlage, M., Chen, F., Miguez-Macho, G., Ireson, A., Li, Z., 2020. Modeling groundwater responses to climate change in the Prairie Pothole Region. Hydrol. Earth Syst. Sci. 24, 655–672. https://doi.org/10.5194/hess-24-655-2020

Zhang, Z., Zhang, R., Cescatti, A., Wohlfahrt, G., Buchmann, N., Zhu, J., Chen, G., Moyano, F., Pumpanen, J., Hirano, T., Takagi, K., Merbold, L., 2017. Effect of climate warming on the annual terrestrial net ecosystem CO2 exchange globally in the boreal and temperate regions. Sci. Rep. https://doi.org/10.1038/s41598-017-03386-5

Zhao, L., Gray, D.M., Toth, B., 2002. Influence of soil texture on snowmelt infiltration into frozen soils. Can. J. Soil Sci. https://doi.org/10.4141/S00-093

Zheng, C., Lu, Y., Liu, X., Šimůnek, J., Zeng, Y., Shi, C., Li, H., 2020. In-situ monitoring and characteristic analysis of freezing-thawing cycles in a deep vadose zone. Water (Switzerland). https://doi.org/10.3390/W12051261

Zheng, D., Hunt, E.R., Running, S.W., 1993. A daily soil temperature model based on air

temperature and precipitation for continental applications. Clim. Res. 2, 183–191. https://doi.org/10.3354/cr002183

APPENDIX A

Biased Correction of Snow Water Equivalent

A systematic bias of about 5.5-cm was noted and removed from the snow depth observations at the black spruce site, which was due to the graduated depth rod penetrating below the snowpack into the fluffy feather moss understory vegetation. The bias was not present at the jack pine and aspen sites because of their comparatively firmer soil-snow interface.

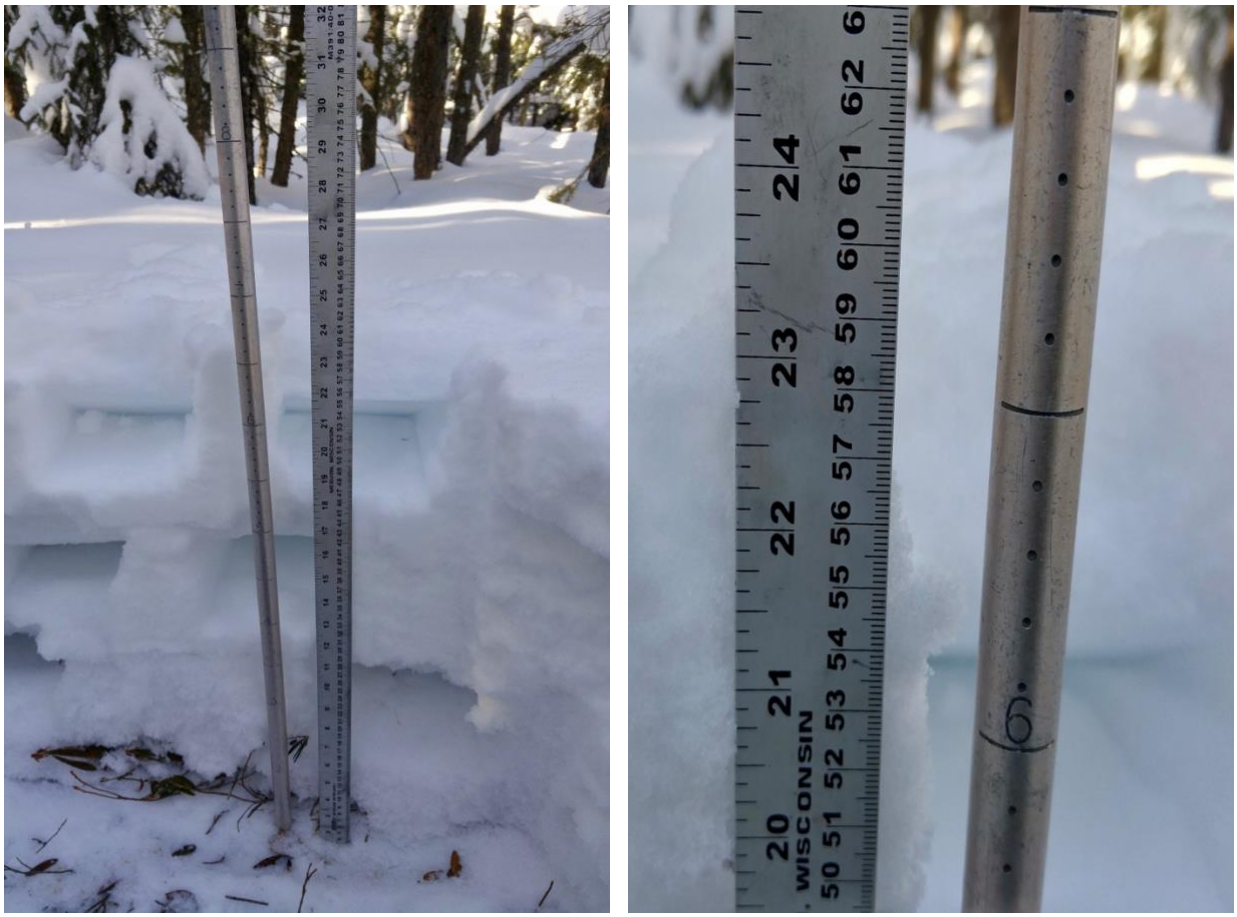

Figure A.1 Difference in snow depth measurements by a measuring rod and a ruler at the black spruce site (Photo Credit: Bruce Johnson)

APPENDIX B

The estimated average ice content based on antecedent conditions prior to soil freezing and the minimum liquid water content in winter from 2001 to 2015 is summarized in Table B.1 along with the minimum soil temperatures for different depths.

Table B.1 The minimum winter soil temperature and ice content for different depths

Site	Soil Depth (cm)	Minimum soil temperature (°C)	Antecedent water content (m^3/m^3)	Minimum liquid water content (m^3/m^3)	Ice content (m^3/m^3)
Aspen	0-15	-2.6	0.236	0.116	0.119
	15-30	-1.6	0.281	0.183	0.099
	30-60	-0.9	0.304	0.248	0.056
	60-90	-0.3	0.317	0.276	0.042
	90-120	0.3	0.282	0.245	0.036
Jack pine	0-15	-5.9	0.089	0.051	0.038
	15-30	-4.8	0.105	0.089	0.016
	30-60	-3.2	0.093	0.057	0.037
	60-90	-2.3	0.083	0.049	0.033
	90-120	-1.5	0.085	0.055	0.031
Black spruce	0-15	-1.5	0.085	0.055	0.031
	15-30	-4.9	0.146	0.047	0.099
	30-60	-0.6	0.317	0.131	0.186
	60-90	0.1	0.349	0.277	0.071

APPENDIX C

Snowpack Energy Balance

The models' (CLASS, CRHM, and SHAW) simulated snowpack energy balance terms are shown in Figure C.1 and Figure C.2 for the year of 2015 and 2016 respectively along with the observations of net radiation. Below canopy radiation data represent single location measurements; therefore, does not capture spatial variability. Net radiation simulations for the CRHM model were slightly higher than the other models but better matched with the observations. A higher sensible heat flux compared to the other models and negligible latent heat flux was simulated by the CRHM model. In contrast, a higher latent heat flux and negligible sensible heat flux was simulated by the SHAW model. A negligible below canopy turbulence was simulated by the CLASS model which suggests that most of the below canopy energy is available for heating and melting the snowpack. Change in internal energy was bigger in magnitude for the CRHM and the SHAW models as compared to the CLASS model.

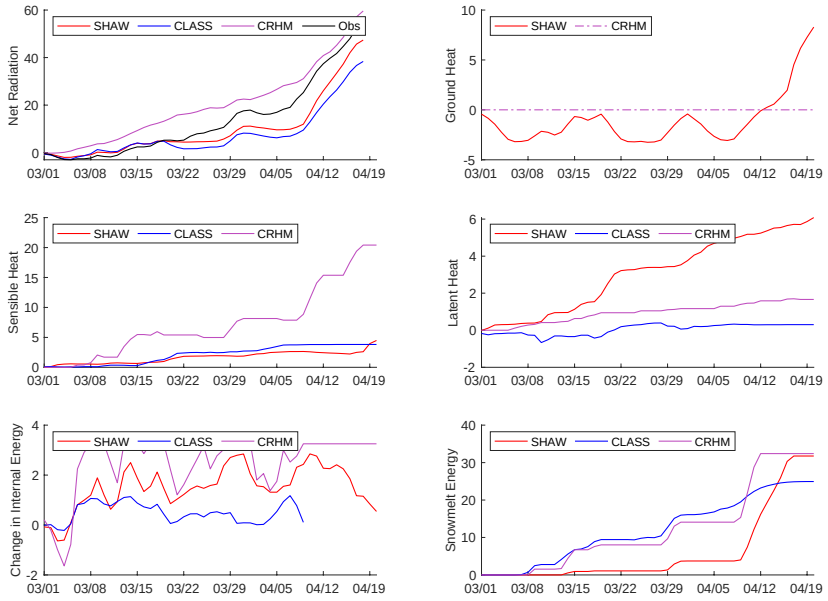

Figure C.1 Snowpack energy balance components (Cumulative in MJ m-2 day-1) for the year of 2015

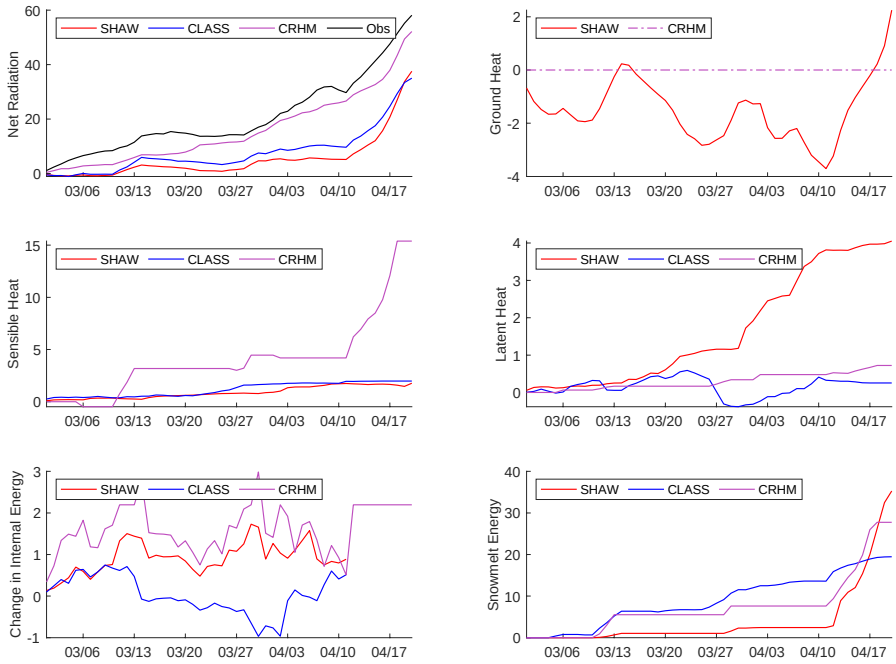

Figure C.2 Snowpack energy balance components (Cumulative in MJ m^{-2} day^{-1}) for the year of 2016

APPENDIX D

For solar radiation function, site specific K_{ST} parameter was needed to relate incoming solar radiation with stomatal conductance. The direct measurements of stomatal conductance were not available and gross ecosystem photosynthesis (GEP) was used as a proxy to stomatal conductance. The values of solar radiation function varies from 0 to 1; thus, GEP data were normalized. The parameter K_{ST} was determined by fitting solar radiation function (f-ST) to the normalized GEP data (Figure D.1).

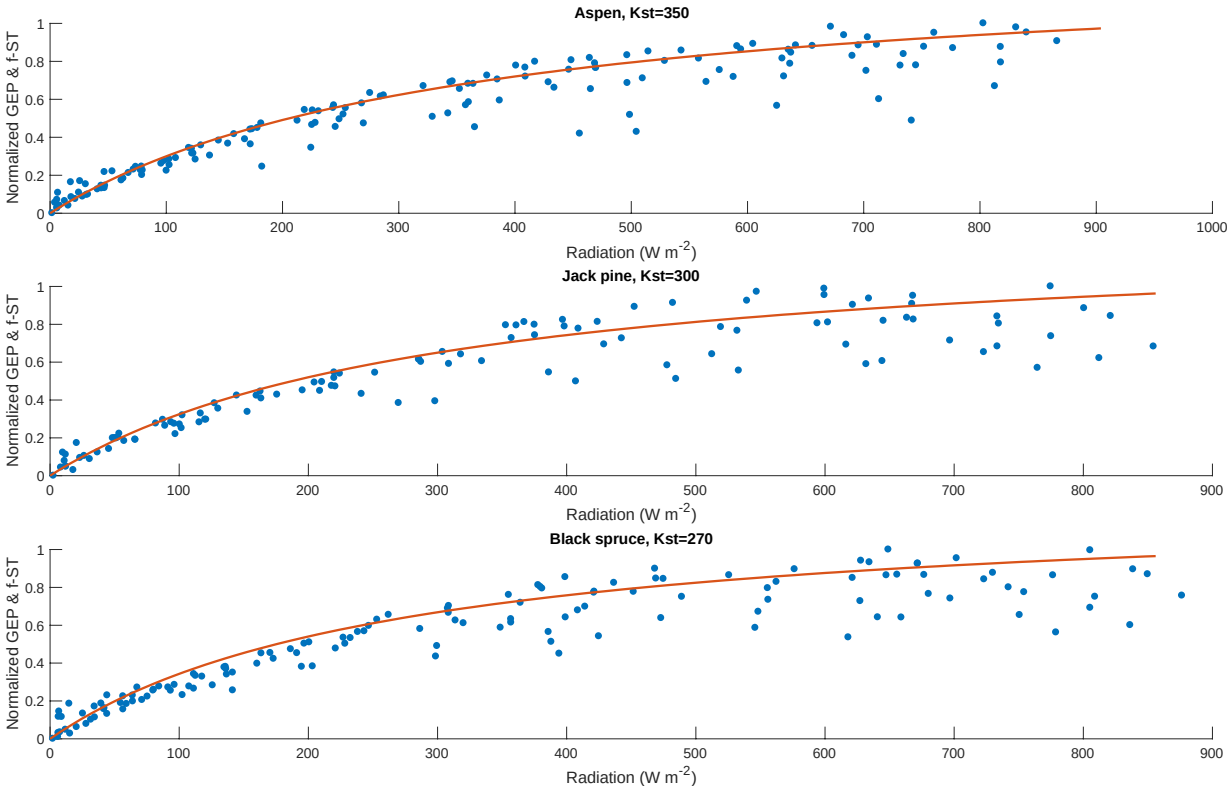

Figure D.1 Scatter plot of normalized Gross Ecosystem Photosynthesis (GEP) vs. solar radiation at all three study sites along with fitted solar radiation function. The observed GEP data is bin averaged (1997 to 2015)

APPENDIX E

The default parameters for VPD function were derived from CLASS technical documentation (Verseghy, 2011) based on vegetation types. The CLASS and SHAW models use different algorithms for vapor pressure deficit function where CLASS relates stomatal resistance with vapor pressure deficit as:

$$f_{VPD\_CLASS} = \frac{(VPD/10)^{cv2}}{cv1}$$

where cv1 is 0.65 and 0.50 for needleleaf and broadleaf trees, respectively and cv2 is 1.05 and 0.60 in the same order. The r_vpd parameter for SHAW was determined by fitting the f_{VPD_CLASS} curve for relating relative conductance with vapor pressure deficit (Figure E.1 and Figure E.2) This was referred as default r_vpd in this study and was estimated to be 0.80 for coniferous and 0.38 for deciduous forests.

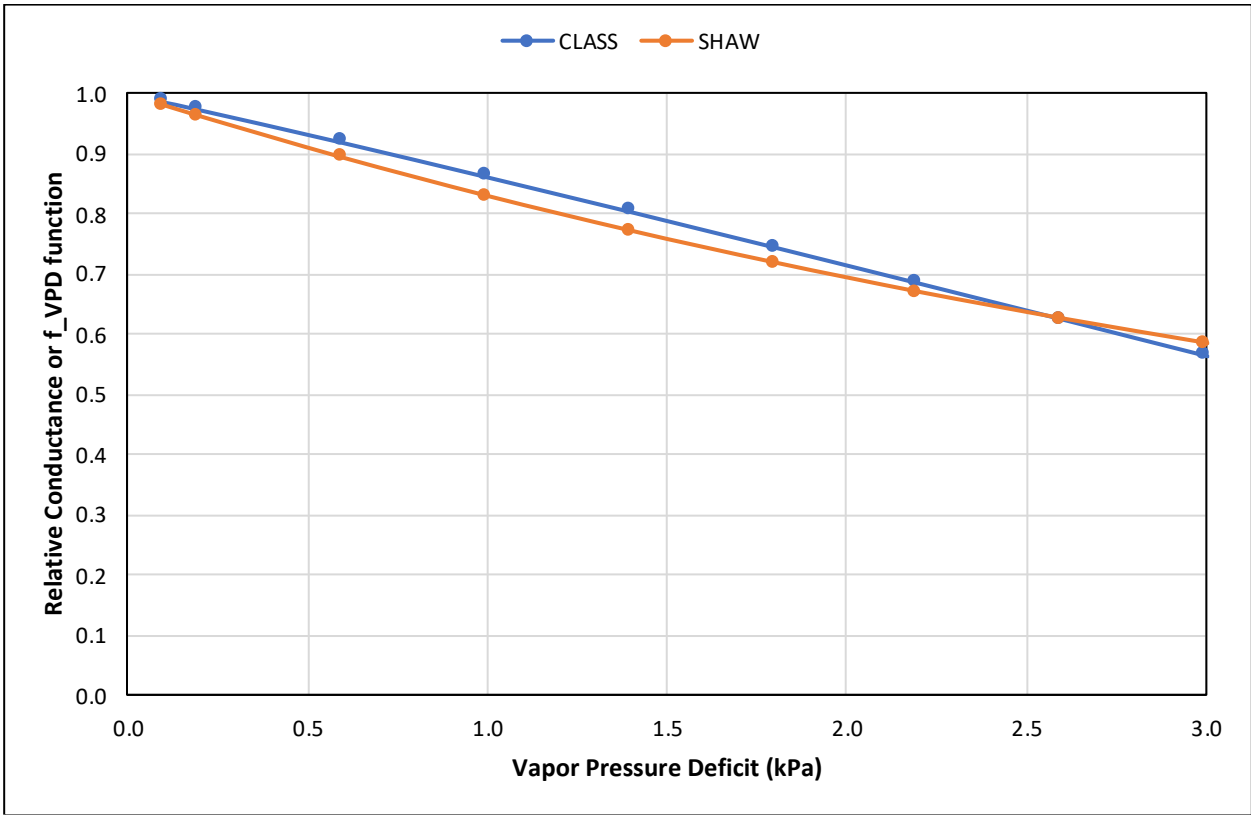

Figure E.1 CLASS and SHAW functions for relating stomatal conductance with vapor pressure deficit for coniferous forests

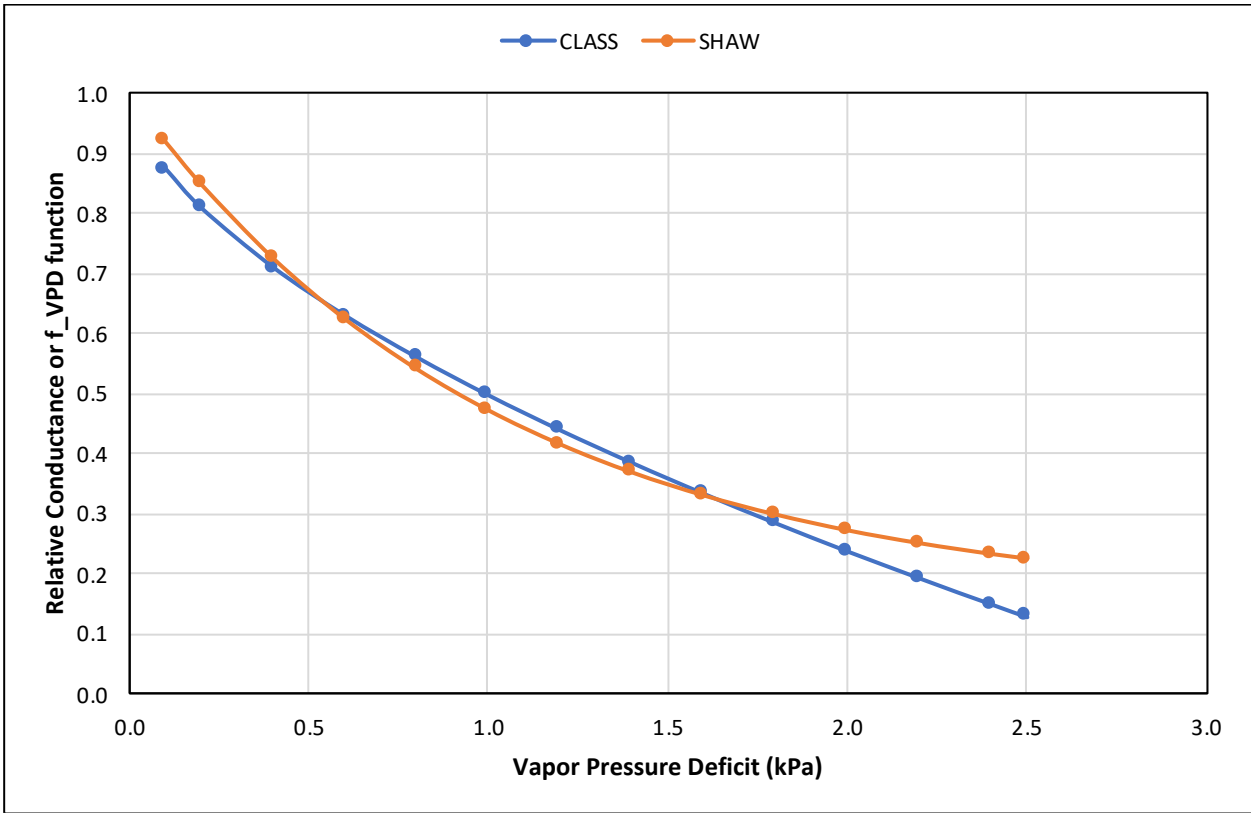

Figure E.2 CLASS and SHAW functions for relating stomatal conductance with vapor pressure deficit for deciduous forests

APPENDIX F

Testing of 0 °C base temperature for Growing Degree Days Calculation

Testing of 0 °C base temperature for growing degree days produced similar results as of 5 °C base temperature. Relationship between gross ecosystem photosynthesis and accumulated growing degree days showed that the onset of recovery of photosynthesis was correlated with the start of GDD accumulation. However, about 675 GDD were required for peak photosynthesis with 0 °C base temperature.

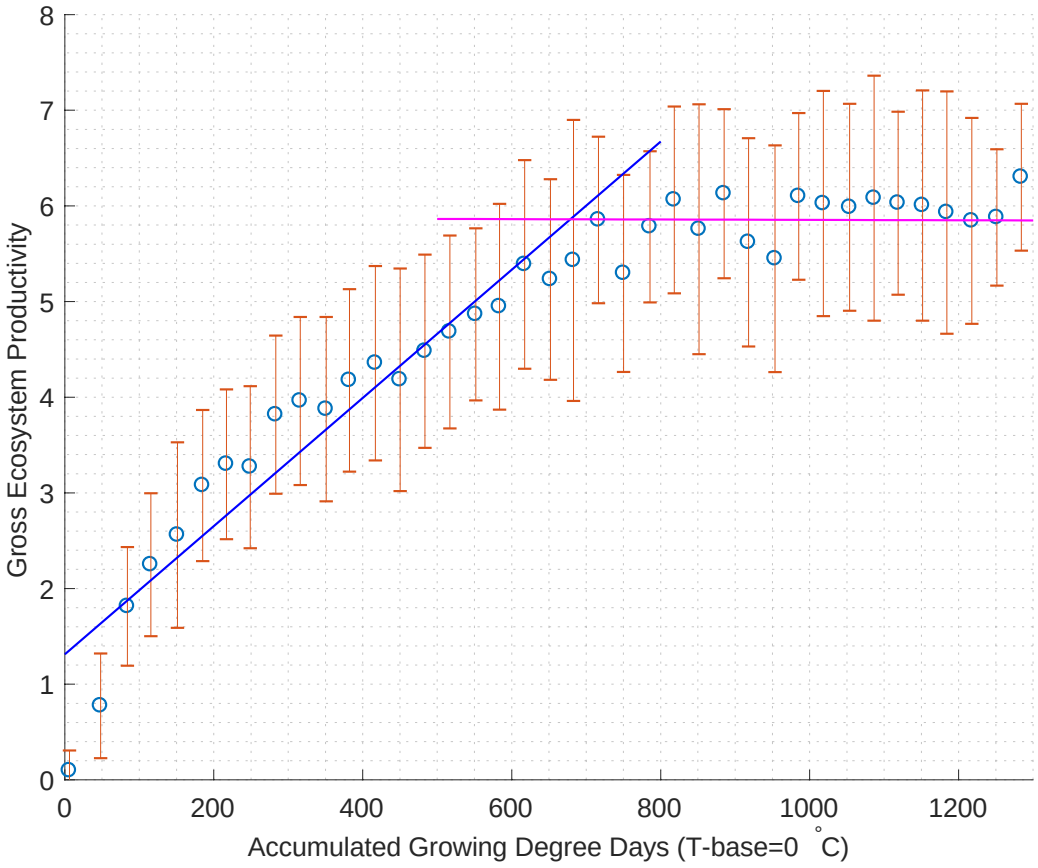

Figure F.1 Relationship between gross ecosystem productivity and accumulated growing degree days based on 0 °C base temperature

APPENDIX G

One-way ANOVA test on Observed and WRF simulated precipitation

One-way ANOVA multiple comparison test was performed to determine if observed and WRF simulated precipitation was statistically different among sites. A graphical representation of test results is provided below. Aspen, jack pine and black spruce sites are represented by 1, 2, and 3, respectively. Two groups are considered to statistically different if comparison interval for their mean don't overlap.

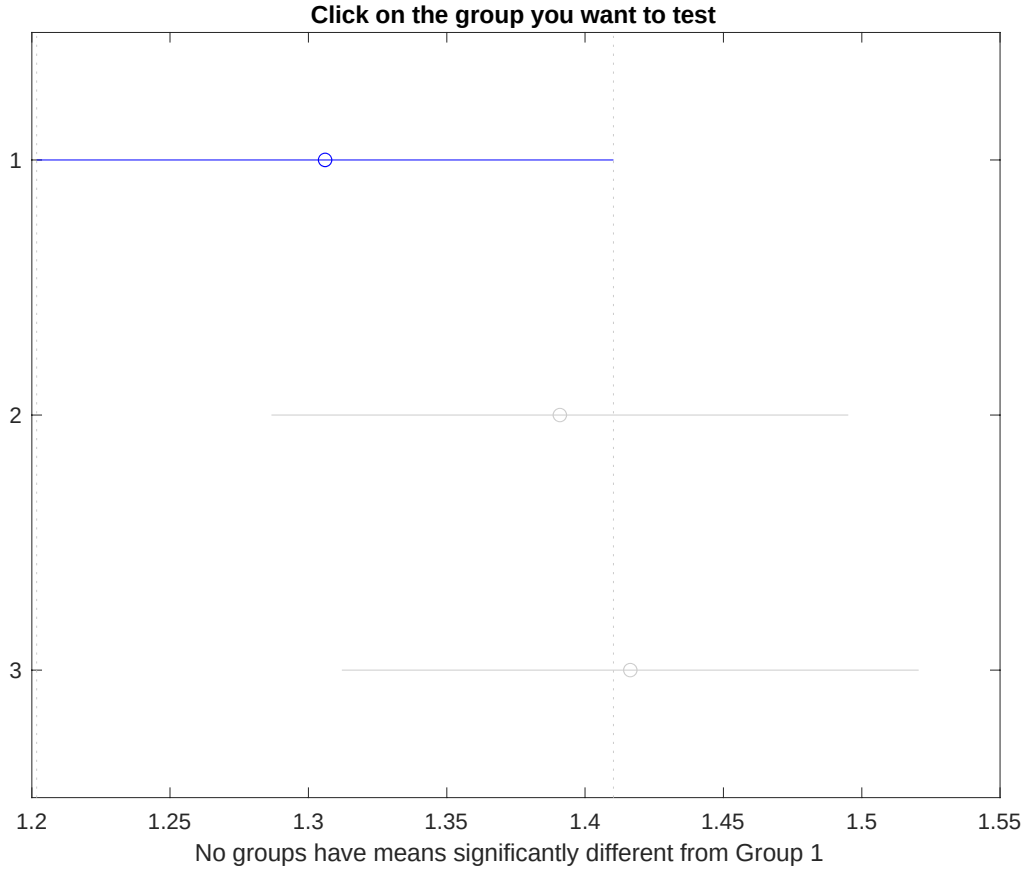

Figure G.1 One-way ANOVA results for observed precipitation at aspen (1), jack pine (2) and black spruce (3).

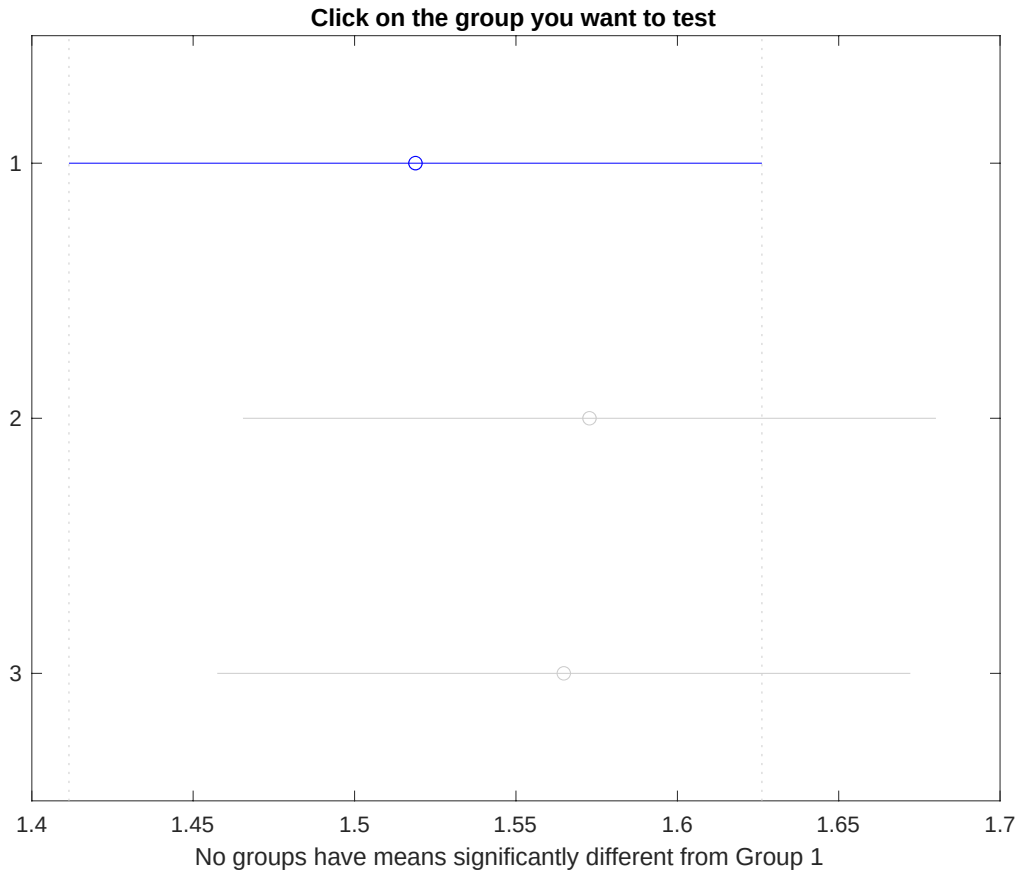

Figure G.2 One-way ANOVA results for WRF-CTL precipitation data at aspen (1), jack pine (2) and black spruce (3) sites.

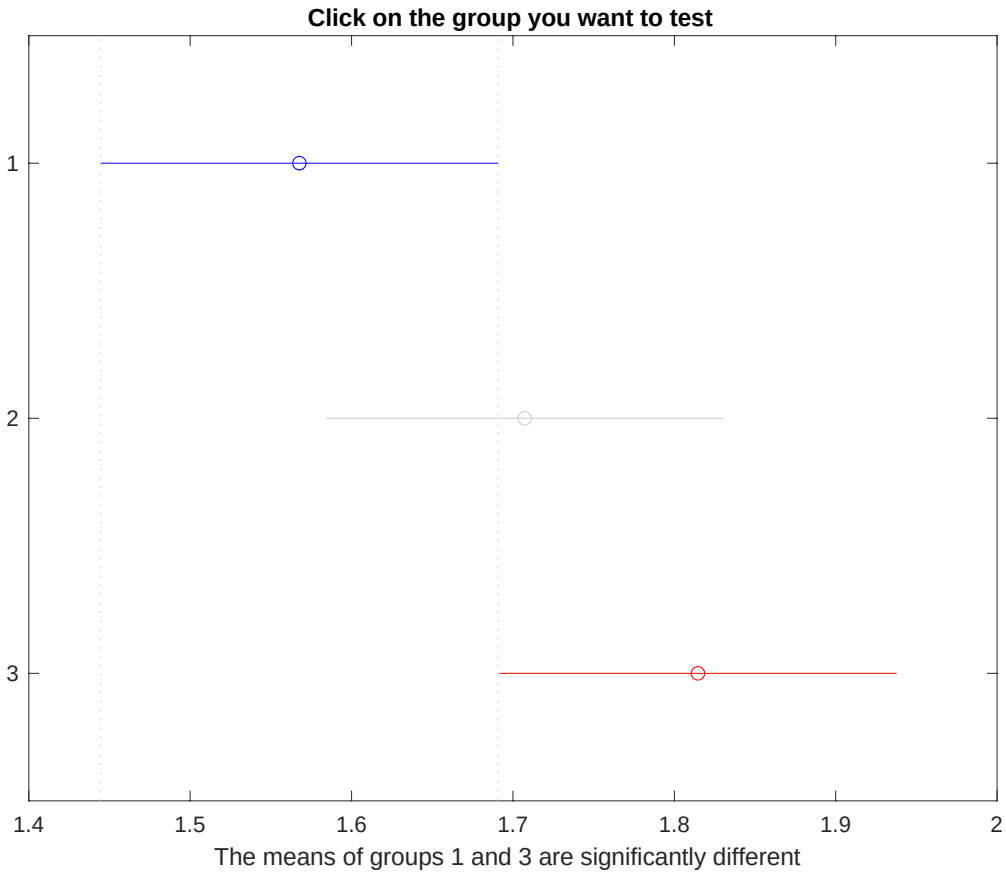

Figure G.3 One-way ANOVA results for WRF-PGW precipitation data at aspen (1), jack pine (2) and black spruce (3) sites.

APPENDIX H

The average daily observed we well as WRF simulated raw and bias corrected data for wind speed, relative humidity and solar radiation are presented in Figure H.1. The bias correction has minor effects on WRF simulated solar radiation and wind speed data but about 15% was bias was removed for relative humidty.

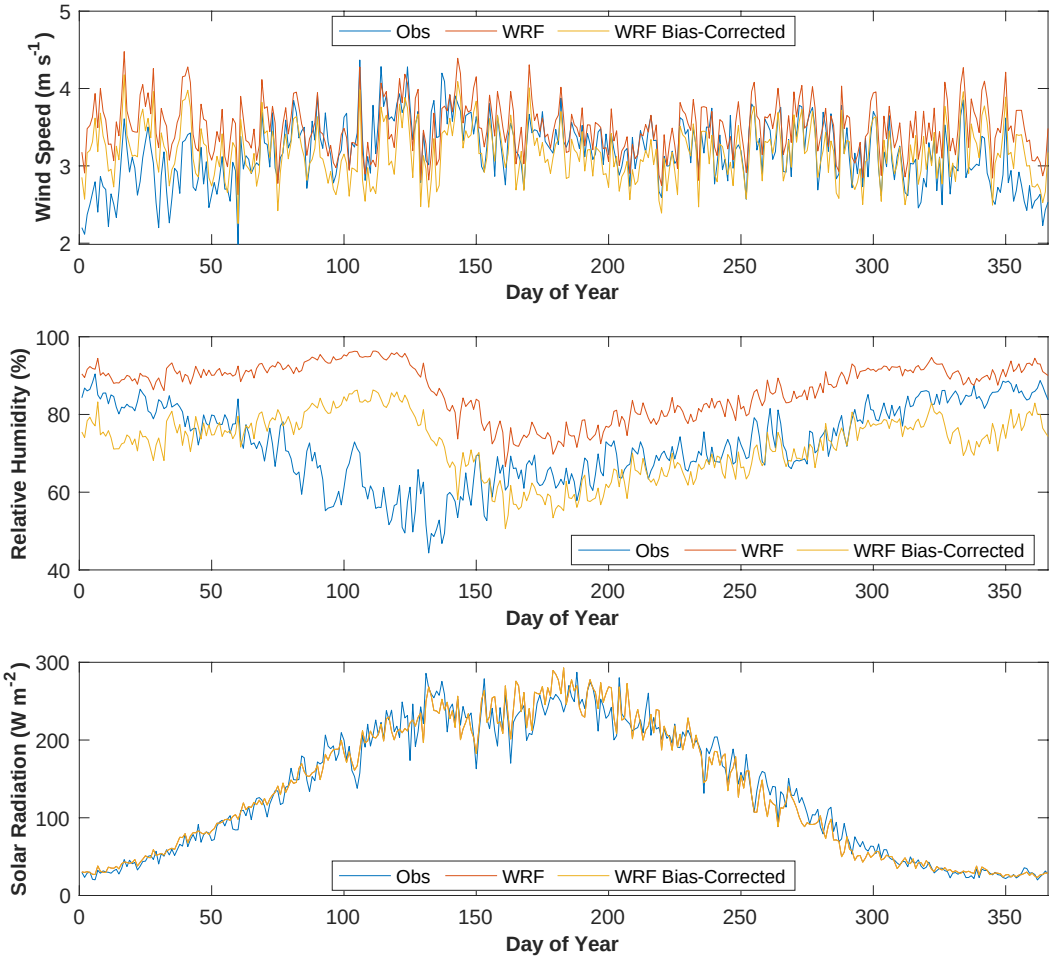

Figure H.1 Observed and WRF simulated data with and without bias correction.